Republic of Iraq
Ministry of Higher Education and Scientific Research
University of Kerbala
College of Engineering
Department of Electrical and Electronic Engineering

Supporting the Electric Motor of A Hybrid Autonomous Vehicle by Intelligent Speed Controller

A Thesis Submitted to the Council of the College of Engineering/University of Kerbala in a Partial Fulfillment of the Requirements for the Degree of Master of Science (M.Sc.) in Electrical Engineering

Written By:

Mohammed Albaker Najm Abed

Supervised By:

Prof. Dr. Ali Abdul Razzaq Altahir

Asst. Prof. Dr. Ahmed Abdulhadi Ahmed

August 2024 Dhu al-Hijjah 1445

ٱقۡرَأۡ بِٱسۡمِ رَبِّكَ ٱلَّذِي خَلَقَ (1)خَلَقَ ٱلۡإِنسَٰنَ مِنۡ عَلَقٍ (2)ٱقۡرَأۡ وَرَبُّكَ ٱلۡأَكۡرَمُ (3)ٱلَّذِي عَلَّمَ بِٱلۡقَلَمِ (4)عَلَّمَ ٱلۡإِنسَٰنَ مَا لَمۡ يَعۡلَمۡ (5)

صدق الله العلي العظيم

(سورة العلق)

Examination Committee Certification

We have read the thesis entitled "**Supporting the Electric Motor of a Hybrid Autonomous Vehicle by Intelligent Speed Controller.**" **As an examining committee, we examined the student "Mohammed Albaker Najm Abed" in its content.** What is connected with it and that, in our opinion, it is adequate as a thesis for the degree of Master of Science (M.Sc.) in Electrical Engineering.

Supervisor

Signature:

Name : *Prof. Dr.* Ali Abdul Razzaq Altahir.

Date: 3 / 9 / 2024

Supervisor

Signature:

Name : *Asst. Prof. Dr.* Ahmed Abdulhadi Al-Moadhen.

Date: 3 / 9 / 2024

Member

Signature:

Name : *Asst. Prof. Dr.* Abduljabbar Owaid Hanfesh.

Date: 3 / 9 / 2024

Member

Signature:

Name : *Asst. Prof. Dr.* Haider Muhamed Umran.

Date: 3 / 9 / 2024

Chairman

Signature:

Name : *Asst. Prof. Dr.* Ammar A. Altameemi.

Date: 3 / 9 / 2024

Signature:

Name : *Asst. Prof. Dr.* Muayad Saleem Kod.

Head of the Department of Electrical and Electronic Engineering

Date: 5 / 9 / 2024

Signature:

Name : *Prof. Dr.* Haider Nadhom Azziz.

Dean of Engineering College

Date: 8 / 9 / 2024

Supervisor Certificate

We certify that the thesis entitled **"Supporting the Electric Motor of A Hybrid Autonomous Vehicle by Intelligent Speed Controller"** was prepared by "**Mohammed Albaker Najm Abed**" under our supervision at the Department of Electrical Engineering, College of Engineering, University of Kerbala as a partial fulfillment of the requirements for the Degree of Master of Science (M.Sc.) in Electrical Engineering.

Signature:

Name: *Prof. Dr.* Ali Abdul Razzaq Altahir

Date: 3 / 9 / 2024

Signature:

Name: *Asst. Prof. Dr.* Ahmed Abdulhadi Ahmed Al-Moadhen

Date: 3 / 9 / 2024

Linguistic Certificate

I certify that the thesis entitled "**Supporting the Electric Motor of a Hybrid Autonomous Vehicle by Intelligent Speed Controller,**" which has been submitted by **Mohammed Albaker Najm Abed,** has been proofread, and its language has been amended to meet the English style.

Signature:

Name: Lecturer Dr. Ahmed Selman Altuma.

Date: ١/٩/2024

Undertaking

I certify that the thesis work "**Supporting the Electric Motor of a Hybrid Autonomous Vehicle by Intelligent Speed Controller**" is mine. The work has not been presented elsewhere for assessment, and the materials used from other sources have been properly acknowledged/referred to.

Signature:

Name: **Mohammed Albaker Najm Abed.**

Date: 3 / 9 / 2024

Dedicated to

((My Family))

Acknowledgments

I would like to thank my supervisors, Prof. Dr. Ali Abdul Razzaq Abbas Altahir and Assist. Prof. Dr. Ahmed Abdulhadi Ahmed, for their support and guidance in helping me conduct my research thesis.

Abstract

Hybrid Electric Vehicles (HEVs) offer a promising solution to mitigate the transportation sector's environmental impact by reducing greenhouse gas emissions. This thesis aims to enhance the performance and control systems of HEVs. A comprehensive investigation of permanent magnet synchronous motor (PMSM) motor control strategies was conducted. Lyapunov stability theory-based backstepping control is the most effective way to track motor speed accurately and efficiently, which is essential for HEV dynamics. This study explored advanced energy management strategies for HEV systems to optimize energy utilization. A hybrid energy storage system was investigated using a rechargeable battery, supercapacitor, and solar energy integration. After evaluating several Maximum Power Point Tracking (MPPT) algorithms, it was found that the Perturbation and Observation (P&O) method performed better at maximizing the power extracted from solar panels.

Moreover, a comparative analysis of DC-DC converter topologies revealed the Super-Lift converter as the most efficient for voltage level conversion. The extracted power from the solar panel is increased to 15% when using P&O with a Super-lift Luo converter. Multi-level inverters were used to ensure smooth operation and reduce torque ripple. The torque ripple decreased to 0.083%. A fractional PID controller was employed for intelligent energy management. To further improve the capabilities of HEVs, this thesis investigated the viability of autonomous operation. An Adaptive Model Predictive Control (AMPC) strategy was developed and simulated to enable precise path tracking for Autonomous Hybrid Electric Vehicles (AHEVs). Simulation results demonstrated exceptional path-tracking accuracy of 99.2%, highlighting the potential of AMPC for safe and efficient autonomous driving. The proposed control strategies and energy management system were rigorously evaluated through MATLAB/Simulink simulations. The results show essential improvements in energy economy, motor performance, and overall HEV system performance. This thesis advances HEV technology by offering practical options for improved motor control, efficient energy management, and autonomous capabilities.

Table of Contents

List of Tables

List of Figures

List of Abbreviations

AHEV	Autonomous Hybrid Electric Vehicle
AV	Autonomous Vehicle
AC	Alternating Current
ANN	Artificial Neural Networks
AMPC	Adaptive Model Predictive Control
BLDC	Brushless DC Motors
BMS	Battery Management Systems
CCM	Continuous Current Mode
CO	Carbon Monoxide
CO2	Carbon Dioxide
DC	Direct Current
DoD	Depth of Discharge
DCM	Discontinuous Current Mode
EMF	Electromotive Force
EM	Electric Motor
EV	Electric Vehicles
EMS	Energy Management System
ESS	Energy Storage System
ESR	Equivalent Series Resistance
EKF	Extended Kalman Filter
EPSO	Enhanced Practical Swarm Optimization
FC	Fuel Cell
FOPID	Fractional-Order PID
FOC	Field-Oriented Control
FCHEV	Fuel Cell Hybrid Electric Vehicles
HESS	Hybrid Energy Storage System
ICHEV	Internal Combustion Engine Hybrid Electric Vehicles
I.M	Induction Motors
IPMSM	Interior Permanent Magnet Synchronous Motor
INC	Incremental Conductance Controller
KF	Kalman Filter
LTVKF	linear-Time-Varying Kalman Filter
LCA	Life Cycle Assessment
MRPT	Maximum Regenerative Power Tracking
MPPT	Maximum Power Point Tracking
MV	Manipulated Variables

PV	Photo Voltaic
PID	Proportional – Integral – Derivative
PM	Permanent Magnets
P&O	Perturbing and Observing
PSO	Particle Swarm Optimization
QP	Quadratic Program
SC	Supercapacitors
SMO	Sliding Mode Observer
SPMSM	Surface Permanent Magnet Synchronous Motor
STD	Standard Test Conditions
SoC	State of Charge
SRM	Switching Reluctance Motors
SMC	Sliding Mode Controller
Sc	Scenario
THD	Total Harmonics Distortion
UPS	Uninterruptible Power Supply

List of Symbols

R_a	Armature resistor
L_a	Armature inductance
Ω_m	Motor PMSM speed
p	The number of poles
i_d,i_q	The stator currents for the d- and q-axes
e_a	Trapezoidal back EMF
I_{sh}	A current of the short circuit for the PV panel
$G1, G2$	The irradiance of the PV panel
N_{cell}	Number of cells in a module connected in series
E_{oc}	Open circuit voltage of Fuel cell
A_{FC}	Photocurrent slope
V_{bat}	Battery voltage
V_{SC}	Supercapacitor voltage
P_{SC}	Supercapacitor power
C_{SC}	Supercapacitor stack's capacity
R_{SC}	Supercapacitor resistor
G_s	Voltage gain
δ	Duty ratio
v_L	The voltage across the inductor
I_{max}, I_{min}	Maximum and minimum inductor currents
L_{min}	Minimum inductor
$\frac{\Delta V_o}{V_o}$	Ripple voltage

$\Delta V_{o,ESR}$	The equivalent series resistance caused a voltage ripple.
k_{slip}	Wheel slip
g_{FB}	The ratio of follower to base gear
τ_B	Torque applied by the gear.
P_{MRPP}	The maximum regenerative power tracking
$s(t)$	The sliding function
$u(t)$	Control signal law
$\mathrm{sgn}(s(t))$	The signum function
$C(s)$	The output of the controller
A_k, B_k, C_k	The state, control, and output matrices
$\dot{Y}$	The global position for the vehicle
j	The cost function for the optimizer of MPC
Ts	Sampling time
Tr	The rise time
T_{ripple}	Torque ripple

Chapter One: Introduction

1.1 Overview

Increasing oil prices and rising rates of carbon monoxide (CO) and carbon dioxide (CO_2) emissions suddenly led to dangerous levels that harm the ecosystem, global warming, health issues, etc. Researchers, scientists, and policymakers were compelled to shift their attention to green technology, which can reduce and eliminate adverse environmental effects [1]. Thus, the 21st century will be remembered as the Century of Technology Evolution, with the automotive industry serving as the primary focus. Autonomous hybrid electric vehicles (AHEVs) are the convergence of two groundbreaking trends in the automotive industry: autonomous driving and hybrid electric propulsion. These vehicles combine the benefits of both technologies, offering the potential for enhanced safety; autonomous systems can react faster and more precisely than human drivers, potentially reducing accidents significantly. Improved fuel efficiency: It combines an internal combustion engine (ICE) or fuel cell (FC) with an electric motor (EM) powered by a battery to provide the best of both worlds for transportation. Compared to ICE, FC, and electric vehicles (EVs), these benefits include long-range, high fuel efficiency, dependability, and low emissions [2].

HEVs can be divided into three primary categories based on recent developments: internal combustion engine hybrid electric vehicles (ICHEVs), fuel cell hybrid electric vehicles (FCHEVs), and all-electric vehicles (EVs). Table 1.1 compares the various attributes of each drivetrain.

Table 1.1: Technical Features of EVs, HEVs, and FCHEVs [3].

Characteristics	EVs	HEVs	FCHEV
Propulsion System	Electric motor based.	Electric motor & ICE.	Electric motor based.
Energy Storage	Battery, Super Ultra-capacitor, Flywheel	Fuel tank Battery, Ultra-capacitor, Flywheel	Fuel cell, Battery, Super-capacitor.
Energy Source Infrastructure	Electric charging facility.	Electric power, Refueling station.	Hydrogen cylinder, Hydrogen refiner, and refuelling station.
Advantages	Zero emission Quite Smooth operation Energy efficient Independency from petroleum product Commercialized.	Low emission Higher fuel economy Long driving range Reliable Commercialized Durability.	Ultra-low emission, competent driving range, highly efficient Independence from petroleum products, reliable durability, and high cost.
Drawbacks	the limited range for driving, Weak dynamic reactions, and the long time needed to recharge.	Complex system Costly Bulky Increased component.	Slow dynamic response Not commercialized Sophisticated electronic controller.
Major Issues	Size and weight of battery pack Infrastructure for the charging station.	Size and weight of battery pack & ICE Integration of components.	Cost of fuel cell Infrastructure for hydrogen conditioning, storage, and refilling system.

The principle of working for an autonomous vehicle (AV) is to use powerful processors to run the software and sophisticated algorithms, actuators, sensors, and machine learning systems to sense its surroundings. That gives the process controller an input signal to make the appropriate decision. As shown in Table. 1.2 there are numerous levels of autonomous driving [4].

Table 1.2: Levels of Driving Automation [4].

Basic Level	1	2	3	4	5
No automation Manual control. The human performs all driving tasks (steering, acceleration, braking, etc.).	Driver assistance The vehicle features a single automated system (e.g., it monitors speed through cruise control).	Partial automation The vehicle can perform steering and acceleration. Humans can still monitor all tasks and take control at any time.	Conditional automation Environmental detection capabilities. The vehicle can perform most driving tasks, but human override is still required.	High automation The vehicle performs all driving under specific circumstances. Geofencing is required. A human override is still an option.	Full automation The vehicle performs all driving tasks under all conditions. Zero human attention is required.
The human monitors the driving environment.			The automated system monitors the driving environment.		

1.2 Research Background

The following are summaries of the hybrid electric vehicle technologies:

1) Propulsion System: Traction motor(s) make up the propulsion system. Electric motors in HEVs come in four primary types:

Brushless DC motors (BLDC), Induction motors(I.M), Permanent magnet synchronous motors (PMSM), and DC motors. While each of these motor types has unique qualities, an HEV must meet three critical criteria: high torque/power density, high efficiency, and continuous power and torque across a wide speed range. Moreover, compactness, cost, reliability, and robustness are the other criteria for electric motor selection. Besides the

electric motor specifications, development for the ICE is also possible, for example, by reducing the engine's size and limiting its speed range to improve emissions and fuel economy [5].

2) Power Converters: General power electronic circuits are rectifiers, DC/DC converters, inverters, etc. One of the main components of the HEV is the electrical power transmission characteristic of the entire system. These characteristics include determining the current type (AC or DC), temperature concerns, magnetic influences, frequency effects, voltage value, cable size, safety measures, and overall transmission efficiency. All parameters must be considered during the design stage due to the high electrical power transmission. It includes safeguarding system components like batteries, supercapacitors (SC), and photovoltaic (PV) panels from unfavourable situations and fluctuations during the bidirectional energy conduction from EM/ICE or EM/FC to batteries and SC [6].

3) Energy Management System (EMS): This is the "head" of the entire system; in addition to driving performance, comfort, and safety, it manages the hybrid system to ensure optimum fuel efficiency and minimum emissions. The hardware device operates the controller techniques and applies the algorithm [7].

4) Energy Storage System (ESS): The fuel tank and the electrical storage unit are the two main storage components of an HEV. The storage of electrical energy is essential to hybrid technologies. It is necessary for regenerative braking, electric-only propulsion, electric propulsion assistance, and charging during coasting. Energy is stored using SC and batteries. However, the capacitor's high specific power (W/kg) makes all the difference against the battery’s high specific energy (Wh/kg). Lead/acid, nickel/cadmium, nickel/metal hydride, zinc/bromine, lithium-ion, and lithium polymer are just

a few of the many types of batteries available. Energy storage capacity, precisely its specific energy value, provided peak power, cycle life, efficiency, self-discharge value, and cost, are all deterministic design factors [8].

1.3 Applications of the Research Thesis in Different Sectors

The following are summaries of the applications of the thesis in different sectors:

a) This thesis can benefit the automotive sector by allowing effective speed controllers for EVs and integrating those controllers into their manufacturing procedures. It could result in more efficient, environmentally friendly EVs with improved performance and range.
b) The thesis on accuracy speed controllers can help advance EV technology. It may lead to developing new, creative control algorithms, power electronics components, and motor designs that can improve electric vehicles' overall efficiency and performance.
c) The accuracy speed controller study also has applications in the renewable energy sector. Controlling the motors ' speed can help improve the efficiency of renewable energy systems, such as wind turbines and solar panels.
d) The thesis on accuracy speed controllers can also be applied to robotics. It can aid in developing the highest accuracy control algorithms for robotic systems—like industrial robots and drones—that utilize electric motors.
e) The thesis focuses on accuracy speed controllers, which can also be applied in education and research. It can teach students and researchers about control systems, power electronics, and motor design and serve as a basis for further research and development.

f) AHEV can transport passengers through airport terminals smoothly and effectively while cutting emissions.

g) These vehicles can be deployed for search and rescue operations in hazardous environments or for transporting medical supplies and personnel during emergencies.

h) Companies can optimize scheduling, fuel efficiency, and driver costs using autonomous hybrid electric vehicles for delivery fleets or service personnel.

1.4 Benefits of Autonomous Hybrid Electric Vehicles

Hybrid electric vehicle technology and autonomous driving promise various real-world uses and could completely transform transportation in several industries. Here are some key areas where these vehicles could shine [9]:

1) Public Transportation:

a) Self-driving buses and shuttles: Imagine a network of AHEV buses operating on defined routes, offering clean, convenient, and on-demand public transportation with reduced traffic congestion and emissions [10].

b) Accessible mobility: People with disabilities or limited mobility can benefit from personalized door-to-door services delivered by autonomous vehicles, increasing their independence and opening up new service options.

2) Logistics and Delivery:

a) Autonomous delivery vehicles: Contactless delivery of groceries, packages, and goods can be facilitated by AHEV, which can enhance efficiency and shorten delivery times [11].

b) On-demand logistics: Companies can use these vehicles to move goods around cities flexibly and effectively, improving inventory control and reducing emissions [12].

c) Supply chains that are automated: By incorporating AHEV into supply chains, real-time tracking is enhanced, logistics are streamlined, and transportation expenses are reduced [13].

3) Personal Transportation:

a) A fleet of AHEV taxis could offer on-demand, shared transportation, reducing car ownership and traffic congestion while promoting cleaner travel[14].

b) People can rent or buy driverless HEVs for their use, taking advantage of the ease of self-driving technology while using less petrol and emitting fewer emissions.

c) Accessible vehicles can offer safe and reliable transportation for older adults, children, and individuals with specific needs, increasing their independence and mobility.

4) Environmental:

a) Adaptive hybrid electric vehicles combine the increased range of gasoline engines with the reduced emissions of electric motors. That has the potential to significantly lower air pollution and greenhouse gas emissions, as shown in Fig 1.1.

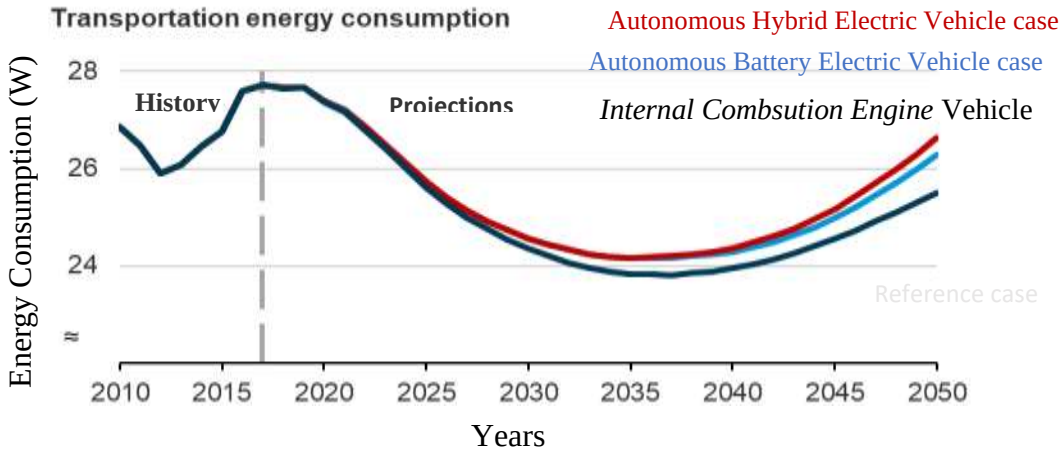

Fig.1.1: Three Predictions of Transportation Energy Usage from 2010 to 2050 [15].

b) Increased energy efficiency: AHEVs can switch between gasoline and electric power to improve their energy use depending on the driving situation. That may result in less reliance on fossil fuels and increased fuel economy[16].

1.5 Problem Statement

1. Current traction motor control algorithms in AHEVs have limited efficiency and performance. It is essential to design a high-performance motor speed controller.
2. Designing a hybrid energy storage system (HESS) with optimal energy management from various sources (FC, grid, PV panels) while considering battery life and efficiency is challenging.
3. Integrating the HEV with an autonomous controller makes the vehicle tracking path one of the challenges.

1.6 Aims of the Thesis

1. Enhance the performance of HEVs by designing an accurate motor speed controller.
2. Design high-performance HESS with accurate EMS to handle any scenario.
3. Investigate the feasibility of converting HEVs into autonomous vehicles by exploring the potential of adaptive model predictive control (AMPC) for path tracking and vehicle control.
4. Develop a comprehensive system integrating advanced motor control, optimized HESS management, and autonomous vehicle control functionalities.
5. Evaluate the performance and efficiency of the proposed system through simulations and potentially experimental testing.
6. Contribute to the advancement of HEV technology by providing insights into potential improvements and future research directions.

1.7 Thesis Objectives

Designing an AHEV involves several steps. Here is the overview of the process:

1. Designing a speed controller is to determine the specifications of the electric motor used. The motor's maximum speed, torque, and power rating must be understood.
2. To adjust the motor's speed must be determined next. Several options include Proportional–integral–derivative (PID) control, slide mode control, model predictive control, and backstepping control.
3. To develop a speed controller with extra capabilities, like the capacity to function as a sensorless controller. That has numerous advantages, such as lower complexity, cost, and maintenance. That procedure occurs when an observer replaces the physical sensor, such as a sliding mode observer (SMO). After designing the controller, it is essential to test the speed controller to ensure it functions as expected.
4. To investigate the suitable energy source and development, batteries, and FC must be ideal for AHEV. Then, SC was added to protect the batteries while regenerating and experiencing high load demand. Furthermore, depending on the charge controller, appropriate MPPT algorithms and PV panel parameters are necessary.

1.8 Research Thesis Methodology Procedures

To achieve the objectives mentioned above, the work steps to carry out the proposed project are as follows: the proposed autonomous hybrid electric vehicle's work steps in Fig.1.2:

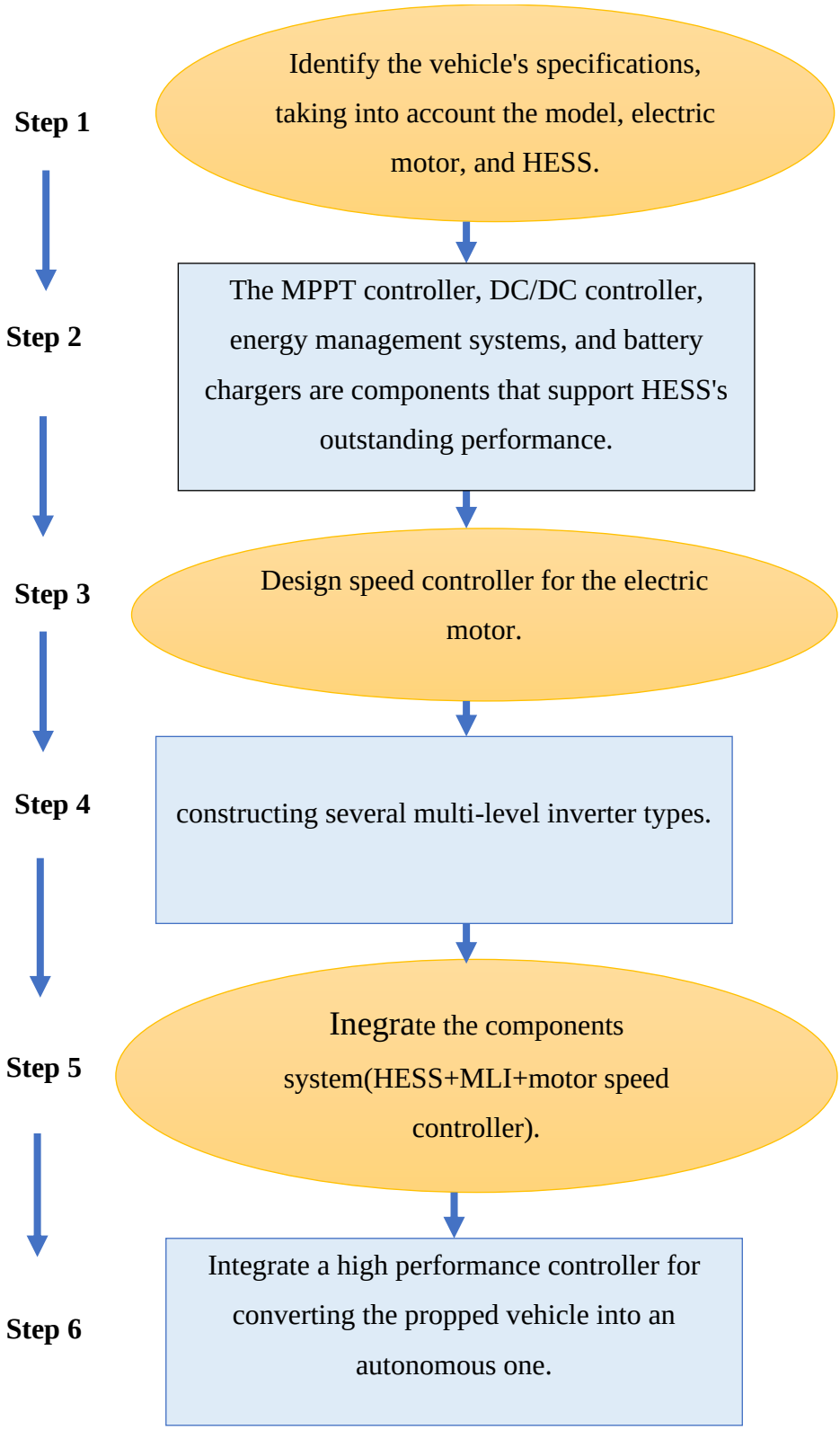

Fig.1.2: The Proposed Autonomous Hybrid Electric Vehicle's Work Steps.

1.9 Thesis Organization

This thesis's subsequent section is divided into four separate chapters. The thesis background, utilizing a mathematical model that includes all the parts and motors used in this investigation., is presented in Chapter Two. In Chapter Three, the thesis methodologies and algorithms are presented in full, together with all the drawings and the corresponding mathematical equations that aid in the development of the vehicle. The comparative results and the effect of each method on the AHEV, depending on the different scenarios, were shown using MATLAB Simulink, with a detailed explanation to discuss the results and indicate the system's best and most efficient method. All of this was presented in chapter four. The conclusion of this work and suggestions for further thesis are listed in chapter five.

Chapter Two:

Backgrounds and Literature Review

2.1 Introduction

The advantages of hybrid electric drivetrains and autonomous technology are combined and named by AHEVs. These vehicles use advanced sensors and algorithms to navigate and make judgments while driving autonomously, negating the need for human participation. The use of hybrid electric powertrains in autonomous vehicles offers several advantages. First, hybrid electric powertrains improve fuel efficiency and reduce emissions compared to traditional ICE. Additionally, combining electric motors with SC and batteries allows smoother and quieter operation, enhancing the overall driving experience. Through regenerative braking, kinetic energy is converted to electrical power and stored in the battery and SC.

Furthermore, integrating autonomous technology with hybrid electric powertrains enables more efficient energy management and optimization. As AHEVs are a promising technology with the potential to improve transportation, they will soon play a significant role in altering the transportation industry. While numerous challenges exist, ongoing research and development efforts pave the way for their successful implementation. Understanding the background, existing literature, and future thesis directions is essential to achieving AHEVs' full potential and developing a more environmentally friendly and effective transportation future.

2.2 Architecture of Hybrid Electric Vehicles

The essential elements of hybrid electric vehicles are:

1. FCHEV contains a Gasoline tank, Converter, Battery, SC, EM, FC, and control methods.
2. EVs include an EM, Battery, SC, DC-DC converters, charger, and Control methods.

This thesis will focus on developing the previous types of HEV by adding PV panels supported by the MPPT techniques, which can enhance the system's efficiency and reduce power consumption.

Three groups can be formed from these components:

a) DriveTrains physically combines the electric drive and the power supply (ICE, FC, charger).

b) Modest energy storage capacities, including battery and SC, are critical to the HESS.

c) Control systems include EM, FC, and EMS. Vehicle designs might vary depending on how these parts are integrated and in what sizes. Drivetrain designs primarily include series, parallel, and power split configurations based on component integration. The architecture of HEVs is divided into three groups: series HEVs [17], parallel HEVs [18], and the combination of parallel and series HEVs[19]. Plug HEVs have a similar architecture to HEVs, except for a substantial onboard battery that offers excellent efficiency and energy density. Making an appropriate charger is crucial, and several varieties are available, including off-board and on-board. A solar-driven HEV has a similar construction to a Plug HEV, except for an extra photovoltaic (PV) panel for battery and SC charging during sun irradiance. PV panels can provide as much power as possible using the MPPT algorithms [20].

2.3 Electric Motors

Many efficient motors and generators are required to reach the demanding standards for efficiency, power density, and drivetrain cost in HEVs. In recent years, traction systems for EVs have improved, particularly with the advancement of drive-control power converter topologies. Fig. 2.1 lists the different motors used in traction and their classification [21]. Table 2.1 summarises the literature on the motors used in EVs and HEVs for traction [22]. An EM type known as a traction motor provides propulsion for vehicles, including trains, EVs, and HEVs. The EM in HEVs supplements an ICE, FC, or HESS's power and efficiency with EM. Although industrial motors are typically optimized at rated conditions, EMs are usually utilized in applications that need to start and stop frequently, high acceleration and deceleration rates, High-torque, low-speed hill climbing, high-speed driving at low torque, and a wide operating speed range, such as HEVs. During the regenerative braking techniques, motors also operate as generators in type PMSM and BLDC motors, returning energy to the energy source [23].

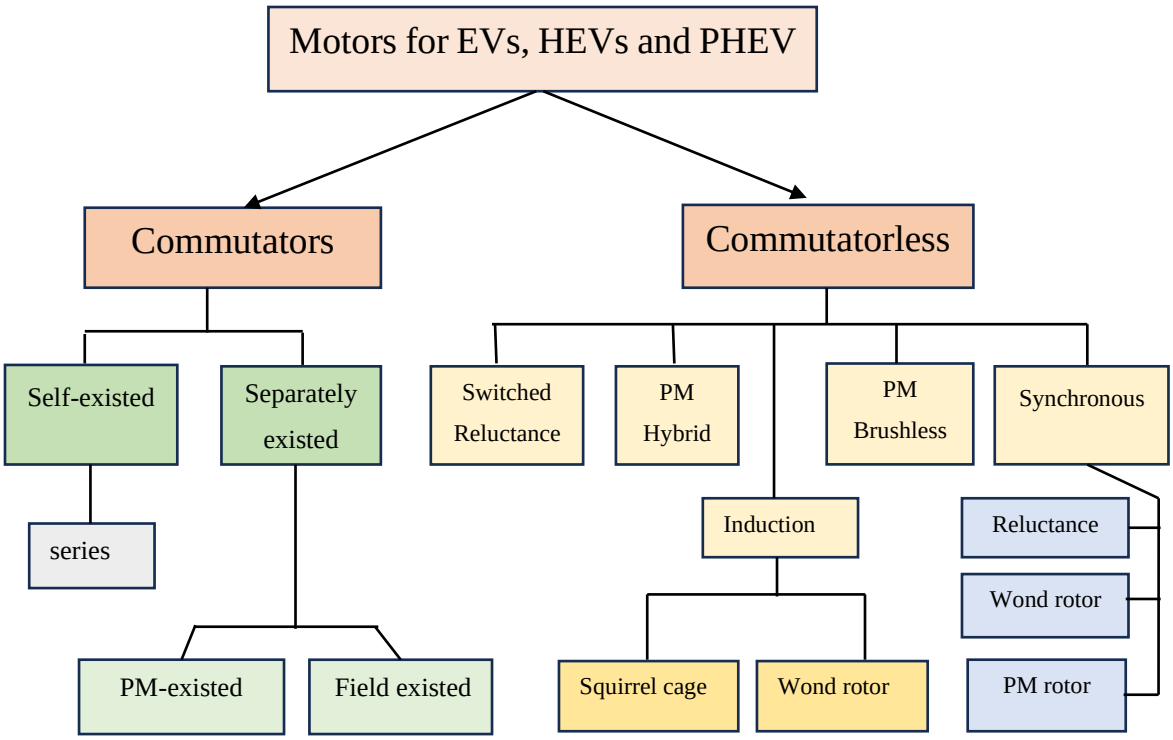

Fig.2.1: Categorization of EM for Applications in HEVs.

Table 2.1: Five Commonly Used EMs for EV/HEV Applications [24].

Category	Brushless DC	Series Motor	PMSM	Switched Reluctance	Induction Motor
Type	DC	DC	AC	DC	AC
Family	Synchronous excited PM	The commutator, separately excited	Separately excited	Synchronous unexcited	Squirrel cage
Power to rotor	PM	DC	PM	Induced	Induced
Power to stator	Pulsed DC	DC	AC	Pulsed dc	AC
Overall cost	High	Low	High	Medium	Medium
Weight	Low	Heavy	Medium	Medium	Medium
Commutation method	Internal electronic	Mechanical Commutation	External electronic	External electronic	External elections

Controller cost	Very high	Low	High	High	High
Maintenance Requirement	Negligible	Brushes wear	Negligible	Negligible	Negligible
Speed control method	Frequency-dependent	PWM or Field weakening	PWM	Frequency-dependent	Frequency-dependent
Starting torque	>175% of the rated	>175% of the rated	>200%of rated	Up to 200% of the rated	High
Speed range	Excellent	Limited by brushes, easy control	Controllable	Controllable	Controllable
Efficiency	High	Low	High	Less than PMDC	High
Application	HEV & EV	HEV & EV	HEV & EV	Normal vehicle	HEV & EV
%Efficiency with electronic	78	78	90	85	84
Examples	Peugeot (France)	Indian Railways	Nissan, Honda Japan	Holden/recommend Australia	Chevrolet (USA)

2.3.1 Permanent Magnet Synchronous Motor

PMSM consists, like any other rotating EM, of a stator and a rotor. The rotor is the rotating part, and the stator is the fixed part. The rotor of an EM is placed inside the stator; however, some constructions have an external rotor or outside stator EM. The magnetic field generated by permanent magnets (PM) interacts with the rotor's current-carrying conductors to produce torque. Due to its many advantages over other types of EM, PMSMs are becoming

more and more common for application in HEVs [25]. Fig.2.2 shows the construction of PMSM with stator and rotor.

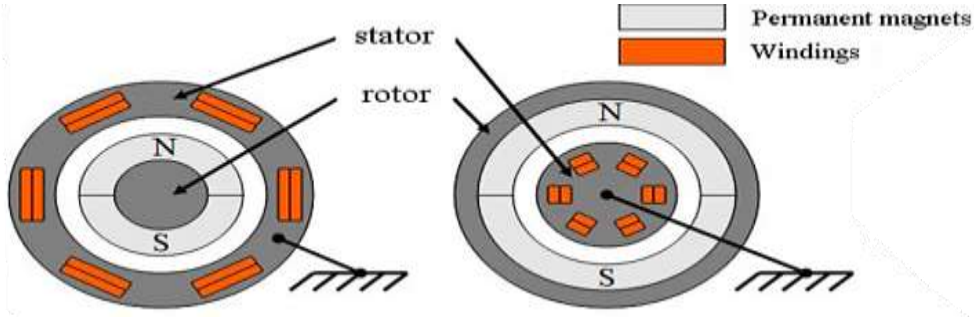

Fig.2.2:The PMSM Construction [26].

The rotor consists of PMs and a winding stator. Synchronous motors are divided based on the rotor design into:

a) Salient pole rotor of motors ($L_d \neq L_q$) The direct inductance and the quadrature inductance are not equal.

b) Non-salient pole rotor of electric moros ($L_d = L_q$) Both direct and quadrature inductances are equal. Fig.2.3 shows the rotor cross-section with various Ld/Lq Ratios.

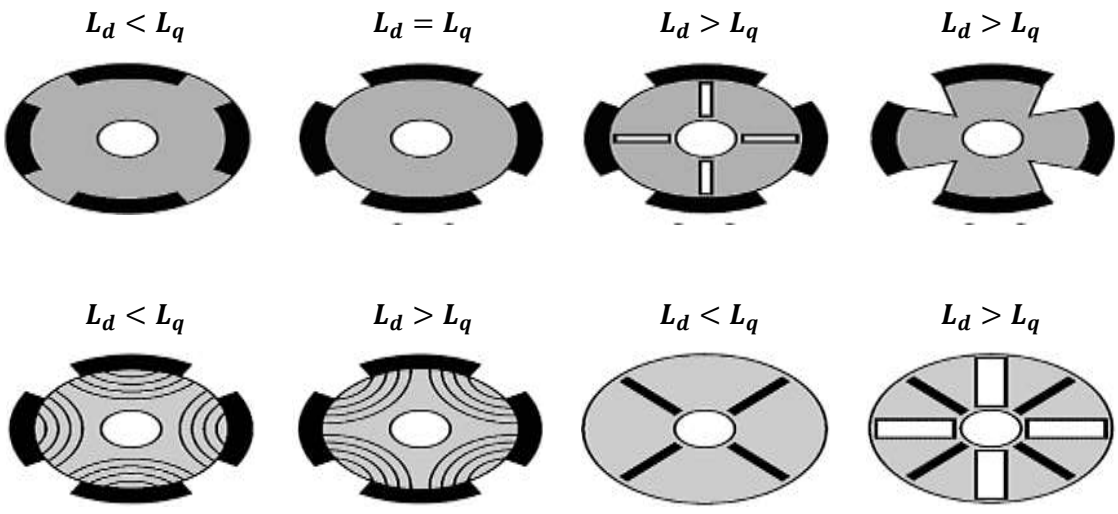

Fig.2.3: Cross Sections of the Rotors with Various Ld/Lq Ratios [27].

The PMSM can be separated into:

a) Surface Permanent Magnet Synchronous Motor (SPMSM).

b) Interior Permanent Magnet Synchronous Motor (IPMSM).

Fig.2.4 shows the construction of PMSM types.

(a) **(b)**

Fig.2.4: PMSM Types (a) SPMSM, (b) IPMSM [28].

The suggested vehicle does not require high speeds, so the non-salient pole SPMSM type will be used. The comparison between the two kinds of PMSM is apparent in Table 2.2.

Table 2.2 Comparison between Types of PMSM [24].

SPMSM	IPMSM
The inductance of the quadrature and direct axes is almost equal.	Quadrature axis inductance and indirect variation are almost equivalent.
Large air-gap	small air-gap
minimal saliency ratio	Large saliency ratio
They are used in low-speed range applications.	Used in high-speed range applications

The SPMSM, when used in AHEVs, provides several significant advantages over I.M. Its excellent effectiveness and precise controllability are two of its main benefits since they swiftly enhance the vehicle's total performance and energy economy. These motors use PM placed on the rotor surface, which combines with the stator's magnetic field to produce motion. Because of its compact and lightweight construction, this motor is ideal for the weight and limitations on space present in modern driverless vehicles [29].

PMs placed on the rotor surface, which interact with the stator's magnetic field, are responsible for this efficiency [30]. Mechanical dependability is also increased because the rotor is robust, and the magnets are not separated by centrifugal force. SPMSM motors can reduce energy usage by 30% while using the same amount of power [31].

PMSMs prove their efficiency with IM in HEV applications. Some of its advantages are less heating, increased power density, and increased efficiency. It has been noted that armature reaction-induced demagnetization is a significant disadvantage of PMSMs [32]. These motors have exceptional efficiency and power density. The back EMF of the BLDC is trapezoidal, whereas the back EMF of the PMSM is sinusoidal. That is the difference between the two types of EMF. In general, the PMSM is recommended for EV/HEV traction.

Below is the PMSM motor's mathematical model [33][34]:

An equation system like this provides the dynamics of the IPMSM in the (d - q) reference frame :

Electric Equation is given in (2.1):

$$\frac{\mathrm{di_d}}{\mathrm{dt}} = -\frac{\mathrm{R_a}}{\mathrm{L_a}}\mathrm{i_d} + p\,\mathrm{i_q}\,\omega_m - \frac{1}{\mathrm{L_a}}\,\mathrm{u_d} \tag{2.1}$$

$$\frac{di_q}{dt} = -\frac{R_a}{L_a} i_d + p\frac{\psi_{PM}}{L_a}\,\omega_m - p\,\omega_m\, i_d - \frac{1}{L_a} u_q \tag{2.2}$$

The formula for electromagnetic torque in (2.3):

$$T_m = \left(\frac{p}{2}\right)\left(\frac{3}{2}\right)(\lambda_{d_{iq}} - \lambda_{q_{id}}) \tag{2.3}$$

where ; $\lambda_d = L_d i_d + \lambda_{pm}$ (2.4)

$$\lambda_q = L_q i_q \tag{2.5}$$

Electric speed equation and mechanical speed relationship in (2.6):

$$\omega_e = \frac{P}{2}\,\omega_m \tag{2.6}$$

The mechanical equation is as follows in (2.7):

$$\frac{d\,\omega_m}{dt} = \; -1.5\,\frac{p}{J}\,\psi_{PM}\,i_q \; - \frac{f}{J}\,\omega_m - \frac{1}{J}T_L \tag{2.7}$$

where is the armature resistor and inductance are R_a and L_a, respectively. The drive train is a single equivalent mass model based on Newton's second law. Hence, the one-mass or lumped-mass model is utilized for tiny signal analysis of PMSM.

i_d, i_q are the stator currents for the d-q representation.

p is the number of poles.

ψ_{PM} is the permanent flux linkage.

u_d, u_q are the d-axes and q-axes stator voltage.

J and f_v are viscous friction and moment of inertia of the motor.

ω_m and T_L represents the motor speed and the load's torque, respectively.

2.3.2 Brushless DC Motor

BLDC motors are PMSMs with an electronic commutation scheme and a trapezoidal back EMF [35]. An EM that operates synchronously and uses DC power is a BLDC motor. BLDC motors have become known for their reliability and high efficiency, making them well-liked for various uses, such as robotics, power tools, HEV, and drones. The windings of a BLDC motor are placed on the stator, while the PMs are fixed to the rotor. The rotor's PMs interact with this spinning magnetic field, creating torque that causes the rotor to turn [36] [37]. The differential voltage equations can be obtained from in (2.8) using the analogous circuit [38]. Though there are several classification schemes for BLDC motors, these two are the most widely used ones:

According to rotor design, it has been classified into two types:

1) Inrunner BLDC Motors: These motors have PMs within the stator windings on the rotor. Compared to outrunners, they are usually smaller and have faster top speeds but lower torque [39].
2) Outrunner BLDC Motors: These motors have PMs outside the stator windings on the rotor. They are usually larger than runners but provide more torque and slower speeds [40].

By winding configuration, it has been classified into two types.

1) Single-phase BLDC Motors: After comparing three-phase motors, it was found that these motors are less frequent and only feature one set of windings. They have less torque and economy and are easier to control [41].
2) Three-phase BLDC Motors: These motors are the most popular variety and have three sets of windings. They offer higher efficiency and torque compared to single-phase motors [42].

The ideal BLDC motor type for a given application will depend on its specific requirements, including size, efficiency, speed, torque, and other factors.

Fig.2.5 depicts the BLDC motor's equivalent circuit.

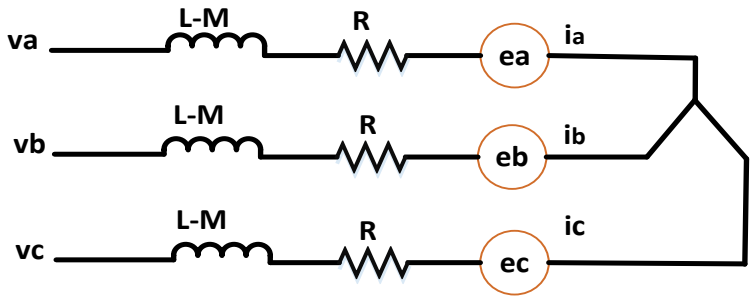

Fig.2.5: Equivalent Circuit of the BLDC Motor [43].

$$\begin{bmatrix} v_a \\ v_b \\ v_c \end{bmatrix} = \begin{bmatrix} R_a & 0 & 0 \\ 0 & R_b & 0 \\ 0 & 0 & R_c \end{bmatrix} \begin{bmatrix} i_a \\ i_b \\ i_c \end{bmatrix} + \frac{d}{dt} \begin{bmatrix} L_a & L_{ab} & L_{ca} \\ L_{ba} & L_b & L_{bc} \\ L_{ca} & L_{cb} & L_c \end{bmatrix} \begin{bmatrix} i_a \\ i_b \\ i_c \end{bmatrix} + \begin{bmatrix} e_a \\ e_b \\ e_c \end{bmatrix} \quad (2.8)$$

BLDC motors often have salient-pole rotors placed on their surface. The self and mutual inductances are considered for simplicity. Over time, the coil's inductance stays constant.

Three-phase stator winding symmetry means that the mutual and self-inductances will be equal, as given in (2.9) [44] [45]:

$$\begin{cases} i_a + i_b + i_c = 0;\ L_a = L_b = L_c = L_S \\ L_{ab} = L_{ac} = L_{bc} = L_{ba} = M \\ R_a = R_b = R_c = R \end{cases} \quad (2.9)$$

The stator winding inductance is La, the mutual inductance is M., and Ra is the stator winding resistance.

The trapezoidal back EMF equations are as follows in (2.10):

$$e_a = K_e \omega_r F(\theta_e); e_b = K_e \omega_r F(\theta_e - \frac{2\pi}{3}); e_c = K_e \omega_r F(\theta_e + \frac{2\pi}{3}) \quad (2.10)$$

where, K_e Is the voltage factor, w_r It is the motor's electrical angular speed. Equation (2.11) can be used to express the developed torque.

$$T_e = K_w \omega_r F(\theta_e) i_a + K_w \omega_r F(\theta_e - \frac{2\pi}{3}) i_b + K_w \omega_r F(\theta_e + \frac{2\pi}{3}) i_c \quad (2.11)$$

K_w It stands for the torque factor. Here is an example of the motor's dynamic expression in (2.12):

$$T_{e-BLDC} = j \frac{d\omega_r}{dt} + B\omega_r + T_l \quad (2.12)$$

where the viscous friction coefficient is B, the load torque is T_l, and the inertia of the rotor is j. Equations (2.8-2.12) describe the mathematical model of a BLDC motor.

2.4 Power Sources for Electric Vehicles

2.4.1 Photovoltaic Panel

Integrating photovoltaic (PV) panels into AHEVs is an exciting concept with the potential to increase their range, decrease your dependency on fossil fuels, and assist in developing a more sustainable future. However, several challenges exist before widespread adoption can occur [46]. Feasibility and Benefits:

a) Solar panels can generate electricity to supplement the battery, potentially extending the driving range of the AHEVs, especially during extended periods of sunshine.

b) AHEVs can decrease fossil fuel demand and greenhouse gas emissions using solar panels.

c) In ideal conditions, solar panels could keep the AHEV's battery topped up, reducing the need for charging from the grid.

Table 2.3 provides the details of the PV panel used in this study. Below: The PV field comprises parallel and series modules to achieve the required power. Every module is made up of individual cells. One of this thesis contributions is utilizing a two-diode model to represent a PV cell, as shown in Fig.2.6 [47][48]. PV system performance can be predicted more accurately using this model because it is more accurate at low irradiation levels.

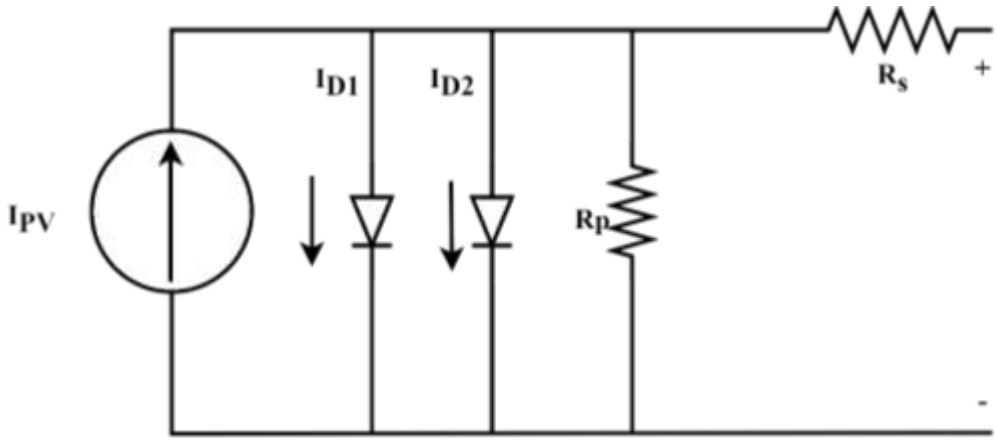

Fig.2.6: Equivalent Circuit of PV Panel [48].

Table 2.3: Specifications of PV Panels.

Parameters	Value
Module	Waaree Energies WU-120
Parallel strings	4
Series-connected modules per string.	2
Maximum Power (W)	120.7 W
Cells per module (Ncell)	72
Open circuit voltage Voc(V)	21 V
Short-circuit current Isc (A)	8 A
MPP voltage (V)	17 V
IMPP (A)	7.1 A

The model was created using the following (2.13) [49]:

$$I_{ph} = [I_{sc} + K_i(T_c - T_{ref})]\frac{G}{G_{ref}} \quad (2.13)$$

The current at the junction is expressed as follows in (2.14):

$$I_d = I_{PV} - I_{01}[exp\left(\frac{V+IR_s}{a1V_{T1}}\right) - 1] - I_{02}[exp\left(\frac{V+IR_s}{a2V_{T2}}\right) - 1] - (\frac{V+IR_s}{R_p}) \quad (2.14)$$

The following (2.15) gives the current flowing through the resistance Rsh:

$$I_{sh} = \frac{(V+R_sI)}{R_{sh}} \quad (2.15)$$

whence

$$I = \left[I_{sc} + K_I(T_c - T_{ref})\right]\frac{G}{G_{ref}} - I\left[\exp\left(\frac{q(V+R_sI)}{N.K.T}\right) - 1\right] - \frac{(V+R_sI)}{R_{sh}} \quad (2.16)$$

1) Impact of solar irradiance on photovoltaic panels: The output current will rise in response to increased irradiance, increasing the output power (P-PV).

The irradiance is measured in units of (W/m^2). Equation (2.17). Provides the mathematical relationship between power, current, and irradiance

$$\frac{G1}{G2} = \frac{I_2}{I_1} = \frac{P_{Pv-2}}{P_{Pv-1}} \quad (2.17)$$

2) Influence of temperature on PV-Panel: Most solar panels' output is assessed using standard test conditions (STC). It is stated at 25 degrees Celsius, or 77 degrees Fahrenheit. Therefore, the PV panel's output voltage and power drop as the temperature rises. Here are a few techniques used in hot and cold climates to manage PV panel temperature changes [50].

$$V_T = \frac{kT}{q} \times nI \times N_{cell} \quad (2.18)$$

where: I_d: current across the diode (A), I_{01} and I_{02} are the diodes 1 and 2's reverse saturation currents, VT1 and VT2 are the corresponding diodes' thermal voltages, and a1 and a2 stand for the ideal constants of the diode. Several investigators believed that a_1 = 1 and a_2= 2.

I_{sc}: current of the short circuit (A), I_o: current for diode saturation (A). , I_1, I_2 : PV panel's current Is the diode's reverse saturation current (A),V_d: diode voltage (V), Rs: series resistance (Ω) of the diode, Rsh: Shunt resistance of the diode (Ω), Vpv: voltage across the diode is (V),P_{Pv-1}, P_{pv-2} : the power of the PV panel (WE), T: the junction's Kelvin cell temperature (K), nI: Ideality factor of the diode, a value near 1.0, Ki: the short-circuit current's temperature coefficient (%/K), q : (1.602×10-19 C) of charge per electron, N: diode's ideality factor,N_{cell}: number of cells in a module connected in series, G1, G2: the irradiance of the PV panel.

2.4.2 Fuel Cell

More research is being done on FC as a possible replacement for power sources for AHEVs.Their capacity to produce electricity via the electrochemical reaction of oxygen and hydrogen makes them perfect for supplying a steady and dependable power source[51]. Furthermore, FC has the potential to significantly extend the range of AHEVs, as they can operate at higher efficiencies than traditional combustion engines [52].

This increased efficiency means that FC-powered AHEVs can travel longer distances on a single charge, reducing the need for frequent stops to recharge or refuel [53]. The benefits of fuel cells for AHEVs include the following:

a) Zero emissions: FCs are a clean and eco-friendly solution because they only release water vapour. It is critical for AHEVs, which are expected to help significantly reduce transportation-related emissions.
b) High efficiency: Compared to ICE, fuel cells are highly efficient at converting hydrogen into electricity with little energy loss. For AHEVs, this means a more excellent range and less fuel usage.
c) Quiet operation: Because FC runs quietly, passengers have a calmer and more enjoyable ride, and urban noise pollution is decreased.
d) Fast refueling: Like gasoline refueling, hydrogen refueling takes only a few minutes, making it a practical choice for lengthy trips.

Toyota, Hyundai, and Honda are among the leading automakers researching AHEVs. Though they are still in the early phases of development, these vehicles portend a bright future for environmentally friendly and sustainable transportation.

The choice of fuel cell technology for an AHEV will depend on factors, including the vehicle's range, performance requirements, and cost [54].

A battery-electric AHEV's range can be increased using an FC. That would extend the vehicle's range before requiring a recharge. That would be ideal for long-haul autonomous trucks or other vehicles requiring long-range and fast refueling [55].

The detailed model matches a particular FC stack according to changes in variables such as pressures, temperatures, fuel and air compositions, and flow rates. The Signal variation pane in the block dialogue box allows the user to select which parameters to modify. These changes have an impact on the photocurrent slope(A_{FC}) and exchange current. (i_0), And also the open circuit voltage (E_{oc}). Fig.2.7 shows the equivalent circuit of the FC source [56] [57].

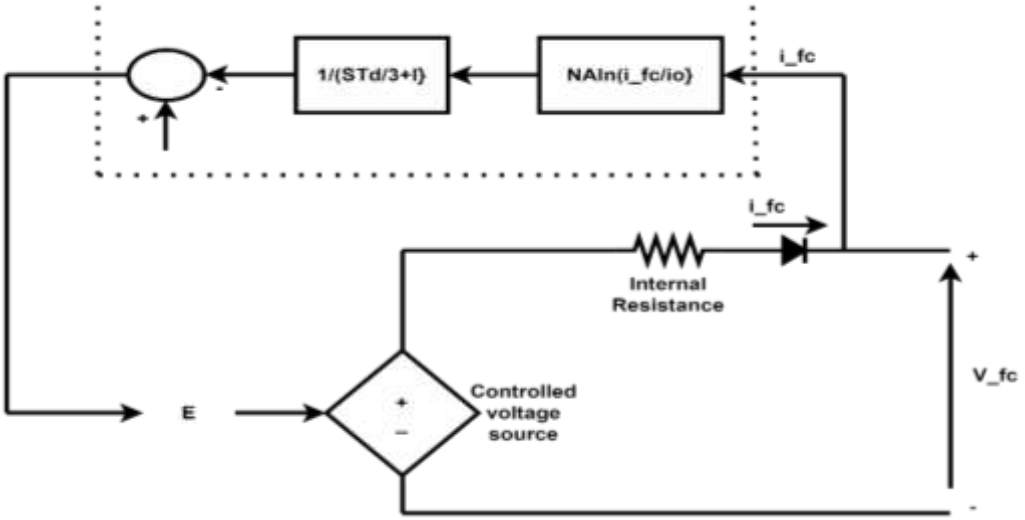

Fig.2.7:Equivalent Circuit of Fuel Cell.

$$E_{oc} = K_c E_n \tag{2.19}$$

$$E_{oc} = \frac{zFK(P_{H2}+P_{o2})\Delta v}{Rh} e^{\frac{-\Delta G}{R_{FC}T}} \tag{2.20}$$

$$A_{FC} = \frac{RT}{z\alpha F} \tag{2.21}$$

where: R_{FC}: 8.3145 J/(mol K),

F: 96485 A s/mol,

z : Quantity of electrons in motion.

E_n : The temperatures and partial pressures of both products and reactants inside the stack determine the thermal voltage of the cells, also known as the Nernst voltage (V),

α: Charge transfer coefficient, which is influenced by the type of electrodes and catalysts used,

P_{H2} : Hydrogen partial pressure inside the stack (Pa),

P_{o2} : Inside the stack, the partial oxygen pressure (Pa).

k: Boltzmann's formula = 1.38 × 10–23 J/K,

h: The Planck constant 6.626 × 10–34 J s,

Δv: Volumetric activation barrier factor assuming Δv = 1, the activation barrier (ΔG) size is calculated, ΔG: The activation barrier's dimensions, measured in J/mol, depend upon the catalyst type and electrode used, T: Operating temperature (K), Kc: voltage steady under the best possible conditions.

The following (2.22) is how block determines the rates of conversion (utilization) of oxygen (U_{fo2}) and hydrogen (U_{fH2}):

$$\begin{cases} U_{fH2} = \frac{n_{H2}^{r}}{n_{H2}^{in}} = \frac{60000RTNi_{fc}}{zFP_{fuel}V_{Ipm(fuel)}x^{\%}} \\ U_{fo2} = \frac{n_{o2}^{r}}{n_{o2}^{in}} = \frac{60000RTNi_{fc}}{2zFP_{air}V_{Ipm(air)}y^{\%}} \end{cases} \quad (2.22)$$

hence:

P_{fuel} : fuel supply pressure in absolute terms (atm), P_{air} : air supply pressure in its whole (atm), Vlpm(fuel): Fuel flow rate (l/min).

Vlpm(air): Airflow rate (l/min), x: The percentage of fuel that is hydrogen (%), y: oxygen content (%) of the oxidizing agent, N: number of cells.

2.4.3 Grid Charger

An AHEV grid charger is a device that links the vehicle to the power grid so that its battery and SC can be charged automatically [58].

There are two primary kinds of grid chargers for AHEVs [59]:

- AC chargers: The vehicle's battery uses alternating current (AC). However, AC chargers are more available and less expensive than DC chargers and generally operate more slowly.
- DC chargers: These chargers use direct current (DC) to charge the battery. DC chargers cost more and are harder to find than AC chargers, but are substantially faster.

As its name implies, AC electricity is needed for charging. AHEVs can be recharged while parked, and because of vehicle-to-grid technology, a vehicle's battery pack can be recharged anywhere. A detailed description of the grid charger used in this investigation may be seen in Fig.2.8[60]. The grid charger characteristics are displayed in Table 2.4.

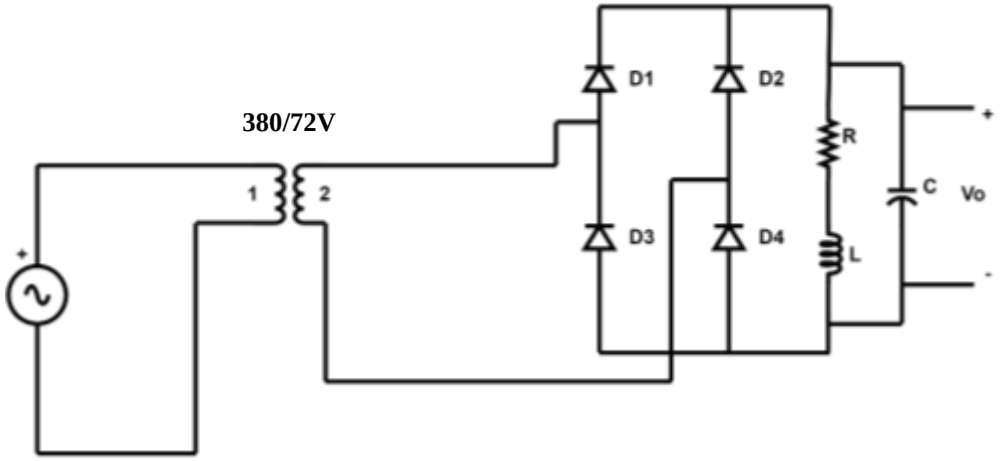

Fig.2.8:Grid Charger Model.

Table 2.4 Grid Charger Specifications.

Parameter	Value
Peak amplitude	312 V
Frequency	50 Hz
Phase	0
Transformer Primary	380 V
Transformer Secondary	72 V
Diode Parameters	
Forward voltage	0.8 V
Resistance Ron	0.01 Ω

2.5 Energy Storage System

2.5.1 Rechargeable Battery Model

Every AHEV has batteries at its core. They are crucial in powering the EM, providing energy for the vehicle's autonomous systems, and enabling regenerative braking [61]. The type of battery used in an AHEV will significantly impact its range, performance, and overall efficiency. Battery provision is required in the proposed HESS. The battery can deliver and store or absorb excess energy in grid-tied mode. The battery and SC supply peak and off-peak power in a standalone application such as AHEV [62].

The comparison of battery types used in AHEVs is given in Table 2.5. A modern trend of AHEVs started with batteries that are based on lithium. The lithium-based battery is one of the most promising technologies due to its high energy density, high power density, lightweight design, low cost, non-toxicity, and ability to charge quickly [63]. This study will employ the $LiFePO_4$ type. The charger device can recharge the battery packs externally from the power grid and PV panel [64]. The equivalent circuit for the battery

is shown in Fig.2.9, which shows several comparisons of various ESS kinds using four more approaches [65] [66].

Table 2.5 Comparing Different Types of EV Batteries [65].

Battery type	Nominal voltage (V)	Energy density (Wh/kg)	Specific energy (W/kg)	Life cycle	Operation temperature (C)	Cost($/ kWh)
Lead acid	2	35	180	1000	-15 to +50	60
ZEBRA	2.6	90-120	155	1200	+245 to +350	230-245
Lithium-ion (Li-ion)	3.6	118-250	200-430	2000	-20 to +60	150
Lithium – ion plumer(LiPo)	3.7	130-225	260-450	1200	-20 to +60	150
Lithium-ion phosphate(LiFeP O_4)	3.2	120	2000-4500	2000	-45 to +70	250
Zinc -air	1.65	460	80-140	200	-10 to +55	90-120

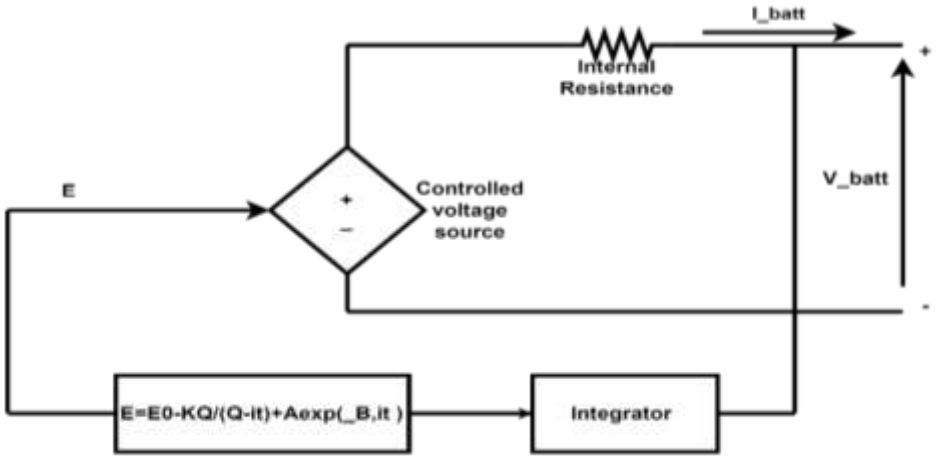

Fig.2.9:Battery's Equivalent Circuit [67].

The model uses the equations below for the lithium-ion battery type[68] [69]. Equation (2.23) describes the battery voltage (V_{bat}).

$$V_{bat} = E - R_{bat} I_{bat} \tag{2.23}$$

Equation(2.24) provides the controlled voltage source.

$$E_{bat} = E_o - K\frac{Q}{Q_D - \int i.dt} + A.\exp(-B\int i.dt) \quad (2.24)$$

- Discharge Model (i* > 0)

$$V_{batt} = E_0 - Ri - k\frac{Q}{Q-it}i^* - k(\frac{Q}{Q-it})it + A\exp(-B.it) \quad (2.25)$$

- Charge Model (i* < 0)

$$V_{batt} = E_0 - Ri - k\frac{Q}{it+0.1Q}i^* - k(\frac{Q}{Q-it})i_t + A\,exp(-B.it) \quad (2.26)$$

where is:

E_0: steady voltage expressed in volts (V), E: voltage when there is no load (V

K: Polarization resistance is measured in Ohms, or polarization constant is measured in V/Ah, I*: dynamics of low-frequency current, in A, i: battery current, expressed in A,i_t : extracted amount, expressed in Ah.

Q: The maximum capacity of the battery is expressed in Ah, A: voltage exponential, given in (V), B: Ah−1, or exponential capacity.

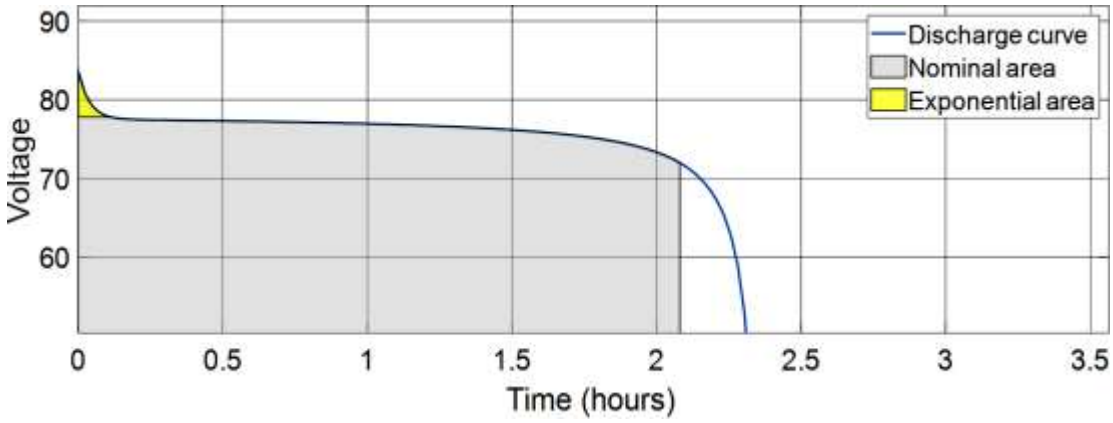

Fig.2.10: Typical Li-ion Battery Discharge Characteristic.

A battery's state of charge (SoC) expresses its charge as a percentage of its overall charge. The SoC's numerical complement is the depth of discharge (DoD), such that DoD = 100% - SoC.

For example, if the SoC is [70]:

- 100% — The DoD is zero %, and the battery is fully charged.
- 75%— The DoD is 25 %, and the battery is 3/4 charged.
- 50% — The DoD is 50%, and the battery has a 50% charge.
- 0% — The battery is 0, and the DoD is 100%.

From the prototype, the battery current value was chosen to be 24 Ah, and the battery voltage was equal to 72V :

the battery power = 72*24= 1728Wh

the rated power of the motor = 1500 W

The number of hours supplied by the battery is:1728/1500 =1.2 h

The specifications of the Lithium-ion phosphate (LiFePO_4) battery in this study is given in Table.2.6:

Table 2.6 Specifications of the Battery.

Nominal voltage(V)	72 V
Rated capacity (Ah)	24 Ah
SoC %	50
Battery response time(S)	0.1 Sec

2.5.2 Supercapacitor Model

Batteries are not the only energy source used in modern energy storage systems. The battery's power density must be high enough to achieve the peak power needed. However, they cost more than their equivalents and have a lower power density. There are still batteries available with higher power densities. While they are accessible, batteries with a higher power density are significantly more expensive than those with a lower power density [71]. SC is used with the battery in HESS to increase the battery's lifecycle. Batteries are essential to operating AHEVs, but SC has become a viable supplementary technology with unique benefits for some uses.

Strengths of Supercapacitors for AHEVs:

1) SC provides and absorbs small power increases, making them ideal for regenerative braking, quickly capturing and storing braking energy for later use, acceleration bursts assisting the battery in providing peak power for rapid acceleration, and sudden power demands, Supporting the powertrain during unexpected events like uphill climbs or quick maneuvers [72].
2) They can charge and discharge much faster than batteries, enabling efficient energy recovery and utilization.
3) Their lifespan is significantly longer than batteries, reducing replacement needs and overall cost.
4) They function better in extreme temperatures compared to some batteries [73].

Potential Applications in AHEVs:

1) Hybrid Energy Storage System (HESS): Combining SCs with batteries can create a synergistic system where batteries provide long-term energy and SCs handle high-power demands. It can optimize overall efficiency and lifespan.
2) Urban Vehicles with Frequent Stops: SCs can be particularly advantageous for AHEVs operating in urban environments with frequent stops and starts, where regenerative braking and power bursts are common.
3) Autonomous Features: SCs can contribute to safe and efficient operation for autonomous-driving features requiring quick responses and power adjustments [74]. The SC is a support and protection device for the battery: the SC can handle sudden overloads in the system because of its characteristics. Fig.2.11 below shows the SC electrical model. The model consists of an analogous series of resistance. R_{SC} connected in series with a

capacitance C_{SC}. Equation (8) provides SC voltage. V_{UC} as a function of SC's current I_{UC}.

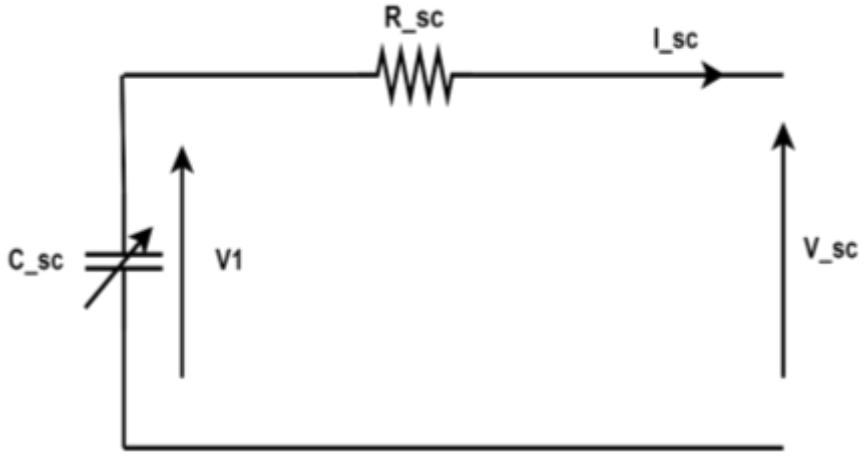

Fig.2.11: Supercapacitor Equivalent Circuit [75].

The output terminals of every bidirectional DC-DC converter are connected in parallel, as seen in Fig.2.12.

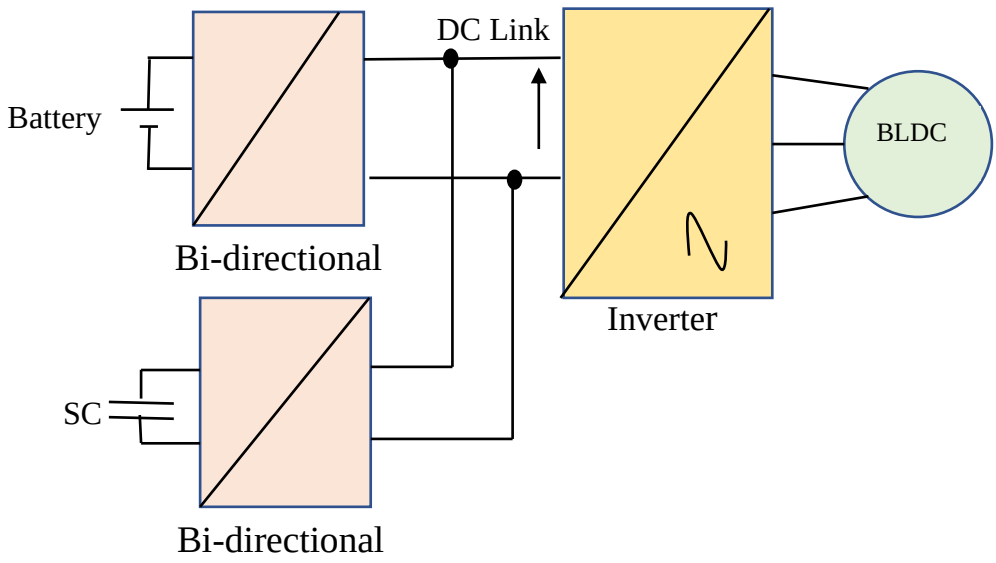

Fig.2.12: Conventional SC_Battery HESS Configuration.

A hybrid design overcomes the limitations of considerable DC bus voltage variations by using multiple DC-DC converters. Several bidirectional DC-DC converters can wholly regulate each SC and battery. The DC-bus potential is constant when several bidirectional DC-DC converters are linked in parallel [76].

The degree of accuracy varies among models based on the number of components and the arrangement of the electric circuit; however, model accuracy increases with circuit complexity.

The mathematical model of SC is given below in (2.27):

$$V_{SC} = V_I - R_{SC} * I_{SC} = \frac{Q_{SC}}{C_{SC}} - R_{SC} * I_{SC} \quad (2.27)$$

Equation (2.28) provides SC power.

$$P_{SC} = \frac{Q_{SC}}{C_{SC}} * I_{SC} - R_{SC} * I_{SC^2} \quad (2.28)$$

employing a storage component called an SC, which comprises many cells coupled in parallel and series, respectively, by Ns and Np. Equations (2.29) and (2.30) define the SC stack's capacity and resistance.

$$C_{SC} = C_{elem} \frac{N_p}{N_s} \quad (2.29)$$

$$R_{SC} = R_{elem} \frac{N_s}{N_p} \quad (2.30)$$

Given the element voltage and element current, the stack's voltage and current are provided by (2.31) and (2.32).

$$V_{SC} = N_s . V_{elem} \quad (2.31)$$

$$I_{SC} = N_p . I_{elem} \quad (2.32)$$

where:

V_{SC}: supercapacitor voltage (V) , R_{SC}: SC resistance,I_{SC}: SC current(A) ,Q_{SC}: the amount of energy that is stored within a cell, C_{SC}: SC stack capacitor, P_{SC}: SC power (W).

Table 2.7 Specifications of the Supercapacitor.

Parameter	Value
Bank of Capacitance (F)	29 F
Series resistance	0.15 Ω
Rated voltage(V)	72 V
Number of series capacitors	5
Parallel capacitors	1
Initial voltage (V)	66V
Operating temperature C^o	25

2.6 DC-DC Converter

The PV module and the load are connected via a DC/DC converter. It is often used in DC power supplies, such as motor drives and PV panels, to achieve the necessary voltage level by converting unregulated DC input into regulated DC output voltage [77]. Here, the converter in the PV system controls the voltage input at the point of maximum PV power, additionally offering load matching to achieve optimal power transfer. The voltage can be adjusted through the solar panel by keeping the input energy in the transformer's inductance for a short while and then releasing it to the output at a variable voltage. Several DC-DC converter types are employed with PV panels. This thesis will compare the proposed Super-Lift luo converter and boost converter.

2.6.1 Super-Lift Luo Converter

New step-up (boost) converters from DC-DC in several models employing the voltage lift technique were developed from prototypes. The construction of these converters is simple, has a high power density, is highly efficient, and has an inexpensive topology for DC-DC voltage-raising conversion. The Super-lift Luo converter produces fewer output voltage ripples and a higher voltage gain than the boost Converter. Based on its capabilities, the Super_lift Luo converter is categorized as a Super-lift Luo converter and a Voltage-Lift Converter. The passive components of the Super-lift luo converter's architecture include two diodes, two capacitors, and an inductor. Discuss the various Super-Lift Luo converters types, which can be found in [78] [79]. Fig.2.13 shows an equivalent circuit for the Super-Lift Luo converter [80]. The Specifications of the Super_lift luo converter are given in Table 2.8 below.

Table 2.8:Specifications of Super-lift Luo Converter.

Parameter	Value
Input capacitance Cin	$3500*10^{-6}$ F
C_2	$550*10^{-6}$ F
Output Capacitance Cout	$570*10^{-5}$ F
Inductance	$100*10^{-6}$ H

The Super-Lift Luo converter can function effectively by keeping to the following premise:

a) The resistance to the load (R_{output}) needs to be high.

b) The switching time must have a time limit.

c) The values of the capacitors $C_{s1}$and C_{s2} must be high.

d) There must be a low duty ratio (δ) value.

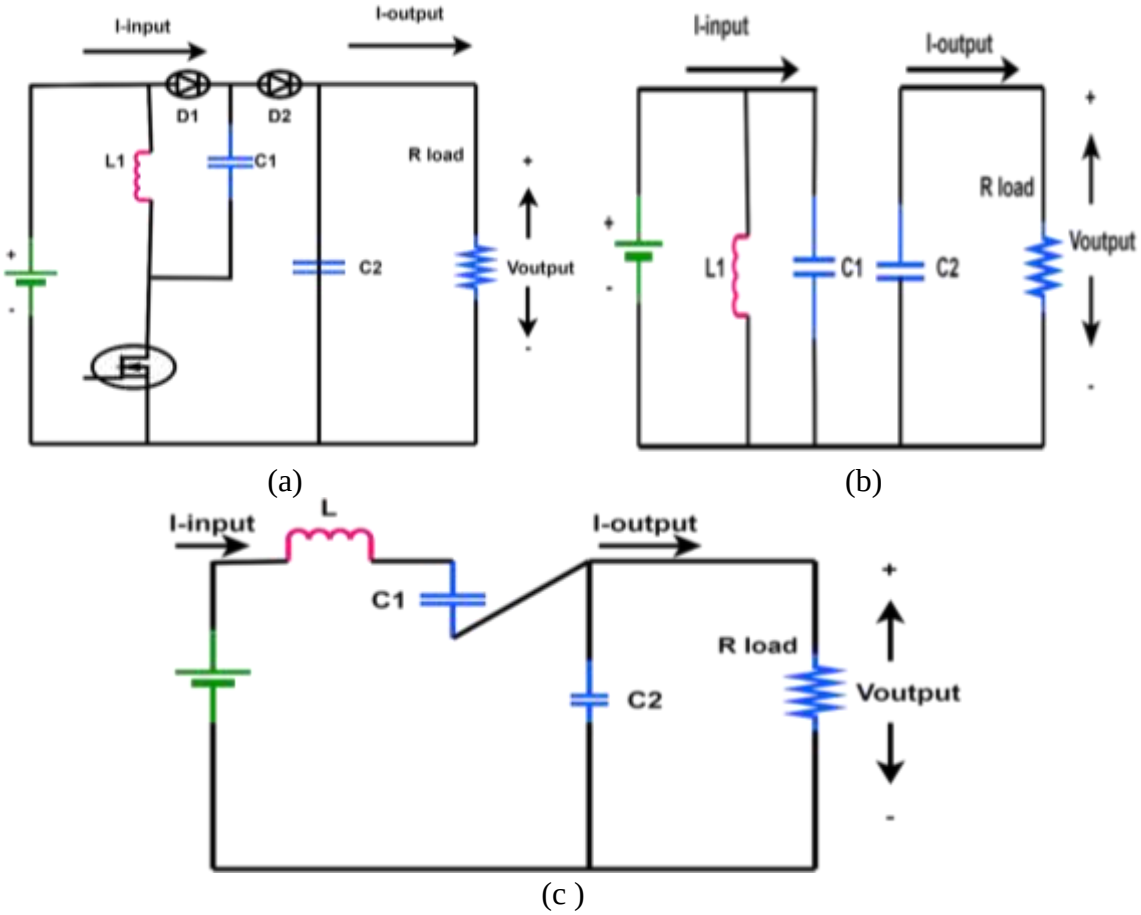

Fig.2.13:(a)Equivalent Circuit Super-lift Luo Converter During (b) Turn On (c) Turn Off.

Equation (2.33) provides the voltage gain equation for the super luo converter.

$$G_s = \frac{V_{output}}{V_{input}} = (\frac{2-\delta}{1-\delta})^n \quad (2.33)$$

V_{output} and V_{input} Are, respectively, the Super-Lift Luo converter's input and output voltages. The Gain G_s depends on the number of stages (n) and the duty ratio (δ). When switch Q is in the off position, V_{input} is the input voltage used to charge the capacitor $Cs-1$. Concurrently, as the inductor current $I_{L_{-1}}$discharges, there is a slight voltage drop of ΔV_{Cs-1}. When the inductance $I_{Ls_{-1}}$ value is high; One takes into account the average inductor current (,Ls-−1.). Equation (2.34) gives the voltage across the capacitor ($Cs-1$).

$$V_{cs\_1} = V_{input} - \Delta V_{Cs-1} \quad (2.34)$$

Equation (2.35) gives the capacitor voltage when the converter switches from the off to the on state when the transition state is adjusted to the on state.

$$\Delta V_{Cs\_1} = \frac{1}{C_{s-1}} \int_{\delta T}^{T} I_{L_{s-1}} dt = \frac{1-\delta}{C_{s-1}} T I_{L_{s-1}} \quad (2.35)$$

Equation (2.36) gives the overall current that passes through the inductor. And capacitor, which is the input current during turn-on.

$$I_{input\_on} = I_{C_{s-1-on}} + I_{L_{s\_1\_on}} \quad (2.36)$$

Equation (2.37) provides the input current as the current passage via the inductor and capacitor when switch Q is open and the input current during the off-time.

$$I_{input\_off} = I_{C_{s-1-off}} + I_{L_{s\_1\_off}} \quad (2.37)$$

The (2.38) and (2.41) calculate the output current, a dependent parameter that is based on the current and duty ratio(δ) of the capacitor.

$$\delta T I_{C_{s\_1\_on}} = (1-\delta) T I_{C_{s\_1\_off}} \quad (2.38)$$

$$I_{input\_off} = I_{C_{s-1-off}} = I_{L_{s\_1}} \quad (2.39)$$

$$I_{input\_on} = I_{L_{s\_1}} + \left(\frac{1-\delta}{\delta}\right) I_{L_{s-1}} = \frac{I_{L_{s\_1}}}{\delta} \tag{2.40}$$

$$I_{C_{s-1-on}} = \left(\frac{1-\delta}{\delta}\right) I_{L_{s-1}} \tag{2.41}$$

The average input current is the total input current in both the on and off modes divided by the duty ratio.

$$I_{input} = \delta I_{input\_on} + (1-\delta) I_{input_{off}} = (2-\delta) I_{L_{s\_1}} \tag{2.42}$$

$$\frac{V_{input}}{I_{input}} = \left(\frac{1-\delta}{2-\delta}\right)^2 \frac{V_{output}}{I_{output}} = \left(\frac{1-\delta}{2-\delta}\right)^2 R_{output} \tag{2.43}$$

Equation (2.44) gives the output voltage ripple as a function of the resistance (R_{output}) and capacitor (C_{s-2}).

$$\Delta V_{output} = \frac{I_{output}(1-\delta)T}{C_{s-2}} = \frac{(1-\delta)V_{output}}{f C_{s-2} R_{output}} \tag{2.44}$$

Raising Cs_ 2 reduces the ripple voltage to a minimum. Capacitor Cs_1 has a higher value than capacitor Cs_2, which is made feasible using duty ratio d values smaller than unity.

2.6.2 Boost Converter

The conventional boost converter has a wide range of power electronic applications, like solar power systems and controlled DC power supplies. Increasing the desired load's DC output voltage from a low DC input voltage is beneficial. There are two current operating modes for the converter. There are two types of current modes: continuous (CCM) and discontinuous (DCM). The traditional boost converter can function at many power levels and in any current mode in power applications, and every setting has unique variation features [81]. Table 2.9 provides the details of the boost converter used in this study.

Table 2.9. Specifications of the Boost Converter.

Parameter	Value
Input capacitance Cin	$3500*10^{-6}$ F
Output Capacitance Cout	$570*10^{-5}$ F
Inductance	$100*10^{-6}$ H

The diode is reverse-biased when the switch is closed. Kirchhoff's voltage law is implemented around the path, including the closed switch, inductor, and source given in (2.45) [82].

$$v_L = V_s = L\frac{di_t}{dt} \tag{2.45}$$

The current change in the inductor comes from calculating the current change from (2.46).

$$\frac{\Delta i_L}{\Delta t} = \frac{\Delta i_L}{\delta T} = \frac{V_s}{L} \tag{2.46}$$

Finding the value of Δi_LWhile the switch is closed,

$$(\Delta i_L)_{closed} = \frac{V_s \delta T}{L} \tag{2.47}$$

When the switch is opened, the diode becomes forward-biased., providing a channel for the inductor current. It prevents the inductor current from changing instantly. The voltage across the inductor is constant when the output voltage Vo in (2.48):

$$v_L = V_s - V_o = L\frac{di_L}{dt} \tag{2.48}$$

Since the inductor current changes constantly, it must vary linearly when the switch opens. The following is how the inductor current varies when the switch is open in (2.49):

$$\frac{\Delta i_L}{\Delta t} = \frac{\Delta i_L}{(1-\delta)T} = \frac{V_s - V_0}{L} \tag{2.49}$$

when calculating Δi_L,

$$(\Delta i_L)_{open} = (V_s - V_0)\frac{(1-\delta)T}{L} \tag{2.50}$$

From (2.49) and (2.50), there must be no net change in inductor current to achieve steady-state operation.

$$\begin{cases}(\Delta \mathrm{i_L})_{\mathrm{closed}} + (\Delta \mathrm{i_L})_{\mathrm{open}} \\ \frac{\mathrm{V_s}\delta \mathrm{T}}{\mathrm{L}} + (\mathrm{V_s} - \mathrm{V_0})\frac{(1-\delta)\mathrm{T}}{\mathrm{L}} \end{cases} = 0 \tag{2.51}$$

From (2.51), the calculation of $\mathrm{V_o}$,

$$\mathrm{V_o} = \frac{\mathrm{V_s}}{1-\delta} \tag{2.52}$$

I_L by calculating the average inductor current and using various substitutes, this can be expressed as follows in (2.53):

$$\mathrm{I_L} = \frac{\mathrm{V_s}}{(1-\delta)^2\mathrm{R}} = \frac{\mathrm{V_o^2}}{\mathrm{V_s R}} = \frac{\mathrm{V_o I_o}}{\mathrm{V_s}} \tag{2.53}$$

The average values of (2.54) and (2.55) and the variation in current are used to calculate the maximum and minimum inductor currents.

$$\mathrm{I_{max}} = \mathrm{I_L} + \frac{\Delta \mathrm{i_L}}{2} = \frac{\mathrm{V_s}}{(1-\delta)^2\mathrm{R}} + \frac{\mathrm{V_s}\delta \mathrm{T}}{2\mathrm{L}} \tag{2.54}$$

$$\mathrm{I_{min}} = \mathrm{I_L} - \frac{\Delta \mathrm{i_L}}{2} = \frac{\mathrm{V_s}}{(1-\delta)^2\mathrm{R}} - \frac{\mathrm{V_s}\delta \mathrm{T}}{2\mathrm{L}} \tag{2.55}$$

In the boost converter, the lowest feasible combination of switching frequency and inductance for continuous current is so. It is helpful to express L in terms of a desired Δi_L, as given in (2.56).

$$\mathrm{L_{min}} = \frac{\delta(1-\delta)^2\mathrm{R}}{2\mathrm{f}} \tag{2.56}$$

It is helpful to express L in terms of a desired $\Delta \mathrm{i_L}$, from a design standpoint.

$$L_{boost} = \frac{\mathrm{V_s}\delta \mathrm{T}}{\Delta \mathrm{i_L}} = \frac{\mathrm{V_s}\delta}{\Delta \mathrm{i_L f}} \tag{2.57}$$

An expression for ripple voltage is given in (2.58).

$$\frac{\Delta \mathrm{V_o}}{\mathrm{V_o}} = \frac{\delta}{\mathrm{RCf}} \tag{2.58}$$

With the switching frequency denoted by f. As an alternative, describing capacitance as the ripple in the output voltage yields.

$$C = \frac{\delta}{R\left(\Delta V_o / V_o\right) f} \tag{2.59}$$

The equivalent series resistance (ESR)-caused voltage ripple is:

$$\Delta V_{o,ESR} = \Delta i_c r_c = I_{L,max} r_C \tag{2.60}$$

The boost converter equivalent circuit is given in Fig.2.14[83].

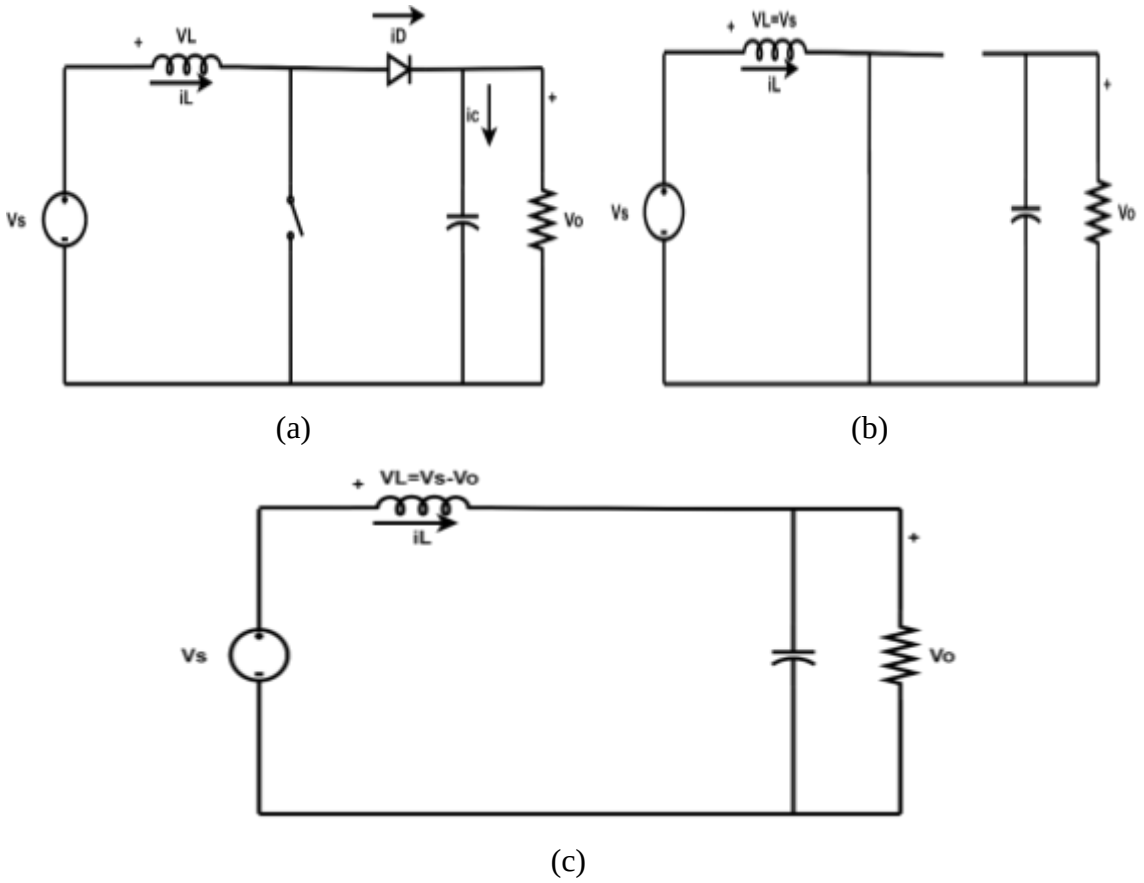

(a) (b)

(c)

Fig.2.14:The Boost Converter :(a) Circuit; (b) Circuit Equivalent for the Closed Switch (c) Circuit Equivalent for the Open Switch.

2.6.3 Bidirectional DC-DC Converters

The bidirectional DC-DC converters are designed to increase the accuracy of EMS. In bidirectional power flow, dependability, weight, cost, and power density are crucial elements, such as AHEVs. It regulates the EMS charge and discharge processes [84].

In HESS, where multiple energy storage technologies like batteries and SCs are combined, bidirectional converters play a crucial role. These converters act as the bridge between different storage units and the DC bus, enabling two-way power flow:

a) Charging: Power from external sources (e.g., solar panels, wind turbines, grid) is converted and directed towards the most suitable storage unit based on factors like charging rate and depth of discharge.
b) Discharging: Stored energy is efficiently extracted from the chosen unit and converted to match the desired voltage and current levels for powering loads or injecting power back into the grid.

Here's a breakdown of why bidirectional converters are essential in HESS:

Benefits[84]:

a) They allow independent control of charging and discharging for each storage unit, optimizing energy utilization based on demand and source availability.
b) By minimizing conversion losses and enabling optimal charging/discharging strategies, they contribute to a more efficient energy storage system.

Types of Bidirectional Converters:

Different converter topologies are used depending on the specific HESS configuration and requirements. Some common types include:

1) Boost converters: Increase voltage from lower storage voltages (e.g., supercapacitors) to match the DC bus voltage.
2) Buck converters: Decrease voltage from higher sources (e.g., solar panels) to match storage unit voltage.
3) Buck-boost converters: Can both increase and decrease voltage, offering greater flexibility. For this thesis, it will use this type.

A diagram of the type of buck-boost bidirectional DC-DC converter implemented in this concept is presented in Fig.2.15[85]. Remember that the SC and battery both contain independent bidirectional DC-DC converters. Switches 1 and 2 type mosfet in the converter switch the output if specific logic-related conditions are satisfied.

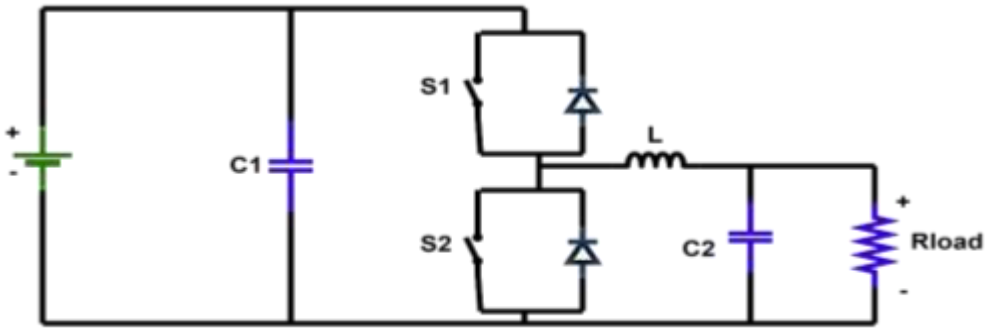

Fig.2.15: Buck-Boost Bidirectional DC-DC Converter.

Switches S1 and S2 are controlled by the fractional order PID (FOPID) controllers to turn ON and OFF according to the controller duty cycle during charge and discharge operations[86].

The system maximizes energy economy and improves overall system performance by utilizing intelligent energy flow balancing and keeping the battery and SC within their specified SoC ranges.

The Capacitors are used to reduce voltage rise. Each energy storage device in this design contains a bidirectional DC-DC converter to measure and compare system frequencies, hence improving the controllability and resilience of charge/discharge processes. Higher prices are a drawback, but overall savings should outweigh this. Battery charging occurs via independent bidirectional DC-DC converters while the supercapacitor is discharged [87].

2.7 Inverter

Inverters are circuits that change DC power into AC power. In some situations, the regulated full-wave bridge converters can act as inverters; however, an AC source has to be present previously. When just a DC voltage source is available, the goal is to produce an AC voltage. An uninterruptible power supply(UPS) is used for inverters, adjustable-speed AC motor drives, and operating AC appliances from a battery bank.
In an AHEV, the inverter manages The flow of power through the EMs that power the vehicle from its numerous energy sources [88].
As technology for autonomous vehicles advances, the inverter will play an even more crucial role in providing effective, dependable, and secure operation.
The full-bridge converter in Fig. 2.16 is the primary circuit for converting DC to AC. The closed switches determine the output voltage (Vo).; it may be either Vdc, Vdc, or zero.
The current waveforms given by (2.61) will change into the following at a steady state [89]:

$$i_o(t) = \begin{cases} \frac{V_{dc}}{R} + (I_{min} - \frac{V_{dc}}{R})e^{-t/\tau} \\ \frac{-V_{dc}}{R} + \left(I_{max} + \frac{V_{dc}}{R}\right) - e^{(t-T/2)/\tau} \end{cases} \quad (2.61)$$

$$I_{max} = -I_{min} = \frac{V_{dc}}{R}\left(\frac{1-e^{-\frac{T}{2\tau}}}{1+e^{-\frac{T}{2\tau}}}\right) \quad (2.62)$$

$$\sqrt{\frac{1}{T}\int_0^T i^2(t)d(t)} = \sqrt{\frac{2}{T}\int_0^{T/2}\left[\frac{V_{dc}}{R} + (I_{min} - \frac{V_{dc}}{R})e^{-t/\tau}\right]^2 dt} \quad (2.63)$$

$$P_{dc} = V_{dc}I_s \quad (2.64)$$

Where:

$$\tau = L/R \quad , \text{T=1/F} \quad (2.65)$$

$i_o(t)$: a load current expression.

I_s: the DC source's average current (A).

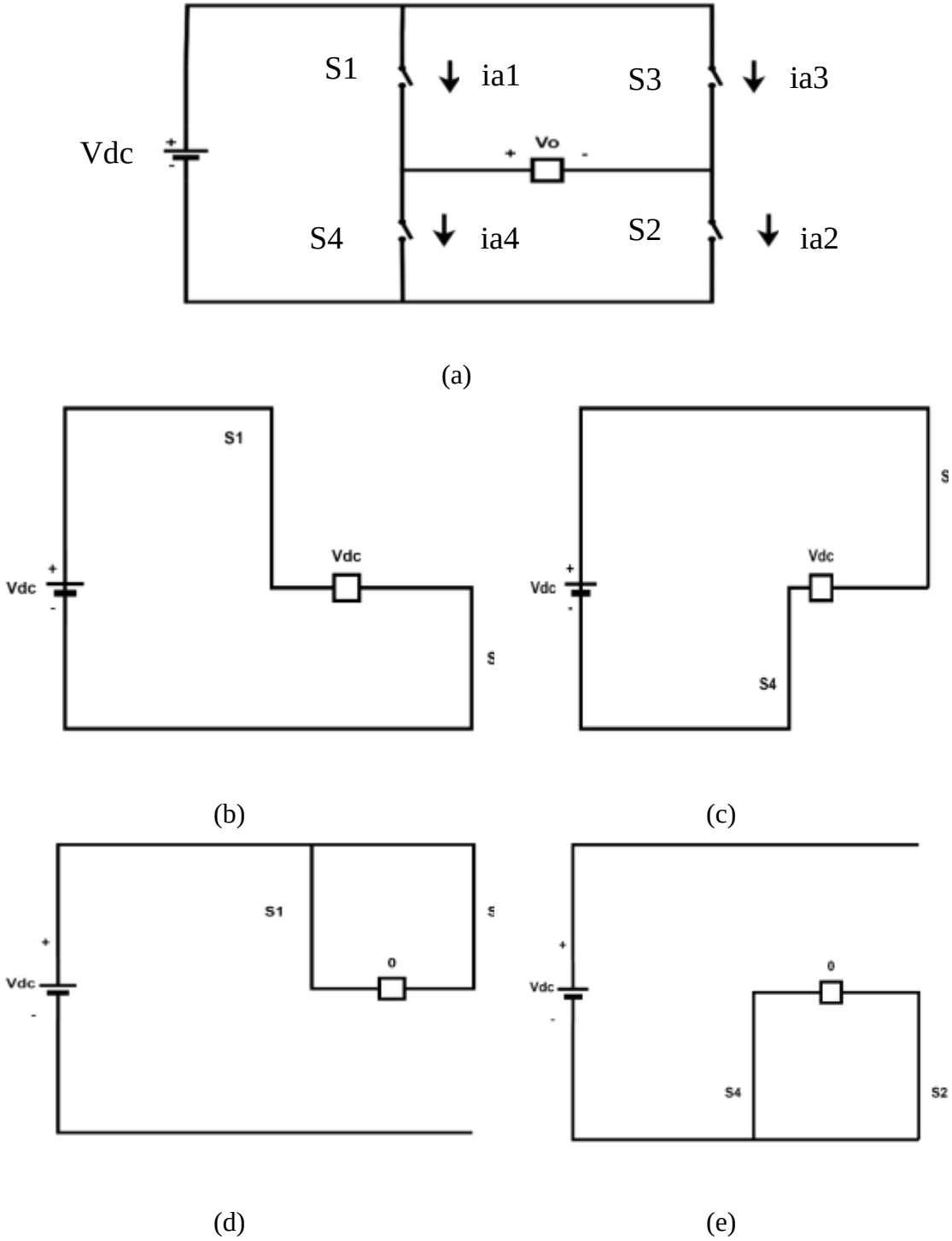

Fig 2.16:(a) Full-Bridge Converter (b) S1 and S2 Closed (c) S3 and S4 Closed; (d) S1 and S3 Closed (e) S2 and S4 Closed.

2.8 Vehicle Structure

Honda mini HEV vehicle combines modern technology and environmentally friendly driving, which sets the standard for creative and environmentally friendly transportation. The vehicle minimizes its environmental impact while providing a smooth driving experience due to its efficient and performant design. The battery, control unit, and 1.5 kW motor are contained within the automaker's Variable Design Platform, upon which it is constructed. It is the skateboard design that Honda has been promising for more than ten years, with a body that can be removed and customized and numerous interior and exterior configurations. The Micro Commuter's lithium-ion battery has a range of 60 miles and a maximum speed of 50 mph. A 2023 Honda vehicle prototype was used in this study [90]. The vehicle prototype is shown in Fig.2.17.

Table 2.10 Vehicle Parameters.

Parameter	Value
Mass	500 kg
Number of wheels per axle	2
Gravitational acceleration	$9.81\ {}^{m}/_{s^2}$
Air density	$1.18\ {}^{kg}/_{m^3}$

Fig.2.17: Prototype of Micro Honda – Hybrid Electric Vehicle.

2.8.1 Tire Modelling

The Tire block models the tire with the longitudinal behavior specified by the Magic Formula, an actual formula with four coefficients of the fitting. Table 2.11 presents the tire dynamics for both constant and varied road conditions.

The tire's motion when rolling over the road parallels its longitudinal direction. The Tire-Road Interaction (Magic Formula) block forms the foundation for this structural block[91]. It can provide parameters like rolling resistance, inertia, and tire compliance to improve the tire model's accuracy. The tire is modified by the Tyre (Magic Formula) block to become an uncomfortable wheel-tire combination that is in contact with the ground and subject to sliding. The tire drives against the ground while enduring contact friction when torque is delivered to the wheel axle, which transfers the force of that pushback onto the wheel. This movement moves the wheel forward or backward. Fig.2.18 shows the forces operating on the tire. Table 2.11 explains the values and variables of the tire model.

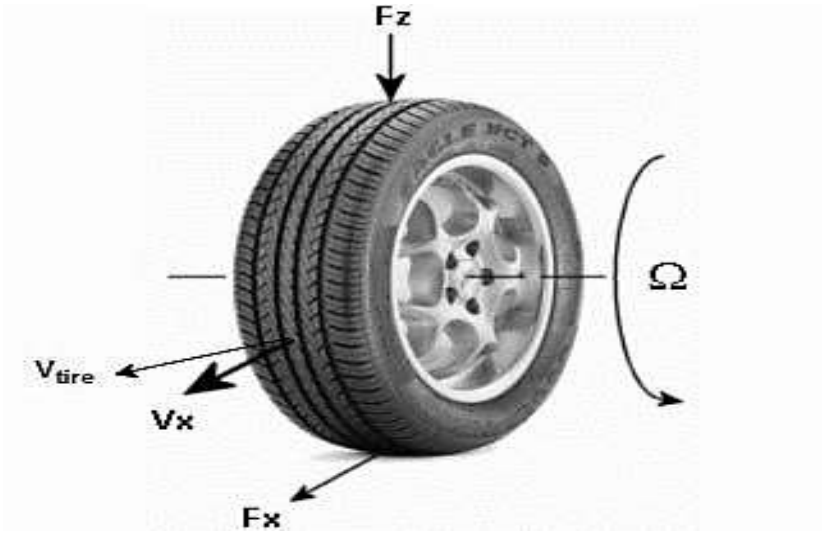

Fig.2.18: Tire Model in Vehicle [92].

Roll and Slip:

Tires do, however, react to slippage by creating a longitudinal force.

$$V_x = r_w \Omega_T \tag{2.66}$$

when tires do slip, though, they react by creating a longitudinal force,F_x.

In (2.68), the wheel slip velocity is given in (2.67).

$$V_{sx} = r_w \Omega - V_x \tag{2.67}$$

The wheel slip is:

$$k_{slip} = \frac{V_{sx}}{|V_x|} \tag{2.68}$$

k_{slip}= -1 for a sliding wheel that is locked. k_{slip}=0 for ideal rolling.

At Low Speed, Slip

For low speeds, as defined by (2.69):

$$|V_x| \leq |V_{th}| \tag{2.69}$$

the wheel slip becomes:

$$k_{slip} = \frac{2V_{sx}}{(V_{th} + \frac{V_x^2}{V_{th}})} \tag{2.70}$$

where: Fz: tire's vertical load, Fx: the force applied longitudinally to the tire at the point of contact, r_w : Radius of the wheels, V_x : Rear wheel longitudinal speed, Ω: Wheel rotational speed, V_{sx}: Velocity of wheel slip, K: a slip of the wheel, V_{th}: Wheel hub threshold speed.

Table 2.11: Specifications of Tire Model Employed in the Thesis.

Parameter	Value
Rated vertical load	$3*10^3$N
Peak longitudinal force at rated load	$3.5*10^3$ N
Slip at peak force at rated load	10%
Longitudinal stiffness	10^5 N/m
Longitudinal damping	400 N/(m/s)
Tire inertia	0.25 Kg*m^2
Initial velocity	0 rad/sec

2.8.2 Simple Gear

A machine's gears transfer rotation or motion from one section to another. Several gear teeth often come into contact with the other gears in the gearbox. By transferring power to the differential, gears assist in regulating rotational speed and power. An automobile's gearbox system typically includes many gear combinations of different sizes. The follower (F) to base (B) tooth ratio (NF/NB) in this thesis is (7.2).Fig.2.19 shows the structure of a simple gear scheme [93].

Fig.2.19:Simple Gear Scheme [94].

The two connected axes are subject to kinematic constraints imposed by the Simple Gear block[95]:

$$r_F \omega_F = r_B \omega_B \tag{2.71}$$

The ratio of follower to base gear is given in (2.72):

$$g_{FB} = \frac{r_F}{r_B} = \frac{N_F}{N_B} \tag{2.72}$$

Reducing the two degrees of freedom to one independent degree yields the torque transfer equation.

$$g_{FB}\tau_B + \tau_F - \tau_{lossed} = 0 \tag{2.73}$$

For the ideal case, $\tau_{lossed} = 0$

where:r_F : the follower gear's radius, ω_F : the follower gear's angle of velocity.

r_B : the base gear's radius,ω_B: the base gear's rotational velocity.

N_B : number of times teeth the base gear has, N_F : number of times teeth are in the follower gear, τ_B : the torque applied, τ_F : the torque produced.

τ_{lossed}: the friction-related loss of torque.

2.4.3 Differential Gear

Placed in between the drive wheels is a gearbox known as the differential. Both a front and a rear differential are found in four-wheel drive vehicles. Variations in wheel speed are made possible via a differential from one another by transferring power from the source to the axle that drives the wheels**;** when cornering compared to the inner wheel, the outer wheel must travel a longer distance. Without a differential, both wheels would be locked together, causing them to scrub and wear excessively. The differential solves this by enabling each wheel to spin at its required speed. The outer wheel must go far more when turning than the inner wheel. Both tires would be locked together in the case of a differential, which would scrape and wear the wheels excessively. That is resolved by the differential, which allows each wheel to spin at the specific speed needed.Fig.2.20 shows the structure of a differential gearbox [96].

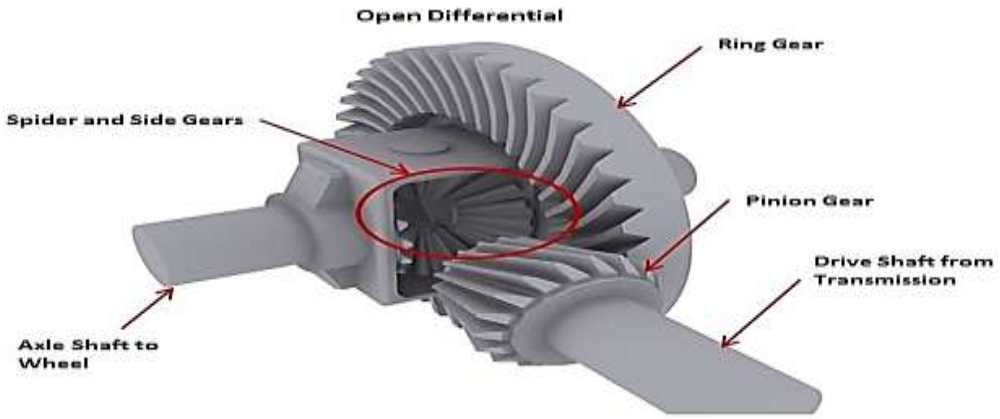

Fig.2.20:Structure of a Differential Gearbox [97].

The longitudinal axis torque reduces the lateral axis torques so that the net power flow equals zero[98] [99]:

$$\omega_{S1}\tau_{S1} + \omega_{S2}\tau_{S2} + \omega_D\tau_D - P_{losses} = 0 \quad (2.74)$$

Combining the kinematic and power limitations results in the ideal case, which is given in (2.75):

$$g_D\tau_D = 2\frac{(\omega_{S1}\tau_{S1}+\omega_{S2}\tau_{S2})}{\omega_{S1}\tau_{S1}} \quad (2.75)$$

where:

τ_{S1} and τ_{S2}: the torques in the lateral directions, τ_D : the torque applied longitudinally, P_{losses} : the loss of power, g_D : the gear ratio for the longitudinal driveshaft. ω_{S1}, ω_{S2} is the velocity of sun gear shafts 1&2.

2.9 Literature Review

Weichao Zhuang et al.2020 [100] examined three alternative HEV configurations: split, series, and parallel that were scaled to keep comparable all-electric ranges (AER), performance, as well as towing capability to track fuel and electrical energy usage (Wh/km).

2.9.1 Control of Electric Motor

Cai-Xue Chen et al.2016[101]**,** this paper presented an SMO-based backstepping control strategy for speed sensorless PMSM. Initially, a thorough dynamical model and space-state equation for the PMSM in the d-q frame are developed. The slide model control approach is used to estimate the electromotive force of a PMSM under a static frame, and the phase loop lock method is utilized to estimate the rotor's location and actual speed.

Sen LI. 2017 [102] explained the uses of electric motors in hybrid and electric vehicles. Every type of controller has been thoroughly detailed, along with its internal components, operation, and various control techniques.

Faisal Amin et al.2017 [103] evaluated the basis for investigating the PMSM dq model and its principle. Researchers produced more accurate simulation results because instead of being built on mathematical building blocks, the PMSM model is based on electronic components. The simulation's modules—including the PWM generator and inverter—are also created from scratch rather than using pre-made Simulink blocks.

Nisha G.K et al.2017 [104] displayed that induction machines with FOC can operate similarly to independently excited DC motors by isolating field control from torque control. In this study, the characteristic control of an induction motor is achieved by effectively altering its design to control the magnetizing current to provide maximum torque in the field weakening zone.

Kumari Suman et al.2018 [105] analyzed the PMSM drive's performance to regulate the speed of the PMSM. The sliding mode controller(SMC), PID, and PI of the PMSM drive have been designed. The SMC method is meant to manage the PMSM drive system's speed without depending on the machine's specifications or the impact of external disturbances.

Marcel Nicola et al.2020 [106], this study used the PMSM field-oriented control (FOC) technique, which takes all the benefits of employing PI-type controllers but is more superficial. However, the PMSM's nonlinear model naturally limits the control performances, the requirement for high-dynamics, wide-range speed, and load torque control, as well as the parameter uncertainties put on, primarily by changes in the rotor-load moment of inertia and the load resistance.

2.9.2 Hybrid Energy Storage System

Yuqing Yang et al.2018 [107]**,** this paper thoroughly analyzed battery sizing standards, procedures, and uses in different renewable energy systems. The uses of storage systems have been divided into groups according to the particular battery storage that will be a part of a renewable energy system. It contrasts with other studies that only considered one type of renewable system or structured the battery sizing procedures as an optimized component in renewable systems.

Praveen Vankadari et al.2021 [108]**,** A thorough examination of a light-electric vehicle design with a propulsion system powered by a BLDC and an ESS made up of a battery or SC has been completed in this proposed system. A simulation is conducted using foundational knowledge about EVs to comprehend the driving dynamics of EVs. Next, to obtain a clear representation of the calculation of several constraints in an EV throughout its

operation, each component and its modeling with control techniques are established.

Institute for Customer Insight et al.2021 [109]**,** the paper further explains how much energy will be needed to meet the rising demand and stresses that the most significant barrier to the growth of EVs will be the production of EV batteries. It also provides several articles on HESS systems and applications.

Fengchen Liu et al.2021[110], this research proposed a novel approach to energy management for urban electric vehicles by utilizing supercapacitors in conjunction with batteries. Using a couple of bidirectional DC-DC converters, the DC bus is connected to these two sources in parallel, giving each source independent control over its power flow. Considering vehicle dynamics when applying load torque to the shaft motor is necessary. Energy management strategy can be distributed between the two sources according to each source's current state of charge as well as the displacement state of the vehicle during stops, accelerations, drives up and down slopes, and decelerations.

Zineb Cabrane et al.2021 [111] created a HESS for photovoltaic systems using batteries and SC. Batteries and solar cells are two separate storage mediums that must have their energy distributed to create an energy management strategy. Thus, a new dimension in PI controller design is presented to manage the buck-boost converters coupled to batteries and SCs and stabilize the DC bus voltage.

2.9.3 Maximum Power Point Tracking Techniques

Pratik Shantaram Gavhane1 et al.2017 [112] this paper uses the enhanced leader particle swarm technique, a modified version of the El-PSO (particle swarm optimization) method. This work simulates MPPT in partially

shaded conditions. The suggested ELPSO approach offers several benefits over PSO, including quick convergence, improved dynamic performance, simplicity in use, and great effectiveness. Siemens S75 is made accessible in three distinct scenarios to evaluate the simulation results of the PV panel using the recommended methodology.

Jubaer Ahmed et al.2018 [113]**,** this work proposed the MPPT method of perturbing and observing (P&O) PV system. The goal is to reduced the steady-state oscillation, tracking direction separation, and global peak identification ability under partial shading.

Kriti Jain et al.2018 [114] presented the application of the P&O and incremental conductance controller (INC) MPPT algorithms and compared results for output parameters. The comparison shows that the MPPT of a PV array may be tracked more quickly and efficiently using the INC technique. The system is modeled using MATLAB/SIMULINK.

Sadeq D. Al-Majid et al.2019 [115]**,** in this paper, prevented a vital training error in the system. It is suggested that an artificial neural network ANN-MPPT method be used based on a sizable practical training data set. For a year, experimental testing of a photovoltaic platform created by Brunel University in London produced such data. The PV system's available power is at MPP, which is the output of the ANN model, and the temperature and radiation levels of the weather are selected as the input variables.

Hoejeong Jeong et al.,2019 [116]**,** this paper presented several DC-DC converter circuit topologies used in solar photovoltaic (PV) applications. This study outlines the three types of DC-DC converters, buck, boost, and buck-boost, which can be connected to solar PV systems for various applications. The application of DC-DC converters for MPPT in solar PV

systems is also presented in this research. It will discuss each topology's benefits and drawbacks regarding price, parts, efficiency, and limitations.

Hossein Gholizadeh et al.2021 [117]**,** in this study, developed and implemented a step-up DC-DC converter with a single switch based on Luo converters and cascaded boost. The suggested converter showed a high efficiency and quadratic voltage gain, making it appropriate for use in renewable energy applications when a high voltage gain ratio is needed without many significant components or a high-duty cycle of the active switches.

Pawan Kumar Pathak et al.2022 [118]**,** this paper proposed a HEV battery charging system that uses FC as the primary energy source and batteries and photovoltaic cells as auxiliary sources. To reduced the impact of tracking direction loss and oscillations near the MPP, a better MPPT system is designed for PV using the P&O method.

2.9.4 Energy Management System

Mauro G. Carignano et al.2017 [119]**,** this paper analyzed an FC/SC architecture that sets up a hard-constrained powertrain and presents a challenge to the EMS regarding driving comfort and fuel efficiency. To minimize this issue, the author introduces a unique EMS based on projecting the energy demand shortly and maintains the supercapacitor's energy state between two online-calculated limits.

Rayavarapu Srinivasa Sankarkumar et al.2021 [120]**,** this paper aims to offer a comparative evaluation of various HESS topologies and EM method types. The quantity of energy regenerated during braking and the design parameters based on the decrease in battery peak current have been compared and discussed. Additionally, the voltage variations and system

design have been compared. Therefore, this review might be a good resource for engineers and researchers working on EVs.

2.9.5 The Vehicle Autonomy System

Christoforos Chatzikomis et al.2018 [121]**,** this paper investigated the benefits of torque sensing in an AEV by including the technology within the path tracking controller or elsewhere. Various route tracking controllers are compared in adaptive control tests simulated with an empirically based vehicle dynamics model.

Monomoy Bujarbaruah et al.2018 [122]**,** this paper suggested a method for Side steering when keeping lane difficulties called AMPC, in which we constantly learn the steering system's unknown but constant steering angle offset. One assumes that longitudinal velocity is constant. The aim is to minimized the movement from the lane centre line and the steady-state heading angle error while keeping to the necessary safety regulations.

2.10 Scope of Thesis

According to the previous literature review, other approaches exist to control the EM besides employing sensors or sensors to identify the rotor position and back EMF. Most authors and researchers also used conventional methods to address these issues.

1) This thesis aims to establish the most advanced control strategies, evaluate them, and select the optimal one based on complexity, tracking speed, torque ripple, and total harmonic distortion (THD). The development of sensorless control for the electric motor through modern observers and their integration with the electric motor's control function will be an addition. SMO will be used with backstepping control.

2) Most authors used two-level inverters, which have many disadvantages affecting the speed controller of electric motors. Depending on the type of electric motor and inverter being utilized, connecting the batteries, solar panels, and SC to the electric motor in a hybrid electrical system might be complicated.

3) Most authors used conventional DC-DC converters, which have many disadvantages in voltage regulation and affect HESS performance. This thesis employed an advanced DC-DC converter with several modern MPPT control techniques to address the issue of how to extract MPP from solar panels.

4) EMS is crucial for companies like HESS since they are essential to cutting expenses and managing energy use. Additionally, EMS helps improve operational efficiency and promote sustainability by monitoring and controlling energy consumption. Therefore, the latest EMS the authors used depends on a conventional PI controller so it will use advanced EMS based on a fractional PID controller.

5) Most researchers and authors used PID controllers for autonomous vehicles. This thesis used Adaptive MPC to control the car and make it autonomous. The control of autonomous vehicles is essential for several reasons. First, it ensures the safety of passengers and pedestrians on the road. Second, it helps avoid accidents by constantly monitoring the vehicle's surroundings and making necessary adjustments to optimal driving conditions. Third, controlling autonomous vehicles allows for efficient navigation and traffic flow optimization, reducing congestion and improving transportation efficiency.

Chapter Three: Methodology

3.1 Introduction

The speed controllers for electric motors will be covered in this chapter. There will be a comparison of three control strategies:

1) FOC is based on an adaptive PID speed controller developed from more conventional FOC strategies.
2) SMC has several benefits over traditional control techniques and may be applied to a wide range of tasks requiring quick and accurate motor control. This chapter covers the fundamental ideas of SMC, how it is utilized for controlling electric motors, and its advantages and disadvantages.
3) Backstepping control is shown to be an effective means of achieving this objective. The principles of backstepping control, its use in EM control, and its benefits over conventional techniques will all be covered in this chapter.
Hardware sensors offer drawbacks such as more maintenance, expense, and temperature. As a result, it was suggested that SMO be added to the best of the mentioned techniques to compare them with sensor control. All EM control methods are affected by the number of inverter levels. An academic analysis of five levels and seven levels of inverters will be presented in this chapter. The super-lift Luo DC-DC converter will be used to develop the HESS. Additionally, the MPPTs will be employed in advanced techniques such as P&O, ANN, EPSO, and INC. based on smart battery charging controllers.

3.2 Speed Control of Electric Motors

Speed control of PMSM and BLDC plays a crucial role in various industrial applications such as robotics, EVs, and renewable energy systems. These motors offer numerous advantages, including high efficiency, compact size, and improved torque-speed characteristics. In addition, the speed control of PMSM and BLDC electric motors ensures precise and reliable operation, allowing for optimal performance in different operating conditions. Furthermore, accurate speed control enables efficient energy utilization and reduces maintenance costs. It also enhances the overall system stability and responsiveness, making it an essential aspect of EM systems. By implementing effective speed control techniques, such as sensorless control algorithms and advanced control strategies, the performance of PMSM and BLDC motors can be significantly improved, leading to enhanced productivity and energy savings.

AC motors are more complex than DC motors and require more sophisticated methods for speed control. The choice of speed control method depends on the specific application requirements, such as the desired speed range, torque requirements, energy efficiency, and cost. It has developed every speed control method listed below by integrating numerous novel methods that improve the performance and efficiency of EMs for HEVs.

Fig.3.1 illustrates the general PMSM scheme.

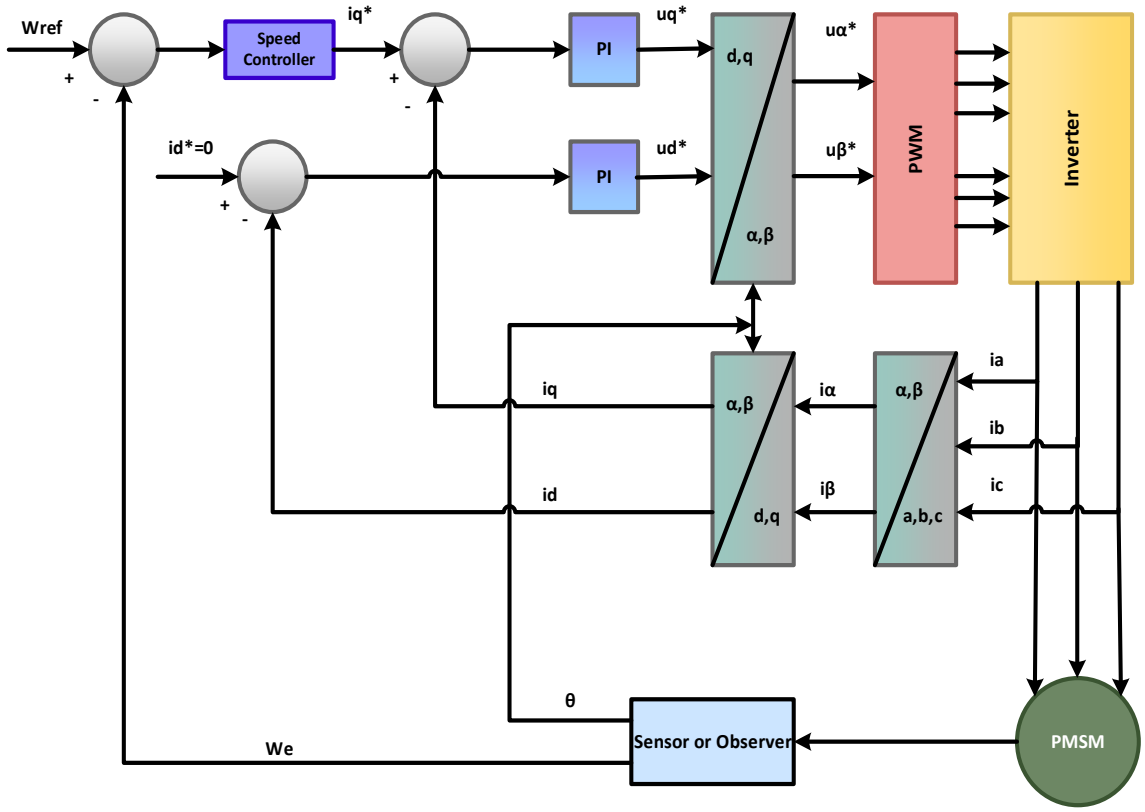

Fig.3.1: General PMSM Control Scheme [123].

3.2.1 Sensorless Backstepping Control

Sensorless backstepping control is a valuable technique for PMSM since it solves the issue of unknown parameters and external disturbances.

Since it can precisely control the speed of PMSM without the need for physical sensors like encoders or resolvers, the controller has attracted much attention in the field of motor control. The benefits of this strategy include lower maintenance costs, increased system reliability, and cost savings. The recursive function links the feedback controller and the control Lyapunov function to ensure that the system is asymptotically stable. Note that the system's stability at the origin point (0,0) was assessed using the Lypononve function; because of their outstanding power density and efficiency, PMSM motors can be used in various applications. However, outside disturbances and uncertainties in parameters such as load torque and stator resistance may

impact their control performance. To solve these problems, the controller does the following:

a) The controller design includes principles for online estimation of the unknown parameters.
b) The control design accounts for and eliminates external disturbances to ensure the motor precisely tracks the specified reference signal (speed).

Benefits of using Sensorless backstepping control:

Compared to conventional control techniques, sensorless backstepping control of PMSMs with an SMO has the following benefits:

a) It saves costs by doing away with the requirement for a physical speed sensor and simplifying the motor design
b) The system's overall reliability is improved because there is one fewer point of failure with fewer sensors.
c) Precise tracking of target Speed and position is made possible by Accurate Speed and Position Tracking backstepping control, which offers a systematic approach to controller design.
d) SMOs are known for managing system uncertainties and outside disturbances, resulting in more seamless functioning under various circumstances.

However, it is crucial to remember that sensorless backstepping control also has limitations. Sensorless estimation accuracy can be impacted by motor saturation and parameter fluctuations, and the design process itself may be more complicated than with simpler control schemes. Fig.3.2 shows the backstepping techniques for the PMSM motor.

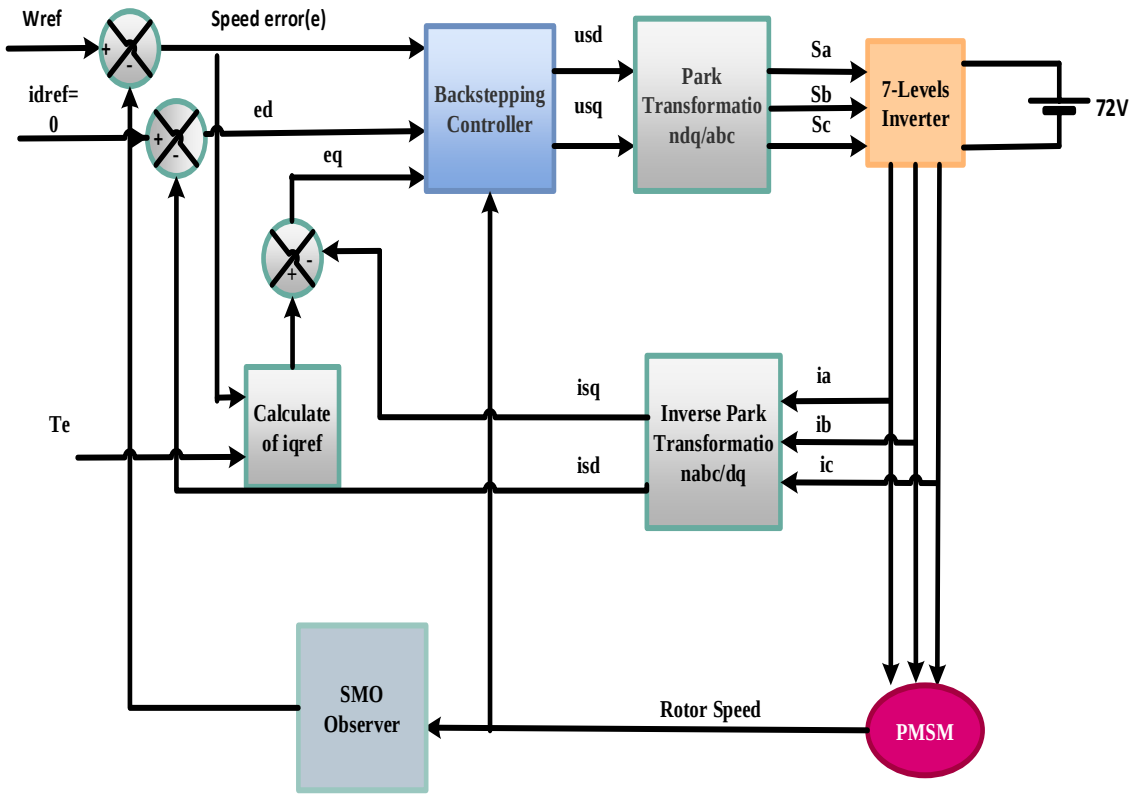

Fig.3.2: Sensorless Backstepping Controller.

For nonlinear systems, backstepping control is an effective technique. Defining a virtual control state is the initial stage in the backstepping technique, after which it becomes a stabilizing function. Thus, the error variable can be stabilized by constructing the related control input based on the Lyapunov stability theory. Establishing the overall controller design using the backstepping design technique is possible [101].

a) Speed Controller Design Methodology

Three steps can be used to design the speed state x1 controller:

Step 1. The state tracking error variable can be created as follows to address the speed tracking issue in (3.1):

$$e_1 = x_1^* - x_1 \tag{3.1}$$

where the reference rotor speed is denoted by x_1^*. x_1 is the rotor's actual speed. To maintain the speed component's stability, the error dynamics of speed tracking can be expressed in (3.2) [101]:

$$e_1 = x_1^* - \dot{x_1} = \frac{1}{J}(Bx_1 + T_L - \frac{3p\phi f}{2}x_2) \quad (3.2)$$

where ϕf is the flux linkage, B is the coefficient of viscous friction, and p is the PMSM's number of pole pairs.

Step 2. Select the following potential Lyapunov function in (3.3):

$$V_1 = \frac{1}{2}e_1^2 \quad (3.3)$$

Step 3. One can derive the time derivative of the Lyapunov function (7) as given in (3.4):

$$\dot{V_1} = e_1\dot{e_1} = \frac{e_1}{J}(Bx_1 + T_L - \frac{3p\phi f}{2}x_2) \quad (3.4)$$

Using Lyapunov's definition of stability, to enable the tracking error to approach zero, It is necessary to satisfy Equation (3.5) and make $\dot{V_1} < 0$.

$$\frac{1}{J}\left(Bx_1 + T_L - \frac{3p\phi f}{2}x_2\right) = -k_1e_1, k_1 > 0 \quad (3.5)$$

Following the backstepping technique with (3.6), the input virtual control variable

$$x_2 = \frac{2}{3p\Phi f}(Bx_1 + T + kJe_1) \quad (3.6)$$

The following Equation can be derived from (3.4) and (3.6) given in (3.7).

$$\dot{V}_1\ 1 = \mathrm{e}_1\ \dot{e}_1 = -k_2\mathrm{e}_{21} \quad (3.7)$$

Consequently, the speed error approaches zero when (3.6) is met. Stated differently, it is possible to achieve global asymptotic speed tracking. The PMSM is a multivariate, high-order, nonlinear system with significant coupling properties. In PMSM control systems, decoupling control is a frequently employed technique. The q-axis current determines the accurate thrust force needed to drive the motor. Additionally, it is recommended that

the d-axis current. x_3 be zero to lower power consumption. Since controlling x_3 to zero will eliminate the coupling term x_1, x_3 , expect the least amount of control effort possible. To put it another way, the control scheme is given below.

$$x_2^* = \frac{2}{3p\phi f}(Bx_1 + T + kJe_1) \tag{3.8}$$

$$x_3^* = 0 \tag{3.9}$$

where x_2^* is the q-axis current reference, and x_3^* is current on the direct axis reference.

b) The Current Controller Design Process

Step 1. To make the q-axis current tracking more accessible, it is selected as the new state variable for current tracking error(e_2).

$$e_{\dot{2}} = x_{\dot{2}}^* - x_{\dot{2}} = \frac{2(B-kJ)}{3p\phi fJ}\left(\frac{3p\phi f}{2}x_2 - Bx_1 - T_L\right) + \frac{Rx_2}{L} + px_1x_3 - \frac{u_q}{L} + \frac{\mathrm{p\Phi f}}{L}x_1 \tag{3.10}$$

Step 2. Regarding a novel system built on e_1 and e_2, the second Lyapunov function is defined as:

$$V_2 = V_1 + \frac{1}{2}e_2^2 \tag{3.11}$$

Step 3. V_2 is time derivative is provided by:

$$V_{\dot{2}} = V_{\dot{1}} + e_2e_{\dot{2}} = -ke_1^2 + e_2\left[\frac{2(B-kJ)}{3p\Phi fJ}\left(\frac{3p\Phi f}{2}x_2 - Bx_1 - T_L\right) + \frac{Rx_2}{L} + px_1x_3 - \frac{u_q}{L} + \frac{p\Phi f}{L}x_1\right] \tag{3.12}$$

where u_q, refers to the actual control variable. The stabilizing control law states in its definition that.

$$u_q = L(\frac{B}{J}x_2 - 2\frac{B^2}{3p\phi fJ}x_1 - \frac{2BT_L}{3p\phi fJ} - \frac{2k^2J}{3p\phi f} + \frac{Rx_2}{L} - px_1x_3 + \frac{P\Phi f}{L}x_1 + k_1e_2) \tag{3.13}$$

hence, the result that follows is as

$$\frac{2(B-kJ)}{3p\phi f}\left(\frac{3p\phi f}{2}x_2 - Bx_1 - T_L\right) + \frac{Rx_2}{L} + px_1x_3 - \frac{u_q}{L} + \frac{p\Phi f}{L}x_1 = -k_1e_2, k_1 > 0 \tag{3.14}$$

$$V_2^{\cdot} = -ke_1^2 - k_1 e_2^2 < 0 \tag{3.15}$$

Similarly, the following steps can be used to develop the d-axis current controller.

Step 1. Choose the d-axis's tracking error as the new state variable. Making a distinction, e_3, in connection to time and using the resulting yield.

$$e_3^{\cdot} = x_3^{*\cdot} - x_3^{\cdot} = \frac{R}{L}x_3 - px_1x_2 - \frac{u_d}{L} \tag{3.16}$$

Step 2. Using, e_1, e_2 and e_3 defining the third Lyapunov function as the basis

$$V_3 = V_2 + \frac{1}{2}e_3^2 \tag{3.17}$$

Step 3. Separating, V_3 it yields

$$V_3^{\cdot} = V_2^{\cdot} + e_3e_3^{\cdot} = -ke_1^2 - k_1e_2^2 + e_3(\frac{R}{L}x_3 - px_1x_2 - \frac{u_d}{L})\ ` \tag{3.18}$$

Equation (3.18), which contains the control variable ud, can be found. The definition of the actual control variable, ud, is as follows:

$$u_d = Rx_3 - pLx_1x_2 + Lk_2e_3, \tag{3.19}$$

Then $V_3^{\cdot} < 0, i.e.,$

$$\frac{R}{L}x_3 - px_1x_2 - \frac{u_d}{L} = -k_3e_3, k_3 > 0 \tag{3.20}$$

Combining (3.17) and (3.19), that results in

$$V_3^{\cdot} = -k_1e_1^2 - k_2e_2^2 - k_3e_3^2 \tag{3.21}$$

Equation (3.20), which makes it clear that the Lyapunov function $V_3^{\cdot} = -k_1e_1^2 - k_2e_2^2 - k_3e_3^2 > 0$ and $V_3^{\cdot} < 0$, it suggests that the tracking error will gradually get closer to zero.

3.2.1.1 Regenerative Braking Techniques

Regenerative braking is an essential component in modern AHEVS that raises energy efficiency. When the braking force is used, mechanical energy can be transformed into electrical energy, allowing the PMSM to function as a generator. Due to regenerative braking, electrical energy can charge ESS [124].

In a PMSM, regenerative braking functions as follows:

1) Motor as Generator: In regular operation, the PMSM functions as a motor, transferring battery-powered electrical energy into mechanical wheel spinning. However, as the driver decelerates when the vehicle is going to stop, the permanent magnets' electrical field is exceeded by the speed at which the motor shaft rotates.
2) Inverter Control: This change in current direction is detected by the inverter, a crucial part of the motor drive system, which modifies the control signals to control the back EMF.

The output voltage and current of the inverter to adjust how much regenerative braking torque is applied. The inverter's switches mosfet works as a diode. Then, the button MOSFET is in operation; it operates as a boost converter. After that, the AC is converted to DC to charge the battery. The inverter operation is shown in Fig.3.3.

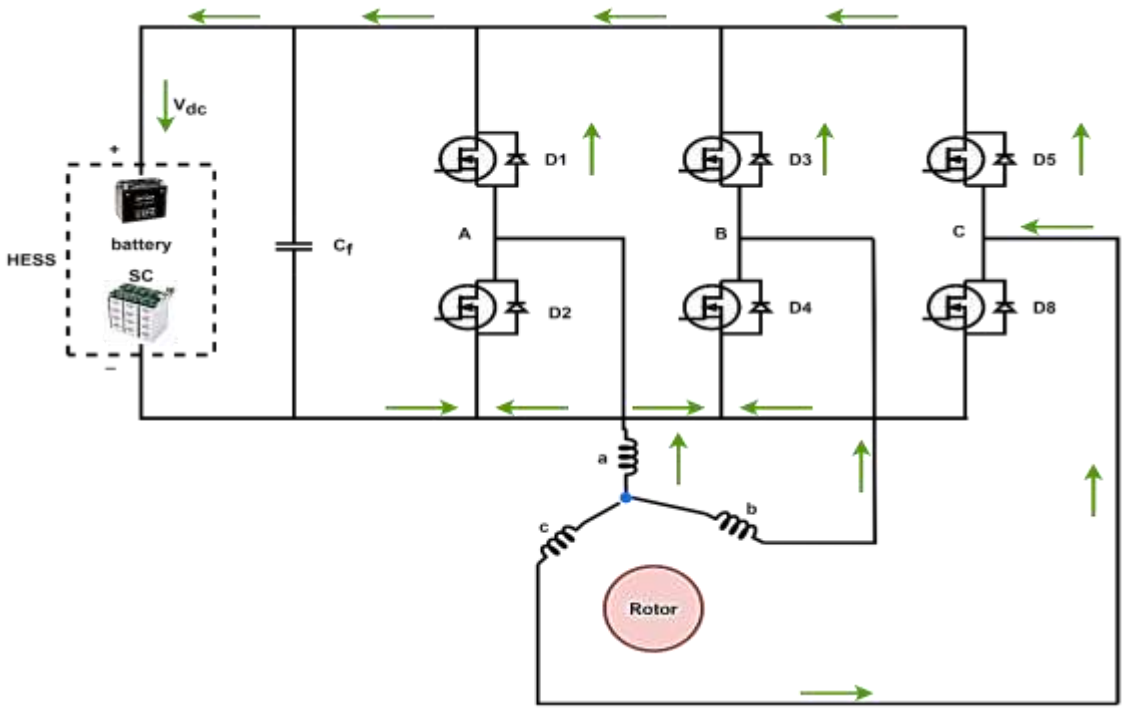

Fig.3.3: Inverter Operation in Regenerative Braking for PMSM.

The electrical braking torque and the mechanical (friction) braking torque make up the braking force of AHEVs. Since the EM-rated torque is constant and unable to stop HEV in situations requiring strong braking, the mechanical torque from the friction brake system must be used to ensure optimal braking performance.Fig.3.4 shows the regenerative braking techniques for the AHEV.

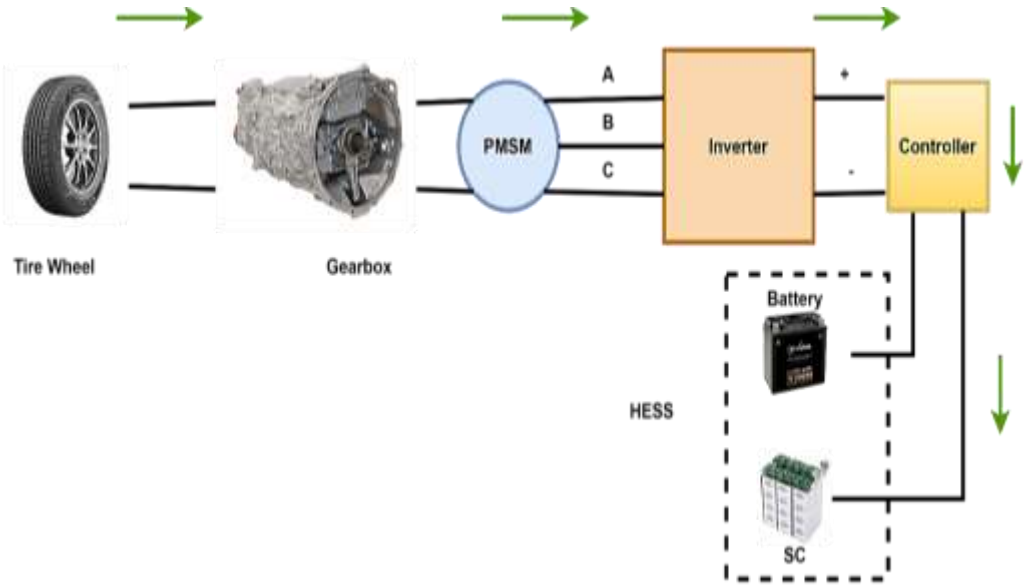

Fig.3.4: Regenerative Braking Techniques for PMSM.

The maximum regenerative power point (MRPP) can be calculated from (3.22):

$$P_{MRPP} = \frac{3}{2}(R_s i_{d-MRPP} + R_s i_{q-MRPP} + \omega_e \phi_e i_{q-MRPP} + (L_d - L_q)\omega i_{d-MRPP} i_{q-MRPP}) \quad (3.22)$$

hence,

$$i_{d-MRPP}(\omega_e) = \frac{(L_d - L_q)\,\omega_e{}^2 \phi_e}{4R_s^2 - (L_d - L_q)^2 \omega_e^2} \quad (3.23)$$

$$i_{q-MRPP}(\omega_e) = \frac{-2R_s\,\omega_e\,\phi_e}{4R_s^2 - (L_d - L_q)^2\,\omega_e{}^2} \quad (3.24)$$

The MRPP torques are computed separately to determine an MRPP torque based on motor speed (3.25).

$$T_{e-MRPP}(\omega_e) = -\frac{3k_b^4 \phi_e^2 P}{8R_s} \frac{\omega_e}{(\omega_e + k_b)^2 (\omega_e - k_b)^2} \quad (3.25)$$

where, $k_b = \frac{2R_s}{L_d - L_q}$ (3.26)

3.2.1.2 Sensorless Control Design

Accurate rotor position and speed data are necessary to properly apply the PMSM control technology. However, due to issues with temperature, signal noise, and space limitations, sensors are not suitable for industrial applications

when used to determine the position and speed of the rotor. For PMSM based on previous control approaches, this study creatively obtains the rotor position and speed data by applying the SMO. PMSM can be controlled sensorless, which has various benefits over traditional methods that depend on mechanical sensors such as encoders or resolvers.

Sensorless control offers a more reliable, robust, and inexpensive PMSM solution for various applications.

The SMO design uses the stationary αβ coordinates. It is the transformation matrix of dq-current (i_{dq}) to α – β current ($i_{\alpha\beta}$).

$$\begin{bmatrix} i_\alpha \\ i_\beta \end{bmatrix} = \begin{bmatrix} cos\theta_e & -\sin\theta_e \\ sin\,\theta_e & cos\theta_e \end{bmatrix} \times \begin{bmatrix} i_d \\ i_q \end{bmatrix} \tag{3.27}$$

where, θ_e shows the electrical angle of the rotor. In the d-q frame, the PMSM equations are presented in chapter two. The electromotive force equation's definition is given (3.28):

$$\begin{cases} e_\alpha = -\Phi_f\ \omega_e \sin\theta_e \\ e_\beta = \Phi_f\ \omega_e\ cos\,\theta_e \end{cases} \tag{3.28}$$

The stator current response is faster than the rotation speed because of the relatively low electric time constant. e_α& e_β are sinusoidal waves. Assuming $\dot{\omega} = 0$ in cycle control time, the (3.28) may be written as

$$\begin{cases} \dot{e_\alpha} = -\omega_e\ e_\beta \\ \dot{e_\beta} = \omega_e\ e_\alpha \end{cases} \tag{3.29}$$

Equation (3.28) demonstrates that the back-EMF eα and eβ are sinusoidal waves and offer information about the rotor's position and speed for the rotor position and velocity to be determined using the estimated back-EMF. The SMO was constructed in the way given in (3.30).

$$\begin{cases} \frac{dis_\alpha}{dt} = -\frac{1}{L}Rs_\alpha + \frac{1}{L}e_\alpha - \frac{k}{L}z_\alpha - \frac{k1}{L}sat(s_\alpha) \\ \frac{dis_\beta}{dt} = -\frac{1}{L}Rs_\beta + \frac{1}{L}e_\beta - \frac{k}{L}z_\beta - \frac{k1}{L}sat(s_\beta) \end{cases} \tag{3.30}$$

where $s_a = \hat{i_a} - i_a$, $s_\beta = \hat{i_\beta} - i_\beta$, $z_a = k_1 sat(s_\alpha) \times \frac{\omega_c}{s+\omega_c}$, $z_\beta = k_1 sat(s_\beta) \times \frac{\omega_c}{s+\omega_c}$, the feedback coefficient is denoted by k, The sliding model coefficient is denoted by k1>0, ω_c shows the one-order cut-off frequency of the low-pass filter SMO reaches the slide model surface in a finite amount of time if the condition of equality is satisfied. The predicted value of the electromotive force can be computed as

$$\begin{cases} \hat{e_\alpha} = kz_\alpha + k1sat(s_\alpha) \\ \hat{e_\beta} = kz_\beta + k1sat(s_\beta) \end{cases} \quad (3.31)$$

The PMSM rotor position and the electromotive force's phase are related. The arc-tangent function of electromotive force is a commonly employed method for determining the actual location of the rotor. However, this strategy has shortcomings, such as low resilience, low resistance to disturbance, and inability to adapt to changing circumstances. Chattering is another severe consequence of parameter variation.

3.2.2 Enhanced Field-Oriented Control

For PMSM, FOC is a popular control technique. With FOC, the electric motors' speed and torque can be independently, accurately, and smoothly controlled. For the FOC algorithm to work, the position of the motor's rotor must be known. FOC consists of two loops. The Controller Algorithm subsystem includes all three PI controllers. The outer loop is an adaptive PID controller that regulates the motor's speed. The two inner-loop PI controllers control the currents on the dq-axes independently. The outer loop PI controller sends a direct signal to the dq-axis to regulate torque [125].

Benefits of using adaptive PID for speed controller:

a) Compared to traditional PID, this method responds more quickly and has fewer steady-state speed errors.

b) Maintains optimal performance even in the face of load delays and parameter changes. Fig.3.5&3.6 shows the proposed adaptive PID control system structure.

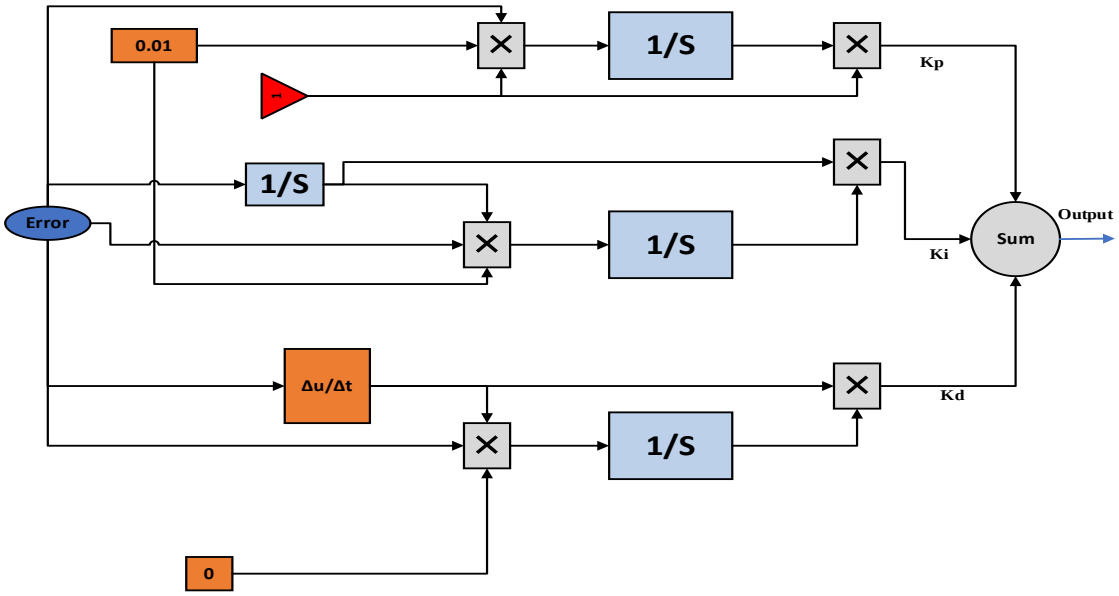

Fig.3.5:Proposed Adaptive PID Control System's Structure.

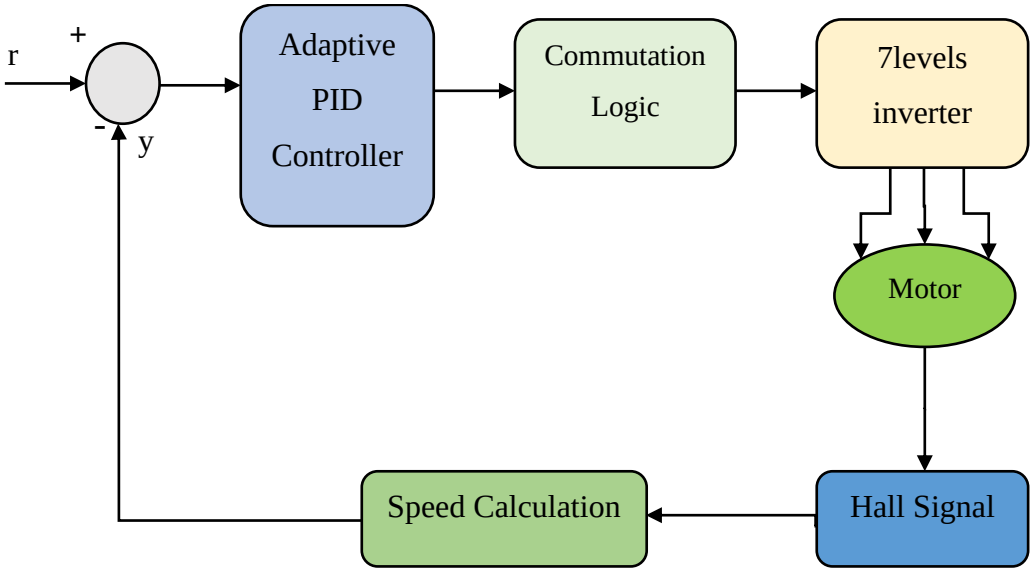

Fig.3.6:Speed Adaptive PID Control's System Structure.

3.2.3 Sliding Mode Control

The SMC surface controller offers several advantages, making it a popular control system choice [105].

1) Ability to handle nonlinear systems, as it does not rely on accurate system modeling. It can effectively handle systems with complex dynamics, nonlinearity, and uncertainty. That makes it a suitable choice for applications where the system characteristics may change or are difficult to model accurately.
2) Additionally, the SMC surface controller offers fast response and high accuracy in tracking the desired trajectory. The control law minimizes the error between the system states and the sliding surface. That leads to quick convergence and accurate tracking of the desired setpoint or trajectory. The fast response time makes the SMC surface controller suitable for applications that require dynamic and precise control, such as robotics, aerospace, and motion control systems[126].

Proper design and implementation techniques, such as boundary layer or reaching law techniques, are often employed to mitigate chattering effects.

$$s(t) = Ce(t) + e^{\bullet}(t) \tag{3.32}$$

$$s^{\bullet}(t) = Ce^{\bullet}(t) + e^{\bullet\bullet}(t) \tag{3.33}$$

where $e(t) = y^* - y$ the error function and the sliding function are. It is demonstrated that the sliding surface results from tracking error, the discrepancy between the reference output and the actual output. C > 0 is a performance parameter that ensures the system's stability on a sliding surface. Both the sliding function $s(t)$ and its derivative $s^{\bullet}(t)$ over the sliding surface are zero. The SMC's control signal law $u(t)$ consists of two components, an

equivalent control signal $u_{eq}(t)$ and a switching control signal $u_{sw}(t)$, both of which are determined by the (3.34) and (3.35) :

$$u(t) = u_{eq}(t) + u_{sw}(t) \tag{3.34}$$

$$u_{sw}(t) = k\,\mathrm{sgn}(s) \tag{3.35}$$

where

$$\mathrm{sgn}\big(s(t)\big) = \begin{cases} +1 & s\ t\ > \\ 0 \quad , & \text{if } s(t) = 0 \\ -1 \ , & \text{if } s(t) < 0 \end{cases} \tag{3.36}$$

$\mathrm{sgn}\big(s(t)\big)$ is the signum function, where k is an optimistic design parameter that is quite large to suppress system uncertainties and unanticipated dynamics. While $s(t)$ it is zero, the $u_{sw}(t)$ signal moves the system's states to the sliding surface. The switching control signal is terminated upon reaching the sliding surface. Although the comparable control signal is continuous, the switching control signal is discontinuous due to the situation. The motion described in (3.37) :

($T_e = J\frac{dw_r}{dt} + Bw_r + T_l$) can be rewritten as follows:

$$J\frac{dw_r}{dt} = k_t u - Bw_r - T_l \tag{3.37}$$

The sliding surface can be expressed as follows in terms of error:

$$s(w) = Ce - e^{\bullet} \tag{3.38}$$

Where the tracking error is equal to:

$e(t) = w_r^* - w_r$ Assume the $s(w^{\bullet}) = 0$, and we have:

$$s(w^{\bullet}) = e = w_r^{\bullet *} - w_r^{\bullet} = w_r^{\bullet *} - \frac{k_t}{J}u + \frac{B}{J}w + \frac{1}{J}T_l = 0 \tag{3.39}$$

According to observer torque, the equivalent control is modelled as follows:

$$u_{eq} = \frac{1}{k_t}(Jw_r^{\bullet *} + Bw + T_l) \tag{3.40}$$

Additionally, the sliding surface signal affects the switching control, which is stated as follows:

$$u_{sw} = k\,\mathrm{sgn}(s) \tag{3.41}$$

Finally, the actual control (output) is

$$u = u_{eq} + u_{sw} \tag{3.42}$$

The actual control equation that depends on simulation has the following final form (3.41 and 3.42) are substituted into (3.43):

$$u = \frac{1}{k_t}(Jw_r^{\bullet *} + Bw + T_l) + k\,\mathrm{sgn}(s) \tag{3.43}$$

Equation (3.40) depicts regulating the BLDC motor's output speed to achieve the desired speed under different conditions, as shown in Fig.3.7.

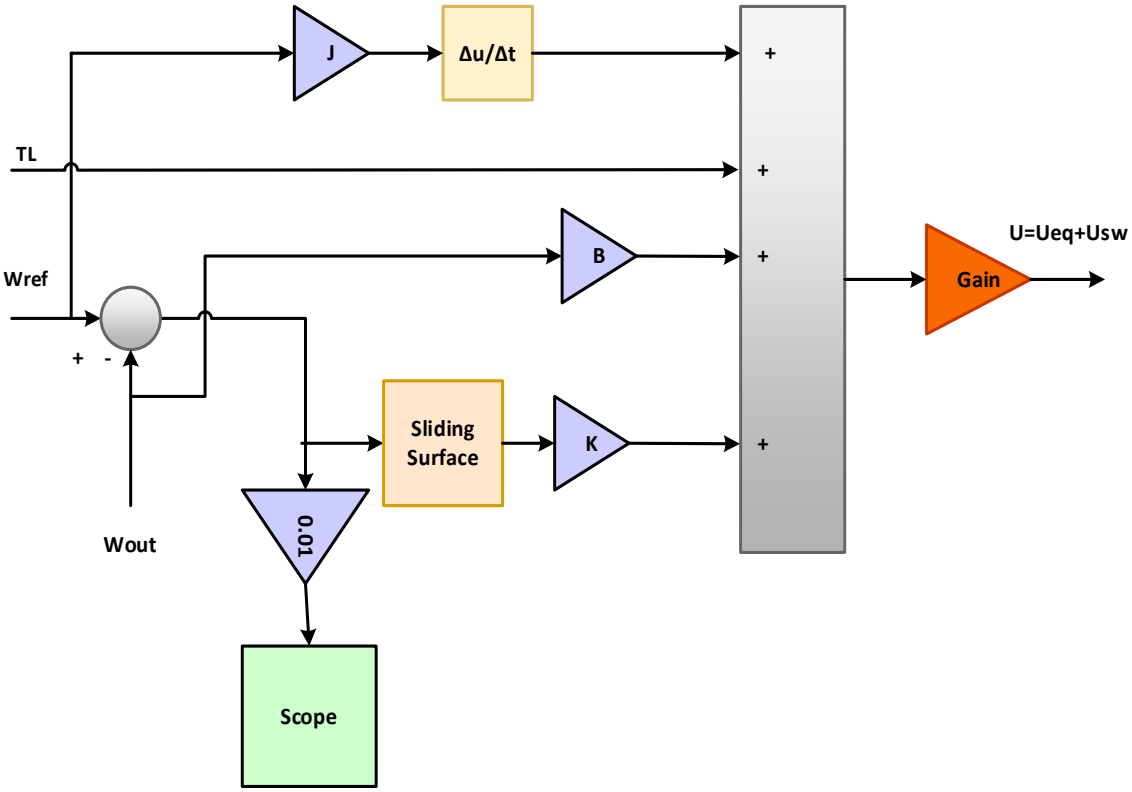

Fig.3.7: Structure of Load Torque Observer-based SMC.

3.3 Multi-Level Inverters in Power Electronics

High-performance motor control systems have recently been in demand across many sectors. Developing reliable and efficient power electronic converters is crucial to meeting this requirement. A highly effective method for controlling motors is the three-phase multi-level diode-clamped inverter. Reduced harmonics at the output, bidirectional power transfer capability, and improved reliability are among the benefits of this type of inverter. Because of their cost and flexibility, these inverters have found extensive use in applications such as EV chargers, solar systems, FC systems, and uninterruptible power supply. PMSM and BLDC motors are two particular applications where the three-phase multi-level diode-clamped inverter performs exceptionally well. MLI for PMSM in HEVs have the following advantages:

1) MLI reduces switching losses and increases total system efficiency by enabling a higher voltage resolution.
2) The output voltage waveform of MLI has less harmonic distortion, which makes the motor run more smoothly and puts less stress on the motor windings.
3) MLI controls the motor's output torque, enabling more accurate and effective operation.
4) MLI contributes to the seamless operation of the vehicle's other electrical components by reducing electromagnetic interference.
5) The motor and other electrical systems in the HEV receive a steady and dependable power supply via MLI, which produces a high-quality output voltage waveform.

6) MLI enhanced control and decreased harmonic distortion, which could lead to the PMSM's longer lifespan.

3.3.1 Three Phase Five Levels Diode-Clamped Inverter

A three-phase, five-level diode-clamped inverter is critical in controlling and operating PMSMs and BLDCs. It enables smooth and efficient power conversion, allowing for precise motor speed and torque control. This thesis will provide a three-phase, five-level diode-clamped inverter and its applications in PMSM and BLDC. Additionally, this chapter will explore the design considerations and optimization techniques for implementing the three-phase, five-level diode-clamped inverter in HEV applications [127].

m (No of level) =5 , active switches Mosfet =6(m-1)=24,

capacitors=(m-1)=4, each capacitor has the same voltage Em, which is given by Em= Vdc/m-1, Fig.3.8 the circuit architecture for the 5-level inverter.

Operation of Five-Level Diode Clamped MLI :

From Table 3.1:

- Turn on all upper-half switches for an output voltage level of Vo = Vdc/2.
- Turn on three upper-half switches and one lower-half switch for an output voltage level of Vo = Vdc/4. Turn on two upper-half and two lower-half switches for an output voltage level of Vo = 0.
- Turn on one upper-half switch and three lower-half switches for an output voltage of Vo = -Vdc/4.
- The upper-half switches are off for a level of output voltage. Vo = -Vdc/2 turns off all switches on the lower and upper halves.
- The desired output voltage is (72V) and the frequency is (50HZ).

Table 3.1: Phase "A" of the 5-Level Diode Clamped Inverter: Switching States.

$S1_a$	$S2_a$	$S3_a$	$S4_a$	$S1_a^*$	$S2_a^*$	$S3_a^*$	$S4_a^*$	V_{ph}
1	1	1	1	0	0	0	0	V_{dc} /2
0	1	1	1	1	0	0	0	V_{dc}/4
0	0	1	1	1	1	0	0	0
0	0	0	1	1	1	1	0	- V_{dc}/4
0	0	0	0	1	1	1	1	- V_{dc}/2

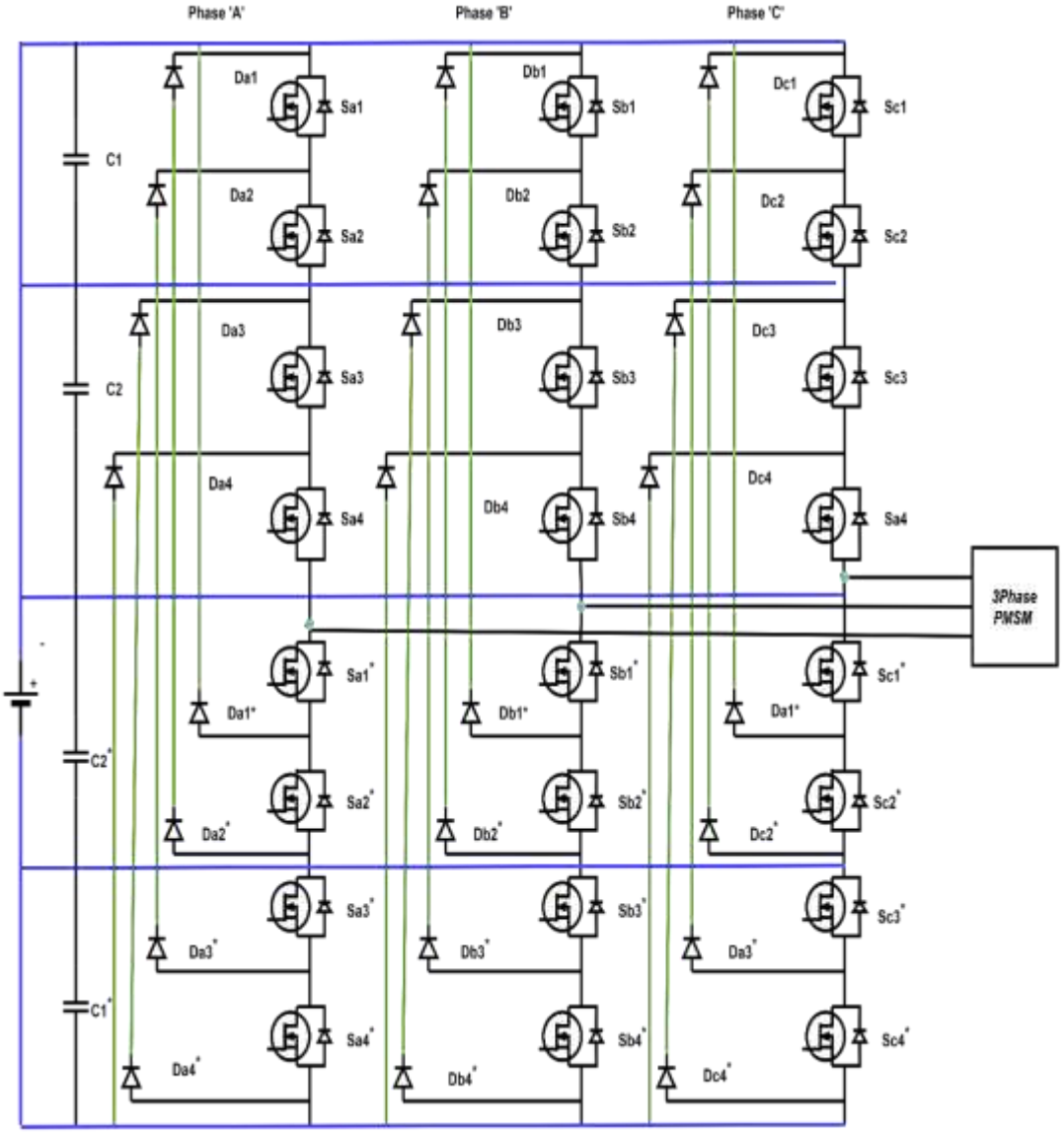

Fig.3.8: Circuit Architecture for a Three-Phase Inverter Including Five Levels of Diode Clamping.

- S1 and S8 are directly clamped to the DC link capacitor depending on the stray inductance. Switches that are indirectly clamped encounter blocking voltages that exceed the nominal value, Vdc/(m-1).
- Reverse-blocking values vary for clamping diodes.
- D1 must block the voltages of three capacitors, D2 must block the voltages of two capacitors, and D3 must block the voltage of one capacitor.
- The voltage levels at the capacitor's terminals and the supply current fluctuate.
- Each capacitor has a varied discharge period, which causes unequal capacitor voltages between levels.
- Batteries or sources of controlled, steady DC voltage can help prevent voltage imbalance.

3.3.2 Three Phase Seven Levels Diode-Clamped Inverter

An advanced and effective technology that has drawn much interest in electrical engineering is the three-phase, seven-level PMSM. EV, renewable energy systems, and industrial automation are just a few of the industrial applications that this system's enhanced performance and control make it suitable.

Because of the seven-level inverter's unique design, the PMSM motor can be tightly controlled, reducing harmonics torque ripple and improving efficiency. As a result, this technology is becoming increasingly common in modern power systems. This publication will address the concepts, design considerations, and advantages of the three-phase seven-level PMSM motor. It will be beneficial for engineers and researchers who are investigating electrical devices and power electronics.

Operation of Five-Level Diode Clamped MLI [128]:

m (No of level) =7 , active switches Mosfet =6(m-1)=36,

capacitors=(m-1)=6, each capacitor has the same voltage Em, which ey = Vdc/m-1 gives, diodes =3(m-1)(m-2)=90, Fig. (2.6) or divided by tow = 45, Fig.3.9.

- Like the five-level case, all switches are turned on, connecting the total DC voltage (Vdc) to the output for a positive voltage of half the DC voltage (+Vdc/2).
- All cases in Table 3.2 have the same idea of a 5-level inverter.

Table 3.2: Switching States for Phase 'A' of 7-Level Diode Clamped Inverter

$S1_a$	$S2_a$	$S3_a$	$S4_a$	$S5_a$	$S6_a$	$S1_a^*$	$S2_a^*$	$S3_a^*$	$S4_a^*$	$S5_a^*$	$S6_a^*$	V_{ph}
1	1	1	1	1	1	0	0	0	0	0	0	Vdc/2
0	1	1	1	1	1	1	0	0	0	0	0	Vdc/3
0	0	1	1	1	1	1	1	0	0	0	0	Vdc/6
0	0	0	1	1	1	1	1	1	0	0	0	0
1	0	1	0	1	0	1	0	1	0	1	0	0
0	0	0	0	1	1	1	1	1	1	0	0	-Vdc/6
0	0	0	0	0	1	1	1	1	1	1	0	-Vdc/3
0	0	0	0	0	0	1	1	1	1	1	1	-Vdc/2

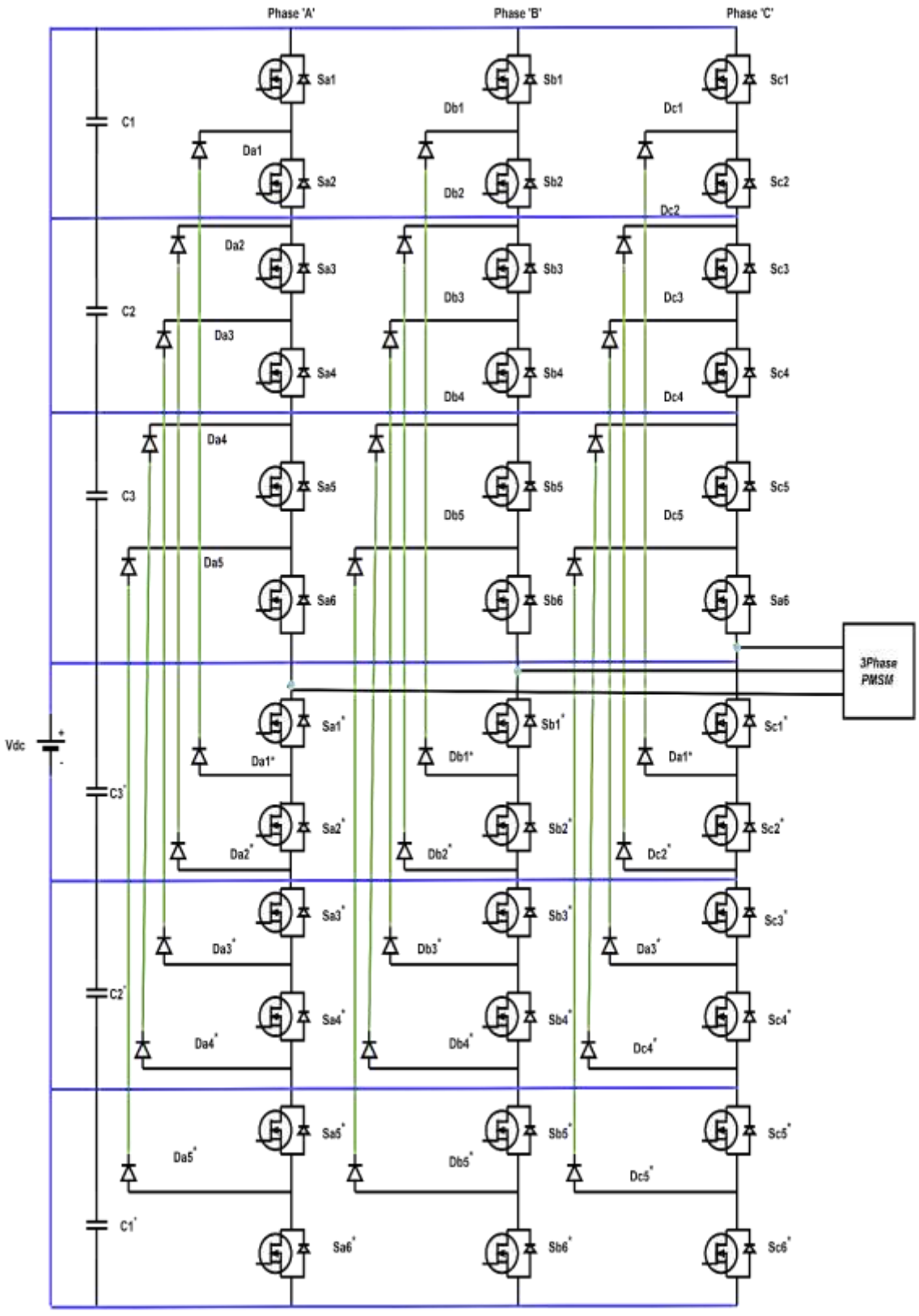

Fig.3.9:Seven Levels Diode Clamping Three-Phase Inverter Circuit Topology.

3.4 Maximum Power Point Tracking Controllers

3.4.1 Perturbation and Observation Controller

Because of its simplicity of implementation, specifically, the P&O algorithm is the one that is utilized in practice the most. As the names indicate, It is dependent on the disturbance of the system caused by a rise or reduction in Vref, which directly affects the duty cycle of the DC-DC converter, then monitoring the effects on the panel's output power. As power increases, the duty cycle also changes in the same direction. It is approaching the MPPT. Therefore, If there is a power failure, it goes away from the MPP. The duty cycle variation must then be reversed in a direction [129]. Fig.3.10 shows the P&O flowchart.

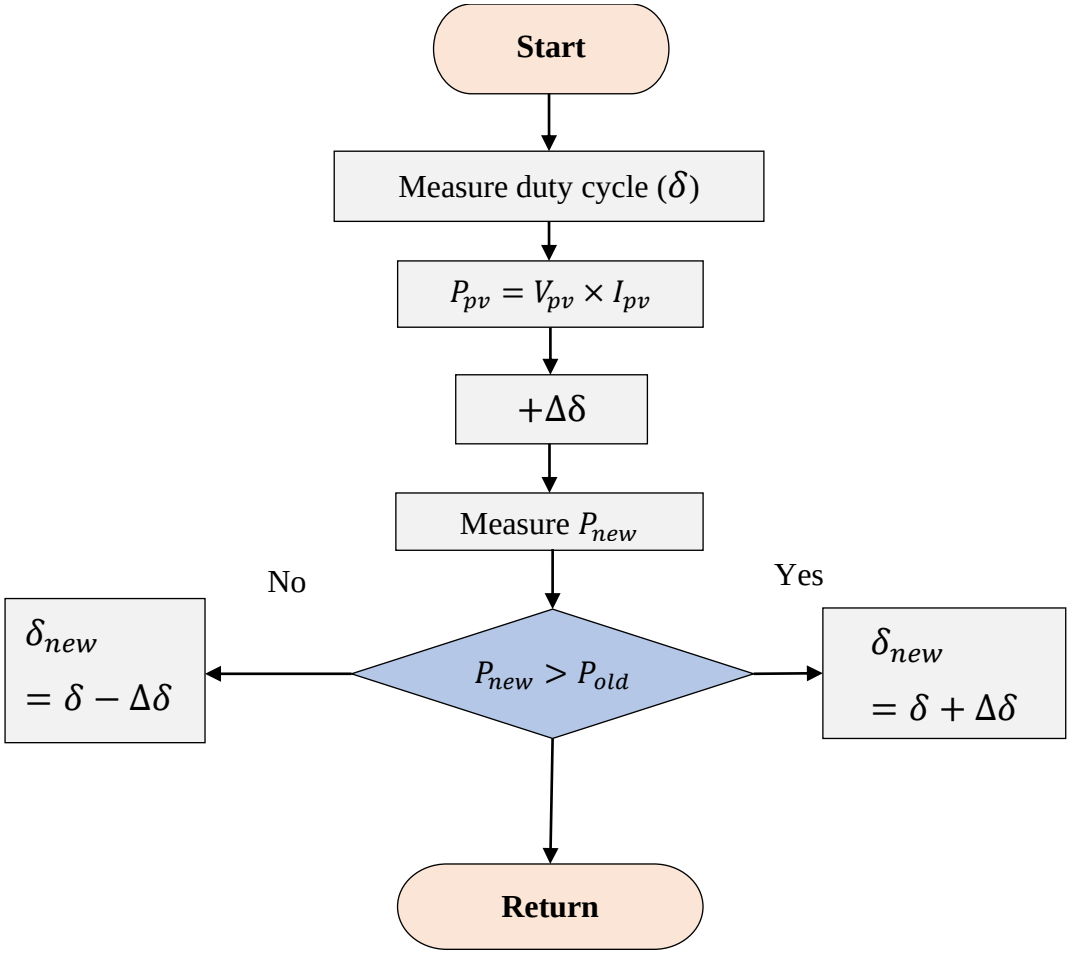

Fig.3.10: Observation and Perturbation of the Flowchart Algorithm.

3.4.2 Enhanced Particle Swarm Optimization

Enhanced Practical Swarm Optimization (EPSO) is a widely used technique for MPP for PV. By constantly tracking the panel's MPPT under various environmental variables, such as temperature and sunlight intensity, this method is intended to maximize the performance of PV. It dynamically modifies the PV panel's operating characteristics, like voltage and current. This algorithm uses a swarm of particles to identify the best solution, each representing a possible solution. Iteratively, the particles' positions are updated based on how well they suit the problem. It has been shown that using EPSO in PV panel MPPT increases the speed and accuracy of the MPP search.

Furthermore, this method has improved the PV system's efficiency, mainly when partial shadowing occurs [130]. The social behavior of animals, including birds, herds, insects, and fish, served as the model for the EPSO algorithm, a metaheuristic optimization technique that Eberhart and Kennedy first presented. To develop a PSO method for resolving any optimization problem, a few concepts must be considered for each particle in the population or particle i. These concepts concern the search space characteristics of algorithms, which fit into the following categories. $V^{(t)}$ and $X^{(t)}$are current velocity and current position, respectively; $P_{B,i}^{(t)}$is the vector's best location at this time. $P_B^{(t)}$is global best position. As each program iteration progresses, each particle aims to increase in position and velocity, as demonstrated mathematically below.

$$X_i^{(t+1)} = V_i^{(t)} + X_i^{(t)} \tag{3.44}$$

$$V_i^{(t+1)} = \left\{IC \times V_i^{(t)}\right\} + \left\{c_1 \times rand \times \left(P_{B,i}^{(t)} - X_i^{(t)}\right)\right\} + \{c_2 \times rand \times \left(G_B^{(t)} - X_i^{(t)}\right) \tag{3.45}$$

$$IC = IC_{max} - \frac{(IC_{max} - IC_{min})}{T_{max}} \times T \tag{3.46}$$

i=1,2,3,….., Nop (3.47)

where, $V^{(t+1)}$ and $X^{(t+1)}$ are, respectively, the position and velocity of the ith particle $(t + 1)$th iteration; IC, IC_{min}, and IC_{max} are the minimum and maximum values of the inertia coefficient, respectively.; $c_1$and c_2 are cognitive factors and social learning factors (positive constant), respectively. T and T_{max} are the current iteration and the previous iteration, respectively. ; Nop indicates the population's size, *rand* is the arbitrary value in the range [0–1]. Remember that random numbers are required for the algorithm's performance to be somewhat unpredictable. That is because any heuristic algorithm starts with a randomly generated initial population. It uses a collection of formulations that vary from algorithm to algorithm based on their intrinsic qualities to progress and converge to a global or nearly global optimal answer. The main benefits of the randomization in the suggested technique are thus the expectation and variance that enable the proposed algorithm to explore and exploit more efficiently. EPSO aims to enhance PSO's ability to handle high-dimensional challenge instances and optimization issues. By reducing the time and effort needed to locate the best answers for complicated situations, EPSO helps to increase search efficiency.

$$0 < C_1 + C_1 < 4(1 + W) \quad (3.48)$$

$$0 < W < 1 \quad (3.49)$$

3.4.3 Artificial Neural Networks

Photovoltaic systems are a critical renewable energy technology, but their efficiency relies heavily on operating at the MPP. Traditional MPPT control methods can struggle with constantly changing environmental conditions. This thesis explores how Artificial Neural Networks (ANNs) offer a promising alternative to MPPT control in PV systems. Fig.3.11 shows the MPPT control that operates on the photovoltaic system.

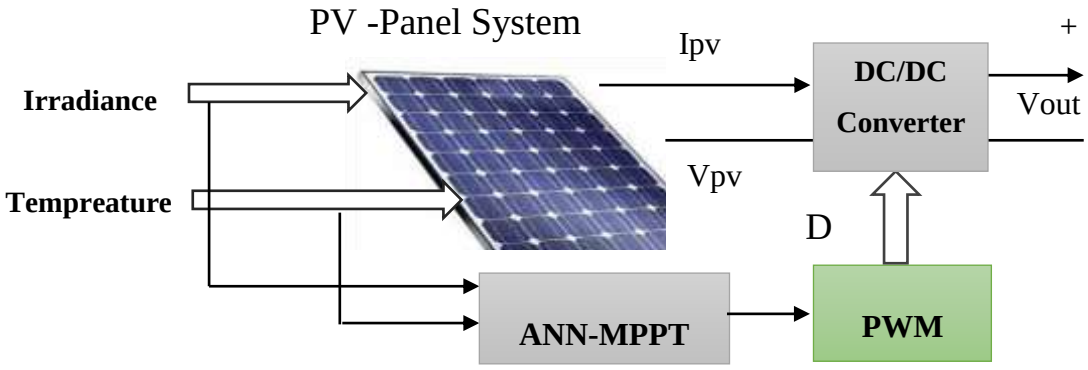

Fig.3.11: ANN - MPPT System Block Diagram.

ANNs are inspired by the structure and function of the human brain. They can learn complex relationships from data, making them well-suited for handling the non-linear characteristics of PV systems. This thesis describes the implementation of an ANN-based MPPT controller for a PV system. The network takes temperature and radiation as inputs and determines the optimal duty cycle for the converter to maximize power output. The thesis also details the training process using the Levenberg-Marquardt algorithm and the chosen network architecture. Finally, it acknowledges the potential for further network structure optimization for even better performance.

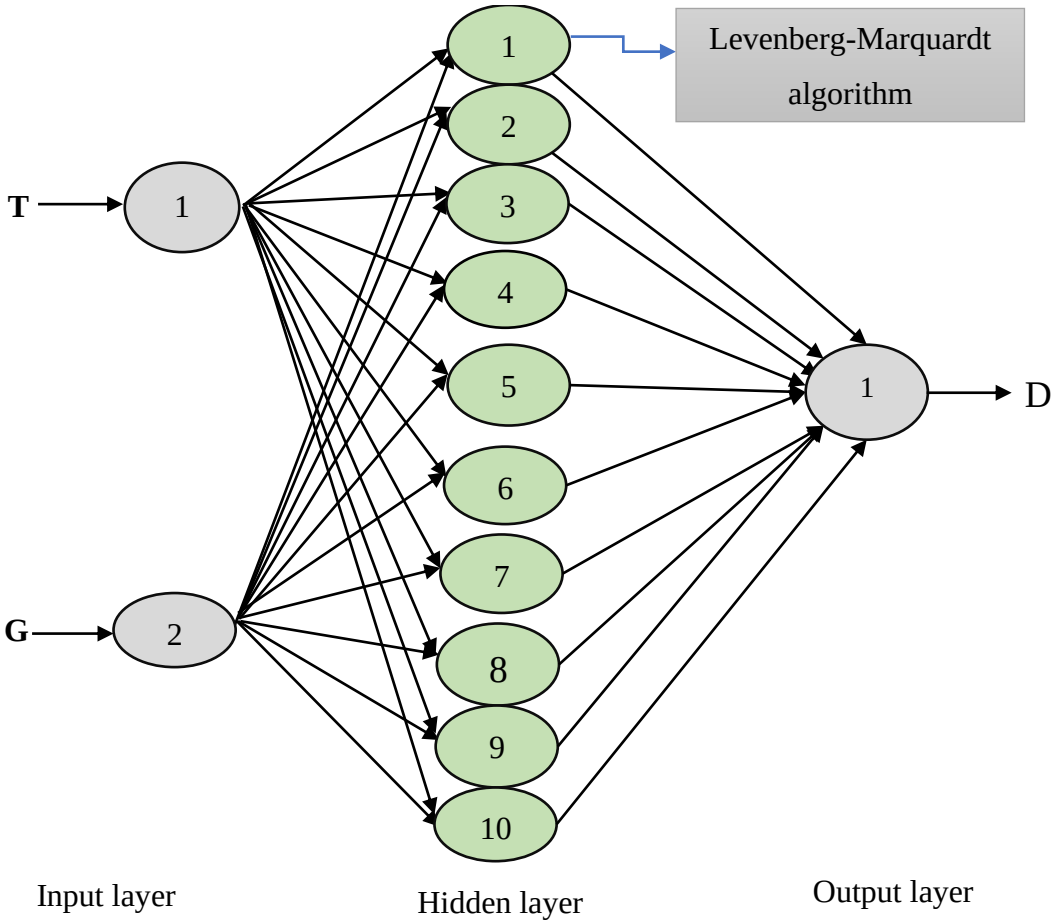

Fig.3.12: Diagram of ANN Structure.

3.4.4 Incremental Conductance Controller

The operating point for the highest power point can be found with instantaneous conductance (I/V) and incremental conductance (dI/dV). Thus, to follow the MPP, one can compare the incremental conductance (dI/dV) and the instantaneous conductance (I/V). The duty cycle will increase if the instantaneous conductance exceeds the opposite of the incremental conductance. Assuming this does not occur, the duty cycle will be decreased. The block's subsystem used the input voltage and current of the PV module to calculate the value of variations in the conduction angle. Fig.3.13 displays the INC flowchart [131].

$$\frac{dP}{dV} = \frac{d(VI)}{dV} = I\frac{dV}{dV} + V\frac{dI}{dV} = I + V\frac{dI}{dV} \tag{3.50}$$

MPP is reached when ($\frac{dP}{dV} = 0$)

$$0 = \mathrm{I} + \mathrm{V}\frac{\mathrm{dI}}{\mathrm{dV}} \Rightarrow \frac{\mathrm{dI}}{\mathrm{dV}} = -\frac{\mathrm{I}}{\mathrm{V}} \tag{3.51}$$

The MPP is achieved when incremental conductance is equal to the negative of instantaneous conductance ($-\frac{\mathrm{I}}{\mathrm{V}}$)

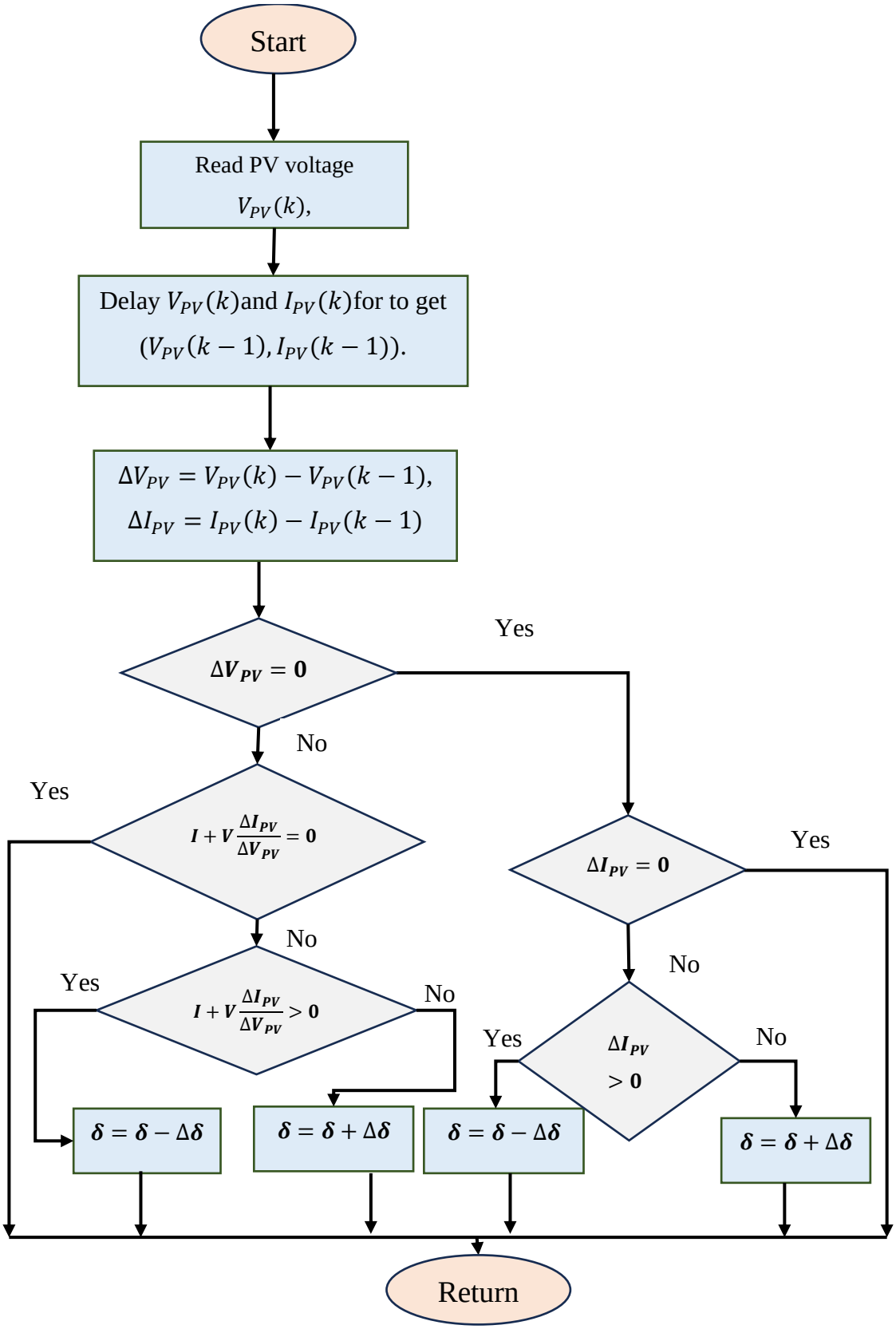

Fig.3.13: Incremental Conductance Flowchart Algorithm.

3.5 Energy Management System-based FOPID Controller

HESS is becoming increasingly crucial for integrating renewable energy sources like solar and wind into the power grid. An EMS plays a vital role in optimizing the performance of a HESS. The EMS determines the power flow between the different components, ensuring efficient energy utilization and extending the lifespan of the storage devices. These systems combine different storage technologies, such as batteries and SCs, to address the intermittent nature of renewables and improve overall grid stability.

When implemented in the EMS, the fractional-order PID (FOPID) allows for more precise control and regulation of the energy flow between the different components of the HESS. The controller considers the system's fractional order dynamics, which can be more accurate in describing its behavior than traditional integer-order PID controllers. Incorporating a FOPID controller into the EMS of an HEV leads to potential benefits such as:

1. Improved tracking of reference power signals
2. Reduced settling time
3. Enhanced robustness to system disturbances
4. Mitigating power fluctuations from renewable sources

The system maximizes energy economy and improves overall system performance by utilizing intelligent energy flow balancing and keeping the battery and SCs within their specified SoC ranges. Fig.3.14 shows the proposed EMS for HESS.

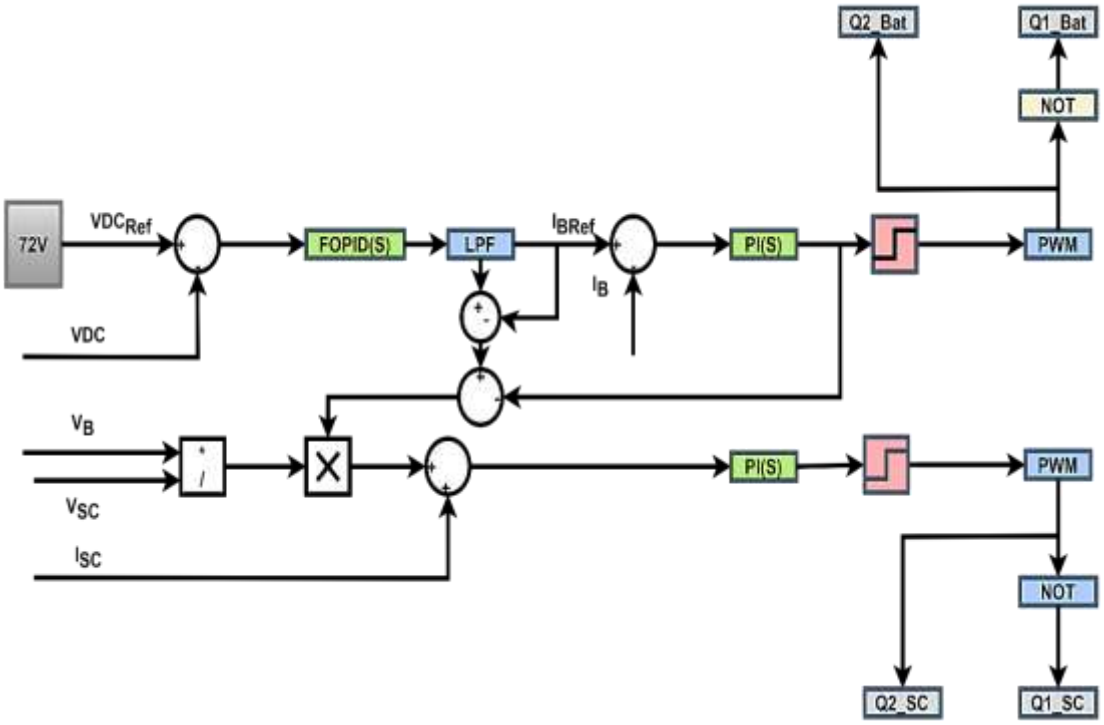

Fig.3.14: Proposed Energy Management System of Hybrid Energy Storage System-based FOPID Controller.

Each energy storage device in this design contains a bidirectional DC-DC converter to measure and compare system frequencies, hence improving the controllability and resilience of charge/discharge processes. Higher prices are a drawback, but overall savings should outweigh this. The battery can be charged while the supercapacitor is discharged thanks to separate bidirectional DC-DC converters. The controller detects three frequencies related to the grid: minimum permissible frequency ($Fmin$), maximum acceptable frequency ($Fmax$), and measured frequency ($Fmea$). Assume the reference frequency is 60Hz, 59Hz, and 61Hz for $Fief$, respectively. When the logic conditions are satisfied, the reference signal and the error signal generated by the FOPID block's comparator are routed. The switches are adjusted to carry out the intended charge/discharge operations [26]. FOPID controller's generalized transfer function is provided in (3.52):

$$C(s) = \frac{U(s)}{E(s)} = K_P + \frac{K_I}{S^{\lambda}} + K_D S^{\mu}, and\ (\lambda, \mu \geq 0) \quad (3.52)$$

where, C(s) is the output of the controller, U(s) is the signal due to control, E(s) is the signal of error , K_P is the gain of proportional constant, K_I is the gain of integration constant.

The transfer function of the PID controller is given in (3.53):

$$\frac{C(s)}{E(s)} = K_p + K_i \frac{1}{s} + K_d s \quad (3.53)$$

where the system's input is represented by E(s), and its output is denoted by C(s).

K_p, K_i, K_d is the proportional-integral-derivative gain.

The complete block diagram of our proposed system can be summarized in Fig.3.15.

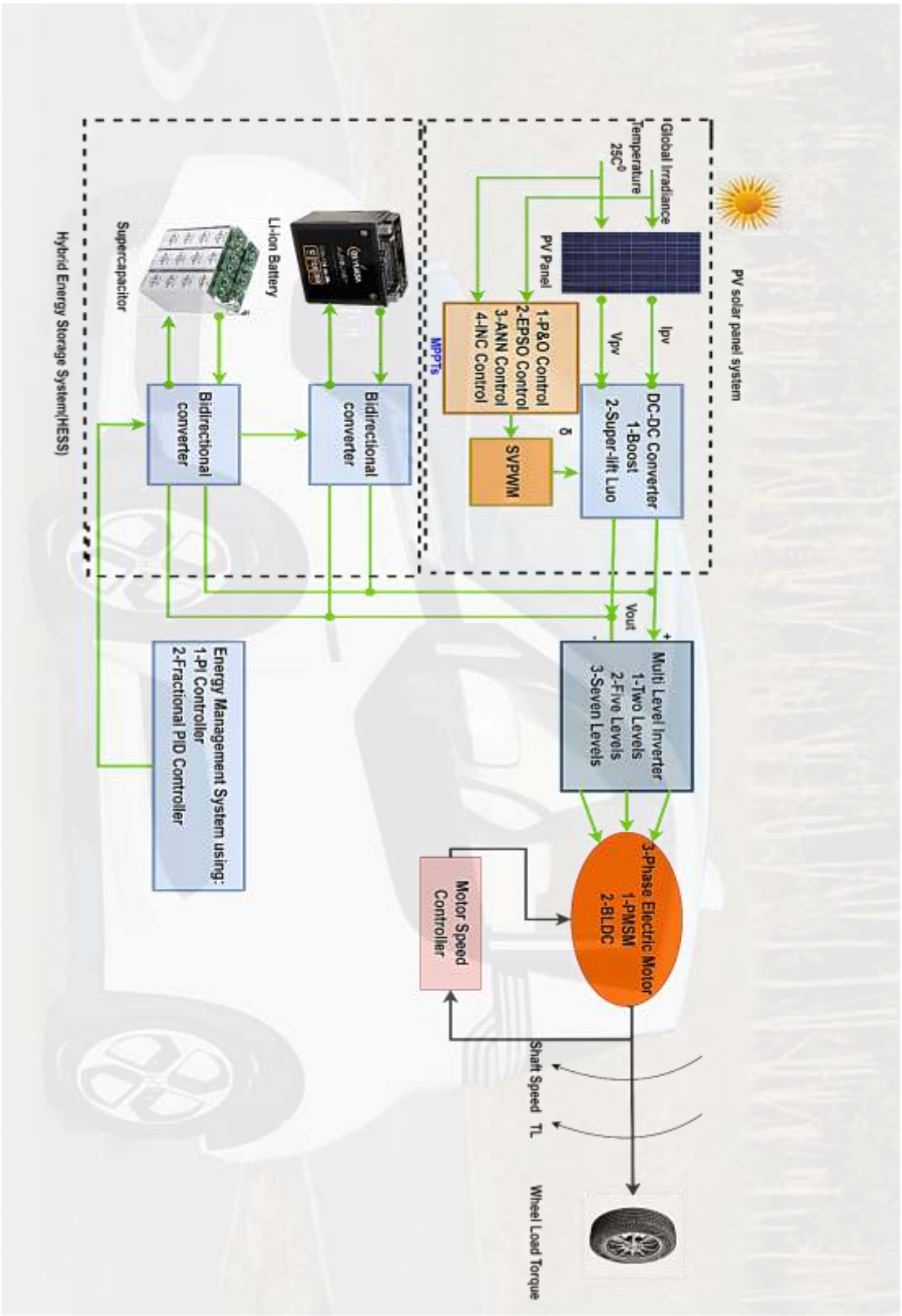

Fig.3.15: Proposed Hybrid Electric Vehicle System.

3.6 Path Tracking Control for Electric Vehicle

Adaptive model predictive control (AMPC) Analyzing the essential parts and workings of AHEV control for path tracking is crucial to understanding this technology. To optimize the vehicle's path tracking based on the present driving conditions, AMPC combines predictive modeling with real-time data from vehicle sensors. Investigating the principal elements and workings of AMPC is crucial to fully understand this technology's path-tracking advantages in AHEVs. To optimize the vehicle's path tracking based on the present driving conditions, AMPC combines predictive modelling with real-time data from vehicle sensors. Fig.3.16 shows the model of vehicle dynamics.

Path tracking is a procedure that depends entirely on the mathematical model of the vehicle (plant) because it is essential when designing the AMPC controller. A 4-wheel vehicle model was used to perform the path-tracking process using MPC, where the dynamics of Inclination and roll were neglected in the Vehicle model because there was no significant impact that might hinder the path-tracking process. The definition of the vehicle model is written in Table.3.3 below [132].

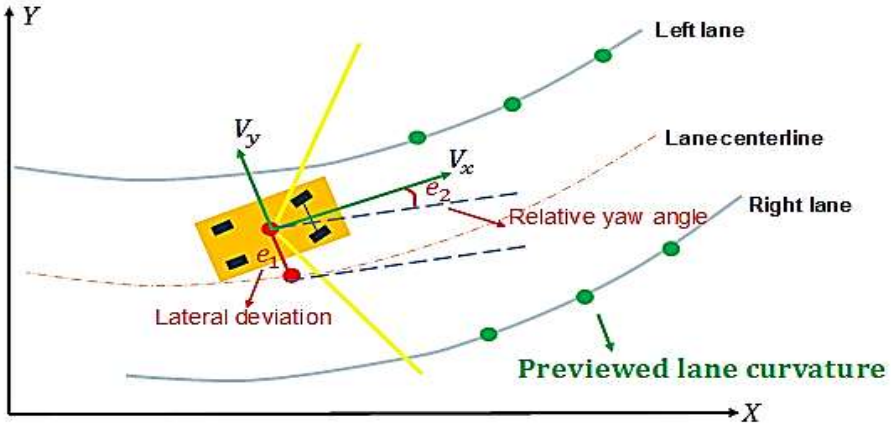

Fig.3.16 : Model of Vehicle Dynamics [133].

Table 3.3: Symbol and Explanation of Vehicle Model.

Symbol	Explanation
V_x	Longitudinal velocity
V_y	Lateral velocity
(X, Y)	Vehicle location globally
ψ	Yaw angle
δ	Frontal steering angle
Y_{ref}	References lateral position
ψ_{ref}	References yaw angle

The discrete state-space equation for the AHEV given by [133]:

$$X(k+1) = A_k X(k) + B_k u(k)` \tag{3.54}$$

$$y(k) = C_k x(k) \tag{3.55}$$

Ak, Bk, and Ck represent the state, control, and output matrices.

The lateral dynamics for the plant [134] :

$$\frac{d}{dt}\begin{bmatrix}\dot{y}\\ \psi\\ \dot{\Psi}\end{bmatrix} = \begin{bmatrix}\frac{-2C_{af}+2C_{ar}}{mV_x} & 0 & -V_x - \frac{2C_{af}\ell_f - 2C_{ar}\ell_r}{mV_X}\\ 0 & 0 & 1\\ \frac{-2\ell_f C_{af} - 2\ell_r C_{ar}}{I_z V_x} & 0 & -\frac{2{\ell_f}^2 C_{af} + 2{\ell_r}^2 C_{ar}}{I_z V_x}\end{bmatrix}\begin{bmatrix}\dot{y}\\ \psi\\ \dot{\psi}\end{bmatrix} + \begin{bmatrix}\frac{2C_{af}}{m}\\ 0\\ 2\frac{\ell_f C_{af}}{I_z}\end{bmatrix}\delta \tag{3.56}$$

The global $\dot{Y}$ is the position for the vehicle:

$$\dot{Y} = V_x \Psi + V_y \tag{3.57}$$

where,V_x is the longitudinal speed at the gravitational center; m represents the vehicle's total mass; I_z is the vehicle's yaw moment of inertia ;I_f is the longitudinal distance between the front tires and the center of gravity;I_r is the longitudinal distance between the rear tires and the center of gravity;C_a Tire cornering stiffness;δ is the front steering angle; Y Lateral position; Ψ It is called the Yaw angle.

3.6.1 Adaptive Model Predictive Control

Path tracking is dealt with in this part using a simple controller method called linear model predictive control, which is more effective than non-linear model

predictive control [135]. MPC finds the key to At each control interval, a quadratic program (QP) optimization issue is given. The correct response is to define the manipulated variables (MVs) employed in the plant until the subsequent control interval. The following characteristics apply to this QP issue:(1) A scalar, a nonnegative measure of controller performance that must be minimized, is the objective, or "cost," function. (2) MVs' physical bounds and plant output variables are a few examples of constraints that the solution must abide by (3) The chosen course of action is the MV change that meets the requirements and minimizes the cost function (J).

3.6.2 Standard Cost Function

The AMPC works to minimize the error between references and the planned output as small as possible to ensure the angle of a steering wheel keeps the vehicle's position within the allowed ranges, referred to as constraints [136],[137]. The sum of four terms makes up the typical cost function. Each focuses on a particular component of controller performance as follows:

$$J(zk) = Jy(zk) + Ju(zk) + J\Delta u(zk) + J\varepsilon(zk) \tag{3.58}$$

where z_k is the QP determination. The MPC controller comes with default weights, but you will typically need to change them to adapt the controller to the application.

3.6.3 Reference Tracking for Output

For most applications, the controller must maintain specific plant outputs at or near predetermined reference values. An AMPC controller utilizes the following scalar performance metric for output reference tracking. By default, MPC updates its controller states, including the plant model states, using a static Kalman filter (KF). Two gain matrices, L and M, are needed for this KF. By default, the MPC controller computes these at initialization.

They are dependent on the predictions made about the random noise signals that power the noise and disturbance models, as well as the characteristics of the plant, disturbance, and noise models.

Adaptive MPC maintains coherence with the updated plant model by using a Kalman filter and adjusting the gains, L and M, at each control interval. A linear-time-varying Kalman filter (LTVKF) is the outcome [138]:

$$L_k = (A_k P_{k|k-1} C_{m,k}^T + N)(C_{m,k} P_{k|k-1} C_{m,k}^T + R)^{-1} \quad (3.59)$$

$$M_k = P_{k|k-1} C_{m,k}^T (C_{m,k} P_{k|k-1} C_{m,k}^T + R)^{-1} \quad (3.60)$$

$$P_{k+1|k} = A_k P_{k|k-1} A_k^T - \left(A_k P_{k|k-1} C_{m,k}^T + N\right) L_k^T + Q \quad (3.61)$$

In this case, the constant covariance matrices Q, R, and N are defined as in the MPC state estimation. The state-space parameter matrices A_k and $C_{m,k}$ represent the controller state as an entire thing; they are defined similarly to traditional MPC but with the plant model's effects updated to time k. Based on information available at time k–1, the state-estimated error covariance matrix at time k is represented by the $P_{k|k-1}$ value. Lastly, the modified KF gain matrices are L_k and M_k. The static KF solution, $P_{0|-1}$, is the initial condition by default before any model modifications.

The model parameters and the assumptions that result in the constant Q, R, and N matrices determine the KF gain and the state error covariance matrix. The formulas for L_k and M_k, converge to the corresponding static KF solution used in conventional MPC if the plant model is constant.

The KF formulation of classical MPC, as detailed in Controller State Estimation, is the same as the equations for the controller state evolution at time k, in addition to the state space matrices and estimator gains updated to time k.

The cost function (j) for the optimizer is given by ;

$$j = \sum_{i=1}^{p} w_e e_k + i^2 + \sum_{i=0}^{p-1} w_{\Delta k} \Delta wk + i^2 \quad (3.62)$$

where p is the left side of the equation, indicates the sum of the predicted errors, and the right side indicates the sum of the steering wheel angle.

To find the optimal balance for Time sampling (T_s) from the given in (3.63):

$$\frac{T_r}{20} \leq T_s \leq \frac{T_r}{10} \quad (3.63)$$

where is; the (T_r) is the rise time of the controller.

The torque ripple can be computed by (3.64):

$$T_{ripple} = T_{max} - T_{min} / T_{avg} \quad (3.64)$$

Chapter Four: Simulation Results and Discussion

4.1 Introduction

As explained in chapter three, the current chapter will investigate the system's performance. The results will be based on comparing motor speed controllers(sliding model control, Backstepping, and enhanced field-oriented control). The comparison will depend on three scenarios. The first scenario(Sc1) will involve a constant reference torque and a variable reference speed. In the second scenario(Sc2), the reference torque will be varied while the reference speed is constant. The third scenario(Sc3) will depend on the suggested vehicle structure to obtain the reference speed and load torque profile that depends on the accelerator. Fig.4.1 shows the reference scenarios in this study. This chapter will compare PMSM and BLDC motors based on several previous scenarios to determine the best options.

The dynamic performance of the multi-level Inverters (two levels, five levels, and seven levels) will be presented in this chapter, depending on a comparison between the different MLIs.

The MPPTs optimization methods will presented based on a comparison depending on several scenarios of irradiance (1000 W/m^2 , 400 W/m^2,1000 – 400 W/m^2 , global irradiance) select the high-performance MPPT for the HESS in the proposed system.

This chapter will analyze the performance of the Boost and Super_lift luo converters in HESS and determine which converter is best for the system based on global irradiance.

The high-performance techniques for the adaptive hybrid vehicle will be chosen after completing all prior comparisons.

The enhanced speed control methods of the electric motor will be integrated with the chosen system to get intelligent control.

This chapter will present and analyze the energy management system and adaptive MPC performance with the proposed system.

This part presents the simulation results using Matlab/Simulink to illustrate and validate the system's operation and the developed control method. The sample time used in this model is 5µs.

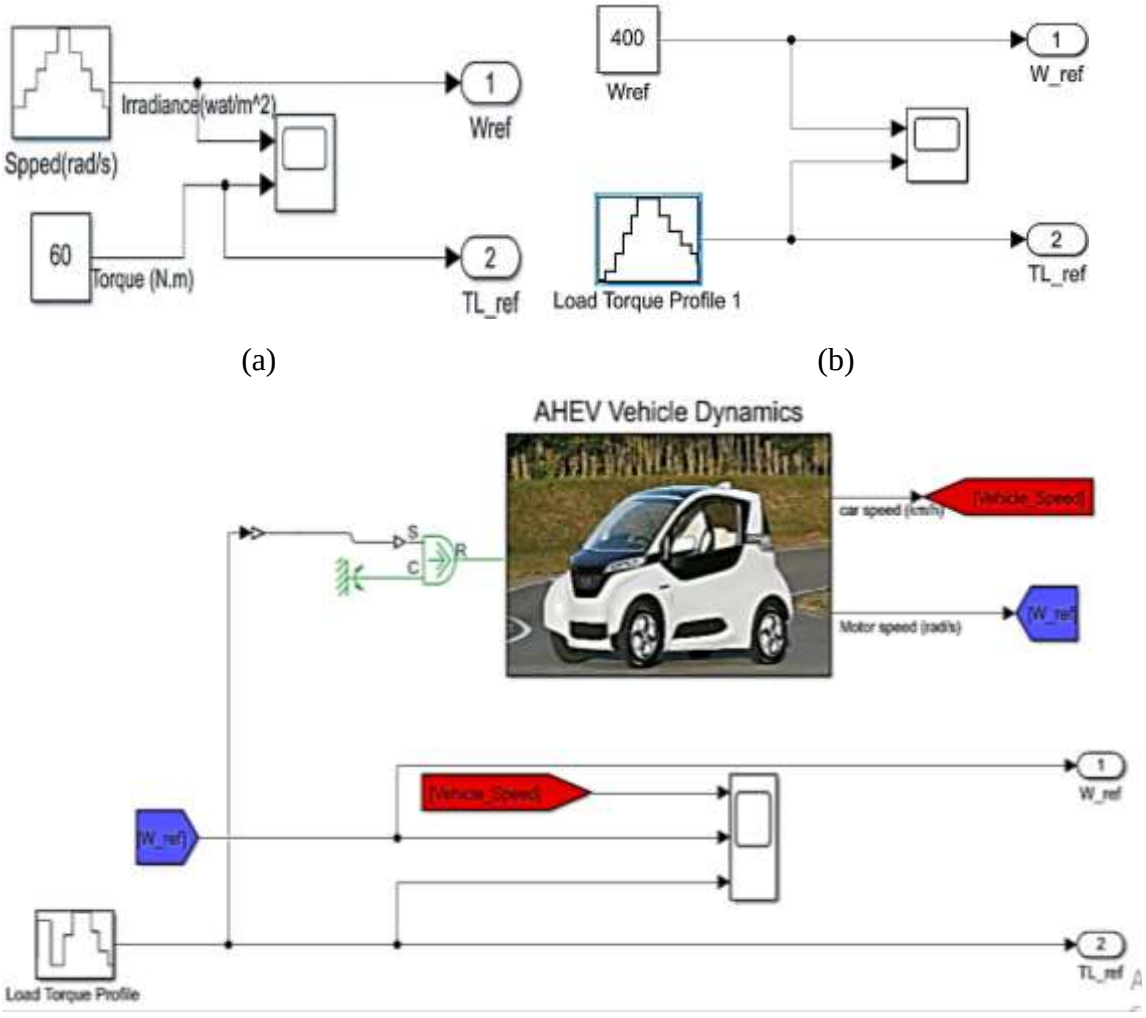

Fig.4.1: Reference Torque and Speed Profile (a) First Scenario,(b) Second Scenario,(c) Third Scenario.

4.2 Best Selection of Electric Motor for Present Work

In the field of electric motors, two notable competitors are PMSM and BLDC. Both perform well in different situations, but choosing one can be crucial. The analysis delves into the key factors that differentiate these motors, focusing on speed and torque ripple, starting current, compatibility with HESS, tracking speed and torque accuracy, and finally, total harmonic distortion (THD). It will be well-equipped to choose the motor that best meets its needs if these factors are understood.

4.2.1 First Scenario Results

Fig.4.2(a) represents the performance of both motors in speed tracking. By observing the figure, the PMSM generally provides more stable superior variable speed tracking capabilities and less fluctuating than BLDC. The reason is that BLDC has a trapezoidal back EMF, which results in uneven torque production throughout the rotation. It is unevenness, known as torque ripple, can cause fluctuations in speed as the motor attempts to maintain a desired setpoint. In contrast, PMSMs boast a sinusoidal back EMF. It translates to a smoother and more consistent flow of torque, minimizing these disruptive fluctuations and enabling the motor to track speed changes more precisely. Fig.4.2(b) shows that the PMSM has smoother output constant torque and fewer fluctuations than BLDC. The reasons of that are the inherent sinusoidal nature of PMSMs leads to smoother torque production, minimizing fluctuations and enabling better constant torque output at variable speeds, and simpler PMSM control schemes allow for faster and more precise adjustments, ensuring the motor maintains the desired torque even during speed changes.

On the other hand, the BLDC has trapezoidal back EMF, which means the voltage induced in the motor windings as they rotate is not constant throughout the rotation cycle. This results in fluctuations in torque production, leading to jerkiness and inconsistencies in maintaining a continuous torque output at varying speeds. These factors make PMSMs the preferred choice for applications requiring smooth and highly accurate constant torque control at variable speeds, such as industrial robots, electric vehicles, and precision control machinery. The fluctuations due to no motor are perfect. Manufacturing tolerances and imperfections in materials can lead to slight variations in magnetic field strength and back EMF. These variations can cause minor torque ripples even in PMSMs. BLDCs are generally more susceptible to these imperfections due to their reliance on discrete permanent magnets and stator windings. Fig.4.2(c) shows that the BLDC has a higher starting current than PMSM because BLDC motors depend on the interaction of a solid initial magnetic field between the stator windings and rotor magnets to start rotation. A high current must be supplied to the windings during start-up to generate this strong field quickly. The high current translates to a surge in the starting current for the BLDC motor. PMSMs, on the other hand, benefit from the inherent alignment between the rotor magnets and the generated magnetic field in the stator. That alignment creates a more natural starting torque, requiring less initial current to overcome inertia and begin rotation. The gain parameters of the backstepping controller for the first scenario are (k1=675.9,k2=414.9,k3=2000).

$$Max\ I_{dc-BLDC} = 10.2\ A,\ Max\ I_{dc-PMSM} = 9.85\ A$$

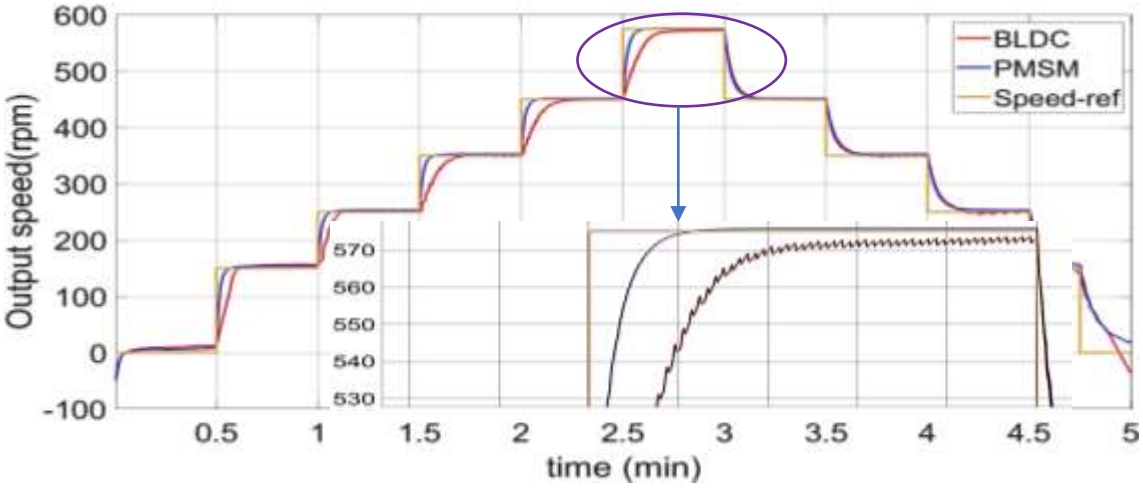

(a)

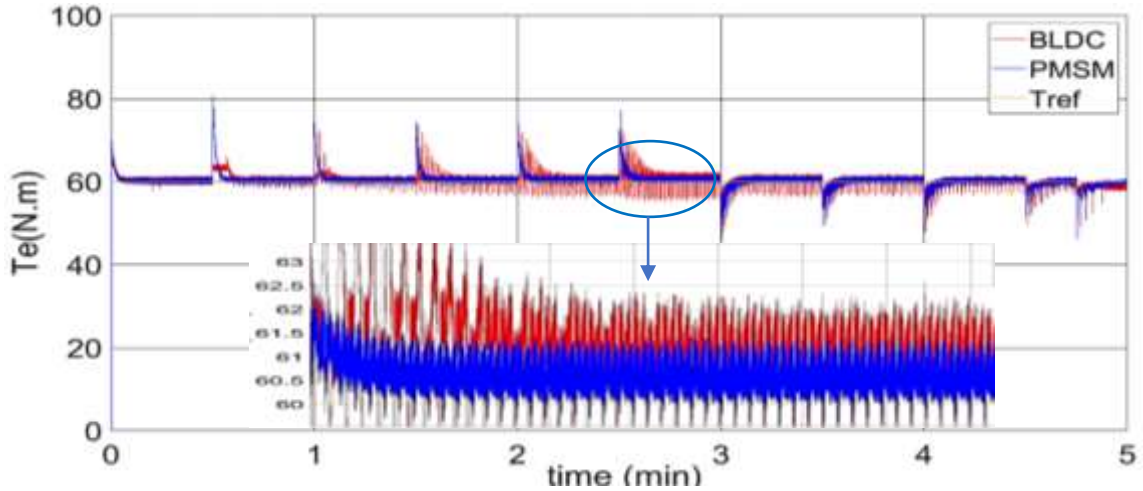

(b)

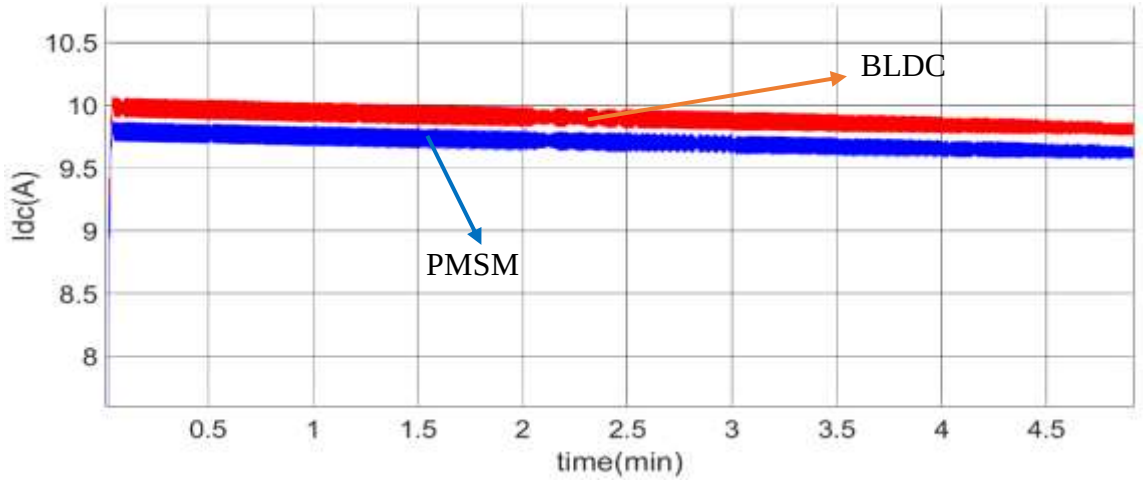

(c)

Fig.4.2: System Response for First Scenario (a)Output Speed, (b)Output Torque, (c)Starting DC-Current.

BLDC and PMSM torque ripple calculations can be complex and involve specialized software or engineering expertise. Advanced control techniques can be employed in both motors to minimize torque ripple. These techniques involve current control strategies, sensor feedback, and advanced control algorithms. Torque ripple is defined as the ratio of the peak-to-peak value of torque to its average value.

$T_{ripple-BLDC} = 35\%, T_{ripple-PMSM} = 2.5\%$

As seen above, the PMSM has a lower torque ripple than BLDC.

4.2.2 Second Scenario Results

The results of the two motors are displayed in Fig. 4.3, assuming that the second scenario will occur. It is clear from Fig. 4.3(a) that a change in torque immediately affects speed, and after that, the controller attempts to move it back into position. It is observed that overshot and ripple are more with the BLDC. From Fig 4.3(b), It is evident that both motors respond similarly to output torque tracking; however, the BLDC has a significant torque ripple when the torque reaches 60 N.m. The gain parameters of the backstepping controller for the first scenario are (k1=668,k2=320,k3=3000).

Torque ripple calculation: $T_{ripple-BLDC} = 5.6\%, T_{ripple-PMSM} = 0.7\%$

BLDC torque ripple is caused mainly by its trapezoidal back EMF waveform. The rotor magnets' synchronization with the stator windings causes the BLDC's back EMF to have sharp transitions, in contrast to the smooth, sinusoidal back EMF of PMSMs. The ripple effect is caused by variations in the motor's torque output due to sudden shifts in back EMF. Fig.4.3 (c) shows the DC response of both motors. The reason is that BLDC motors require a strong initial magnetic field interaction between the rotor magnets and stator windings to initiate rotation. A high current must be supplied to the windings

during start-up to generate this strong field quickly. This translates to a surge in starting current for the BLDC motor.

$Max\ I_{dc-BLDC} = 7.2A, Max\ I_{dc-PMSM} = 5.4\ A.$

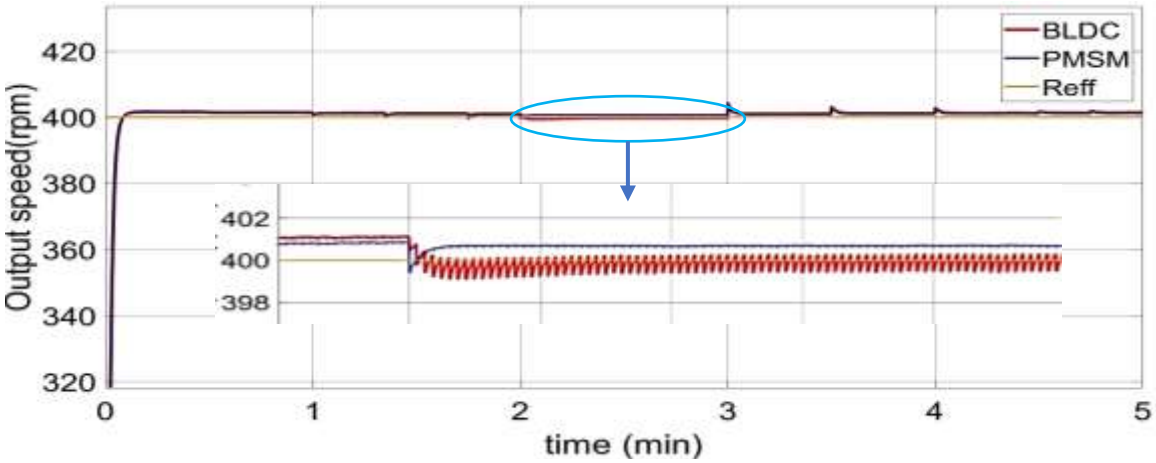

(a)

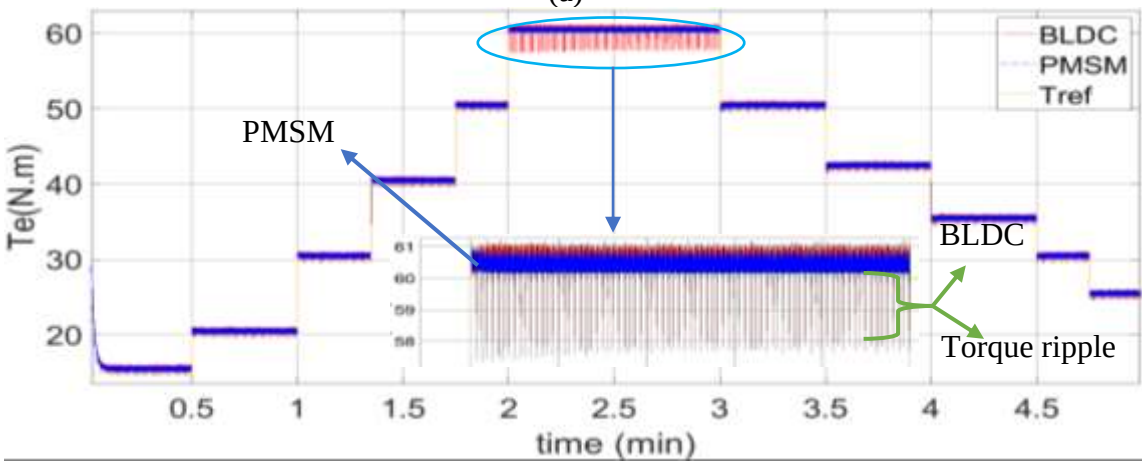

(b)

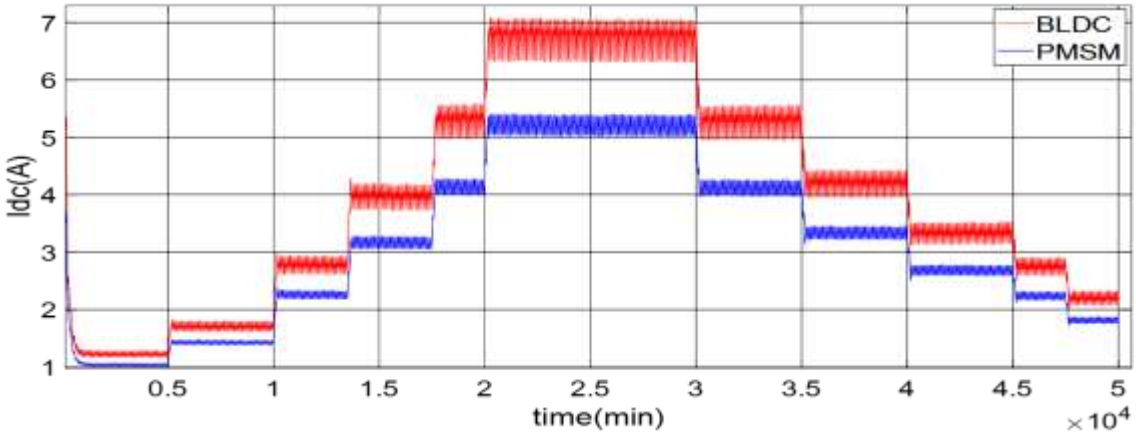

(c)

Fig.4.3: System Time Response for the Second Scenario (a)Output Speed, (b) Output Torque, (c)Starting DC_ Current.

4.2.3 Third Scenario Results

The results of the two motors for the third scenario are displayed in Fig.4.4 (a&b), which show the output speed and torque response.

In a variable speed and variable torque scenario, PMSMs offer superior performance due to their inherent characteristics and control advantages. The sinusoidal back EMF, simpler control schemes, and sensorless control options all contribute to their ability to track speed changes more precisely with minimal fluctuations and overshoot. While BLDC control techniques are constantly evolving, these inherent advantages solidify PMSMs as the preferred choice for applications demanding high precision control in variable speed and torque conditions. These advantages solidify PMSMs as the preferred choice for applications demanding high precision control in variable speed and torque environments, such as robotics, electric vehicles, and industrial automation. The gain parameters of the backstepping controller for the first scenario are (k1=668,k2=320,k3=1100).

Torque ripple: According to eq (3.64).

$T_{ripple-BLDC} = 16.5\%, T_{ripple-PMSM} = 1\%$

Fig.4.4(c) illustrates that the BLDC motor has a more significant DC-current than the PMSM in the variable speed and torque scenario.

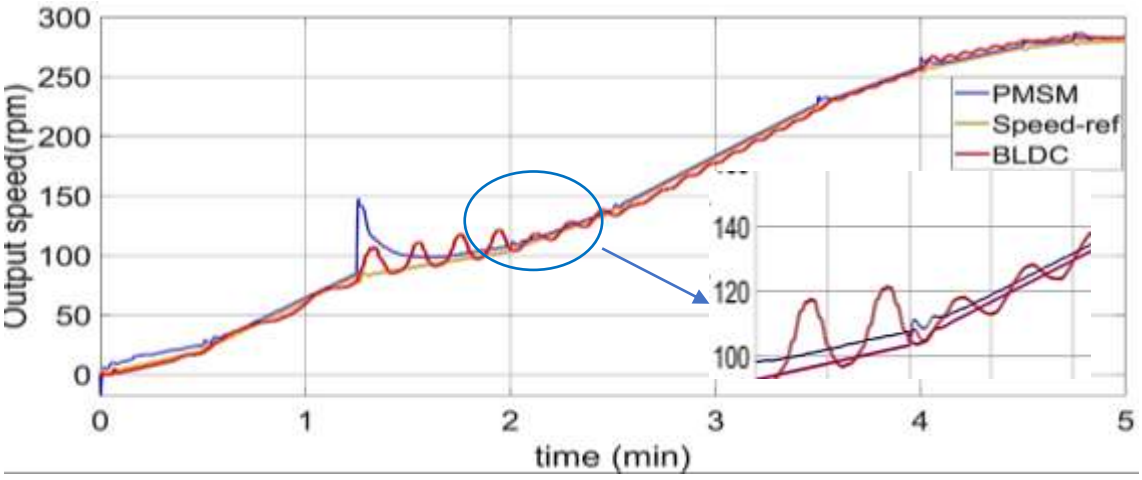

(a)

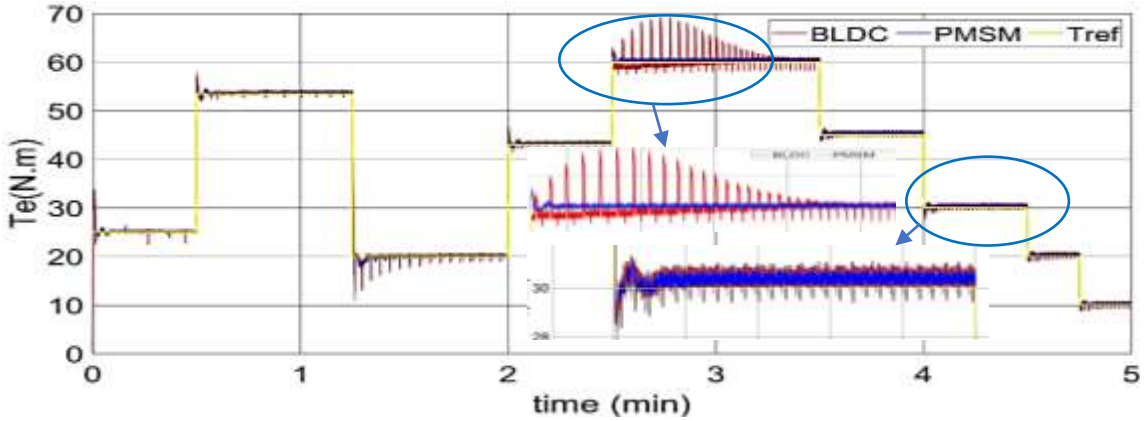

(b)

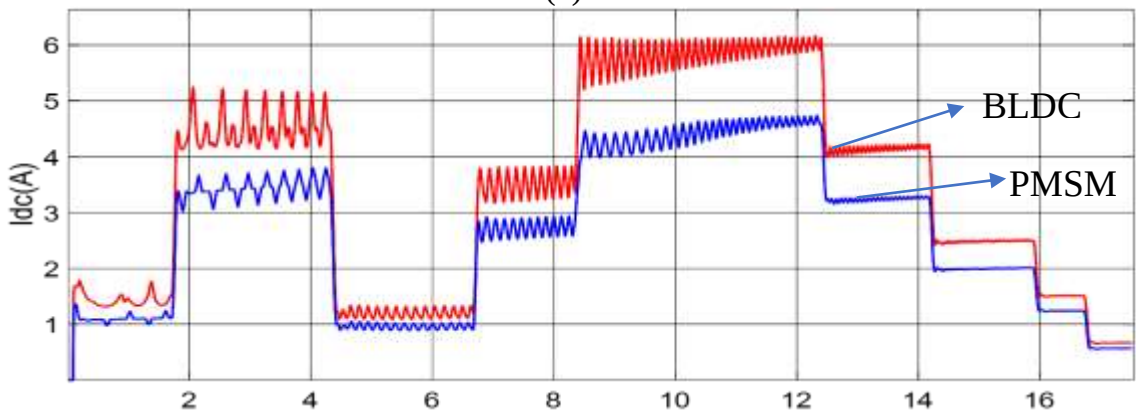

(c)

Fig.4.4: System Response Model for the Third Scenario (a)Output Speed,(b)Output Torque,(c)Starting DC_Current.

Table 4.1 shows that PMSM and BLDC depend on the HEV system results.

Table 4.1 Comparison between PMSM and BLDC under Different Scenarios.

Feature	PMSM	BLDC
Torque Production	Smoother, sinusoidal back EMF	Uneven, trapezoidal back EMF (torque ripple)
Control Scheme	Simpler, directly aligns with back EMF	More complex, needs to compensate for back EMF
Sensorless Control	Possible estimates based on back EMF	It is not ideal; it relies on physical sensors
Speed & Torque Tracking	More precise, faster response	Less precise, potential delays
Fluctuations	Less fluctuation due to smoother torque	More fluctuations due to torque ripple
Overshoot	Minimized due to faster response	This can occur during speed/torque changes

4.3 Speed Controllers Comparisons

The chosen speed controller heavily influences the performance of a PMSM. This comparison dives into three prevalent control techniques: SMC, Backstepping Control, and EFOC. It will analyze their strengths and weaknesses, but it is crucial to recognize that the optimal choice hinges on the specific application's speed and torque profile. Here is why understanding the scenario matters:

a) The application prioritizes rapid acceleration, high constant speed, and precise torque control during operation. The desired dynamics will influence which controller offers the best trade-off between performance and complexity.

b) The evaluation will focus on critical parameters like output torque, tracking torque errors, tracking speed (ability to maintain reference speed), tracking speed error, and their impact on the system's power dynamics, including photovoltaic power input, DC bus voltage (V_{dc}), and direct current (I_{dc}).

4.3.1 Traditional Power Electronic Inverter

4.3.1.1 First Scenario Results

Fig.4.5 compares speed controller results depending on variable speeds and constant torque. After zooming the peak output speed response in Fig. 4.5(a), the backstepping control responds more accurately in variable speed scenarios than the other controller. Backstepping control employs a systematic process in which every action builds on the one before. The controller can better maintain the intended speed reference by adjusting its output and explicitly considering the speed variations. It allows control law to incorporate variable

speed dynamics of variable speed directly. By explicitly considering the speed variations, the controller can adjust its output more effectively to maintain the desired speed reference. Fig 4.5(b) shows the controller's constant torque response. All controllers have the same reaction with less distortion for the backstepping control. The main reason is that Backstepping control's efficacy depends on accurate controller tuning. Torque distortion can be considerably reduced with carefully selected parameters.

$T_{ripple-EFOC} = 4.5\%, T_{ripple-SMC} = 2.5\%, T_{ripple-Backstepping} = 3.34\%$

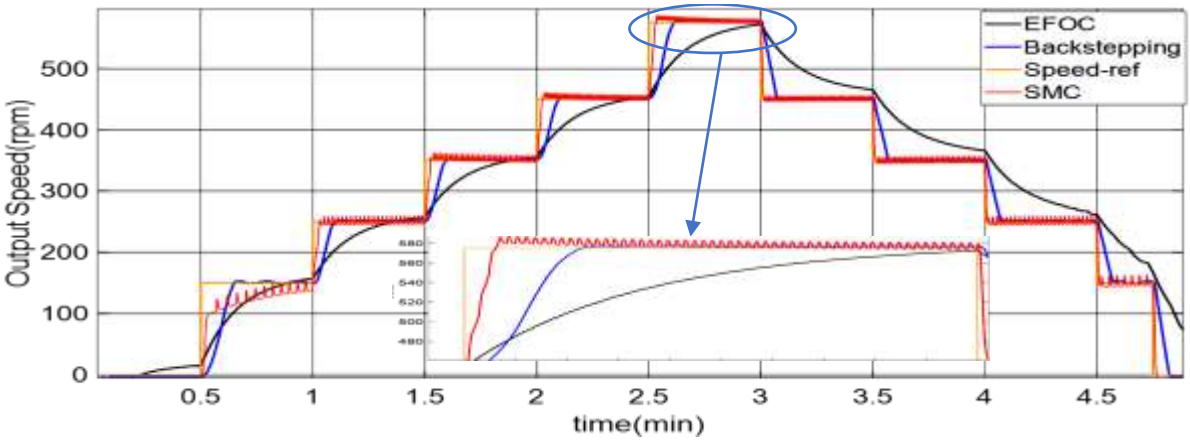

(a)

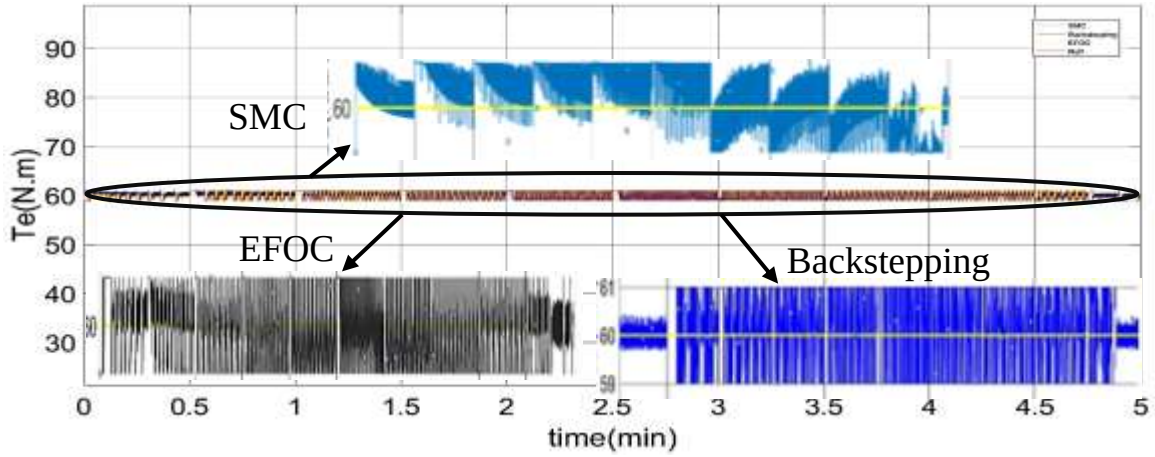

(b)

Fig.4.5: System Response for First Scenario (a) Output Speed,(b) Output Torque.

Fig.4.6 shows the controllers' speed tracking error. Based on the previous discussion, backstepping control generally offers the best speed-tracking error due to performance among the three controllers (SMC, Backstepping, EFOC) for PMSM. Error integration causes it to accumulate speed variations gradually, and this data is used to modify the control signal, improving tracking accuracy over time.

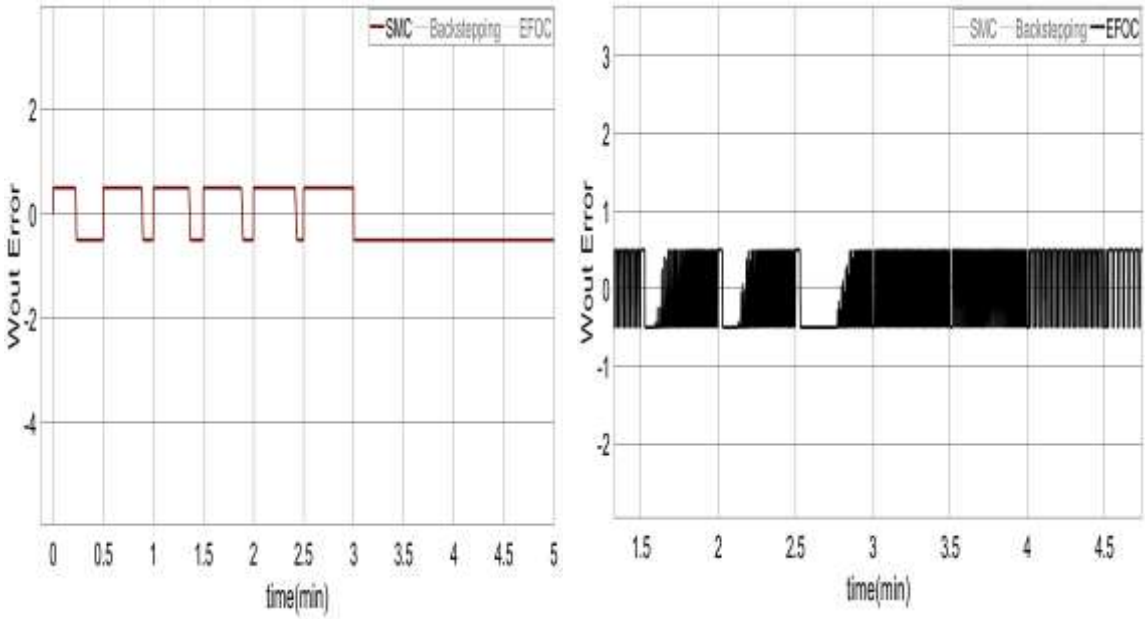

(a) (b)

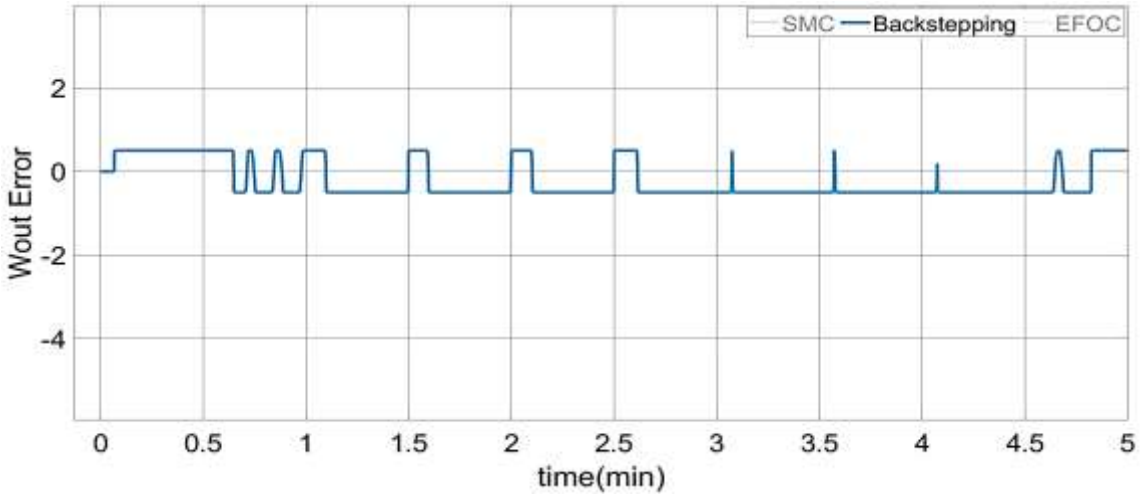

(c)

Fig.4.6 : Speed Tracking Error (a) SMC,(b) Enhanced FOC,(c) Backstepping Control.

4.3.1.2 Second Scenario Results

Fig.4.7 shows the controllers response to constant speed and variable torque. As seen in Fig.4.7(a), The backstepping control's fast response, low distortion, and low fluctuations make it ideal for situations involving variable torque and constant speed. Backstepping's flexibility and error-minimization capabilities make it a strong option for these challenging circumstances, even though correct tuning and other computational constraints require consideration. Fig.4.7(b) shows that EFOC has more significant torque vibrations in variable torque situations than backstepping control. Due to the focus on torque control, EFOC prioritizes precise torque control. It may not be as good at limiting torque ripple as Backstepping control, which focuses on overall system stability and lowers errors, even if it can sometimes handle speed variations.

$T_{ripple-EFOC} = 37\%, T_{ripple-SMC} = 5.84\%, T_{ripple-Backstepping} = 3.55\%.$

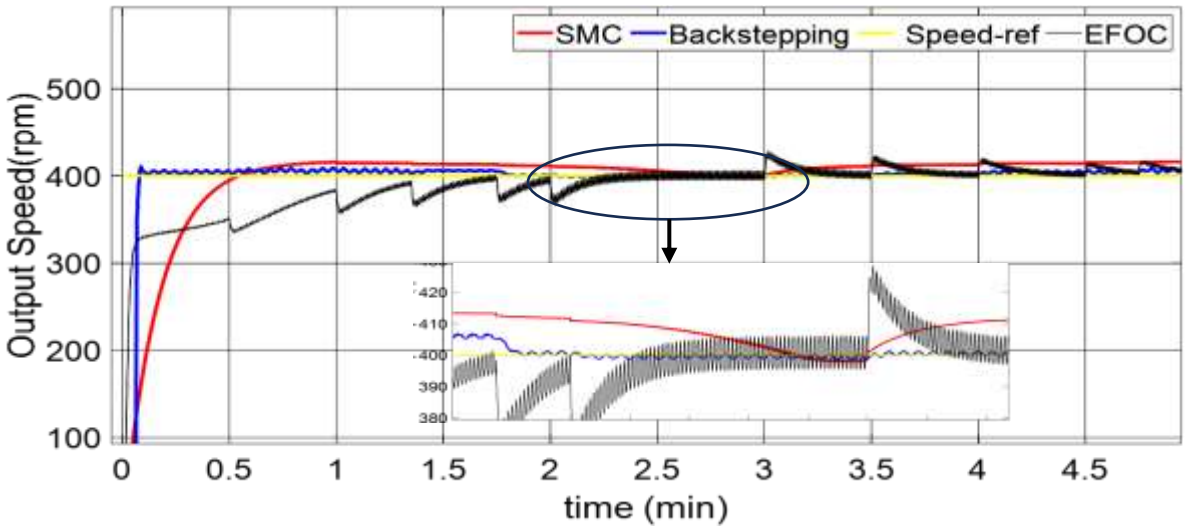

(a)

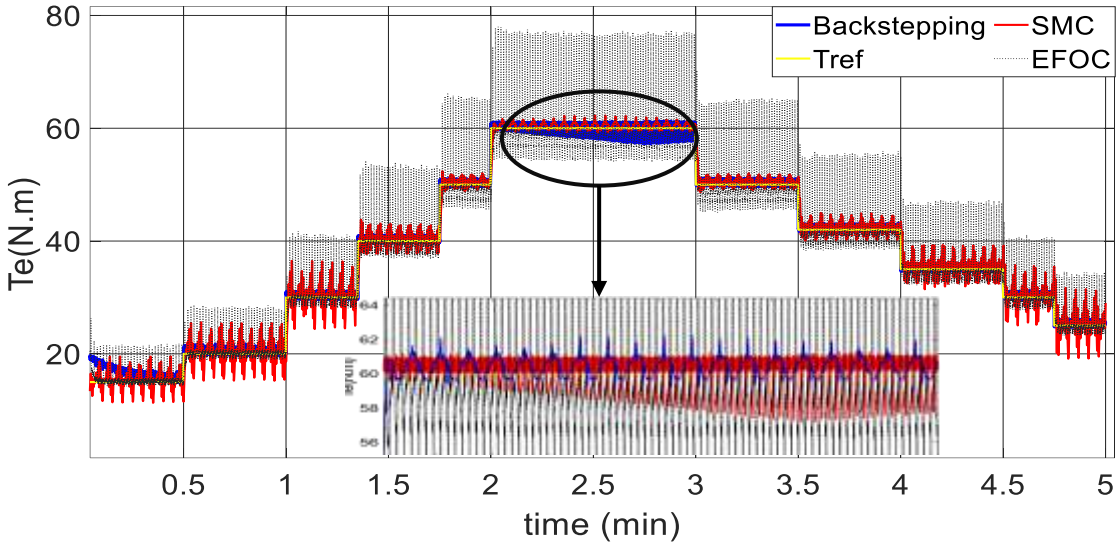

(b)

Fig.4.7: System Response Model for Second Scenario (a) Output Speed,(b) Output Torque.

4.3.1.3 Third Scenario Results

Fig.4.8 shows the controller's response for the variable speed and torque scenario. Based on our discussion, Backstepping control emerges as the frontrunner for several critical aspects in controlling PMSMs, mainly when dealing with variable speed and torque:

a) Backstepping excels at tracking speed and torque references due to its systematic design, error integration, and ability to handle uncertainties.

b) Focusing on stability and error minimization during design leads to smoother operation and minimal distortion in the output.

c) Backstepping's ability to continuously learn and adjust for errors helps reduce torque ripple, especially during rapid changes in torque demand.

d) Combining these factors allows Backstepping to achieve high accuracy in tracking speed and torque references.

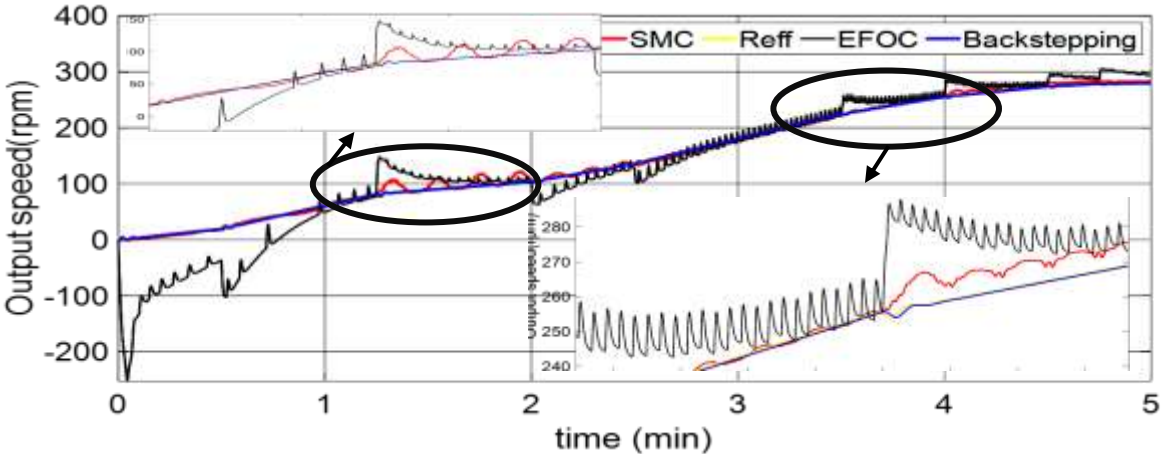

(a)

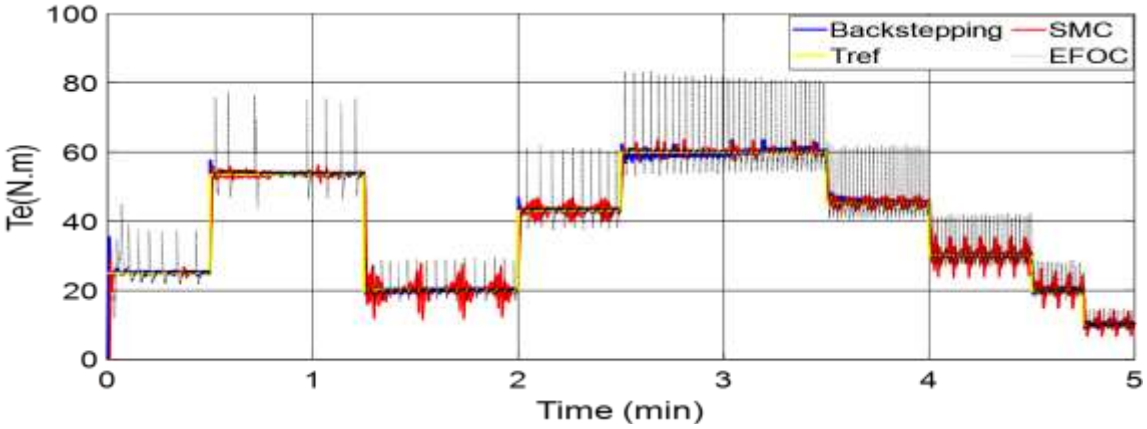

(b)

Fig.4.8: System Response for the Third Scenario (a) Output Speed,(b) Output Torque.

Here's Table 4.2 summarizing the key points:

Table 4.2 Simple Comparison between EFOC, Backstepping, and Slide Mode Controllers.

Feature	Backstepping Control	SMC	Enhanced FOC
Variable Speed Tracking	Best	Good	Good
Torque Ripple	Low	Low	High
Distortion	Low	Moderate	High
Complexity	High	Moderate	Low
Computational Resources	High	Low	Low

Backstepping control is a strong option for HEV applications because of its flexibility, improved tracking performance, and capacity to reduce torque ripple. The possible advantages for overall performance, drivetrain efficiency, and passenger comfort outweigh the implementation hurdles. Backstepping control is an excellent option for HEVs that stress smooth operation and accurate control.

4.3.2 Speed Controllers with Multi-Level Inverter

As PMSMs are highly controllable and efficient, they are widely used in many applications. On the other hand, traditional two-level inverters have the potential to produce significant harmonics, which raises motor losses and torque ripple. Here, it will explore the relationship between the advantages of employing a 7-level MLI in PMSM drives and the control strategy selection. Best control approaches will be the main emphasis of this comparison:

- SMC
- Backstepping Control

It will examine how each controller makes the most of a seven-level MLI to maximize PMSM drive performance.

4.3.2.1 First Scenario Results

The reason for the removal of the EFOC method was that it was an outdated approach with numerous issues.

Fig.4.9 shows the speed controllers with MLI in the first scenario's system response.

Fig.4.9(a,b) presented that Backstepping control is beneficial for utilizing a 7-level MLI in a PMSM drive since it can handle varying speeds, integrate errors, and take advantage of the MLI's more precise voltage control. The combination leads to superior speed-tracking performance and lower speed-tracking errors than the SMC control technique.

As seen in Fig.4.9(c,d) below, backstepping control offers several advantages that lead to lower torque ripple and a better torque response than SMC. The reason is that backstepping can react to slight variations from the desired constant torque reference more quickly due to its continual learning and error-adjusting capability, which results in better overall torque flexibility, particularly in quick situations.

Toque ripple calculations:

$T_{ripple-SMC} = 3.34\%,\ T_{ripple-Backstepping} = 0.62\%$

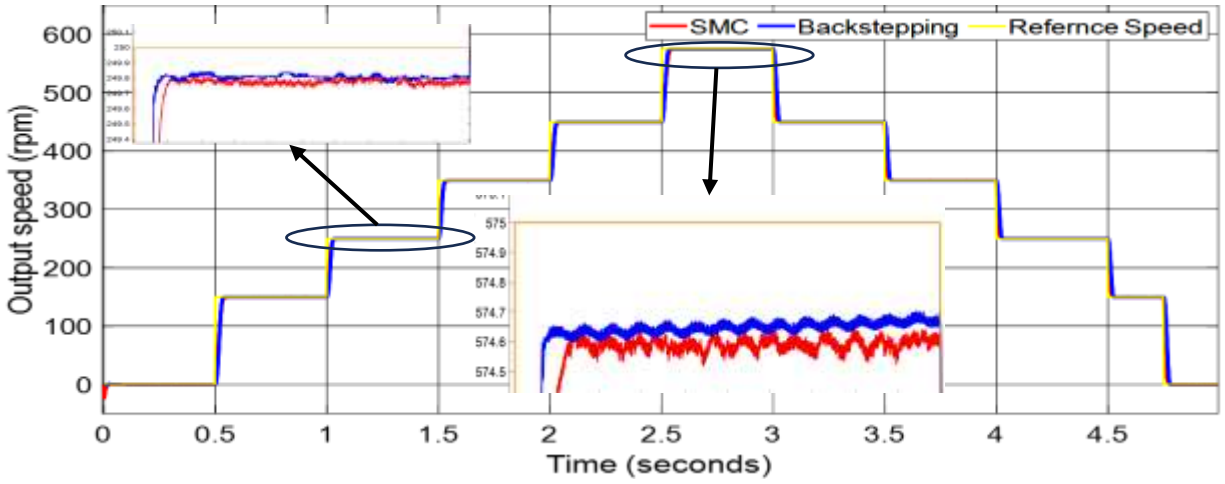

(a)

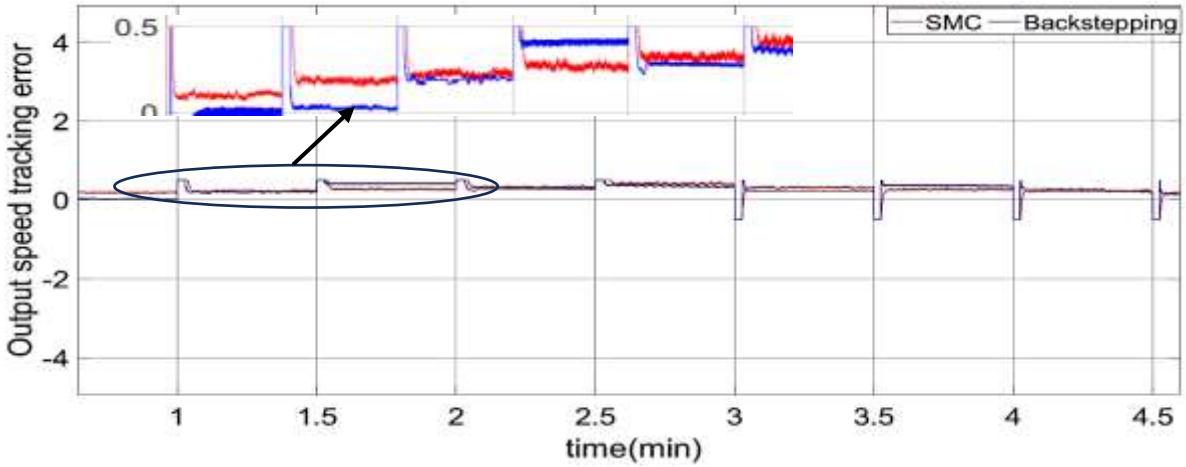

(b)

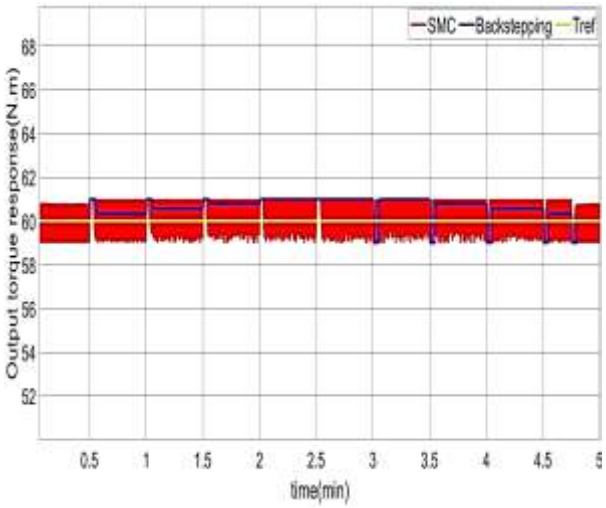

(c)

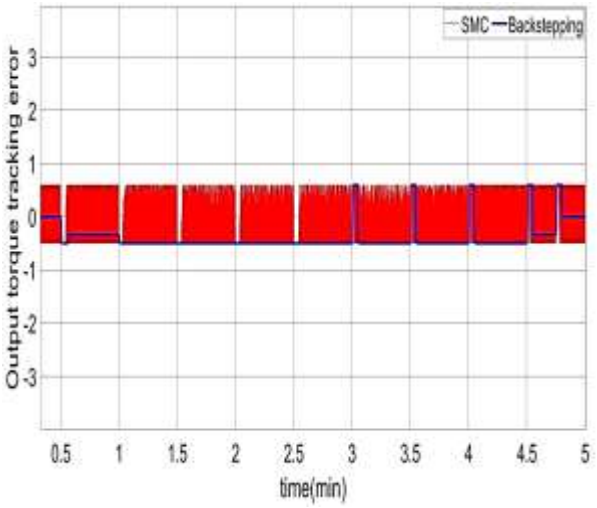

(d)

Fig.4.9: System Response for the First Scenario (a) Output Speed,(b) Speed Tracking Errors,(c) Output Torque,(d) Torque Tracking Error.

4.3.2.2 Second and Third Scenario Results

Fig.4.10 shows the scenarios' speed response and tracking errors for the second and third scenarios. Although both controllers can operate in situations with varying speeds, backstepping control performs slightly better in speed tracking, reduces errors in speed tracking, and shows less speed fluctuation. That is because of its design philosophy, emphasis on error minimization, and capacity to take advantage of the finer control offered by the 7-level inverter. Backstepping control is recommended for applications requiring the most accurate speed control.

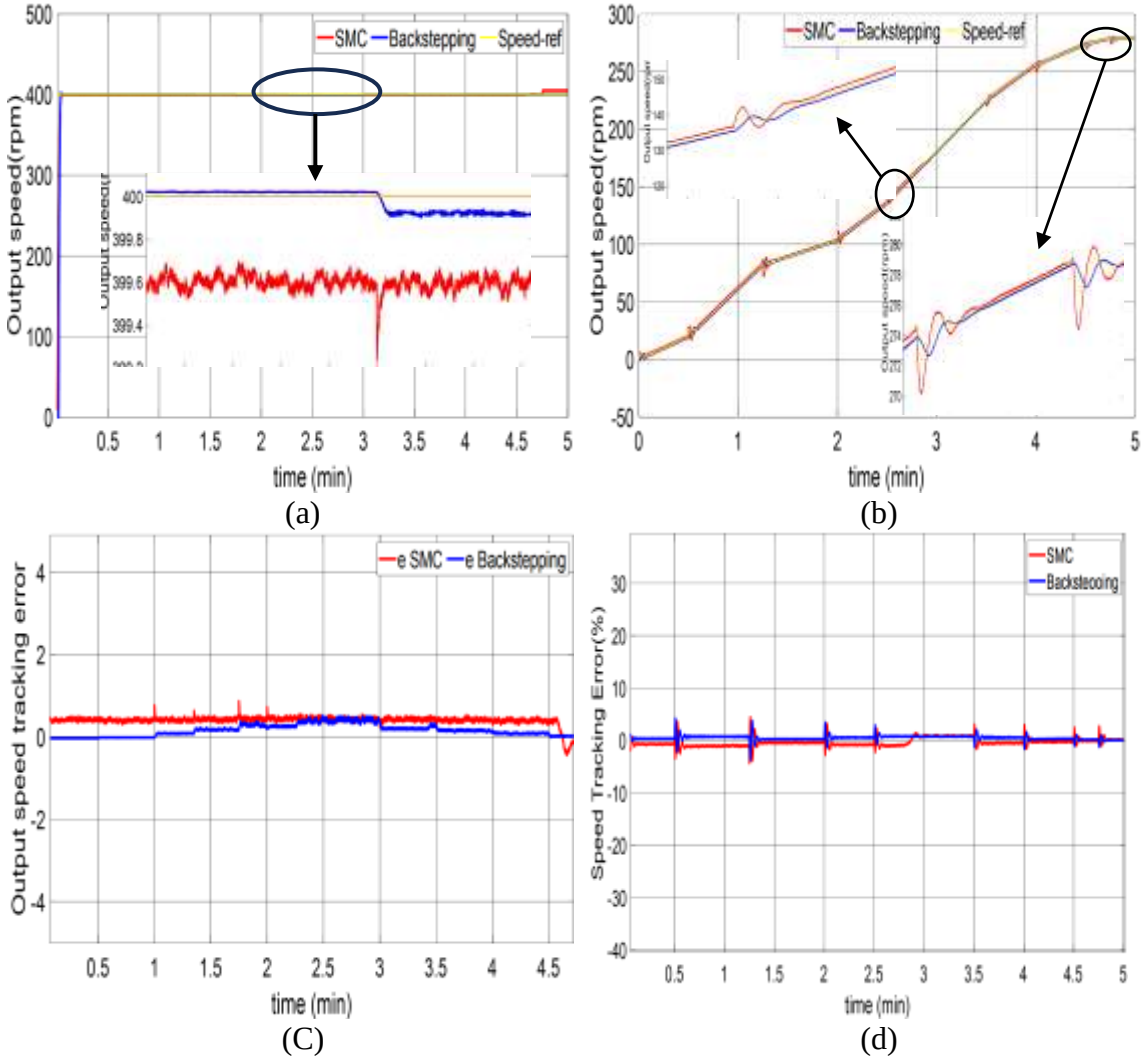

Fig.4.10 : Output Speed of (a) Second Scenario,(b) Third Scenario,(c)Second Scenario Speed Tracking Error,(d) Third Scenario Speed Tracking Error.

Fig.4.11 shows scenarios' torque-speed response and tracking error (2&3). The best option for scenarios requiring accurate and responsive torque control is backstepping control. Particularly in changing torque scenarios, its design philosophy, capacity to take advantage of the 7-level MLI's finer control, and emphasis on error minimization help produce better torque tracking, fewer torque tracking errors, and less torque ripple. Although both controllers can operate, Backstepping control provides a significant advantage in scenarios 2 and 3.

As seen in Fig.4.11(b), the SMC has some overshoot in torque response in Scenario 3 (variable speed and variable torque) for a PMSM drive using a 7-level MLI due to reaching the switching boundary in SMC, the controller rapidly switches between different control actions based on the system state. In Scenario 3, with both speed and torque references changing, SMC might reach the boundary conditions for switching more frequently. As a result, the torque response may overshoot as the controller alternates between several control actions, exceeding the target torque value before settling.

Torque ripple calculations

Sc2:

$$T_{ripple-SMC} = 0.25\%, T_{ripple-Backstepping} = 0.12\%$$

Sc3:

$$T_{ripple-SMC} = 1.333\%, T_{ripple-Backstepping} = 0.083\%$$

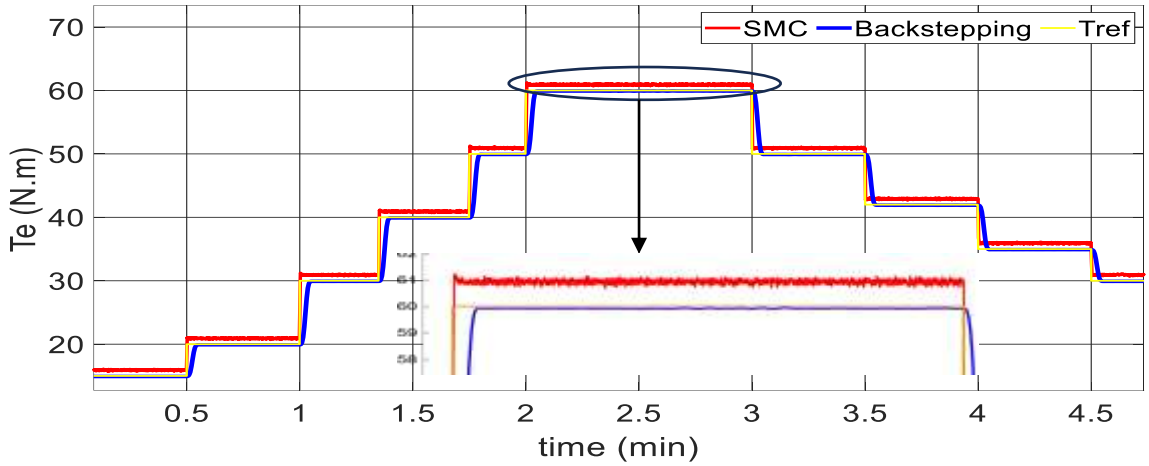

(a)

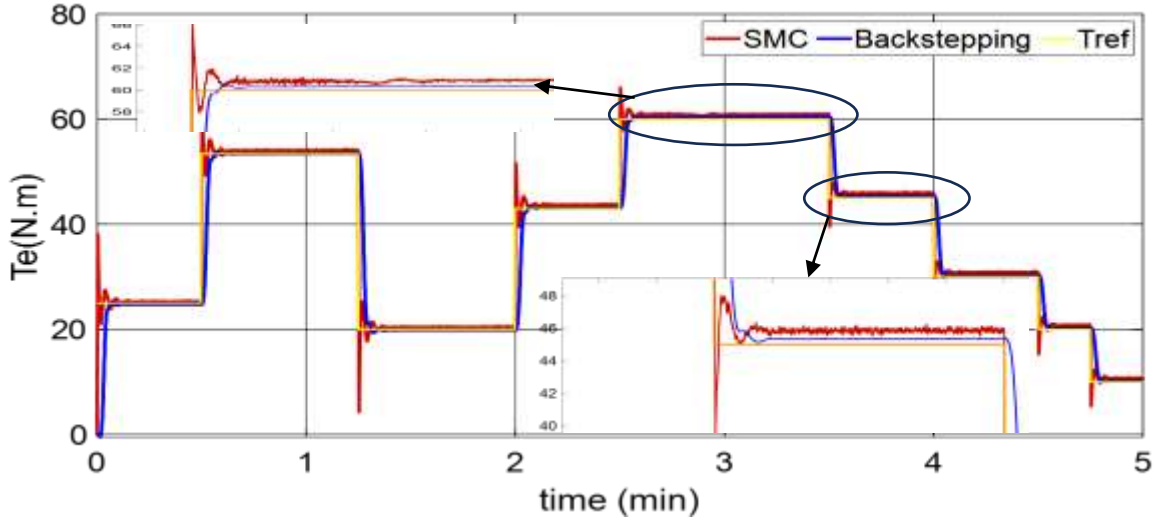

(b)

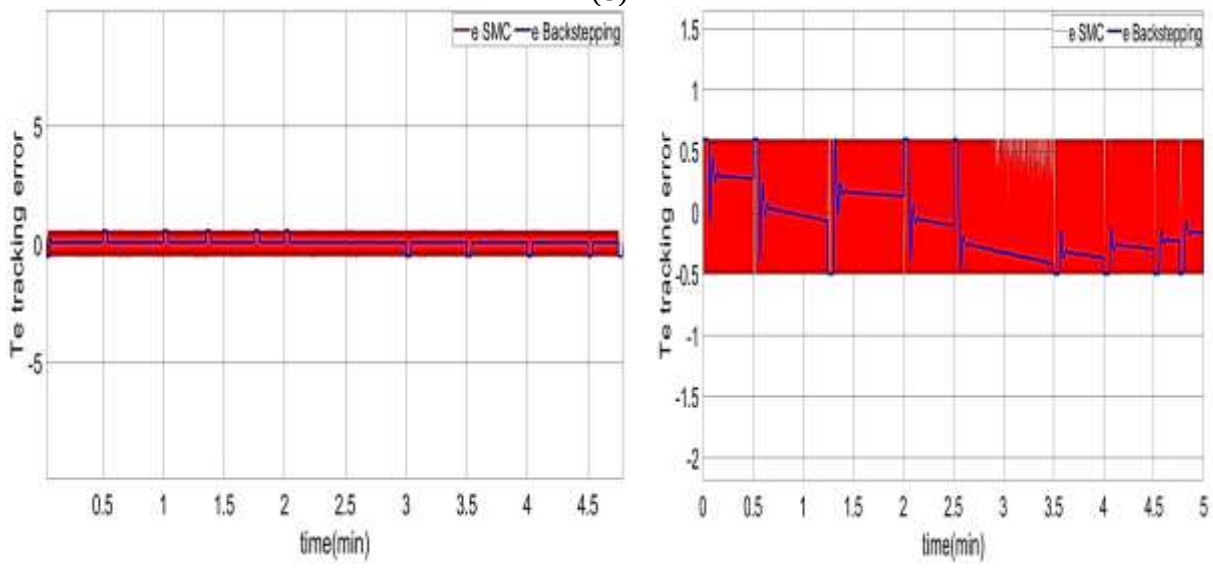

(c) (d)

Fig.4.11: Output Torque Response (a) Sc2,(b) Sc3,(c) Tracking Torque Errors of Sc2 ,(d) Tracking Torque Error of Sc3.

Fig.4.12 shows the THD of the output torque. Backstepping control offers a significant advantage over SMC in achieving a lower THD for torque in a PMSM drive, especially when combined with an MLI.

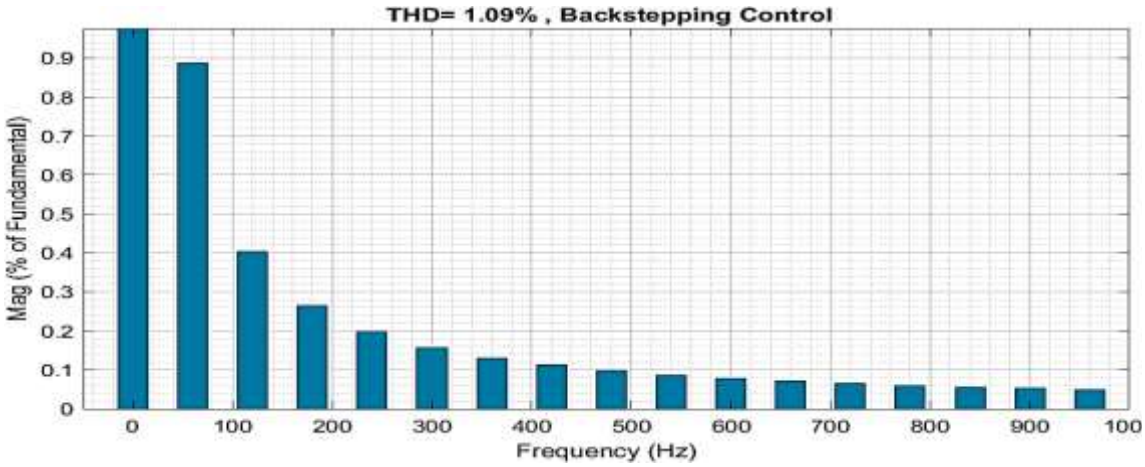

(a)

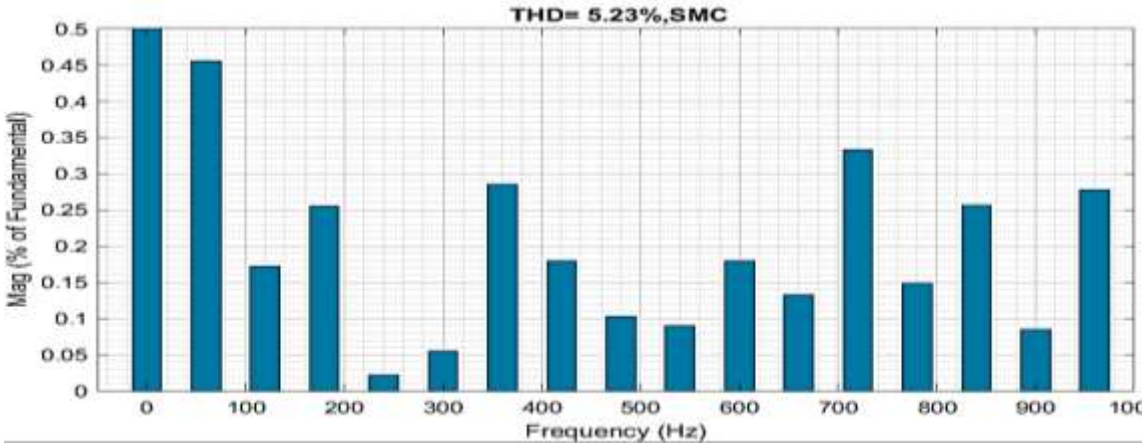

(b)

Fig.4.12: THD of Output Torque (a) Backstepping Control,(b) Slide Mode Control.

Fig.4.13 shows the total output speed distortion. Stability, error minimization, fast response to errors, and utilizing the advantages of MLI are all critical components of the design philosophy of backstepping control, which helps achieve a much lower degree of distortions in the output speed compared to SMC. It results in a more accurate and seamless regulation of the

motor's speed. Although both controllers can work with MLIs, backstepping control has a significant advantage in reducing speed distortions.

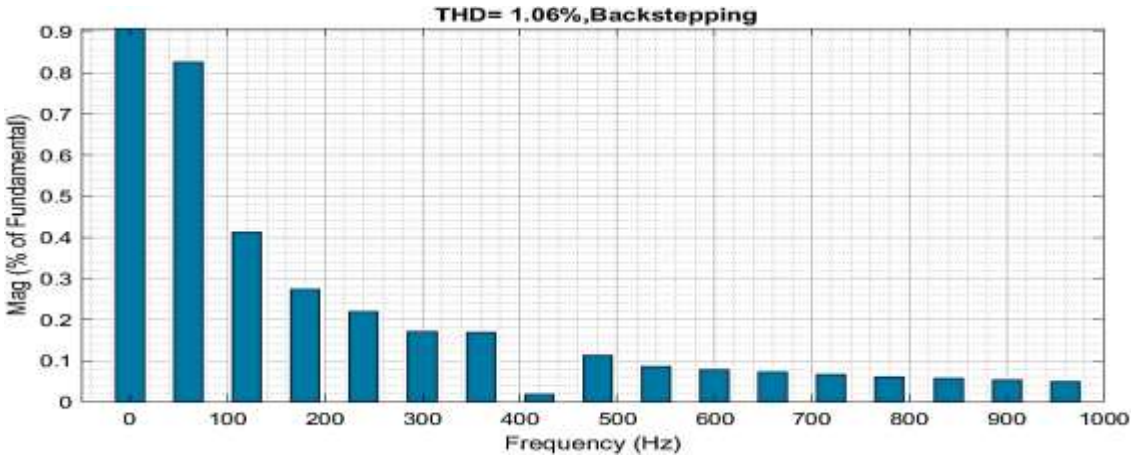

(a)

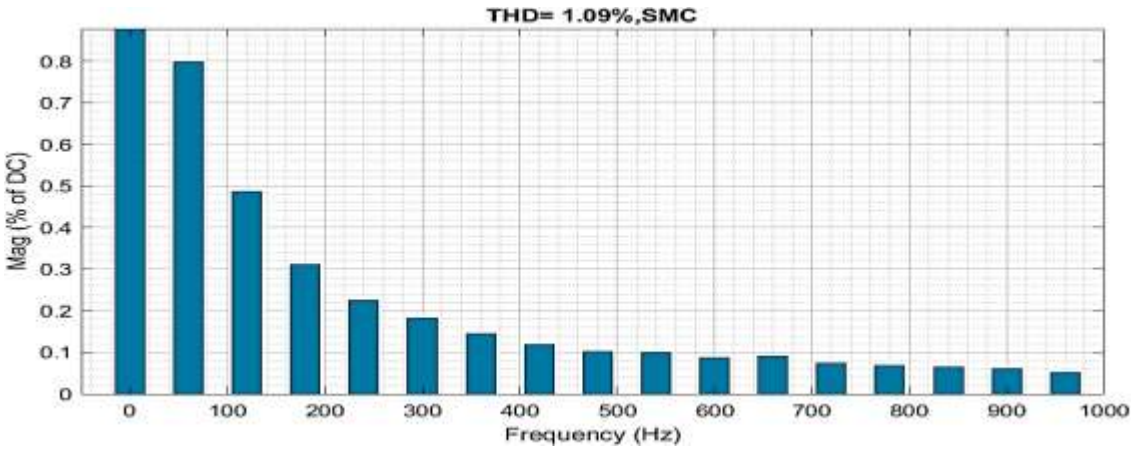

(b)

Fig.4.13: THD of Output Speed (a) Backstepping Control, (b) Slide Mode Control.

Fig.4.14 shows the THD of output voltage from HESS. In a HESS application, backstepping control provides a notable benefit over SMC when obtaining a lower THD for the DC-link voltage (Vdc). Reducing errors at all levels of the control loop, including DC bus voltage regulation, is the top priority for backstepping control. It reduces Vdc voltage distortion by giving the power converter a smoother control signal. The objectives of a specific application determine the best controller to select. Backstepping control is better if accurate speed and torque control, small torque ripple, and quick

response time are important considerations. On the other hand, SMC could be a good choice if ease of use and cheap processing resource requirements are the primary priorities, particularly in situations with less demanding torque variations.

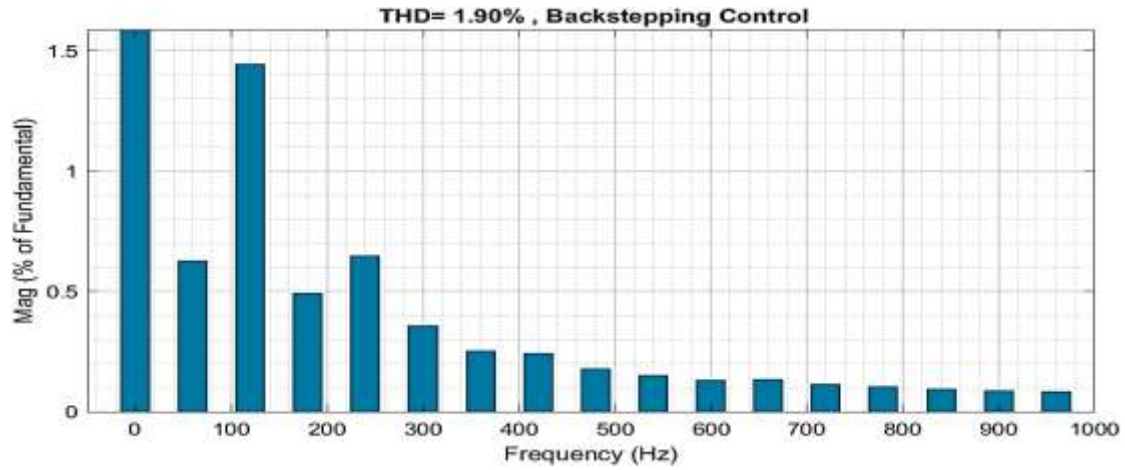

(a)

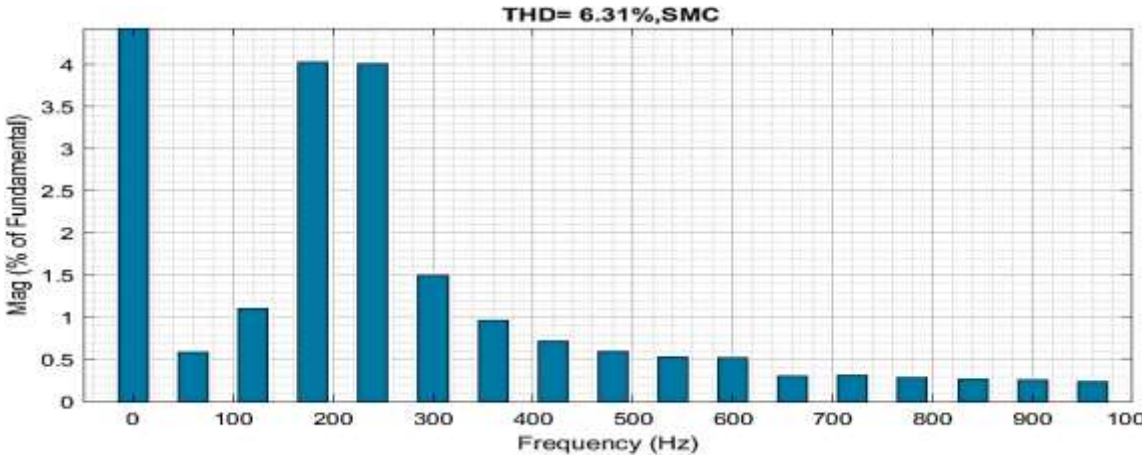

(b)

Fig.4.14: THD of Output Voltage (a) Backstepping Control,
(b) Slide Mode Control.

Table 4.3 shows the general comparison between backstepping and SMC in our proposed system.

Table 4.3 Simple Comparison between Backstepping Control and SMC for PMSM Driven by 7-Level Inverter.

Features	First Scenario (Variable Speed, Constant Torque)	Second Scenario (Variable Torque, Constant Speed)	Third Scenario (Variable Speed & Variable Torque)
Speed Tracking	Backstepping: Superior(98.5%)	Backstepping: Superior (99%)	Backstepping: Superior(99.3%)
	SMC: Good (90.4%)	SMC: Good(92%)	SMC: Good (92%)
Speed Tracking Error	Backstepping: Lower	Backstepping: Lower	Backstepping: Lower
	SMC: Moderate	SMC: Moderate	SMC: Higher
Speed Fluctuations	Backstepping: Lower	Backstepping: Lower	Backstepping: Lower
	SMC: Moderate	SMC: Moderate	SMC: Higher
Torque Tracking	Backstepping: Superior (93.2%)	Backstepping: Superior (99.34%)	Backstepping: Superior(98%)
	SMC: Moderate (91%)	SMC: Good (84%)	SMC: Good (92%)
Torque Tracking Error	Backstepping: Lower	Backstepping: Lower	Backstepping: Lower
	SMC: Moderate	SMC: Moderate	SMC: Higher
Torque Ripple	Backstepping: Lower(0.083%)	Backstepping: Lower	Backstepping: Lower
	SMC: Higher(1.333%)	SMC: Higher	SMC: Highest
Overshoot in Torque Response	Backstepping: Minimal	Backstepping: Minimal	Backstepping: Minimal
	SMC: Potential for Overshoot	SMC: Potential for Overshoot	SMC: Likely Overshoot
Complexity	Backstepping: Higher SMC: Moderate	Backstepping: Higher SMC: Moderate	Backstepping: Higher SMC: Moderate
Computational Resources	Backstepping: Higher SMC: Moderate	Backstepping: Higher SMC: Moderate	Backstepping: Higher SMC: Moderate

4.4 Comparison Results of Multi-Level Inverter

The comparative efficiency of 2-level, 5-level, and 7-level MLIs utilized with backstepping control for PMSMs is examined in this section. The effect of the voltage level, torque ripple, current harmonics, control design complexity, torque tracking, and speed tracking will all be examined. The aim

is to offer a thorough grasp of the trade-offs related to choosing the best MLI configuration for a particular PMSM application.

4.4.1 First Scenario Simulation Results

Fig.4.15(a) shows that 7-level- and 5-level inverters generally have better variable speed tracking performance than a 2-level inverter. The MLI can produce a closer approximation to a sinusoidal waveform—the ideal input for the PMSM—due to their higher voltage accuracy, which comes with higher voltage levels. The Results are smoother torque and better speed control by lowering the quantization errors that happen with fewer levels.

As illustrated in Fig.4.15(b), a 7-level MLI provides the best tracking performance with minimum torque fluctuation and ripple compared to 2-level- and even 5-level inverters in constant torque scenarios. When attempting to produce a smooth sine wave, 2-level inverters' limited ability to flip between positive and negative voltage results in significant quantization errors. While 5-level inverters are an improvement, 7-level inverters minimize these problems with better control.

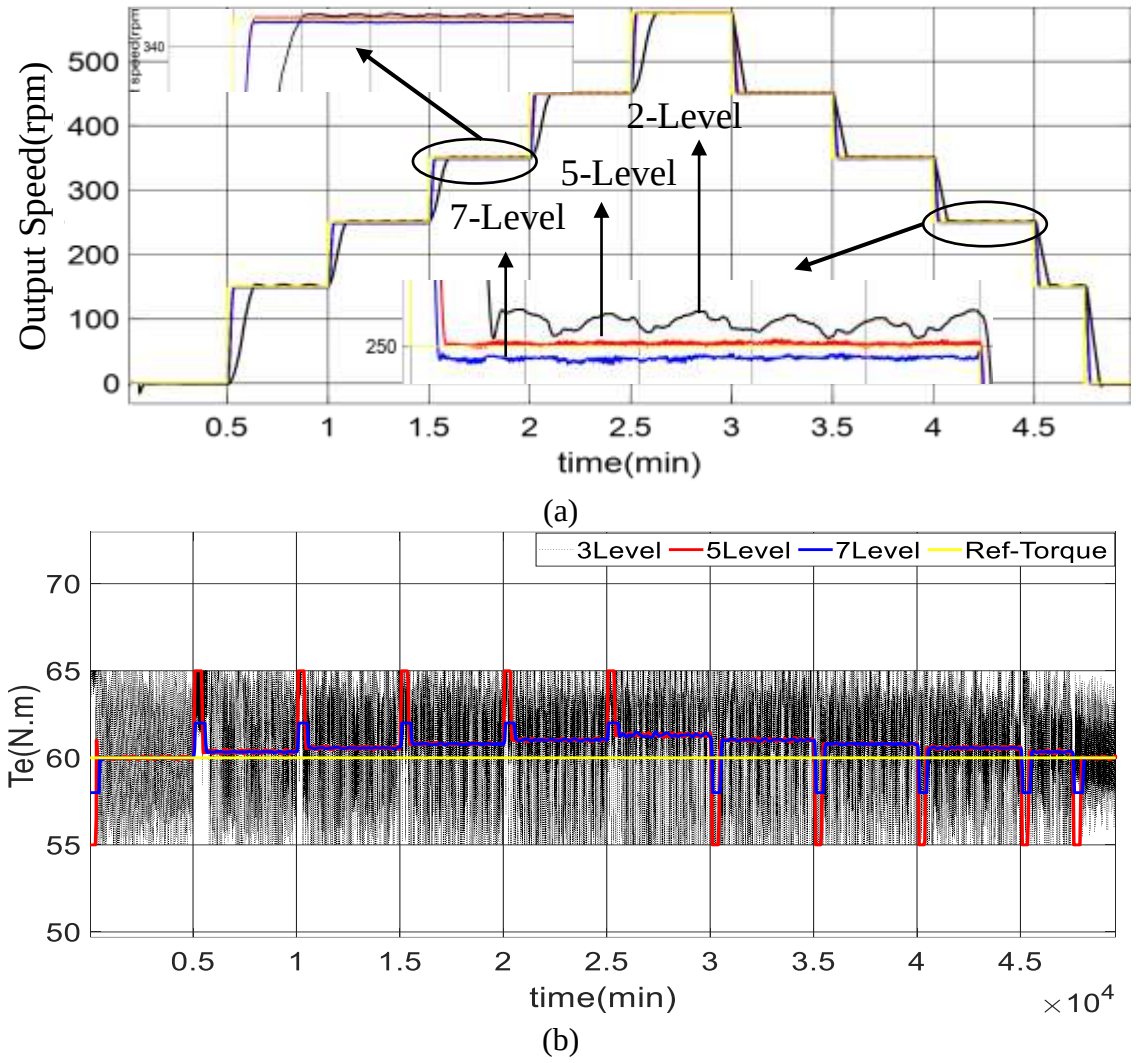

Fig.4.15: System Response (a) Speed Response,(b) Torque Response.

4.4.2 Second Scenario Simulation Results

As illustrated in Fig.4.16, a 7-level inverter tends to outperform 2-level and even 5-level inverters regarding realistic speed and torque monitoring while limiting torque error in the second scenario of variable torque and constant speed. It is difficult to precisely match the voltage required for specific speed commands because of the general "staircase" (restricted voltage levels) that causes the higher speed variations in a 2-level inverter during variable torque and constant speed operation. As a result, the motor speed oscillates around the intended value.

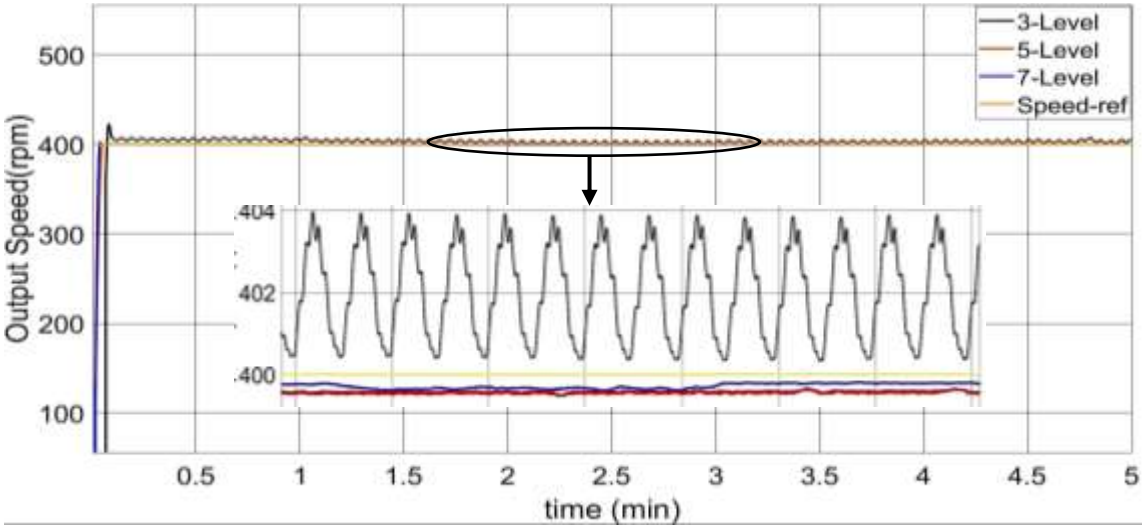

(a)

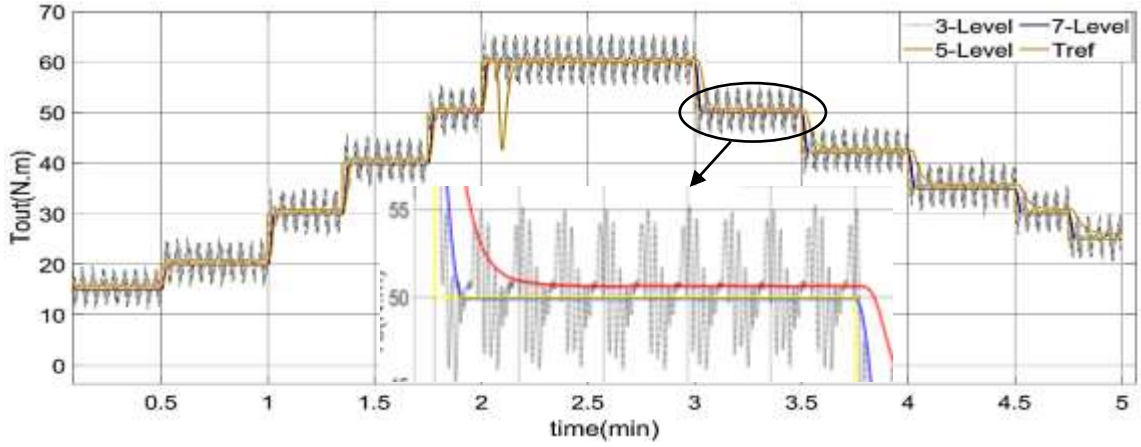

(b)

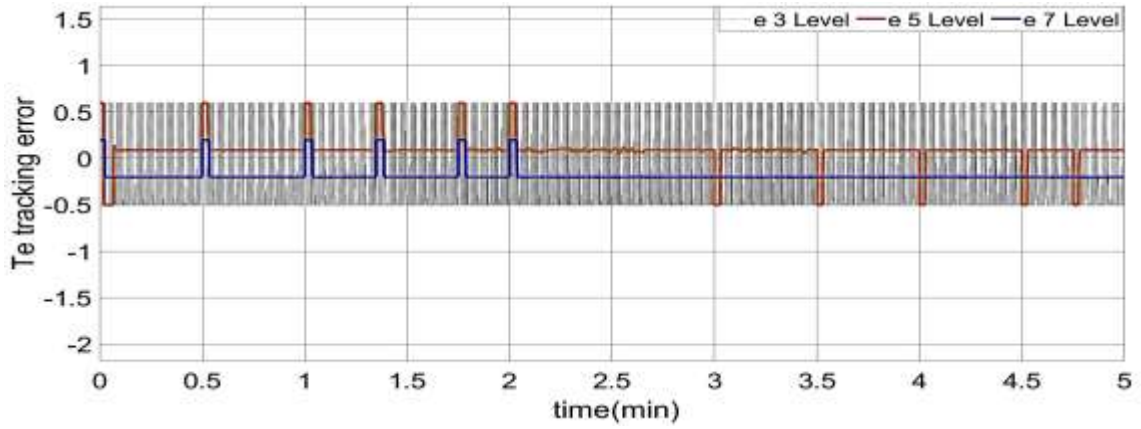

(c)

Fig.4.16: System Response (a) Speed Response,(b) Torque Response,(d) Output Torque Tracking Error.

4.4.3 Third Scenario Simulation Results

Fig.4.17 shows the MLI response for the third scenario. A 7-level inverter excels at achievable speed and torque tracking in the most demanding scenario involving variable speed and torque. The 7-level MLI can modify the voltage profile more precisely to achieve the required back EMF for the new speed when the desired speed changes. As a result, speed instructions are tracked more accurately than lower-level inverters with less voltage resolution. Because of its more muscular control, the 7-level MLI may produce a smoother voltage transition when torque demands change. That reduces torque ripple, unwanted variations in the motor's torque output that might happen during abrupt variations. Lower torque ripple translates to smoother operation and potentially improved efficiency.

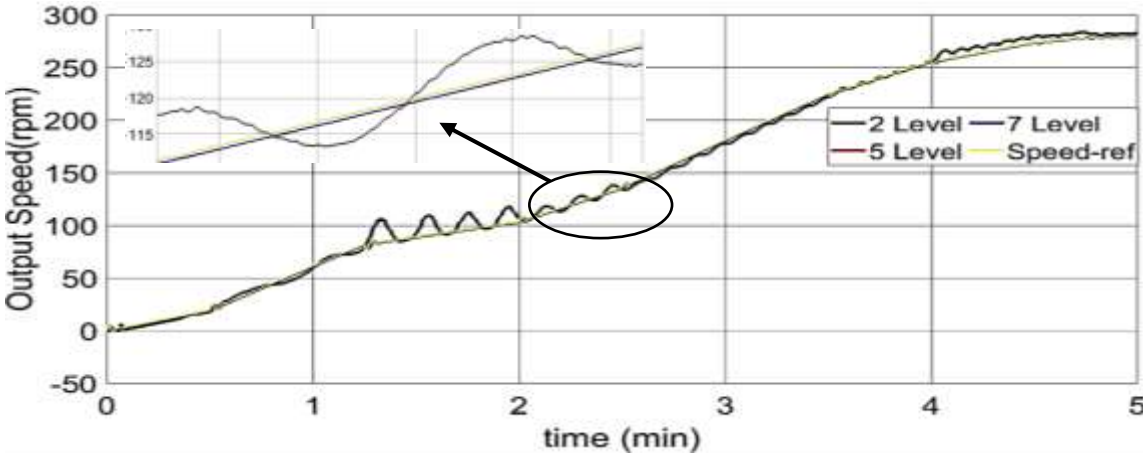

(a)

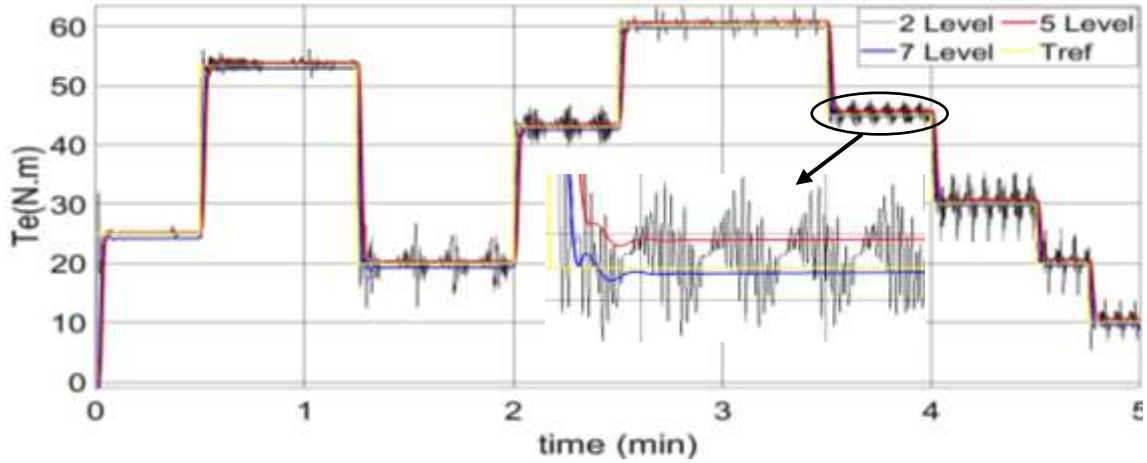

(b)

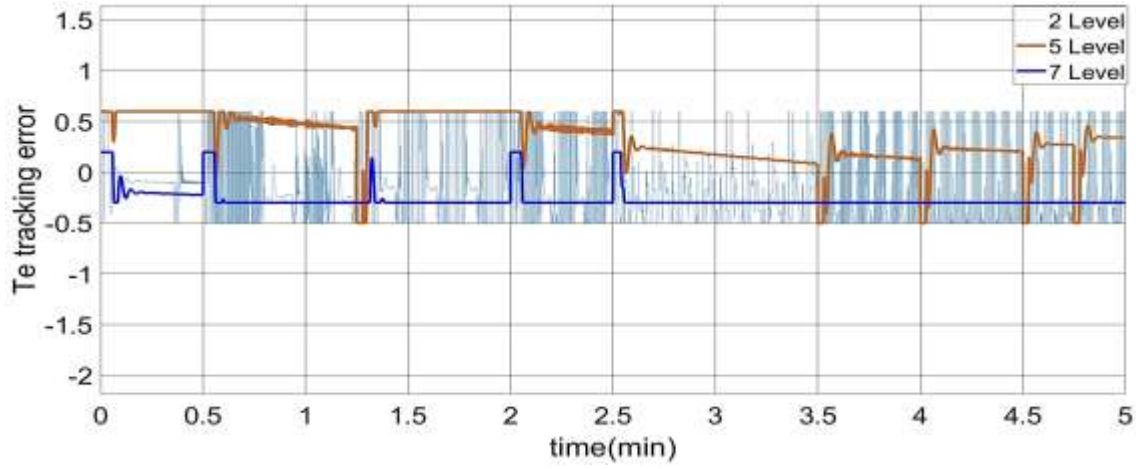

(c)

Fig.4.17: System Response (a) Speed Response, (b)Torque Response, (c) Torque Tracking Error.

4.4.4 Effects of Multi-Level Inverter on Hybrid Electric Storage System

Fig.4.18 shows the extracted power with different inverter levels. In contrast, power quality and efficiency can be improved with a 7-level inverter. Rather than directly resulting from the number of voltage levels, the observed increased power extraction at 1000 (W/m^2) irradiance most likely comes from an improved system design or a more effective MPPT algorithm. Because a 7-level inverter may occasionally have lower switching losses than a lower-level inverter, this may result in a marginally higher percentage of the extracted electricity reaching the grid or slightly improved overall system efficiency.

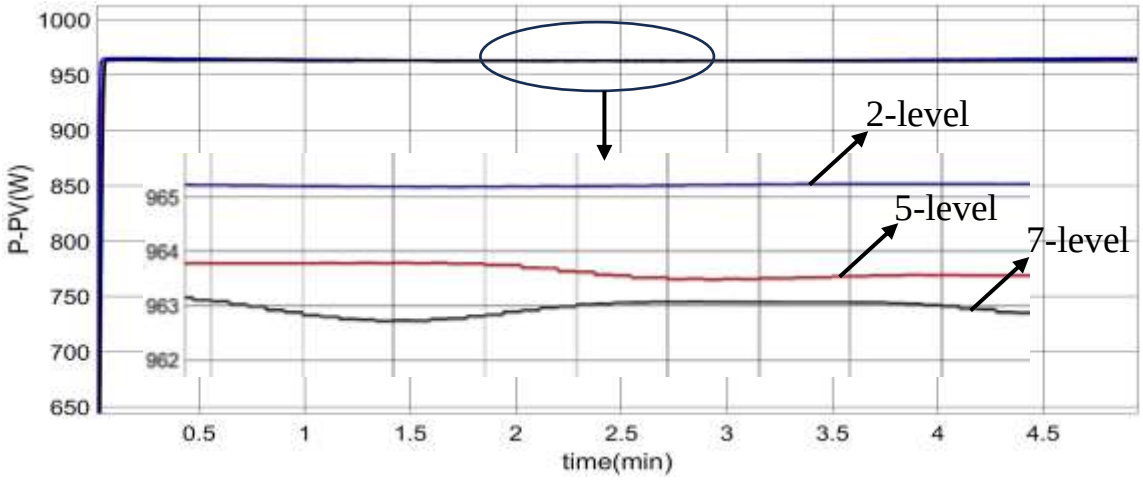

Fig.4.18:Performance of Extracted PV-Power Under 1000(Watt/m^2) Irradiance.

Fig.4.19 shows the effect of MLI on the SoC of ESS. When charging a Supercapacitor (SC) in a HESS, 5-level and 7-level inverters have advantages over 2-level inverters because ESS's SoC is higher at the 5 and 7 levels. These inverters can produce lower voltage steps throughout the charging process with higher voltage levels. Comparing this smoother voltage transition to the

more significant voltage jumps seen with a 2-level inverter may help minimize charging inefficiencies and time.

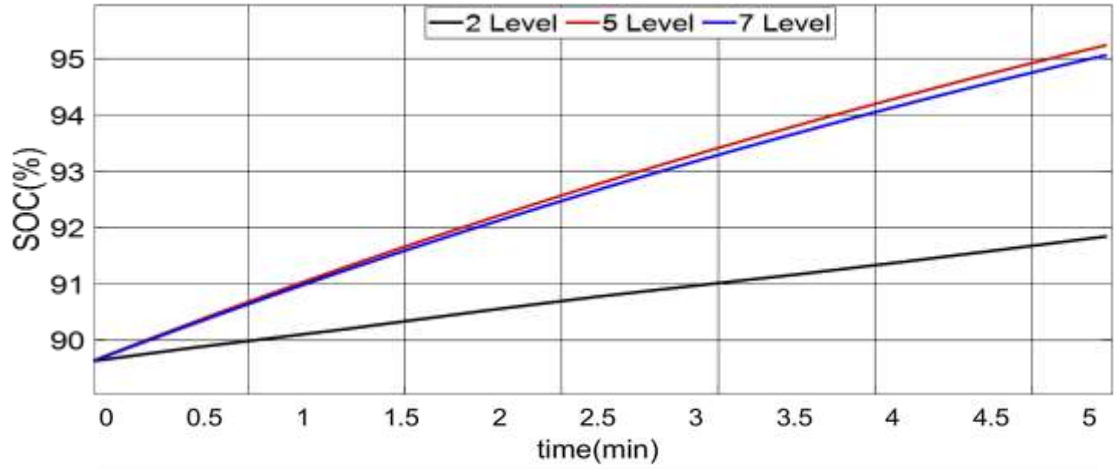

(a)

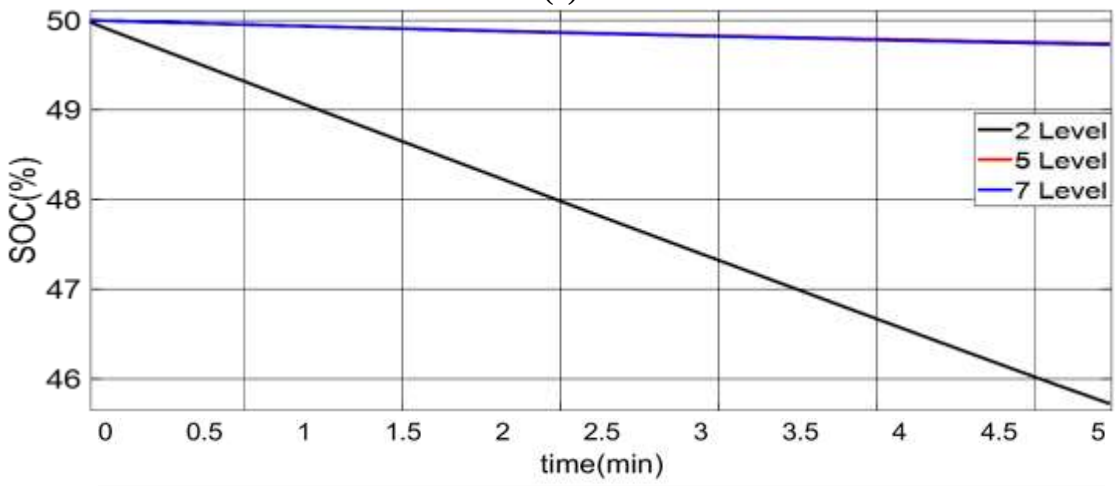

(b)

Fig.4.19: Impact of MLI on SoC of Rechargeable (a)Battery and (b) Supercapacitor.

Fig.4.20 shows the DC-starting current with all MLI types. Compared to 5-level and 2-level inverters, a 7-level inverter may demand less DC starting current from the HESS. With a 2-level inverter, the initial application of voltage to the DC link (connection between HESS and inverter) can result in a high inrush current surge. That is because the inverter can only switch between a positive and negative DC voltage, resulting in an abrupt voltage rise at startup. Due to the reduced voltage levels, a 5-level inverter still has limitations, even though it can raise voltage more smoothly than a 2-level

inverter. With its more precise control, the 7-level inverter can produce a more gradual voltage rise at the start, significantly lowering the inrush current drawn by the HESS. The principal cause of the significant fluctuations in the DC extracted from the HESS is the limiting voltage control of a 2-level inverter. Even while it is still functional in a HESS, these variations may shorten component life and reduce system effectiveness.. 5-level or 7-level inverters are typically the better options in applications where reducing DC variations is essential.

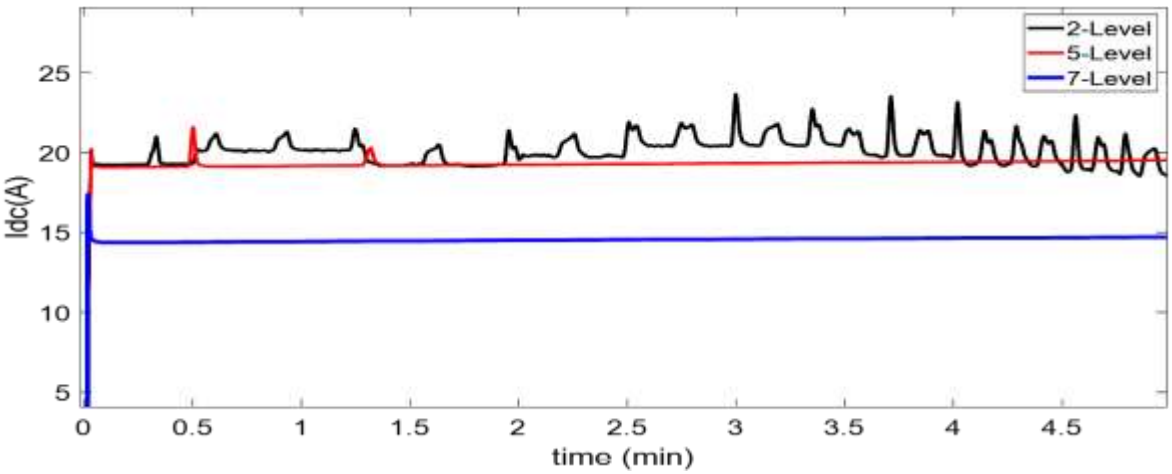

Fig.4.20 : Output HESS DC-Current with Multi-Level Inverter.

Fig.4.21 shows the power delivered to the load from HESS. There are two main issues with power delivered to the load by a 2-level inverter in a HESS: significant fluctuations and perhaps excessive average power compared to the intended output. High power variations due to sudden voltage shifts mean the power delivered changes significantly**.** The power output does not follow the smooth sinusoidal behavior required for most AC loads; instead, it appears "choppy" or pulsing. Poor voltage regulation is the leading cause of the significant variations in load current and power when using a 2-level inverter in an HESS. For HEV applications where smooth power delivery, high efficiency, and precise control are crucial, a 7-level inverter is the preferred choice due to its superior voltage control capability.

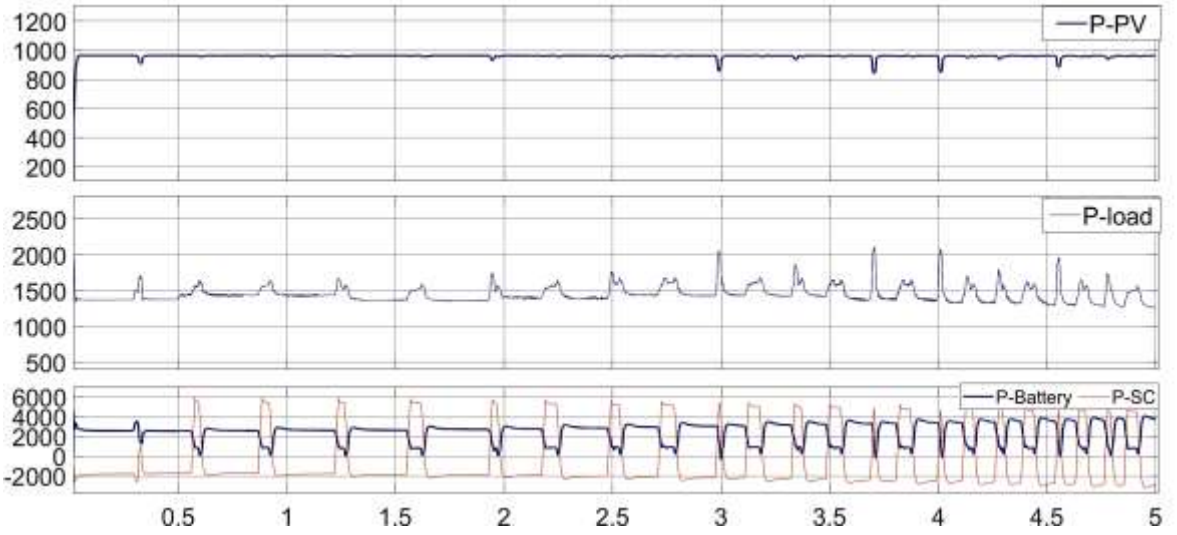

(a)

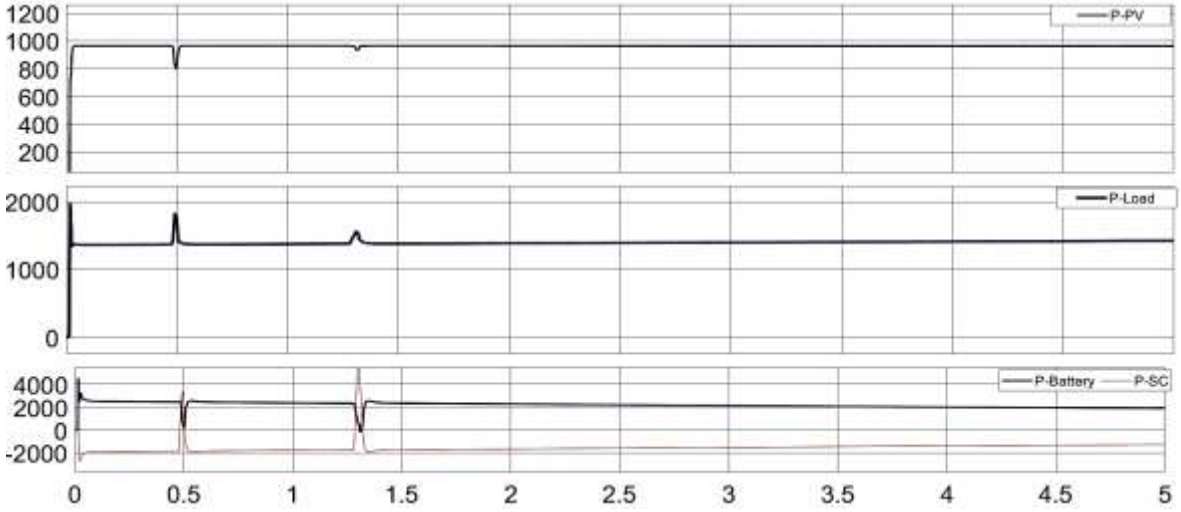

(b)

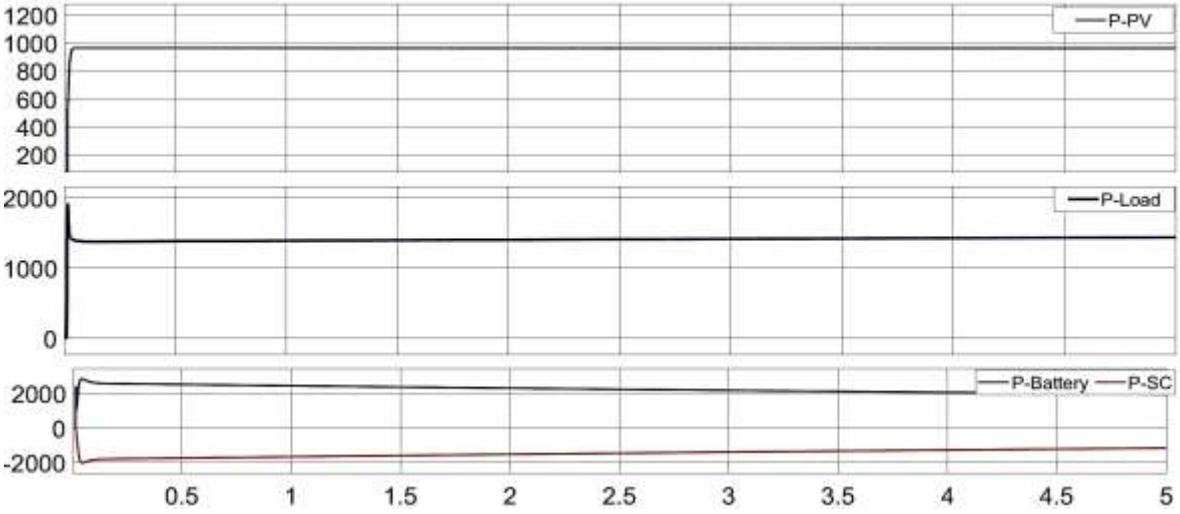

(c)

Fig.4.21: Power HESS Supplied Load Via (a) 2-Level, (b) 5-Level, (c) 7-Level.

Fig.4.22 shows the THD of Vdc from HESS. The 7-level inverter has the lowest THD. That much is evident. Compared to 2-level and 5-level inverters, a 7-level inverter's improved voltage management capability enables it to produce a DC voltage waveform with significantly reduced THD. It may increase effectiveness, less stress on the parts, and higher overall power quality in a HESS. However, thoroughly examining the unique HESS requirements and goals should be the foundation for selecting the inverter type.

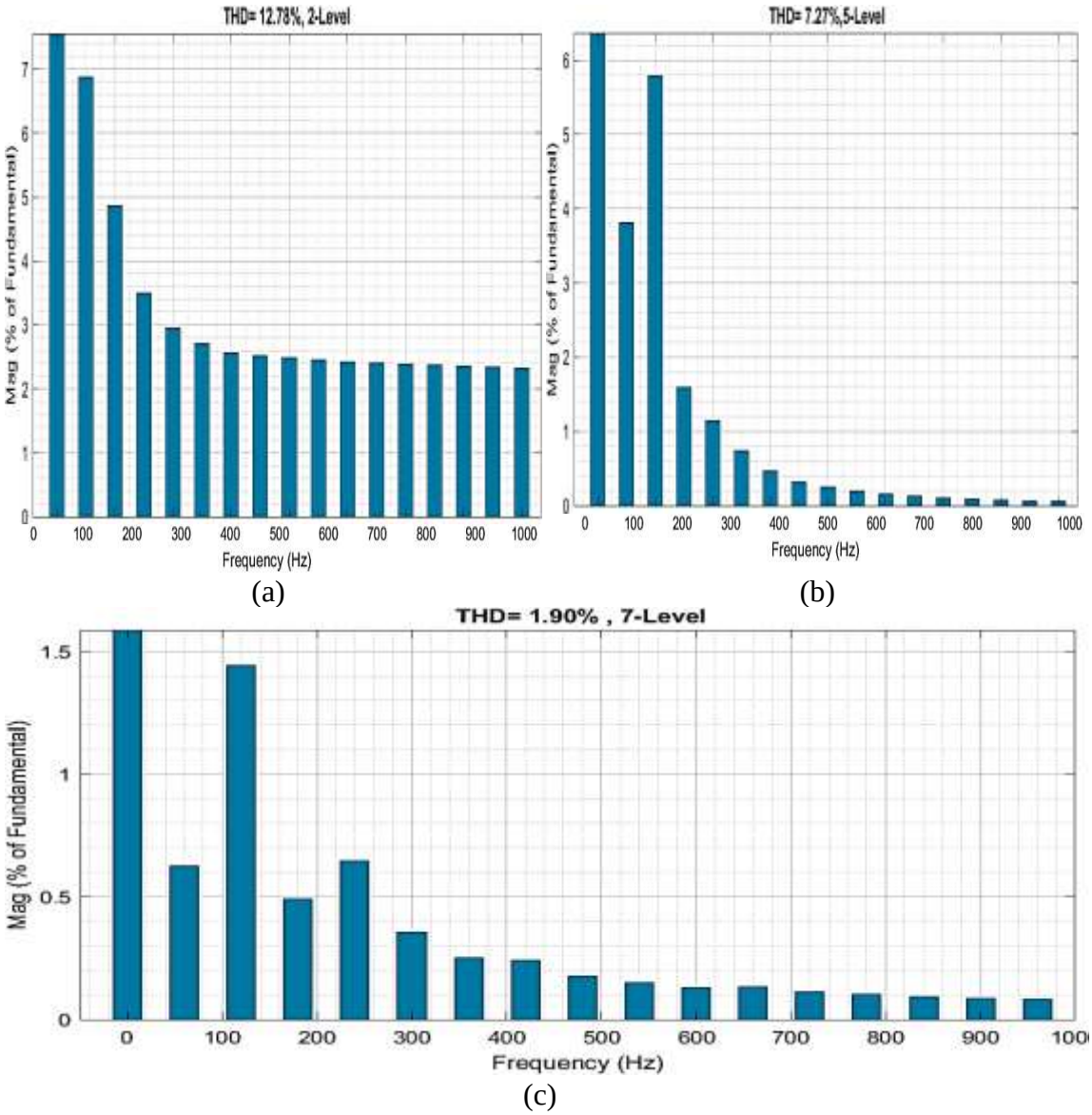

Fig.4.22: THD of Vdc from HESS with (a)2-Level, (b)5-Level, (c)7-Level.

Fig.4.23 shows the THD of the load current. The 7-level inverter has the lowest other types in the AHEV system. Fig 4.24 and Fig.4.25 show the total distortion in output torque and speed with MLI. According to earlier discussions, the 7-level inverter responds to torque and speed changes and distortion less than other inverters.

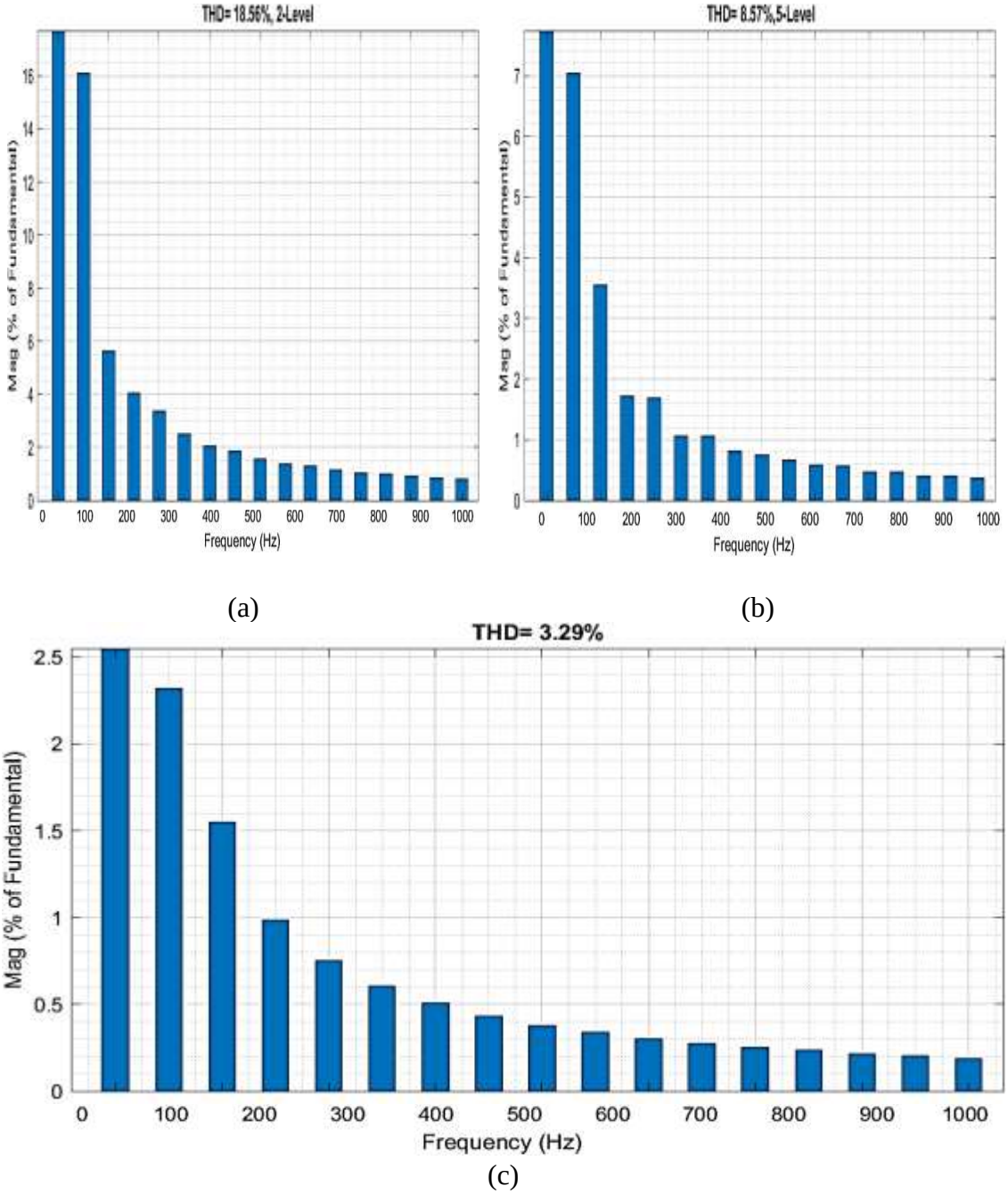

Fig.4.23: THD of I_{DC} from HESS with (a)2-Level, (b)5-Level, (c)7-Level Inverter

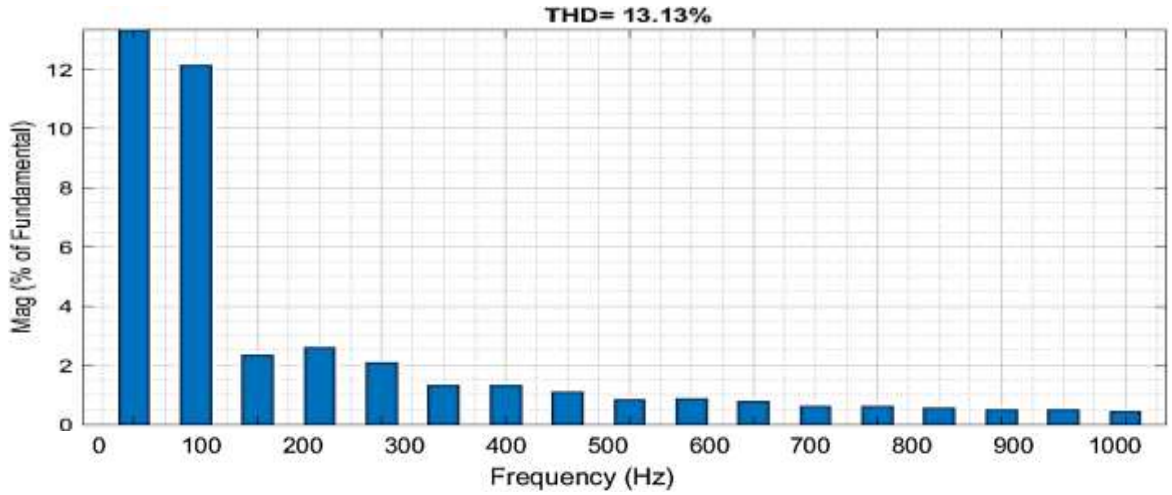

(a)

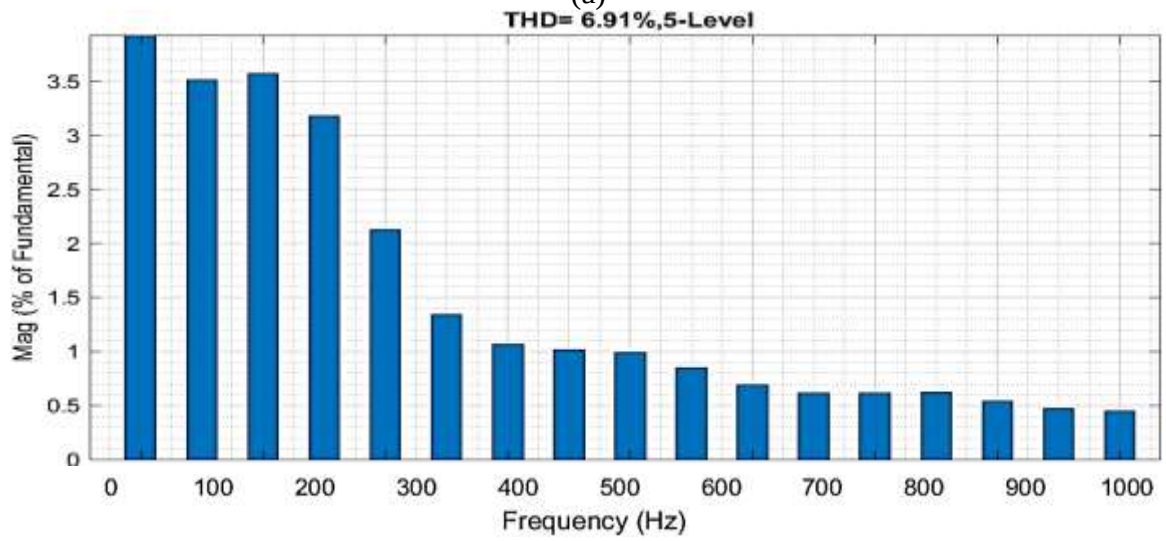

(b)

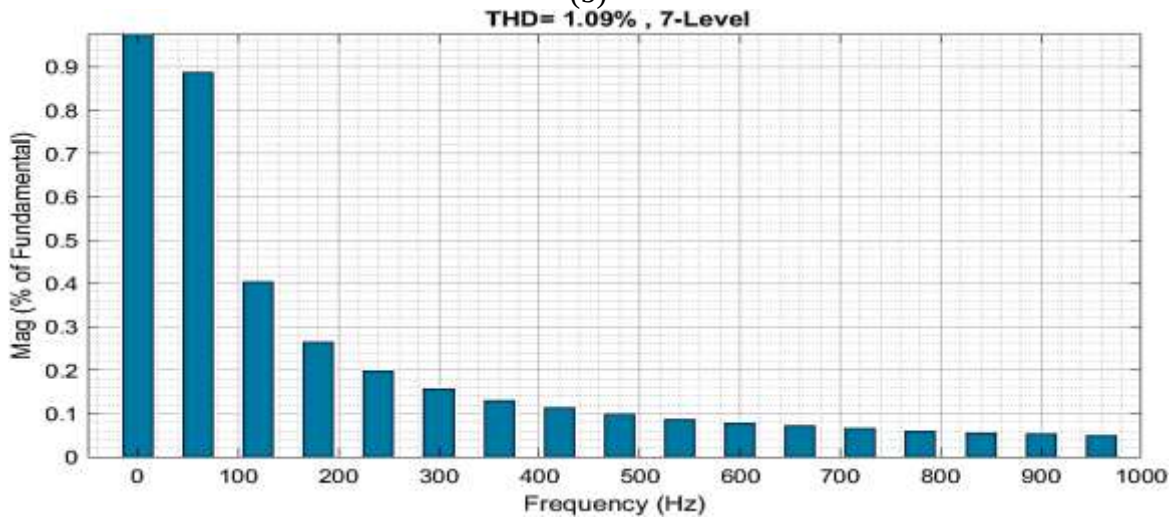

(c)

Fig.4.24: THD of Output Torque with (a) 2-Level, (b) 5-Level, (c) 7-Level Inverter.

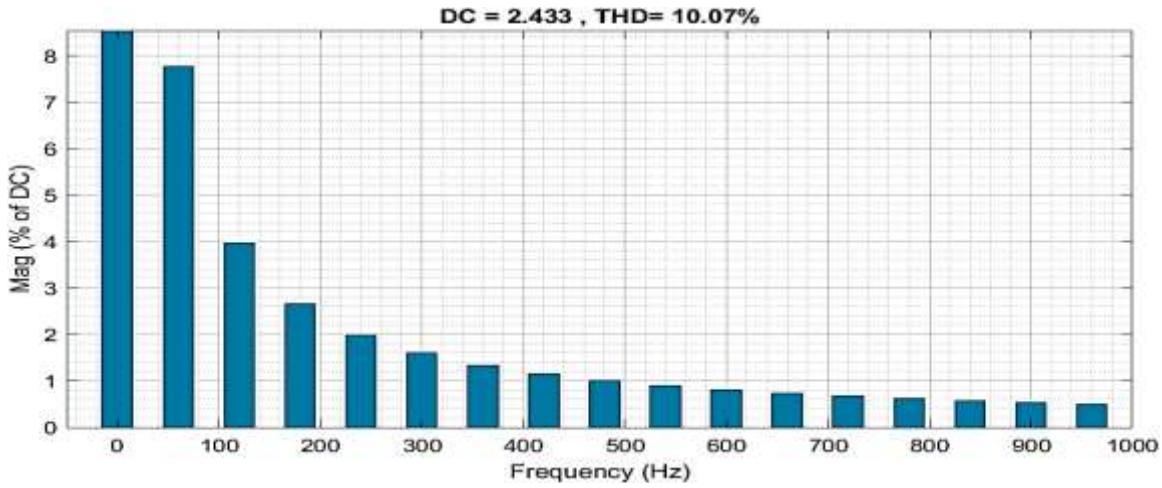

(a)

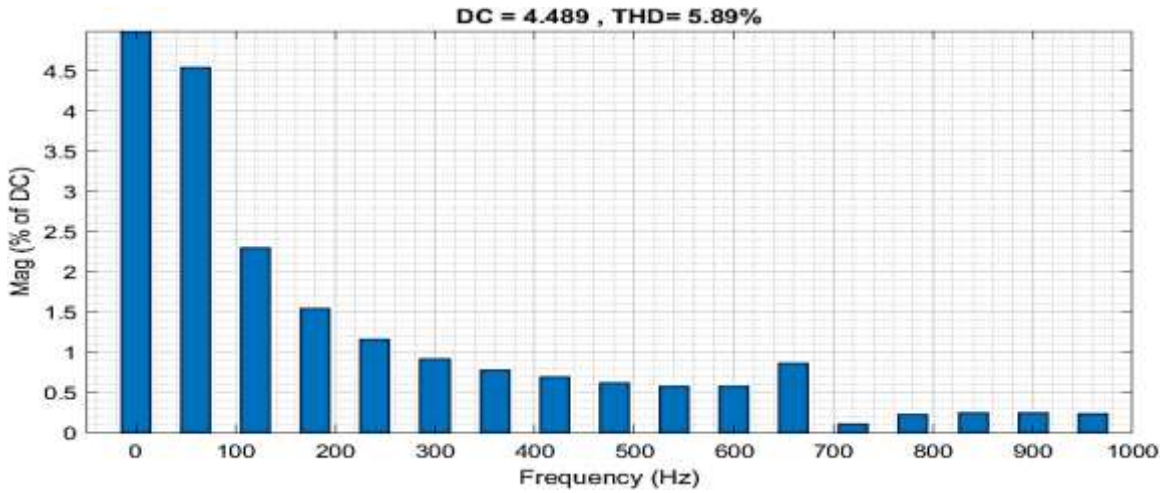

(b)

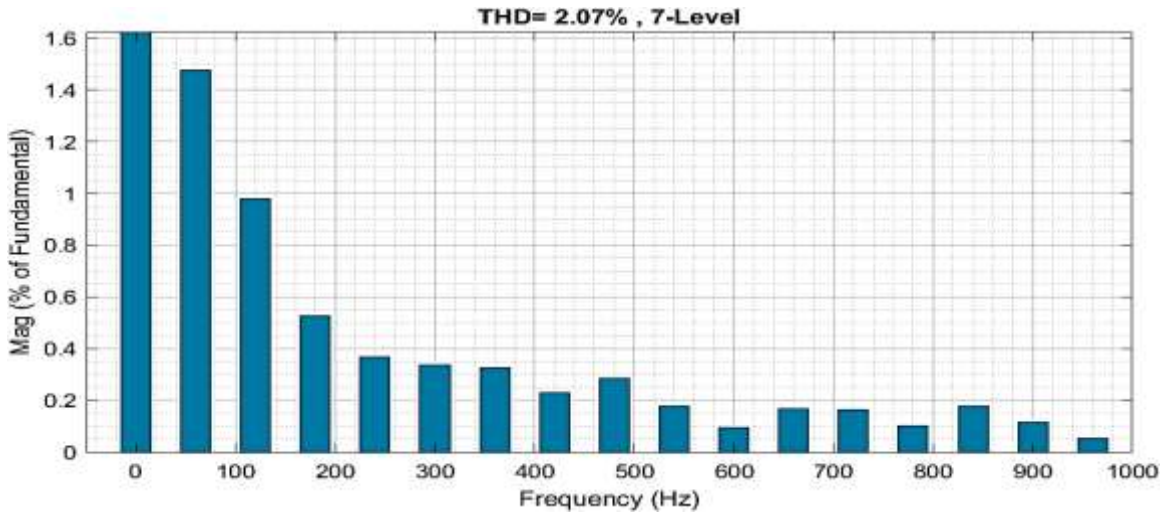

(c)

Fig.4.25: THD of Output Speed with (a) 2-Level,(b)5-Level, (c)7-Level Inverter.

Table 4.4 compares the 2,5, and 7 levels inverters depending on system response.

Table 4.4: Comparison of Inverter Ievels in Autonomous Hybrid Electric Vehicle Applications.

Feature	2-Level Inverter	5-Level Inverter	7-Level Inverter
Voltage Control	Limited (Binary: Positive/Negative DC)	Improved (More Voltage Levels)	Superior (Finer Voltage Control)
THD of Vdc	High	Moderate	Low
Starting Current	High Inrush Surge	Lower Inrush Current	Lowest Inrush Current (Gradual Rise)
Power Quality (AC Output)	High Fluctuations, High Harmonics	Reduced Fluctuations, Lower Harmonics	Smoothest Power Delivery, Lowest Harmonics
Speed & Torque Tracking (Variable Speed/Torque)	Poor	Improved	Best
Complexity & Cost	Low	Moderate	High

All inverter levels can operate in a HESS, but because of its improved voltage control capability, a 7-level inverter typically provides the optimum performance in several sectors. This corresponds to the following:

a) Reduced stress on HESS components.
b) Improved efficiency.
c) Smoother power delivery.
d) More precise control over speed and torque (for variable conditions).

4.5 Performance of DC Converters

Fig.4.26 displays the P-V and V-I properties of the PV module at various amounts of solar radiation.

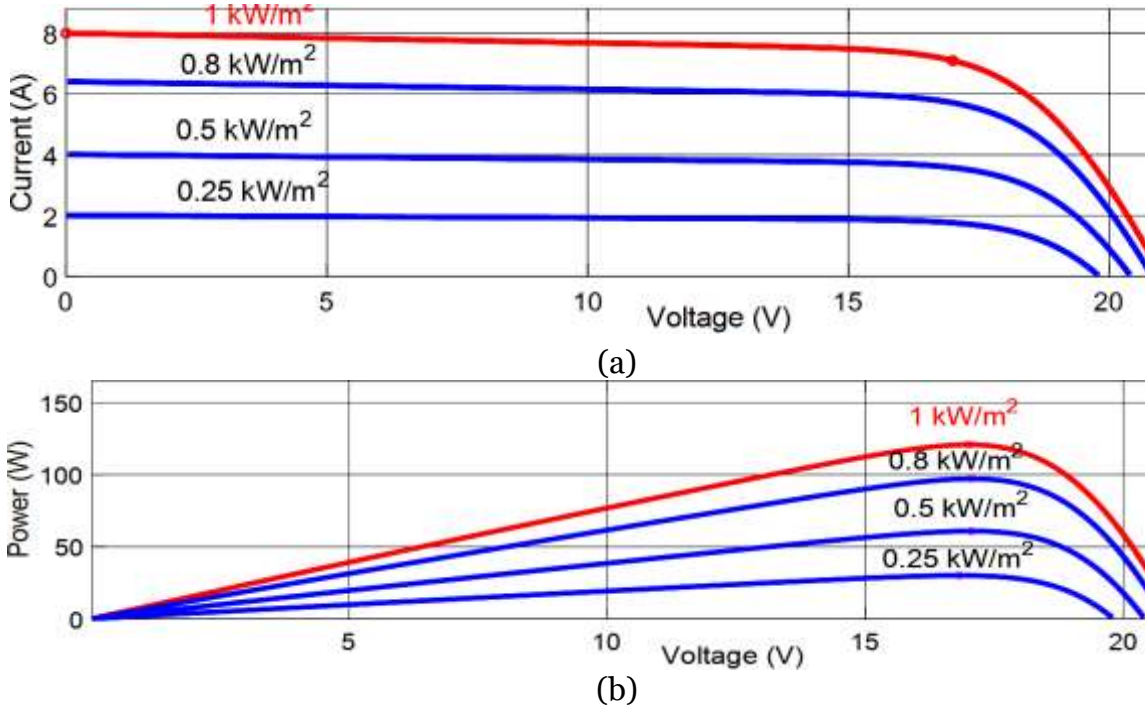

Fig.4.26: PV Solar Panel Characteristics (a)I-V Curves,(b)P-V Curves.

The tuning parameters of the proposed system are given in Table 4.5.

Table 4.5: Controllers' Tuning Parameter in HESS.

Parameter	Value
$K_p, K_i, K_d, \lambda, \mu$	1.477, 3077,0,110,55
Battery charge PI controller(K_p, K_i)	0.043,0.65
Supercapacitor PI controller (K_p, K_i)	0.45,14800
P&O (D_{old},V_{old},P_{old})	0.35,17,120
EPSO(C)	244

Operation of a boost and super Lift Luo circuit is used to calculate a circuit's efficiency according to the input/output power ratio. The motor load is varied by about 1500W. This test takes advantage of the input sources of the PV module. The simulation results are given in the figures below. The temperature of the PV system is $25C^0$. As shown in Fig.4.27(a), the irradiance

ranges from 6 to 18 hours. Thus, the simulation used in this work will depend on this region.

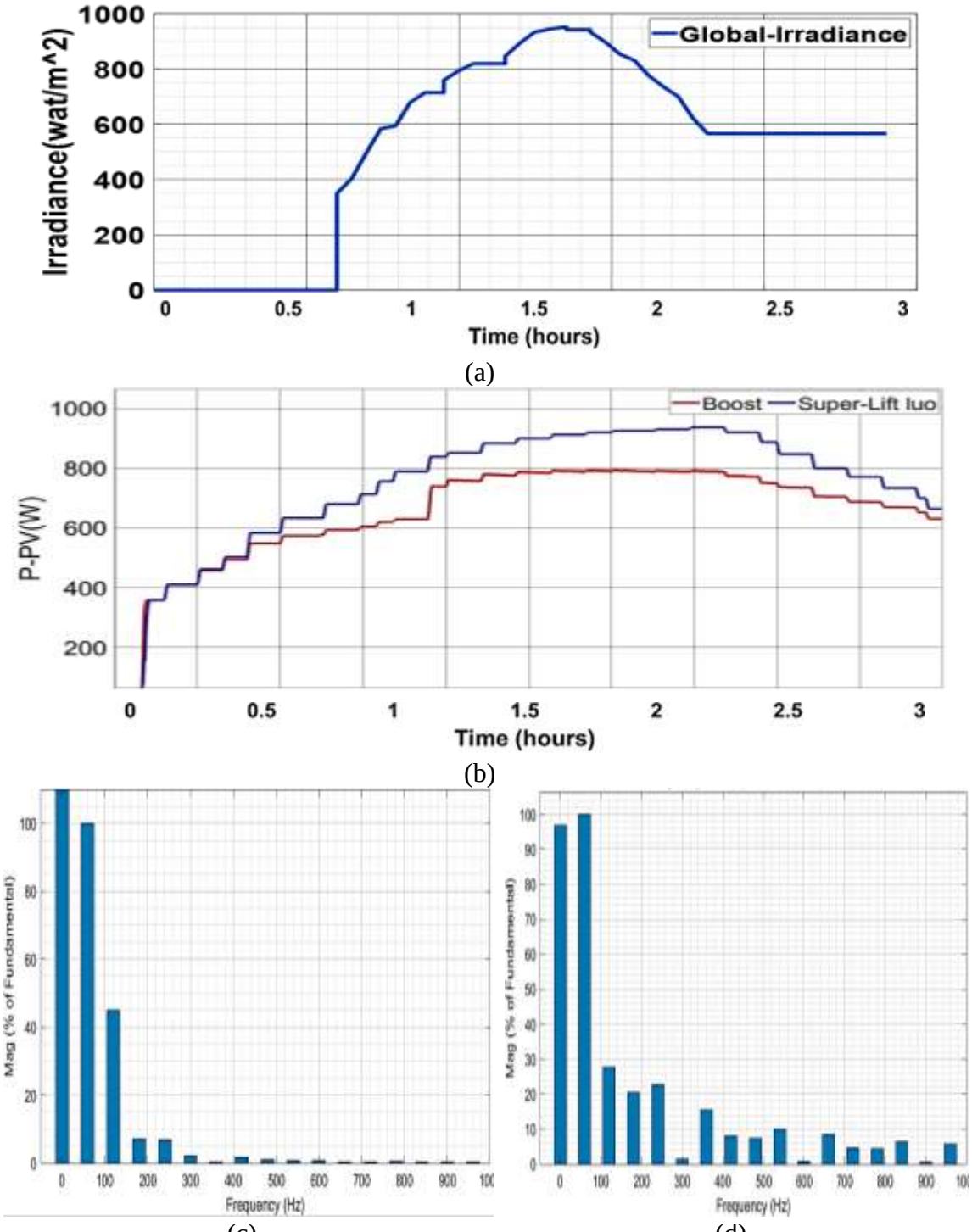

Fig.4.27: Boost and Super lift - Luo Converters with (a) Solar Irradiance Profile, (b) Input PV Tracked Power, (c) THD of the Super-lift Luo, and (d) Boost Converter Output Voltage.

As seen below in Fig.4.28, the THD voltage for both converters that satisfied the super lift luo load was less than 1%, as stated in IEEE standards. The Super-Lift Luo converter's design includes additional circuitry that helps bend the input voltage waveform and get it closer to a sine wave, which explains why. THD is lowered as a result of the harmonic content. In contrast, the boost circuit's THD variations are 10-15%. The super-Lift Luo circuit with HESS offers higher, better, smoother performance and provides a potential advantage in reducing THD compared to a boost converter. The voltage gain of the Super-Lift Luo circuit is substantially more significant. It uses a more complex circuit with capacitors and an extra inductor to achieve this. It makes it possible to increase the output voltage significantly, often several times the input value.

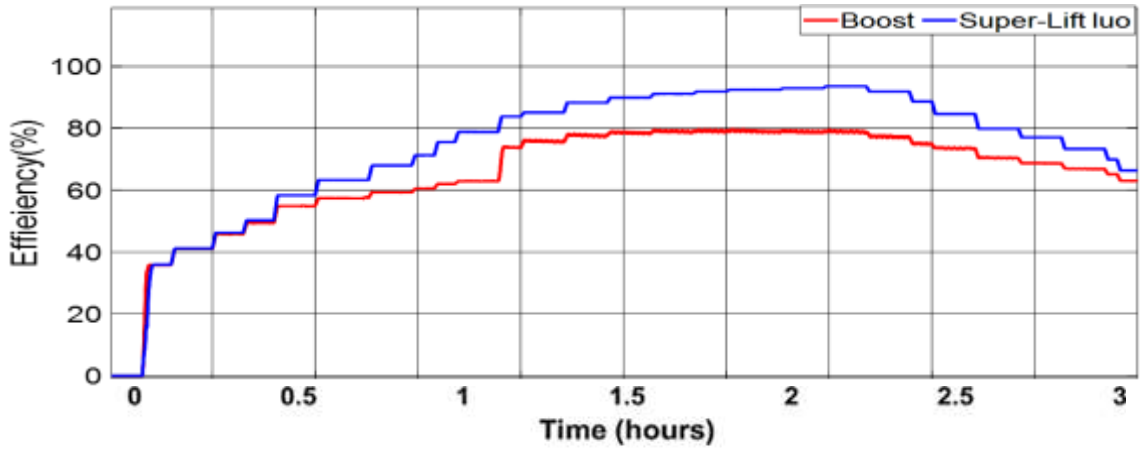

(a)

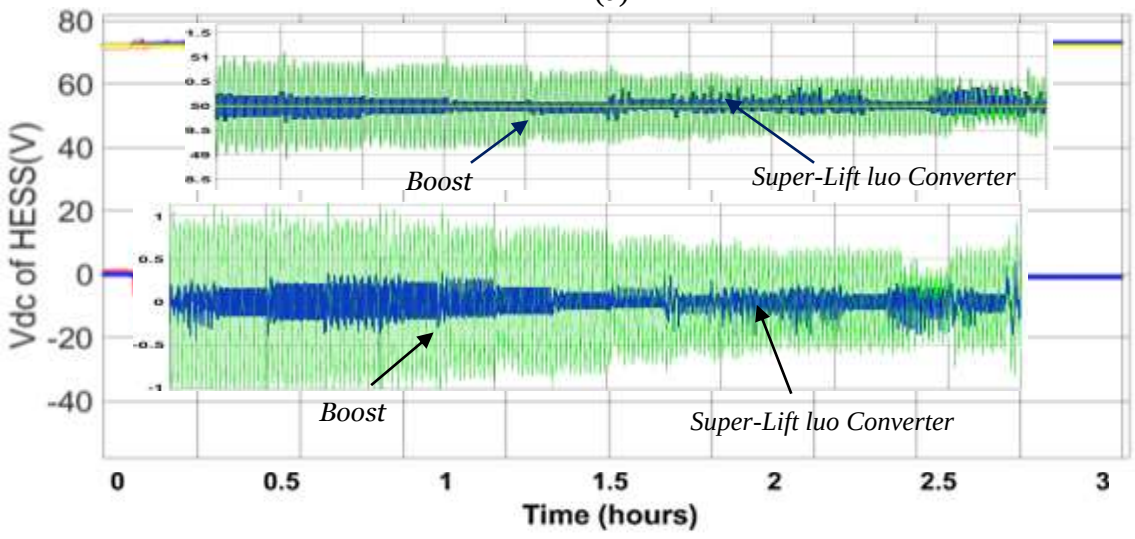

(b)

Fig.4.28:Boost and Super lift - Luo Converters (a) Terminal Voltage-Based Reference DC Voltage (72V) with Their Errors,(b) DC-DC Converters' Efficiency.

Super Lift Luo converters can achieve higher efficiency, especially under low irradiance, due to lower duty cycle operation, as seen in Fig.4.29(a). Because a high-duty cycle is required for high voltage gain, boost converter efficiency decreases in low irradiance. However, efficiency increases with higher irradiance. That improves the system's reliability when the super lift Luo converter is used. As shown in Fig.4.29(b), under global irradiance or changing daily light intensity, the Super Lift Luo converter offers PV systems with MPPT with several advantages. Compared to a conventional boost converter, it can handle a broader range of input voltages, achieve higher efficiency, and increase MPPT performance. It is challenging to operate a PV panel under global irradiation. However, the Super Lift Luo converter consistently produces higher output power and low overshooting to meet the desired load (1500W) than a boost converter. Super_lift Luo converters have extra filtering components to provide a shallow ripple compared to a well-designed boost converter with appropriate filtering. Luo converters can deliver smoother output voltage than boost converters.

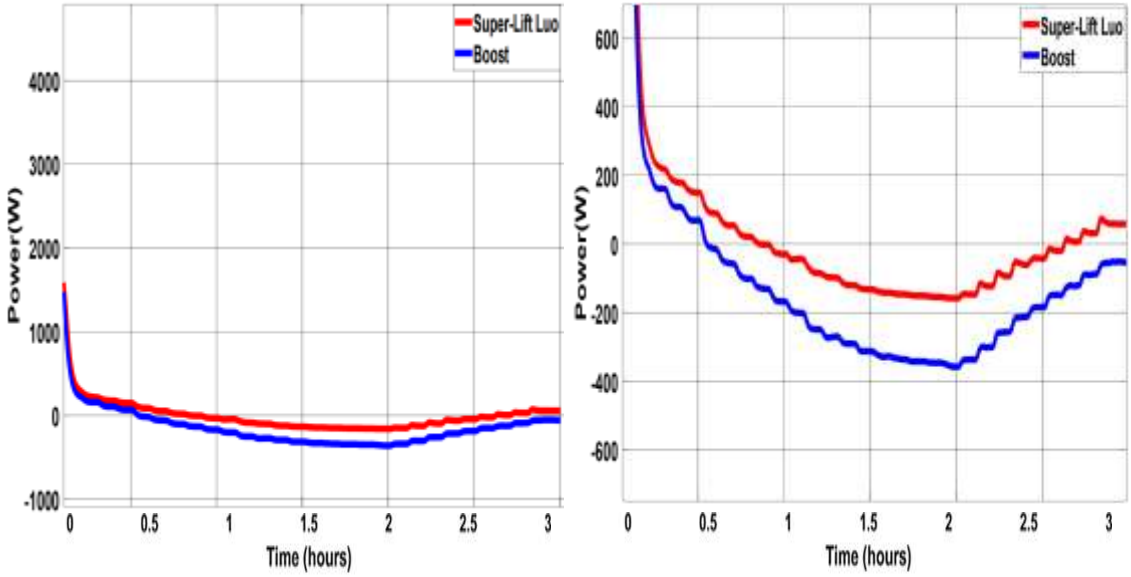

(a) (b)

Fig.4.29: Effect of Boost and Super-Lift Luo Converter with (a) Battery Output Power and (b) Super Capacitor Output Power.

The effect of both converters, when connected with the battery and SC that make up the HESS, is seen in Fig.4.30. With the Super Lift Luo converter, the HESS can extract more power from the supercapacitor and battery, even in situations where the solar energy input varies due to the global irradiance; it is because energy losses during the conversion process are minimized by the super-lift Luo converter design. It is evident that when utilizing a super lift Luo, the battery's state of charge is approximately 0.2% greater than when using a boost converter. Additionally, super lift Luo is higher for supercapacitors, reaching 0.4% more significantly than a boost converter. The battery and supercapacitor can be charged faster and more efficiently due to the HESS with a super-lift Luo converter's higher efficiency and power output.

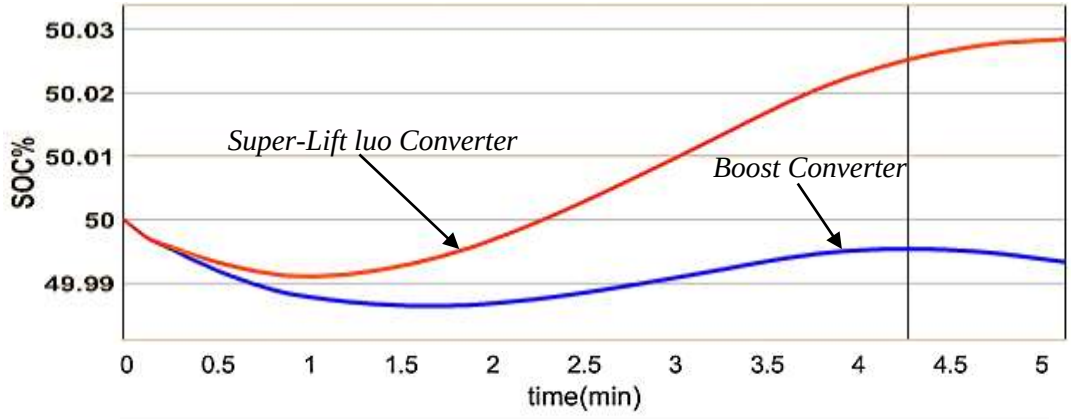

(a)

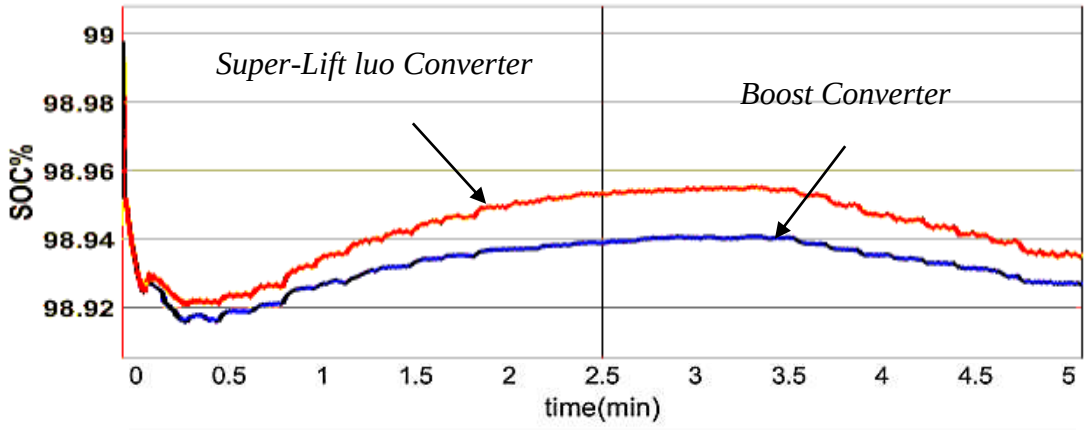

(b)

Fig.4.30: Effect of Boost and Super-Lift Luo Converters on (a) Battery State of Charge and (b) Supercapacitor State of Charge.

4.6 Performance of MPPT Tracking Algorithm

Comparative outcomes of the MPPTs in various scenarios. The MPP reached by every algorithm will determine the result of this study. The scenarios are based on an irradiance of 1000(W/m^2), 400 (W/m^2), a combination of 1000 - 400 (W/m^2), and finally, the global irradiance of Kerbala City, and the results are shown in Fig.4.31. Depending on how radiation input affects MPPT module power, it is clear that power output would decrease with decreasing irradiation input.

After comparing the outcomes of the four algorithms, P&O has a more considerable output power than techniques and a higher current and constant voltage value. However, in the case of 400(W/m^2), the INC is more accurate in tracking and requires less power than other algorithms. The particular reason for Inc MPPTs is that they employ advanced algorithms and enhanced perturbation control to overcome the drawbacks of conventional MPPT methods in low-irradiance scenarios. For this reason, it is utilized for MPP in areas with low solar irradiance levels. The P&O is more efficient and has the best MPP among PV panels regarding global irradiation.

Table 4.6 determines the duty cycle under global irradiation for each MPPT technique. P&O's ability to rapidly locate the MPP is beneficial. As irradiance changes throughout the day, the MPP also shifts. P&O's quick response allows it to adjust the duty cycle effectively to maintain operation closer to the MPP, potentially leading to a better overall duty cycle across varying irradiance levels.

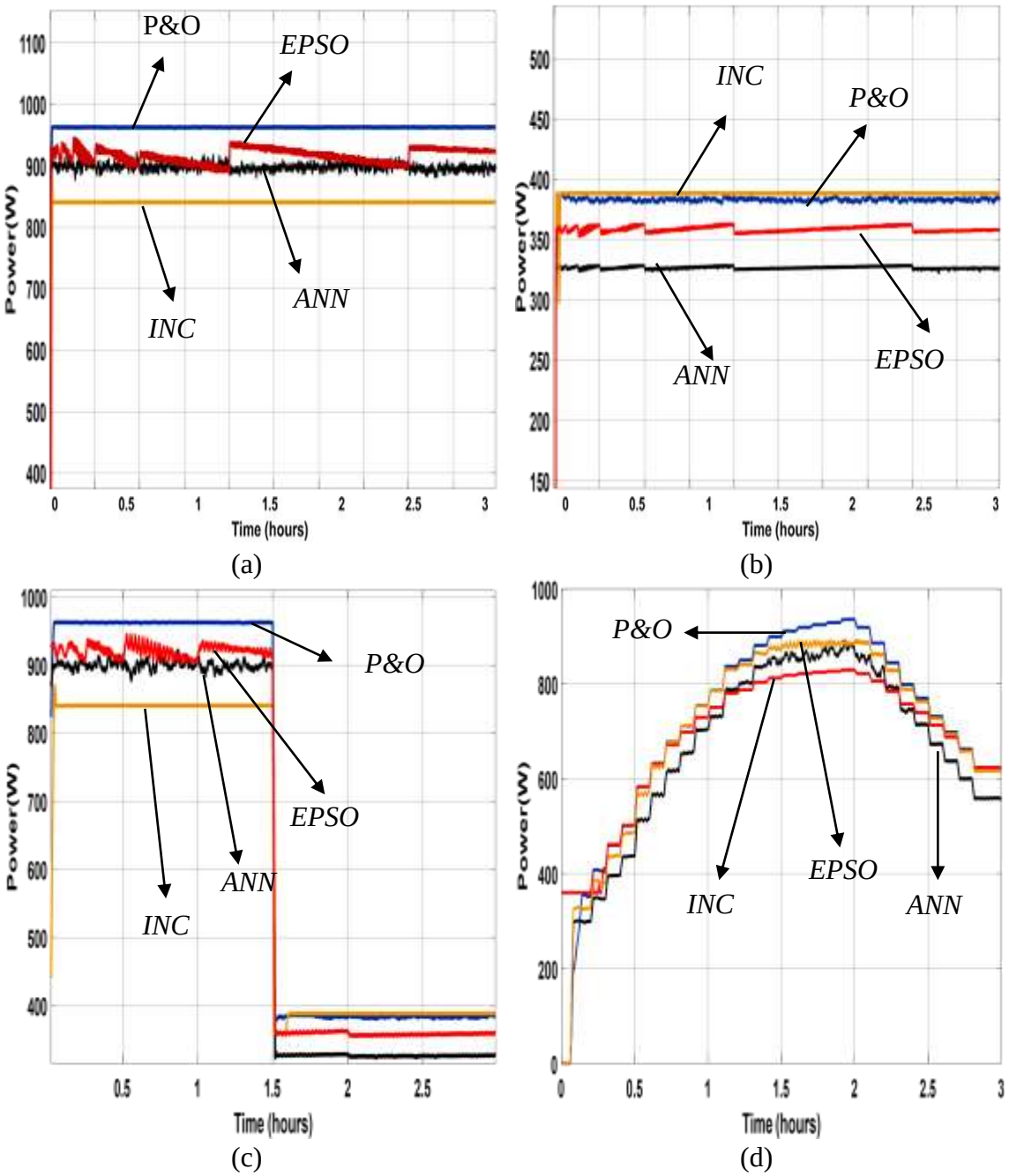

Fig.4.31 : MPPTs Response Under (a)1000(W/m^2), (b)400(W/m^2), (c)1000-400(W/m^2), (d)Global Irradiance.

Fig.4.32 shows the SoC of the battery with different MPPTs.The P&O algorithm has the highest SoC when charging for operation. P&O can improve battery SoC faster, especially in situations with global irradiation.

Table 4.6 :The MPPT Controllers' Duty Cycle.

MPPT	P&O	ANN	INC	EPSO
δ_{max}	0.5	0.9	0.2	0.09
δ_{min}	0.05	0.1	0.03	0.05

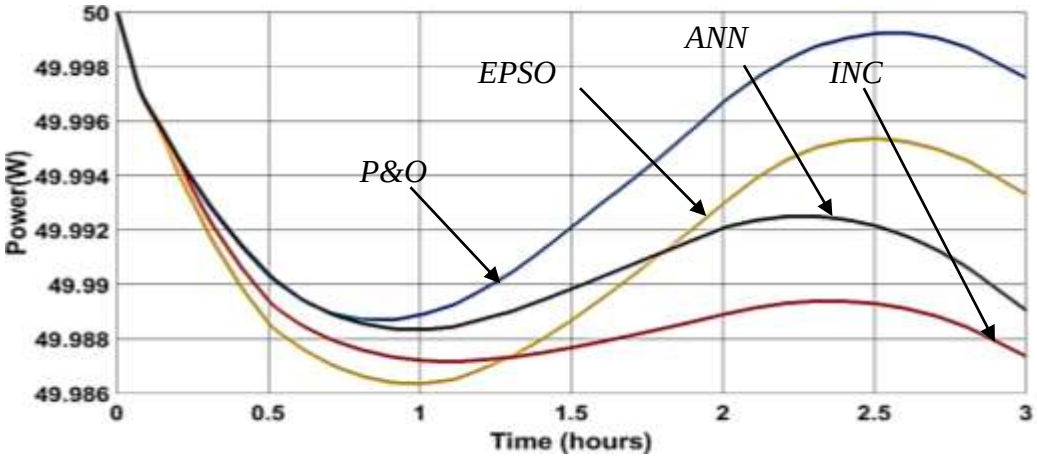

Fig.4.32 : Battery SoC with Different Tracking Algorithms: P&O, ANN, EPSO, and INC

The following things may be the cause of the disparity. The specifications of the Simulink Lithium-ion battery model differ from those of the actual Li-ion battery Gel. Considering the current integration in time and capacity, the SoC calculation for the Simulink model uses the battery voltage level as a starting point. Simulink's battery model never simulates an ageing or capacity-derated battery; instead, it always runs under new conditions. A greater power output from the P&O solar panel means more power is available for battery charging. It immediately quickens the rate at which the battery's SoC changes.

4.7 Sensorless Backstepping Controller Results

The integration of an SMO with backstepping control for PMSM speed control in HEVs is covered in this section. By estimating unmeasured states and minimizing the impact of uncertainties and disruptions, the SMO increases the resilience of the control system. In practical HEV applications, the combined method seeks to deliver better speed-tracking performance and increased system robustness.

Fig.4.33 shows the speed tracking response when using sensorless control. The SMO successfully addresses the limitations of backstepping control by offering good speed-tracking accuracy and robustness against uncertainties in an HEV environment.

Even though the SMO with backstepping control has several advantages for PMSM speed control in HEVs, there is a chance that speed tracking will have a slight fluctuation and overshoot reach (0.1-0.25) higher than sensor control. Aggressive switching gains cause this; the SMO needs a switching term to produce sliding mode behavior. Selecting excessively aggressive switching gains might cause chattering, characterized by abrupt changes in the control signal. That can lead to variations and possible overshoot as the speed oscillates around the desired value. These unmodeled dynamics have the potential to introduce errors into the state estimation process, which could cause fluctuations or overshoot as well as deviations from the intended speed trajectory.

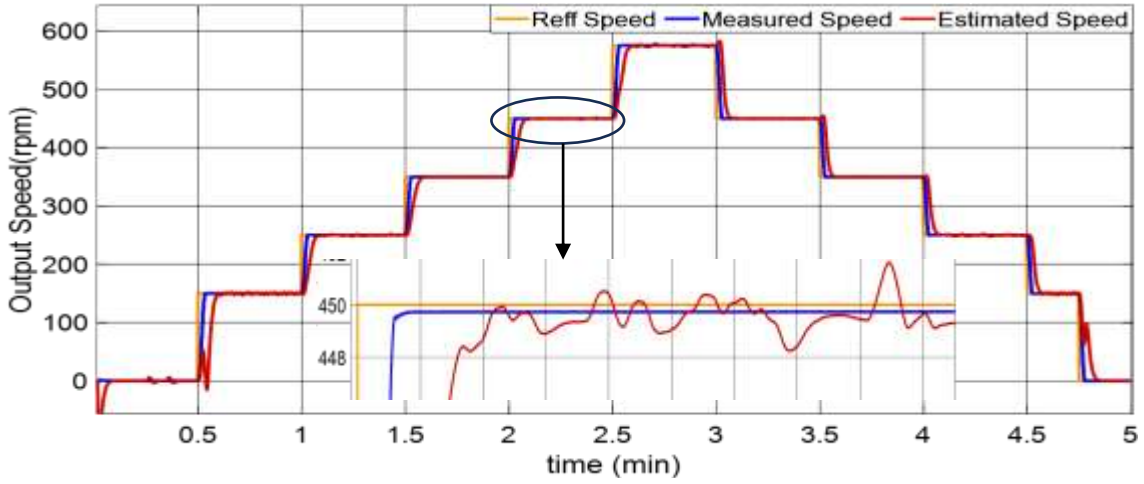

(a)

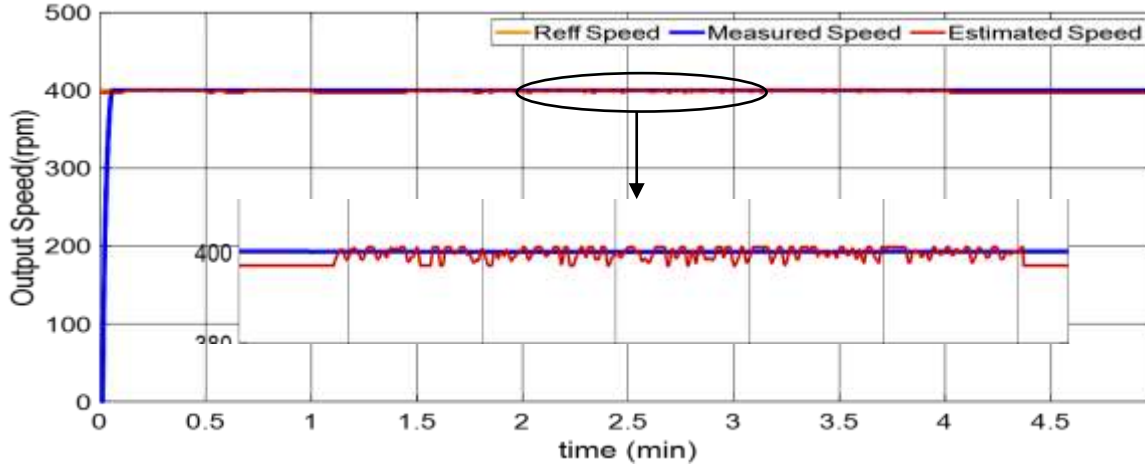

(b)

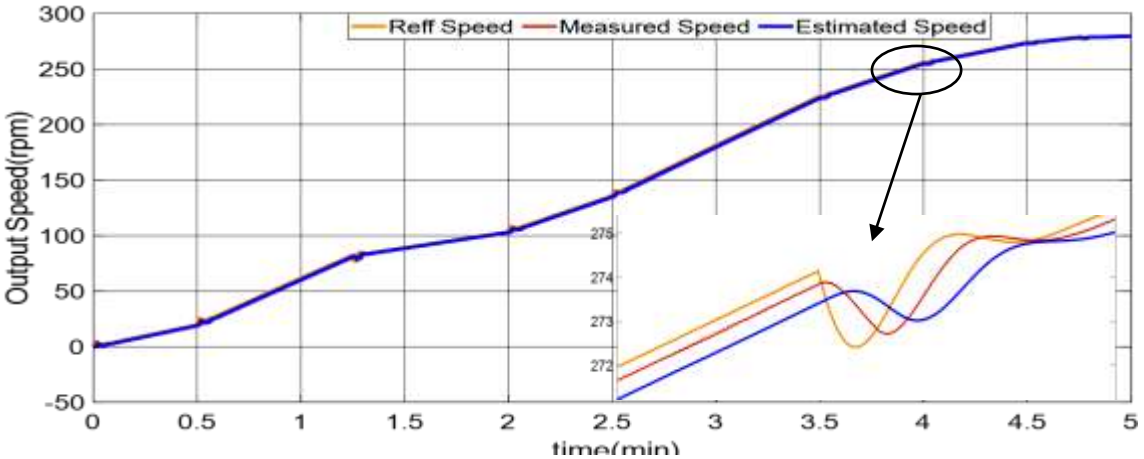

`(c)

Fig.4.33: Speed Response of Sensorless Speed Controller for (a) First Scenario, (b)Second Scenario, (c)Third Scenario.

4.8 Fuel Cell Hybrid Electric Vehicle

With its 7-level inverter, sensorless backstepping speed control, and intelligent energy management, this FCHEV system provides a potential way forward for electric vehicles. Further research and development can raise these vehicles' performance, efficiency, and cost. As shown in Fig.4.34(a), the reference speed and torque for FCHEV will depend on the accelerator pedal. Fig.4.34 shows how sensorless backstepping control combined with a 7-level inverter can provide FCHEVs with optimal speed and torque response for the previously mentioned reasons. The torque response error shows that it converges to zero after(0.2sec) using backstepping control for FCHEV.

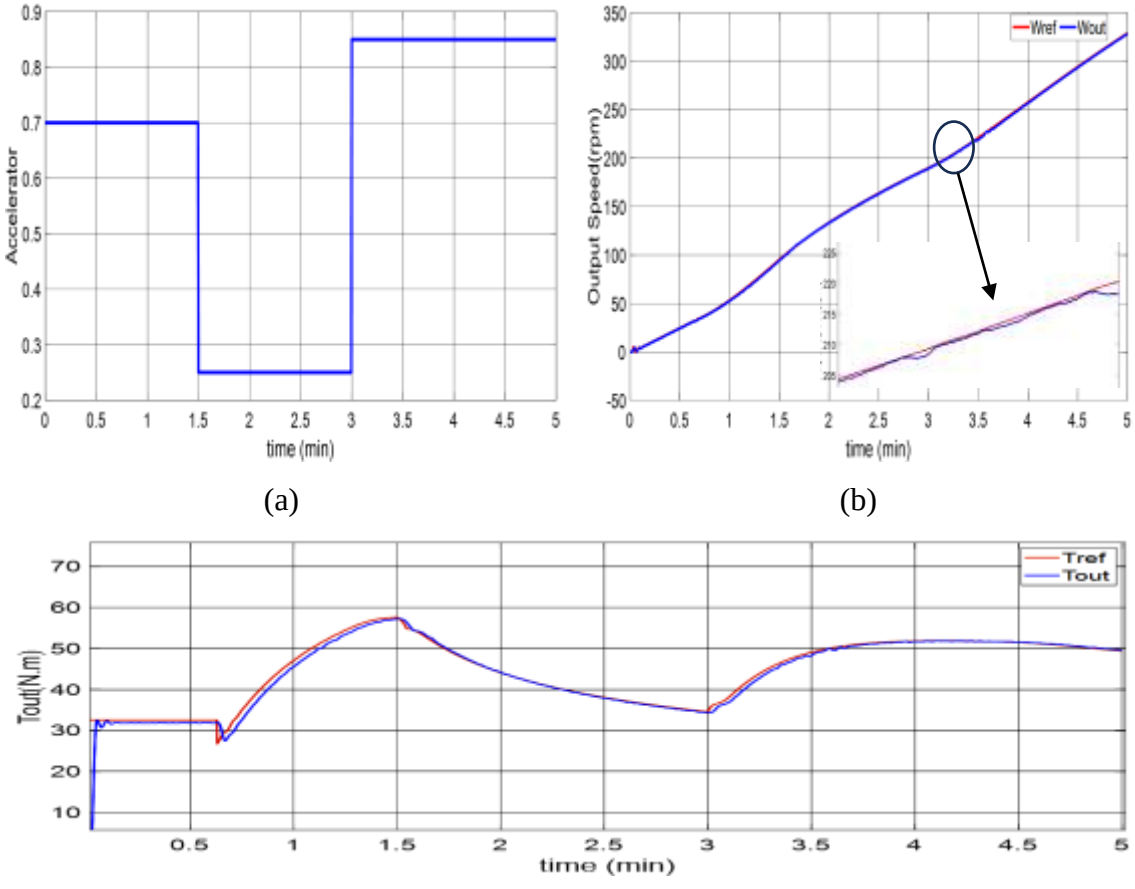

(a) (b)

(c)

Fig.4.34: System Response with Fuel Cell,(a) Pedal Speed (Accelerator),(b) Speed Response,(c) Torque Response.

Fig.4.35 demonstrates the intelligent EMS that, using an adaptive PID controller, indicates that when the speed exceeds 45 km/h, the fuel cell's energy will be utilized to protect the battery from excessive load. Otherwise, the energy from FC and HESS will be used. The advantages of this strategy:

- Giving the FC the most significant importance at high speeds can keep the battery from being overworked and increase its life.
- The FC operates more effectively at its ideal power range, which could consume less hydrogen.
- Enough power is provided for all driving conditions when FC and battery are used together.
- This feature allows the system to modify its plan in response to changing circumstances, improving overall performance. After 3sec, when the throttle is used for the brake, the motor will operate as a generator and convert the mechanical energy to electrical energy, as shown in Fig.4.35(b).

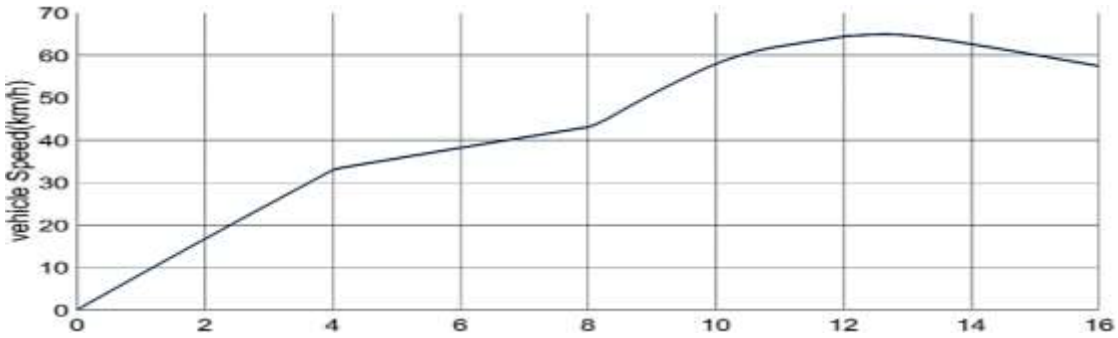

(a)

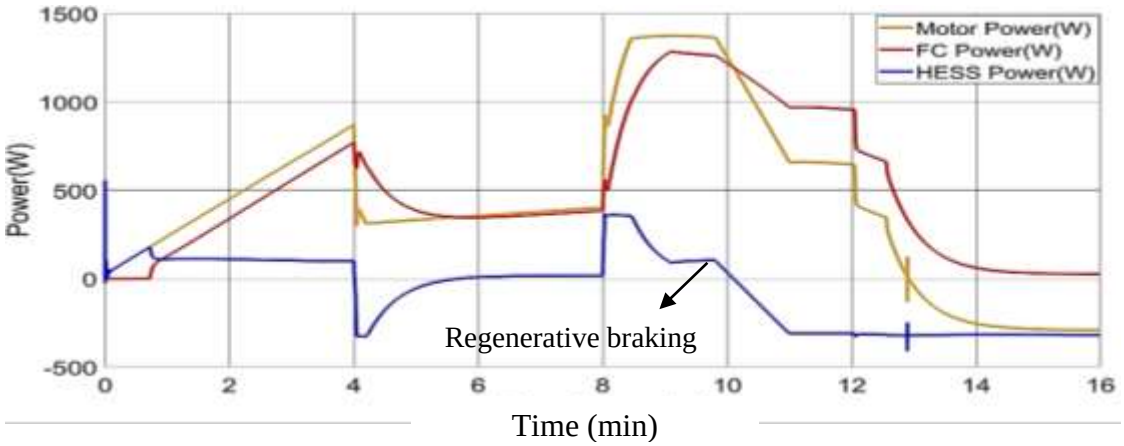

(b)

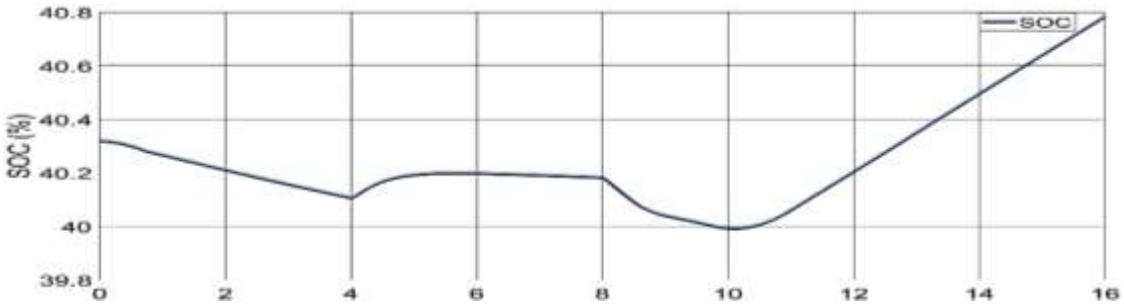

(c)

Fig.4.35 : EMS Response with (a) Vehicle Speed, (b) Power Delivered, (c) Battery SoC.

The vehicle's electric range increases by recharging the battery and SC with the energy captured, and its dependency on the primary power source decreases. Fig.4.35(c) shows the battery SoC. It was evident that using regenerative techniques would result in a higher SoC.

4.9 Autonomous Hybrid Electric Vehicle Performance

The potential of adaptive model predictive control AMPC as an effective strategy for improving AHEV path tracking performance is examined in this thesis. AMPC provides a unique ability to predict future vehicle behaviour, optimize control inputs, and actively adjust to conditions. This method promises to significantly increase path-tracking accuracy, stability, and driving comfort by tackling model uncertainty and external disturbances.

Fig.4.36 shows the three scenarios that will be used for the HEV to conduct tests and perform the AMPC. The first path has many waypoints; for the longest, the vehicle must move away from the large cuboid in the trajectory and back to the correct trajectory. The second path has the shortest waypoints shortest. The vehicle only needs to track the path trajectory, and the third scenario depends on the Geographic Information System (GIS) for the University of Kerbala Streets.

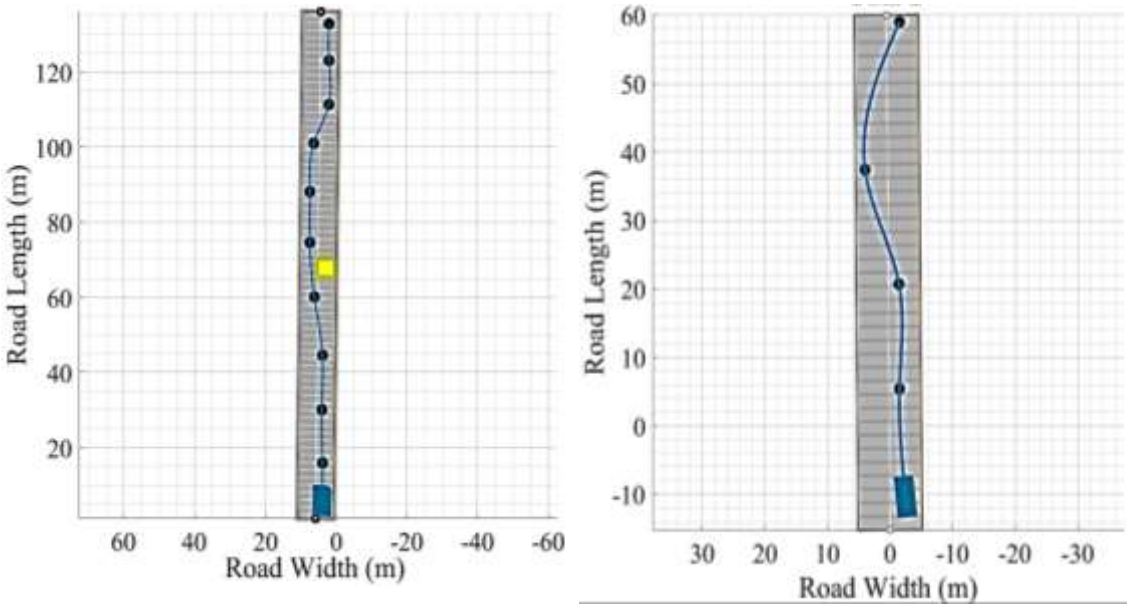

(a) (b)

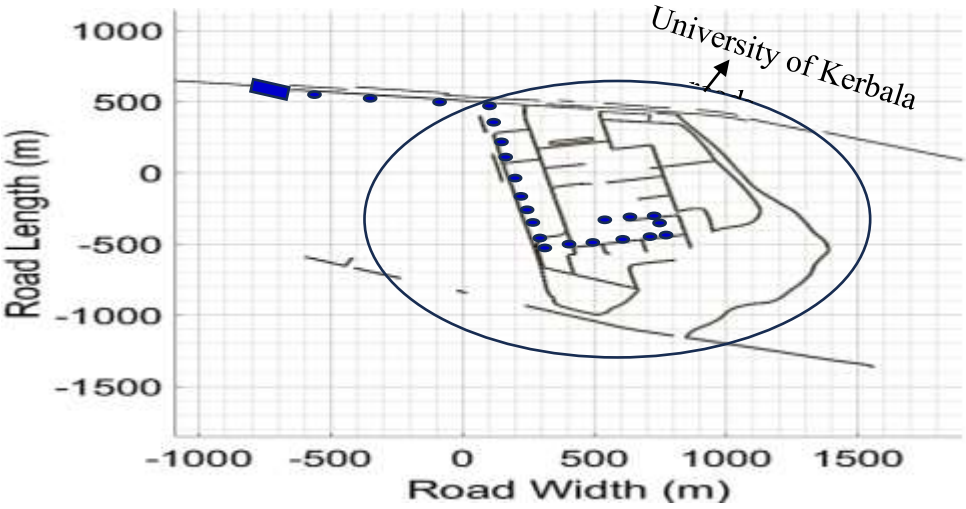

(c)

Fig.4.36 : The Reference Path Scenario (a) First Scenario (b) Second Scenario (c) Third Scenario.

After creating the two paths, the references can be represented by position laterally and the angle of Yaw, as shown in Fig.4.37. The response of the first path shows that the lateral position starts in a slight overshoot in a short time of about (1.2 sec) and then becomes quite close to the reference. Fig.4.37(c) demonstrates that the response of the second lateral position was close to ideal

because the turn was small, making it easy to control. Fig.4.37(b,d,f). Yaw1, Yaw-2, and Yaw-3 results were as close to reference as possible, while the tracking error reached zero for the first and second Yaw-Angle, equal to lateral tracking errors. As shown from the results above at time-space for (15 seconds), the time response of all scenarios system was almost similar to the reference signal, and the vehicle overcame the collision with the large cuboid without problems and with high accuracy. The results were just that steady-state error for the angles of yaw and lateral and undershoot when positioned laterally. The AMPC gives many advantages to the path-tracking process; if the number of waypoints is high, that makes the control of the vehicle more difficult, and it takes more time to reach a steady state, but it has an advantage by increasing the efficiency of the path tracking process.

The steering angle remains within the permitted range. The primary benefit of the suggested AMPC controller is that it guarantees the driving immovability of vehicles, which could be decided as shown in Fig.4.38. The steering angle in the front can be adjusted using an MPC-based controller. Driving efficiency and consistency are ensured when the vehicle stays on the selected route. Autonomous MPC significantly benefits when attaining smooth steering angle commands for path tracking in AHEVs. The integration of prediction, optimization, and real-time adaptability facilitates the development of autonomous vehicles that offer enhanced comfort and efficiency for drivers.

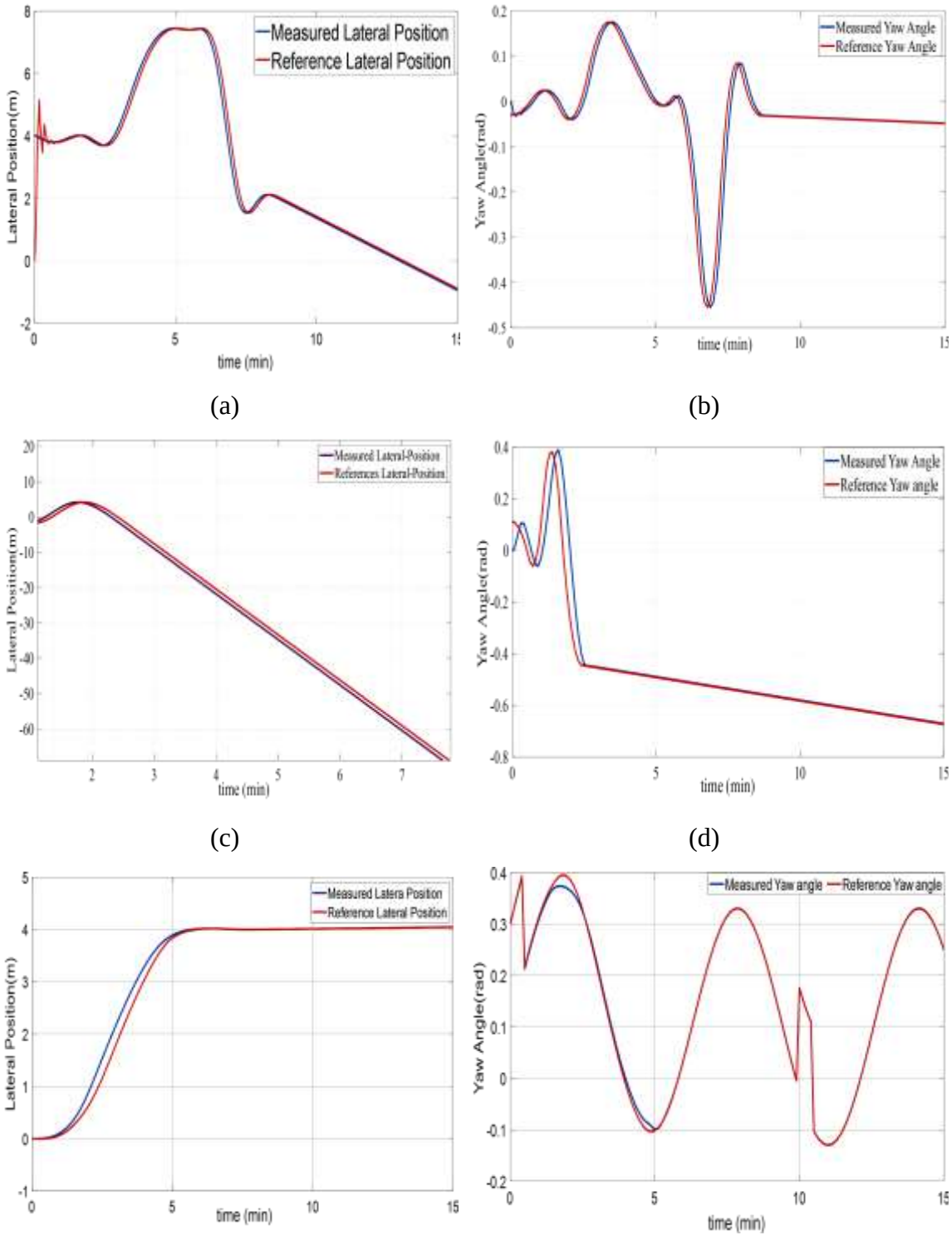

Fig.4.37 : Response of the System Model of (a) Lateral-1,(b) Yaw Angle-1, (c) Lateral-2 , (d)Yaw Angle -2, (e) Lateral-3,(f) Yaw Angle -3.

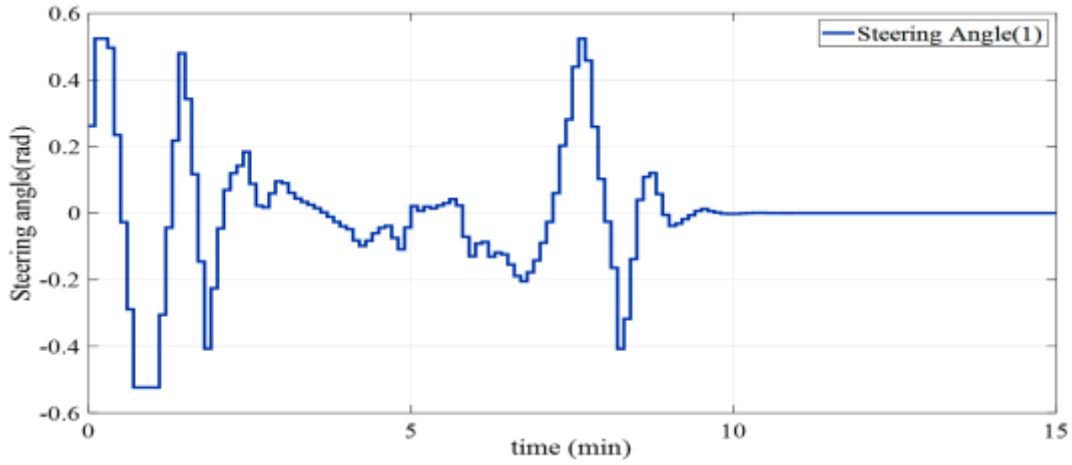

(a)

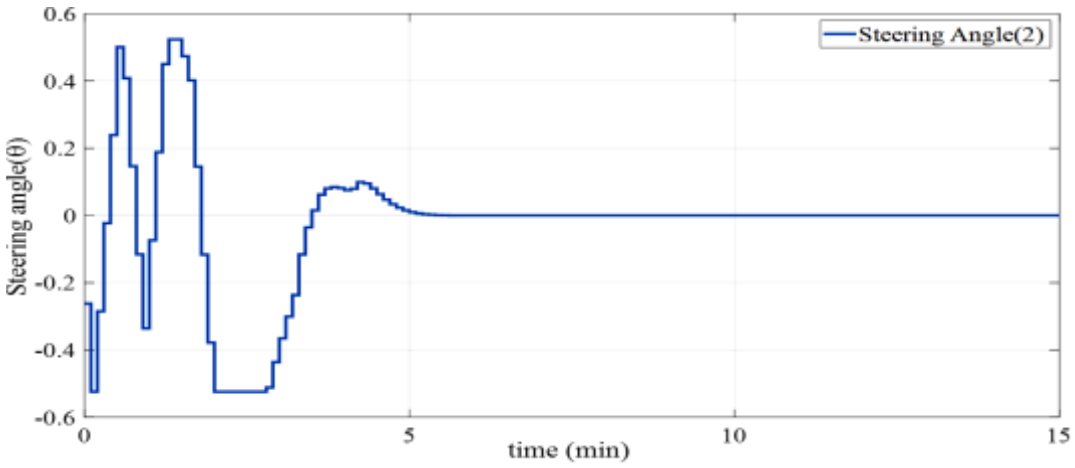

(b)

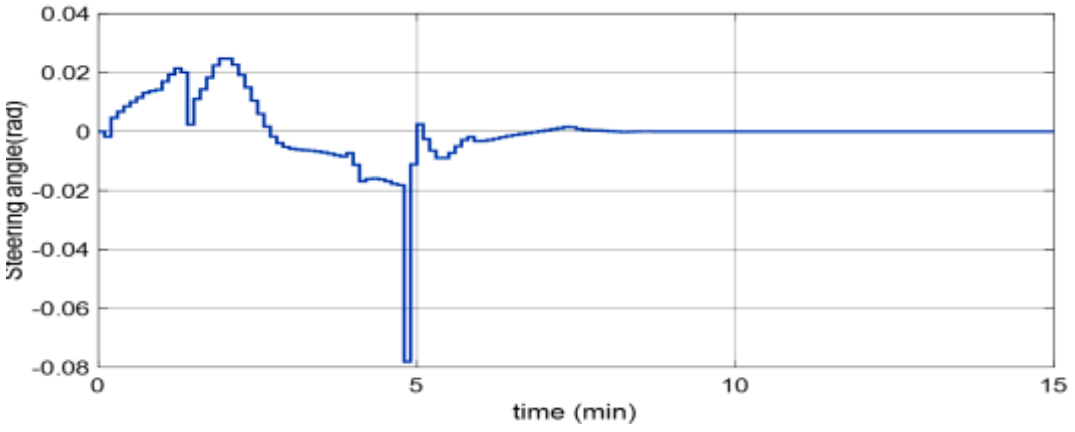

c

Fig.4.38 : Time Response for Steering Angle-1 (a) First Scenario,(b) Second Scenario, (c) Third Scenario.

Chapter Five: Conclusion and Future Work

5.1 Conclusion

This research investigated the potential for enhancing the dynamic performance of HEVs and explored the feasibility of autonomous operation through a novel system. To assess the effectiveness of the system, numerical simulation was applied to three different operating scenarios:

1) The results highlight the advantages of a PMSM combined with backstepping speed control based on Lyapunov stability theory over other motor-control designs. Better energy efficiency, torque ripple reduction reach of about (0.083%), and overall system smoothness were all proved by this combination. In particular, torque and speed variations were substantially reduced using backstepping control, which improved driving comfort and possibly increased component lifetime.
2) Supercapacitors, batteries, and solar energy integration improved HESS. A Perturbation and Observation (P&O) algorithm proved instrumental in maximizing solar power extraction, accelerating battery and supercapacitor charging, and improving overall HEV efficiency. The Super-Lift Luo converter demonstrated superiority over the boost converter regarding MPPT efficiency of about (15%) and voltage regulation. Additionally, by successfully decreasing torque and speed fluctuations, the 7-level inverter enhanced HESS performance and decreased the THD.
3) Incorporating a fuel cell expanded the HESS's operational range by alleviating battery load at higher speeds. This strategy has been demonstrated to protect the battery from undue stress and increase its lifespan. This further

proved the motor control technique's effectiveness in managing demands for different torque and speed.

4) The research extended to the realm of autonomous operation by exploring the application of AMPC for path tracking. The outcomes proved that it was possible to convert the HEV into an autonomous HEV (AHEV). While the achieved path-tracking accuracy of 99.2% is promising, further integration of sensors, high-resolution maps, and sophisticated decision-making algorithms is required for practical implementation.

In this thesis, a study has significantly contributed to the advancement of HEV technology. The potential for improving vehicle performance, efficiency, and sustainability is evident with the proposed AHEV. To maximize the potential of autonomous HEVs, future research should focus on cost-benefit analysis, real-world validation, and the smooth integration of the AMPC with other autonomous vehicle subsystems.

5.2 Future Work

This thesis has laid a strong foundation for advancing HEV performance and autonomous integration. However, the quest for a more sustainable and efficient future demands further exploration. Here are some exciting avenues for future work, building upon the findings of this study:

1) Enhancing Motor Control:

- Improve control over backstepping by utilizing adaption strategies for this approach.
- Examine how sensorless backstepping control is implemented on current HEV devices.

2) Optimizing hybrid energy storage system through the following:

- Examine the inclusion of cutting-edge battery technology, such as lithium-sulfur or solid-state batteries. These innovations could increase energy density, speed up charging, and boost safety, increasing the practicality of hybrid electric vehicles.
- Create more advanced energy management algorithms that can balance the relations between the fuel cell, supercapacitor, and battery within the hybrid energy storage system, depending on power requirements and driving conditions, in real-time.

3) Multi-level inverter advancement through the following:

- Examine the viability and possible advantages of utilizing higher-level MLIs in HEVs (such as 11-level and 13-level) for minimizing torque ripple in electrical machines.
- Examine the possibility of designing MLIs using such devices as Silicon Carbide and Gallium Nitride. These devices offer superior switching characteristics and higher efficiency, potentially leading to further performance improvements in HEVs.

4) Beyond the Core Technologies through the following:

- Examine how communication technology might be included in HEV. In addition to improving safety and traffic flow, this would allow communication with vehicles and infrastructure and may help develop cooperative autonomous driving systems.
- Conduct a comprehensive life cycle assessment of HEVs, considering the environmental impact throughout their life cycle, from material sourcing and manufacturing to operation and disposal. That can help identify areas for improvement and promote genuinely sustainable HEVs' development.

5) Integration with autonomous technologies through the following:

- Investigate integrating several sensors (LiDAR, Radar, Cameras) and create robust sensor fusion algorithms enabling autonomous HEVs to detect their surroundings accurately and consistently.
- Develop sophisticated path planning algorithms to navigate complex traffic scenarios and make real-time decisions for safe and efficient autonomous operation.

Researchers and engineers can expand on the groundwork this study provided by exploring these directions for future research. It will open the door for creating even more eco-friendly, autonomous, and efficient hybrid electric vehicles, resulting in a more sustainable transportation future.

References

[1] R. Vidhi and P. Shrivastava, "A review of electric vehicle lifecycle emissions and policy recommendations to increase EV penetration in India," *Energies*, vol. 11, no. 3, pp. 1–15, 2018, doi: 10.3390/en11030483.

[2] Z. P. Cano *et al.*, "Batteries and fuel cells for emerging electric vehicle markets," *Nat. Energy*, vol. 3, no. 4, pp. 279–289, 2018, doi: 10.1038/s41560-018-0108-1.

[3] A. Sachdeva and D. D. Mohite, "Recent Development in Green Fuel Vehicles and their Future Advancements," *Int. Res. J. Eng. Technol.*, 2020, [Online]. Available: www.irjet.net

[4] F. Novakazi, M. Johansson, H. Strömberg, and M. A. Karlsson, "Levels of What?Investigating Drivers' Understanding of Different Levels of Automation in Vehicles," *J. Cogn. Eng. Decis. Mak.*, vol. 15, no. 2–3, pp. 116–132, 2021, doi: 10.1177/15553434211009024.

[5] I. López, E. Ibarra, A. Matallana, J. Andreu, and I. Kortabarria, "Next generation electric drives for HEV/EV propulsion systems: Technology, trends and challenges," *Renew. Sustain. Energy Rev.*, vol. 114, no. April 2018, p. 109336, 2019, doi: 10.1016/j.rser.2019.109336.

[6] A. Matallana *et al.*, "Power module electronics in HEV/EV applications: New trends in wide-bandgap semiconductor technologies and design aspects," *Renew. Sustain. Energy Rev.*, vol. 113, no. June, p. 109264, 2019, doi: 10.1016/j.rser.2019.109264.

[7] L. Guo, H. Chen, B. Gao, and Q. Liu, "Energy management of HEVs based on velocity profile optimization," *Sci. China Inf. Sci.*, vol. 62, no. 8, 2019, doi: 10.1007/s11432-018-9529-7.

[8] W. Sarwar, T. Engstrom, M. Marinescu, N. Green, N. Taylor, and G. J. Offer, "Experimental analysis of Hybridised Energy Storage Systems for automotive applications," *J. Power Sources*, vol. 324, pp. 388–401, 2016, doi: 10.1016/j.jpowsour.2016.05.114.

[9] Saleh A, Faiqotul Azmi KS, Hardianto T, Hadi W. Comparison of MPPT fuzzy logic controller based on perturb and observe (P&O) and incremental conductance (InC) algorithm on the buck-boost converter. *Proceedings - 2018 2nd International Conference on Electrical Engineering and Informatics: Toward the Most Efficient Way of Making and Dealing with Future Electrical Power System and Big Data Analysis, ICon EEI 2018* 2018(October): 154–158.

[10] C.- Nd, "http://creativecommons.org/licenses/by-nc-nd/4.0/," pp. 0–24, 2021.

[11] S. J. Rind, M. Jamil, and A. Amjad, "Electric Motors and Speed Sensorless Control for Electric and Hybrid Electric Vehicles: A Review," *Proc. - 2018 53rd Int. Univ. Power Eng. Conf. UPEC 2018*, no. September 2018, 2018, doi: 10.1109/UPEC.2018.8541871.

[12] Z. Zhang, Y. Dong, and Y. Han, "Dynamic and Control of Electric Vehicle in Regenerative Braking for Driving Safety and Energy Conservation," *J. Vib. Eng. Technol.*, vol. 8, no. 1, pp. 179–197, 2020, doi: 10.1007/s42417-019-00098-0.

[13] A. R. Jordehi, "Maximum power point tracking in photovoltaic (PV) systems: A review of different approaches," *Renew. Sustain. Energy Rev.*, vol. 65, pp. 1127–1138, 2016, doi: 10.1016/j.rser.2016.07.053.

[14] H. N. De Melo, J. P. F. Trovão, P. G. Pereirinha, H. M. Jorge, and C. H. Antunes, "A controllable bidirectional battery charger for electric vehicles with vehicle-To-grid capability," *IEEE Trans. Veh. Technol.*,

vol. 67, no. 1, pp. 114–123, 2018, doi: 10.1109/TVT.2017.2774189.

[15] H. Hao, Y. Geng, W. Li, and B. Guo, “Energy consumption and GHG emissions from China’s freight transport sector: Scenarios through 2050,” *Energy Policy*, vol. 85, pp. 94–101, 2015, doi: 10.1016/j.enpol.2015.05.016.

[16] R. P. Denaro, J. Zmud, S. Shladover, B. W. Smith, and J. Lappin, *Implications for Transportation Automated Vehicle Technology : Driverless Cars : Plus :*, no. 292. 2014. [Online]. Available: https://onlinepubs.trb.org/onlinepubs/trnews/trnews292.pdf

[17] B. Anton and A. Florescu, “Design and Development of Series-Hybrid Automotive Powertrains,” *IEEE Access*, vol. 8, pp. 226026–226041, 2020, doi: 10.1109/ACCESS.2020.3044500.

[18] P. G. Anselma *et al.*, “Comparing parallel hybrid electric vehicle powertrains for real-world driving,” *2019 AEIT Int. Conf. Electr. Electron. Technol. Automotive, AEIT Automot. 2019*, no. August, pp. 1–6, 2019, doi: 10.23919/EETA.2019.8804609.

[19] Y. Wang, X. Wang, Y. Sun, and S. You, “Model predictive control strategy for energy optimization of series-parallel hybrid electric vehicle,” *J. Clean. Prod.*, vol. 199, no. October, pp. 348–358, 2018, doi: 10.1016/j.jclepro.2018.07.191.

[20] O. Singh and S. K. Gupta, “A review on recent Mppt techniques for photovoltaic system,” *2018 IEEMA Eng. Infin. Conf. eTechNxT 2018*, pp. 1–6, 2018, doi: 10.1109/ETECHNXT.2018.8385315.

[21] F. Un-Noor, S. Padmanaban, L. Mihet-Popa, M. N. Mollah, and E. Hossain, “A comprehensive study of key electric vehicle (EV) components, technologies, challenges, impacts, and future direction of development,” *Energies*, vol. 10, no. 8, 2017, doi: 10.3390/en10081217.

[22] T. A. Zarma, A. A. Galadima, and M. A. Aminu, "Review of Motors for Electrical Vehicles," *J. Sci. Res. Reports*, pp. 1–6, Oct. 2019, doi: 10.9734/jsrr/2019/v24i630170.

[23] A. Eldho Aliasand and F. T. Josh, "Selection of Motor foran Electric Vehicle: A Review," *Mater. Today Proc.*, vol. 24, pp. 1804–1815, 2020, doi: 10.1016/j.matpr.2020.03.605.

[24] H. T. ARAT, "Numerical Comparison of Driving Cycles with Different Electric Motors (IM and PM) Operated in a Hybrid Electric Vehicle," *Eur. J. Sci. Technol.*, no. 14, pp. 378–387, 2018, doi: 10.31590/ejosat.494127.

[25] Z. Zhong, S. Jiang, Y. Zhou, and S. Zhou, "Magnetic coenergy based modelling of PMSM for HEV/EV application," *Prog. Electromagn. Res. M*, vol. 50, no. September, pp. 11–22, 2016, doi: 10.2528/PIERM16061501.

[26] D. Mohanraj, J. Gopalakrishnan, B. Chokkalingam, and L. Mihet-Popa, "Critical Aspects of Electric Motor Drive Controllers and Mitigation of Torque Ripple - Review," *IEEE Access*, vol. 10, no. July, pp. 73635–73674, 2022, doi: 10.1109/ACCESS.2022.3187515.

[27] D. K. Athanasopoulos, V. I. Kastros, and J. C. Kappatou, "Electromagnetic analysis of a PMSM with different rotor topologies," *Proc. - 2016 22nd Int. Conf. Electr. Mach. ICEM 2016*, no. September, pp. 306–312, 2016, doi: 10.1109/ICELMACH.2016.7732543.

[28] C. Ogbuka, C. Nwosu, and M. Agu, "Dynamic and steady state performance comparison of line-start permanent magnet synchronous motors with interior and surface rotor magnets," *Arch. Electr. Eng.*, vol. 65, no. 1, pp. 105–116, 2016, doi: 10.1515/aee-2016-0008.

[29] K. D. Hoang and H. K. A. Aorith, "Online Control of IPMSM Drives

for Traction Applications Considering Machine Parameter and Inverter Nonlinearities," *IEEE Trans. Transp. Electrif.*, vol. 1, no. 4, pp. 312–325, 2015, doi: 10.1109/TTE.2015.2477469.

[30] L. Li and Q. Liu, "Research on IPMSM drive system control technology for electric vehicle energy consumption," *IEEE Access*, vol. 7, pp. 186201–186210, 2019, doi: 10.1109/ACCESS.2019.2958944.

[31] M. Salehifar, M. Moreno-Eguilaz, G. Putrus, and P. Barras, "Simplified fault tolerant finite control set model predictive control of a five-phase inverter supplying BLDC motor in electric vehicle drive," *Electr. Power Syst. Res.*, vol. 132, pp. 56–66, 2016, doi: 10.1016/j.epsr.2015.10.030.

[32] S. Sharifan, S. Ebrahimi, A. Oraee, and H. Oraee, "Performance comparison between brushless PM and induction motors for hybrid electric vehicle applications," pp. 719–724, 2016, doi: 10.1109/optim.2015.7492473.

[33] R. Thike and P. Pillay, "Mathematical Model of an Interior PMSM with Aligned Magnet and Reluctance Torques," *IEEE Trans. Transp. Electrif.*, vol. 6, no. 2, pp. 647–658, 2020, doi: 10.1109/TTE.2020.2991369.

[34] A. A. R. Altahir, "Park and Clark Transformations: A Short Review," *no. April*, no. April, pp. 2–5, 2020, doi: 10.13140/RG.2.2.20287.46241.

[35] W. Cao, A. A. S. Bukhari, and L. Aarniovuori, "Review of Electrical Motor Drives for Electric Vehicle Applications," *Mehran Univ. Res. J. Eng. Technol.*, vol. 38, no. 3, pp. 525–540, 2019, doi: 10.22581/muet1982.1903.01.

[36] D. Mohanraj *et al.*, "A Review of BLDC Motor: State of Art, Advanced Control Techniques, and Applications," *IEEE Access*, vol. 10, pp. 54833–54869, 2022, doi: 10.1109/ACCESS.2022.3175011.

[37] M. Yildirim and H. Kurum, “Electronic Differential System for an Electric Vehicle with Four In-wheel PMSM,” *IEEE Veh. Technol. Conf.*, vol. 2020-May, 2020, doi: 10.1109/VTC2020-Spring48590.2020.9129139.

[38] B. Ren, H. Chen, H. Zhao, and W. Xu, “MPC-based torque control of permanent magnet synchronous motor for electric vehicles via switching optimization,” *Control Theory Technol.*, vol. 15, no. 2, pp. 138–149, 2017, doi: 10.1007/s11768-017-6193-z.

[39] E. YORAT, N. S. ÖZBEK, and L. SARIBULUT, “Performance Evaluation of Brushless Direct Current Motor Control Methods through Low-Cost Microcontroller-Based Real-Time Experiments,” *Gazi Üniversitesi Fen Bilim. Derg. Part C Tasarım ve Teknol.*, vol. 11, no. 2, pp. 498–510, 2023, doi: 10.29109/gujsc.1229896.

[40] O. Tosun and N. F. O. Serteller, “The Design of the Outer-Rotor Brushless DC Motor and an Investigation of Motor Axial-Length-to-Pole-Pitch Ratio,” *Sustain.*, vol. 14, no. 19, 2022, doi: 10.3390/su141912743.

[41] H. J. Hu, G. Z. Cao, S. D. Huang, C. Wu, and Y. P. Peng, “Drive circuit-based torque-ripple suppression method for single-phase BLDC fan motors to reduce acoustic noise,” *IET Electr. Power Appl.*, vol. 13, no. 7, pp. 881–888, 2019, doi: 10.1049/iet-epa.2018.5234.

[42] I. Shchur and D. Jancarczyk, “Electromagnetic torque ripple in multiple three-phase brushless dc motors for electric vehicles,” *Electron.*, vol. 10, no. 24, 2021, doi: 10.3390/electronics10243097.

[43] M. Ridwan, M. N. Yuniarto, and Soedibyo, “Electrical equivalent circuit based modeling and analysis of brushless direct current (BLDC) motor,” *Proceeding - 2016 Int. Semin. Intell. Technol. Its Appl. ISITIA 2016*

Recent Trends Intell. Comput. Technol. Sustain. Energy, pp. 471–478, 2017, doi: 10.1109/ISITIA.2016.7828706.

[44] D. Chowdhury, M. Chattopadhyay, and P. Roy, "Modelling and Simulation of Cost Effective Sensorless Drive for Brushless DC Motor," *Procedia Technol.*, vol. 10, pp. 279–286, 2013, doi: 10.1016/j.protcy.2013.12.362.

[45] D. Yadav, U. Parekh, K. Patel, R. Parmar, P. Prakash, and U. G. Student, "Application of Modified Three Phase Conduction Method to Minimize Torque Ripple in BLDC Motor," vol. 6, no. 1, pp. 3–4, 2019.

[46] A. K. Tripathi, S. Ray, M. Aruna, and S. Prasad, "Evaluation of solar PV panel performance under humid atmosphere," *Mater. Today Proc.*, vol. 45, no. xxxx, pp. 5916–5920, 2020, doi: 10.1016/j.matpr.2020.08.775.

[47] J. D. Bastidas-Rodriguez, G. Petrone, C. A. Ramos-Paja, and G. Spagnuolo, "A genetic algorithm for identifying the single diode model parameters of a photovoltaic panel," *Math. Comput. Simul.*, vol. 131, pp. 38–54, 2017, doi: 10.1016/j.matcom.2015.10.008.

[48] K. Ishaque, Z. Salam, and H. Taheri, "Accurate MATLAB simulink PV system simulator based on a two-diode model," *J. Power Electron.*, vol. 11, no. 2, pp. 179–187, 2011, doi: 10.6113/JPE.2011.11.2.179.

[49] V. Stornelli, M. Muttillo, T. de Rubeis, and I. Nardi, "A new simplified five-parameter estimation method for single-diode model of photovoltaic panels," *Energies*, vol. 12, no. 22, 2019, doi: 10.3390/en12224271.

[50] M. Nadia, H. Lassad, Z. Abderrahmen, and C. Abdelkader, "Influence of temperature and irradiance on the different solar PV panel technologies," *Int. J. Energy Sect. Manag.*, vol. 15, no. 2, pp. 421–430,

2021, doi: 10.1108/IJESM-06-2020-0002.

[51] S. T. Thompson *et al.*, “Direct hydrogen fuel cell electric vehicle cost analysis: System and high-volume manufacturing description, validation, and outlook,” *J. Power Sources*, vol. 399, no. March, pp. 304–313, 2018, doi: 10.1016/j.jpowsour.2018.07.100.

[52] B. Tanç, H. T. Arat, E. Baltacıoğlu, and K. Aydın, “Overview of the next quarter century vision of hydrogen fuel cell electric vehicles,” *Int. J. Hydrogen Energy*, vol. 44, no. 20, pp. 10120–10128, 2019, doi: 10.1016/j.ijhydene.2018.10.112.

[53] M. A. Baba, M. Labbadi, M. Cherkaoui, and M. Maaroufi, “Fuel cell electric vehicles: A review of current power electronic converters Topologies and technical challenges,” *IOP Conf. Ser. Earth Environ. Sci.*, vol. 785, no. 1, pp. 1–29, 2021, doi: 10.1088/1755-1315/785/1/012011.

[54] H. S. Das, C. W. Tan, and A. H. M. Yatim, “Fuel cell hybrid electric vehicles: A review on power conditioning units and topologies,” *Renew. Sustain. Energy Rev.*, vol. 76, no. February, pp. 268–291, 2017, doi: 10.1016/j.rser.2017.03.056.

[55] A. Ajanovic and R. Haas, “Economic and Environmental Prospects for Battery Electric- and Fuel Cell Vehicles: A Review,” *Fuel Cells*, vol. 19, no. 5, pp. 515–529, 2019, doi: 10.1002/fuce.201800171.

[56] S. L. Chavan and D. B. Talange, “Electrical equivalent circuit modeling and parameter estimation for PEM fuel cell,” *2017 Innov. Power Adv. Comput. Technol. i-PACT 2017*, vol. 2017-Janua, pp. 1–6, 2017, doi: 10.1109/IPACT.2017.8244980.

[57] Z. Ural and M. T. Gencoglu, “Mathematical Models of PEM Fuel Cells,” *5th Int. Ege Energy Symp. Exhib.*, no. June, pp. 27–30, 2010.

[58] K. M. Tan, S. Padmanaban, J. Y. Yong, and V. K. Ramachandaramurthy, "A multi-control vehicle-to-grid charger with bi-directional active and reactive power capabilities for power grid support," *Energy*, vol. 171, pp. 1150–1163, 2019, doi: 10.1016/j.energy.2019.01.053.

[59] D. S. Abraham *et al.*, "Electric vehicles charging stations' architectures, criteria, power converters, and control strategies in microgrids," *Electron.*, vol. 10, no. 16, 2021, doi: 10.3390/electronics10161895.

[60] G. Saldaña, J. I. S. Martin, I. Zamora, F. J. Asensio, and O. Oñederra, "Electric vehicle into the grid: Charging methodologies aimed at providing ancillary services considering battery degradation," *Energies*, vol. 12, no. 12, 2019, doi: 10.3390/en12122443.

[61] A. R. Dehghani-Sanij, E. Tharumalingam, M. B. Dusseault, and R. Fraser, "Study of energy storage systems and environmental challenges of batteries," *Renew. Sustain. Energy Rev.*, vol. 104, no. November 2018, pp. 192–208, 2019, doi: 10.1016/j.rser.2019.01.023.

[62] I. Azizi and H. Radjeai, "A new strategy for battery and supercapacitor energy management for an urban electric vehicle," *Electr. Eng.*, vol. 100, no. 2, pp. 667–676, 2018, doi: 10.1007/s00202-017-0535-1.

[63] Y. Miao, P. Hynan, A. Von Jouanne, and A. Yokochi, "Current li-ion battery technologies in electric vehicles and opportunities for advancements," *Energies*, vol. 12, no. 6, pp. 1–20, 2019, doi: 10.3390/en12061074.

[64] H. Kraiem, F. Aymen, L. Yahya, A. Triviño, M. Alharthi, and S. S. M. Ghoneim, "A comparison between particle swarm and grey wolf optimization algorithms for improving the battery autonomy in a photovoltaic system," *Appl. Sci.*, vol. 11, no. 16, 2021, doi:

10.3390/app11167732.

[65] C. Iclodean, B. Varga, N. Burnete, D. Cimerdean, and B. Jurchiş, "Comparison of Different Battery Types for Electric Vehicles," *IOP Conf. Ser. Mater. Sci. Eng.*, vol. 252, no. 1, 2017, doi: 10.1088/1757-899X/252/1/012058.

[66] D. N. T. How, M. A. Hannan, M. S. H. Lipu, K. S. M. Sahari, P. J. Ker, and K. M. Muttaqi, "State-of-Charge Estimation of Li-Ion Battery in Electric Vehicles: A Deep Neural Network Approach," *IEEE Trans. Ind. Appl.*, vol. 56, no. 5, pp. 5565–5574, 2020, doi: 10.1109/TIA.2020.3004294.

[67] N. Campagna *et al.*, "Battery models for battery powered applications: A comparative study," *Energies*, vol. 13, no. 15, 2020, doi: 10.3390/en13164085.

[68] U. Krewer, F. Röder, E. Harinath, R. D. Braatz, B. Bedürftig, and R. Findeisen, "Review—Dynamic Models of Li-Ion Batteries for Diagnosis and Operation: A Review and Perspective," *J. Electrochem. Soc.*, vol. 165, no. 16, pp. A3656–A3673, 2018, doi: 10.1149/2.1061814jes.

[69] Y. Zhang, X. Song, C. Ma, D. Hao, and Y. Chen, "Effects of the structure arrangement and spacing on the thermal characteristics of Li-ion battery pack at various discharge rates," *Appl. Therm. Eng.*, vol. 165, no. October, p. 114610, 2020, doi: 10.1016/j.applthermaleng.2019.114610.

[70] S. Podder and M. Z. R. Khan, "Comparison of lead acid and Li-ion battery in solar home system of Bangladesh," *2016 5th Int. Conf. Informatics, Electron. Vision, ICIEV 2016*, pp. 434–438, 2016, doi: 10.1109/ICIEV.2016.7760041.

[71] Q. Zhang, L. Wang, G. Li, and Y. Liu, "A real-time energy management control strategy for battery and supercapacitor hybrid energy storage systems of pure electric vehicles," *J. Energy Storage*, vol. 31, no. May, p. 101721, 2020, doi: 10.1016/j.est.2020.101721.

[72] S. S. Patil *et al.*, "Hybrid Solid State Supercapacitors (HSSC's) for High Energy & Power Density: An Overview," *Eng. Sci.*, vol. 12, pp. 38–51, 2020, doi: 10.30919/es8d1140.

[73] V. Kumaravel, J. Bartlett, and S. C. Pillai, "Solid Electrolytes for High-Temperature Stable Batteries and Supercapacitors," *Adv. Energy Mater.*, vol. 11, no. 3, 2021, doi: 10.1002/aenm.202002869.

[74] S. M. Beladi-Mousavi, B. Khezri, S. Matějková, Z. Sofer, and M. Pumera, "Supercapacitors in Motion: Autonomous Microswimmers for Natural-Resource Recovery," *Angew. Chemie*, vol. 131, no. 38, pp. 13474–13478, 2019, doi: 10.1002/ange.201906642.

[75] S. Fletcher, I. Kirkpatrick, R. Dring, R. Puttock, R. Thring, and S. Howroyd, "The modelling of carbon-based supercapacitors: Distributions of time constants and Pascal Equivalent Circuits," *J. Power Sources*, vol. 345, pp. 247–253, 2017, doi: 10.1016/j.jpowsour.2017.02.012.

[76] R. Drummond, S. Zhao, D. A. Howey, and S. R. Duncan, "Circuit synthesis of electrochemical supercapacitor models," *J. Energy Storage*, vol. 10, pp. 48–55, 2017, doi: 10.1016/j.est.2016.11.003.

[77] N. H. Baharudin, T. M. N. T. Mansur, F. A. Hamid, R. Ali, and M. I. Misrun, "Topologies of DC-DC converter in solar PV applications," *Indones. J. Electr. Eng. Comput. Sci.*, vol. 8, no. 2, pp. 368–374, 2017, doi: 10.11591/ijeecs.v8.i2.pp368-374.

[78] S. S. Dheeban, N. B. M. Selvan, and L. Krishnaveni, "Performance

improvement of Photo-Voltaic panels by super-lift luo converter in standalone application," *Mater. Today Proc.*, vol. 37, no. Part 2, pp. 1163–1171, 2020, doi: 10.1016/j.matpr.2020.06.352.

[79] K. Pavithra, H. Pooja, D. Tamilselvan, and T. D. Sudhakar, "Solar power based positive output super-lift Luo converter using fuzzy logic controller," *J. Phys. Conf. Ser.*, vol. 2040, no. 1, 2021, doi: 10.1088/1742-6596/2040/1/012034.

[80] M. P. Chand and G. Ramesh, "Design of new positive output super-lift luo converter for solar input in comparison with different DC-DC converters," *Int. Res. J. Eng. Technol.*, vol. 03, no. 09, pp. 1588–1594, 2016.

[81] A. Pradhan and B. Panda, "A simplified design and modeling of boost converter for photovoltaic sytem," *Int. J. Electr. Comput. Eng.*, vol. 8, no. 1, pp. 141–149, 2018, doi: 10.11591/ijece.v8i1.pp141-149.

[82] W. Hart Danial, *Commonly used Power and Converter Equations*. 2010.

[83] A. Thiyagarajan, S. G. Praveen Kumar, and A. Nandini, "Analysis and comparison of conventional and interleaved DC/DC boost converter," *2nd Int. Conf. Curr. Trends Eng. Technol. ICCTET 2014*, vol. 38, no. 0, pp. 198–205, 2014, doi: 10.1109/ICCTET.2014.6966287.

[84] S. Punna, U. B. Manthati, and A. Chirayarukil Raveendran, "Modeling, analysis, and design of novel control scheme for two-input bidirectional DC-DC converter for HESS in DC microgrid applications," *Int. Trans. Electr. Energy Syst.*, vol. 31, no. 10, pp. 1–23, 2021, doi: 10.1002/2050-7038.12774.

[85] S. N. Soheli, G. Sarowar, M. A. Hoque, and M. S. Hasan, "Design and Analysis of a DC -DC Buck Boost Converter to Achieve High Efficiency and Low Voltage Gain by using Buck Boost Topology into

Buck Topology," *2018 Int. Conf. Adv. Electr. Electron. Eng. ICAEEE 2018*, no. 1, p. 1, 2018, doi: 10.1109/ICAEEE.2018.8643001.

[86] S. Pourjafar, H. Shayeghi, F. Sedaghati, S. Seyedshenava, and F. Blaabjerg, "A bidirectional multiport DC-DC converter applied for energy storage system with hybrid energy sources," *Int. J. Circuit Theory Appl.*, vol. 49, no. 8, pp. 2453–2478, 2021, doi: 10.1002/cta.2988.

[87] B. H. Nguyen, R. German, J. P. F. Trovao, and A. Bouscayrol, "Real-time energy management of battery/supercapacitor electric vehicles based on an adaptation of pontryagin's minimum principle," *IEEE Trans. Veh. Technol.*, vol. 68, no. 1, pp. 203–212, 2019, doi: 10.1109/TVT.2018.2881057.

[88] B. S. E. Schulz, "Exploring the High-Power Inverter," no. March, pp. 28–35, 2017.

[89] I. Kim, "Short-Circuit Analysis Models for Unbalanced Inverter-Based Distributed Generation Sources and Loads," *IEEE Trans. Power Syst.*, vol. 34, no. 5, pp. 3515–3526, 2019, doi: 10.1109/TPWRS.2019.2903552.

[90] Q. Xun, Y. Liu, and N. Zhao, "Energy Efficiency Comparison of Hybrid Powertrain Systems for Fuel-Cell-Based Electric Vehicles," *2020 IEEE Transp. Electrif. Conf. Expo, ITEC 2020*, pp. 1234–1239, 2020, doi: 10.1109/ITEC48692.2020.9161586.

[91] E. C. Acosta, J. J. C. Aguilar, J. A. C. Carrillo, J. M. V. Garcia, J. P. Fernandez, and M. G. A. Vargas, "Modeling of Tire Vertical Behavior Using a Test Bench," *IEEE Access*, vol. 8, pp. 106531–106541, 2020, doi: 10.1109/ACCESS.2020.3000533.

[92] Mohamed Belrzaeg, Abdussalam Ali Ahmed, Amhimmid Q

Almabrouk, Mohamed Mohamed Khaleel, Alforjani Ali Ahmed, and Meshaal Almukhtar, "Vehicle dynamics and tire models: An overview," *World J. Adv. Res. Rev.*, vol. 12, no. 1, pp. 331–348, 2021, doi: 10.30574/wjarr.2021.12.1.0524.

[93] J. O. Han, J. W. Shin, J. C. Kim, and S. H. Oh, "Design 2-speed transmission for compact electric vehicle using dual brake system," *Appl. Sci.*, vol. 9, no. 9, 2019, doi: 10.3390/app9091793.

[94] S. Wang, Z. Wu, D. Peng, W. Li, S. Chen, and S. Liu, "An angle displacement sensor using a simple gear," *Sensors Actuators, A Phys.*, vol. 270, pp. 245–251, 2018, doi: 10.1016/j.sna.2017.12.064.

[95] J. Pei, X. Han, and Y. Tao, "An improved stiffness model for line contact elastohydrodynamic lubrication and its application in gear pairs," *Ind. Lubr. Tribol.*, vol. 72, no. 5, pp. 703–708, 2020, doi: 10.1108/ILT-11-2019-0465.

[96] Y. Avula, V. R. N. Reddy, and V. S. | V. Srisailam, "Modelling and 3D Printing of Differential Gear Box," *Int. J. Trend Sci. Res. Dev.*, vol. Volume-3, no. Issue-3, pp. 1163–1167, 2019, doi: 10.31142/ijtsrd23287.

[97] M. Hofstetter, D. Lechleitner, M. Hirz, M. Gintzel, and A. Schmidhofer, "Multi-objective gearbox design optimization for xEV-axle drives under consideration of package restrictions," *Forsch. im Ingenieurwesen/Engineering Res.*, vol. 82, no. 4, pp. 361–370, 2018, doi: 10.1007/s10010-018-0278-9.

[98] Z. Pusztai, P. Kőrös, and F. Friedler, "Vehicle Model for Driving Strategy Optimization of Energy Efficient Lightweight Vehicle," *Chem. Eng. Trans.*, vol. 88, no. April, pp. 385–390, 2021, doi: 10.3303/CET2188064.

[99] A. Efimov, O. Polushkin, S. Kireev, and M. Korchagina, "A Mathematical Model of a Differential Drive with a Limited Gear Ratio," *Transp. Res. Procedia*, vol. 54, no. 2020, pp. 699–711, 2021, doi: 10.1016/j.trpro.2021.02.123.

[100] W. Zhuang *et al.*, "A survey of powertrain configuration studies on hybrid electric vehicles," *Appl. Energy*, vol. 262, no. October 2019, p. 114553, 2020, doi: 10.1016/j.apenergy.2020.114553.

[101] C. X. Chen, Y. X. Xie, and Y. H. Lan, "Backstepping control of speed sensorless permanent magnet synchronous motor based on slide model observer," *Int. J. Autom. Comput.*, vol. 12, no. 2, pp. 149–155, 2015, doi: 10.1007/s11633-015-0881-2.

[102] S. Li, "A Review of Electric Motor Drives for Applications in Electric and Hybrid Vehicles," *Model. Anal. Electr. Mot. Drive Syst.*, no. April, 2017, doi: 10.13140/RG.2.2.14806.52802.

[103] F. Amin, E. Bin Sulaiman, W. M. Utomo, H. A. Soomro, M. Jenal, and R. Kumar, "Modelling and simulation of field oriented control based permanent magnet synchronous motor drive system," *Indones. J. Electr. Eng. Comput. Sci.*, vol. 6, no. 2, pp. 387–395, 2017, doi: 10.11591/ijeecs.v6.i2.pp387-395.

[104] N. G.K., L. Z.V., and U. S., "Torque capability improvement of sensorless FOC induction machine in field weakening for propulsion purposes," *J. Electr. Syst. Inf. Technol.*, vol. 4, no. 1, pp. 173–184, 2017, doi: 10.1016/j.jesit.2016.10.002.

[105] K. Suman and A. T. Mathew, "Speed Control of Permanent Magnet Synchronous Motor Drive System Using PI, PID, SMC and SMC plus PID Controller," *2018 Int. Conf. Adv. Comput. Commun. Informatics, ICACCI 2018*, pp. 543–549, 2018, doi:

10.1109/ICACCI.2018.8554788.

[106] M. Nicola and C. I. Nicola, "Sensorless fractional order control of pmsm based on synergetic and sliding mode controllers," *Electron.*, vol. 9, no. 9, pp. 1–45, 2020, doi: 10.3390/electronics9091494.

[107] Y. Yang, S. Bremner, C. Menictas, and M. Kay, "Battery energy storage system size determination in renewable energy systems: A review," *Renew. Sustain. Energy Rev.*, vol. 91, no. June 2017, pp. 109–125, 2018, doi: 10.1016/j.rser.2018.03.047.

[108] P. Vankadari, "Comparison Study of Battery & Supercapacitor Standalone Storage System Based Light Electric Vehicle Using MATLAB/SIMULINK," *Int. J. Res. Appl. Sci. Eng. Technol.*, vol. 9, no. 12, pp. 1071–1082, Dec. 2021, doi: 10.22214/ijraset.2021.39471.

[109] A. K. Podder, O. Chakraborty, S. Islam, N. Manoj Kumar, and H. H. Alhelou, "Control Strategies of Different Hybrid Energy Storage Systems for Electric Vehicles Applications," *IEEE Access*, vol. 9, pp. 51865–51895, 2021, doi: 10.1109/ACCESS.2021.3069593.

[110] F. Liu, C. Wang, and Y. Luo, "Parameter matching method of a battery-supercapacitor hybrid energy storage system for electric vehicles," *World Electr. Veh. J.*, vol. 12, no. 4, 2021, doi: 10.3390/wevj12040253.

[111] Z. Cabrane, J. Kim, K. Yoo, and M. Ouassaid, "HESS-based photovoltaic/batteries/supercapacitors: Energy management strategy and DC bus voltage stabilization," *Sol. Energy*, vol. 216, no. January, pp. 551–563, 2021, doi: 10.1016/j.solener.2021.01.048.

[112] P. S. Gavhane, S. Krishnamurthy, R. Dixit, J. P. Ram, and N. Rajasekar, "EL-PSO based MPPT for Solar PV under Partial Shaded Condition," *Energy Procedia*, vol. 117, pp. 1047–1053, 2017, doi: 10.1016/j.egypro.2017.05.227.

[113] J. Ahmed and Z. Salam, "An Enhanced Adaptive P&O MPPT for Fast and Efficient Tracking Under Varying Environmental Conditions," *IEEE Trans. Sustain. Energy*, vol. 9, no. 3, pp. 1487–1496, 2018, doi: 10.1109/TSTE.2018.2791968.

[114] K. Jain, M. Gupta, and A. K. Bohre, "Implementation and Comparative Analysis of P & O and INC MPPT Method for PV System," *2018 8th IEEE India Int. Conf. Power Electron.*, pp. 1–6, 2018.

[115] S. D. Al-majidi, "Design of an intelligent MPPT based on ANN using a real photovoltaic system data," *2019 54th Int. Univ. Power Eng. Conf.*, pp. 1–6, 2019, doi: 10.1109/UPEC.2019.8893638.

[116] H. Jeong, H. Lee, Y. C. Liu, and K. A. Kim, "Review of Differential Power Processing Converter Techniques for Photovoltaic Applications," *IEEE Trans. Energy Convers.*, vol. 34, no. 1, pp. 351–360, 2019, doi: 10.1109/TEC.2018.2876176.

[117] H. Gholizadeh, R. Sharifi Shahrivar, M. R. Hashemi, E. Afjei, and S. A. Gorji, "Design and implementation a single-switch step-up dc-dc converter based on cascaded boost and luo converters," *Energies*, vol. 14, no. 12, pp. 1–18, 2021, doi: 10.3390/en14123584.

[118] P. K. Pathak, A. K. Yadav, S. Kumar, B. Twala, and I. Kamwa, "Design of smart battery charging circuit via photovoltaic for hybrid electric vehicle," *IET Renew. Power Gener.*, 2023, doi: 10.1049/rpg2.12656.

[119] M. G. Carignano, R. Costa-Castelló, V. Roda, N. M. Nigro, S. Junco, and D. Feroldi, "Energy management strategy for fuel cell-supercapacitor hybrid vehicles based on prediction of energy demand," *J. Power Sources*, vol. 360, pp. 419–433, 2017, doi: 10.1016/j.jpowsour.2017.06.016.

[120] R. S. Sankarkumar and R. Natarajan, "Energy management techniques

and topologies suitable for hybrid energy storage system powered electric vehicles: An overview," *Int. Trans. Electr. Energy Syst.*, vol. 31, no. 4, pp. 1–30, 2021, doi: 10.1002/2050-7038.12819.

[121] C. Chatzikomis, A. Sorniotti, P. Gruber, M. Zanchetta, D. Willans, and B. Balcombe, "Comparison of Path Tracking and Torque-Vectoring Controllers for Autonomous Electric Vehicles," *IEEE Trans. Intell. Veh.*, vol. 3, no. 4, pp. 559–570, 2018, doi: 10.1109/TIV.2018.2874529.

[122] M. Bujarbaruah, X. Zhang, H. E. Tseng, and F. Borrelli, "Adaptive MPC for Autonomous Lane Keeping," 2018, [Online]. Available: http://arxiv.org/abs/1806.04335

[123] A. Benevieri *et al.*, "Surface Permanent Magnet Synchronous Motors' Passive Sensorless Control: A Review," *Energies*, vol. 15, no. 20, 2022, doi: 10.3390/en15207747.

[124] K. M. Choo and C. Y. Won, "Design and Analysis of Electrical Braking Torque Limit Trajectory for Regenerative Braking in Electric Vehicles with PMSM Drive Systems," *IEEE Trans. Power Electron.*, vol. 35, no. 12, pp. 13308–13321, 2020, doi: 10.1109/TPEL.2020.2994615.

[125] Y. Ahmed, A. Hoballah, E. Hendawi, S. Al Otaibi, S. K. Elsayed, and N. I. Elkalashy, "Fractional order pid controller adaptation for pmsm drive using hybrid grey wolf optimization," *Int. J. Power Electron. Drive Syst.*, vol. 12, no. 2, pp. 745–756, 2021, doi: 10.11591/ijpeds.v12.i2.pp745-756.

[126] F. M. Zaihidee, S. Mekhilef, and M. Mubin, "Fractional Order SMC for Speed Control of PMSM," *iEECON 2018 - 6th Int. Electr. Eng. Congr.*, pp. 1–4, 2018, doi: 10.1109/IEECON.2018.8712281.

[127] M. G. Majumder, A. K. Yadav, K. Gopakumar, R. Krishna, U. Loganathan, and L. G. Franquelo, "A 5-Level Inverter Scheme Using

Single DC Link with Reduced Number of Floating Capacitors and Switches for Open-End im Drives," *IEEE Trans. Ind. Electron.*, vol. 67, no. 2, pp. 960–968, 2020, doi: 10.1109/TIE.2019.2898594.

[128] D. D. Julasana, S. B. Dabhi, and C. H. Raval, "Simulation and analysis of PMBLDC motor fed by seven level inverter with K-map logic," *2018 Int. Conf. Comput. Power Commun. Technol. GUCON 2018*, no. 1, pp. 743–747, 2019, doi: 10.1109/GUCON.2018.8674911.

[129] A. Saleh, K. S. Faiqotul Azmi, T. Hardianto, and W. Hadi, "Comparison of MPPT fuzzy logic controller based on perturb and observe (P&O) and incremental conductance (InC) algorithm on buck-boost converter," *Proc. - 2018 2nd Int. Conf. Electr. Eng. Informatics Towar. Most Effic. W. Mak. Deal. with Futur. Electr. Power Syst. Big Data Anal. ICon EEI 2018*, no. October, pp. 154–158, 2018, doi: 10.1109/ICon-EEI.2018.8784324.

[130] A. P. Yoganandini and G. S. Anitha, "A modified particle swarm optimization algorithm to enhance MPPT in the PV array," *Int. J. Electr. Comput. Eng.*, vol. 10, no. 5, pp. 5001–5008, 2020, doi: 10.11591/IJECE.V10I5.PP5001-5008.

[131] L. X. Eulg *et al.*, "3Huwxue 2Evhuyh Dqg , Qfuhphqwdo & Rqgxfwdqfh," pp. 354–359, 2014.

[132] S. Xu and H. Peng, "Design, Analysis, and Experiments of Preview Path Tracking Control for Autonomous Vehicles," *IEEE Trans. Intell. Transp. Syst.*, vol. 21, no. 1, pp. 48–58, 2020, doi: 10.1109/TITS.2019.2892926.

[133] S. Kamat, "Lane Keeping of Vehicle Using Model Predictive Control," *2019 IEEE 5th Int. Conf. Converg. Technol. I2CT 2019*, pp. 1–6, 2019, doi: 10.1109/I2CT45611.2019.9033958.

[134] C. E. Beal and J. C. Gerdes, “Model predictive control for vehicle stabilization at the limits of handling,” *IEEE Trans. Control Syst. Technol.*, vol. 21, no. 4, pp. 1258–1269, 2013, doi: 10.1109/TCST.2012.2200826.

[135] G. V. Raffo, G. K. Gomes, J. E. Normey-Rico, C. R. Kelber, and L. B. Becker, “A predictive controller for autonomous vehicle path tracking,” *IEEE Trans. Intell. Transp. Syst.*, vol. 10, no. 1, pp. 92–102, 2009, doi: 10.1109/TITS.2008.2011697.

[136] A. Seabridge and M. Radaei, “Vehicle Systems,” *Aircr. Syst. Classif.*, vol. 15, no. 3, pp. 37–126, 2022, doi: 10.1002/9781119771876.ch3.

[137] F. Borrelli, P. Falcone, T. Keviczky, J. Asgari, and D. Hrovat, “Biographical notes: Francesco Borrelli received thèLaurea’ degree in computer science engineering in 1998 from the University of Naples`Federico Naples`Federico II’, Italy. In 2002 he received his PhD from the Automatic Control Laboratory Int,” *J. Veh. Auton. Syst.*, vol. 3, no. 2, p. 265, 2005.

[138] J. Hanema, M. Lazar, and R. Tóth, “Tube-based LPV constant output reference tracking MPC with error bound,” *IFAC-PapersOnLine*, vol. 50, no. 1, pp. 8612–8617, 2017, doi: 10.1016/j.ifacol.2017.08.1430.

Appendices

List of Publications:

1. A paper entitled "Model Predictive Control based Autonomous Electric Vehicle for Monitoring Path Tracing Process" has been accepted for publication in the 7th International Conference on Engineering Sciences, December 2023.

2. The paper " Enhancing the Dynamic Performance of Hybrid Storage Systems Provided by PV Solar Panels " was submitted to the Tikrit Journal of Engineering Sciences in May 2024.

3. A Review of Hybrid Electric Vehicle Configurations: Advances and Challenges

4. A paper has been submitted to Almustashar Journal entitled " Integrating electric vehicle charging stations with solar panels: innovative solutions to enhance electric transportation". It as been published in middle of August, No.3, 2024.

5. A patent has been submitted to Central Organization for Standardization and Quality Control – Industrial Property Department - Iraq entitled " Innovative Intelligent Speed Control Technology to Maximize Electric Motor Performance in Hybrid Vehicles", by Ali Altahir, Mohammed Albaker,and Ahmed Abdulhadi Ahmed, 2024.

1) First paper

ID-Code: ICES-135
Authors: Mohammed Albaqer Najim, Ali Abdul Razzaq Altahir, Ahmed Abdulhadi Al-Moadhen
Date: 22/11/2023

Dear Authors,

On behalf of the scientific and organizing committees of the 7th International Conference on Engineering Sciences (ICES 2023), I am pleased to inform you that your manuscript entitled "**Model Predictive Control-Based Autonomous Vehicle for Monitoring Path Tracing Process**" has been accepted for publication in the conference proceedings of ICES2023. The accepted paper will be published in the AIP Conference Proceedings which is indexed in the Scopus Journals database. The 7th ICES will be held on 13-14 December 2023. Thank you for your interest in participating in the 7th ICES.

Best Regards,

University Of Kerbala
Dean Office
College of engineering

L. Sh. Rash

Prof. Dr. Laith Sh. Rasheed
Chair of the Organizing Committee -ICES
Dean of Engineering College at Kerbala University

Model Predictive Control-Based Autonomous Vehicle for Monitoring Path Tracing Process

Mohammed Albaqer Najim[1], Ali Abdul Razzaq Altahir[1],
Ahmed Abdulhadi Al – Moadhen[1]

[1] *Department of Electrical and Electronics Engineering, University of Kerbala, Karbala, Iraq.*
e09163265@s.uokerbala.edu.iq; ali.altahir@uokerbala.edu.iq, ahmedh1333@uokerbala.edu.iq

Abstract. This paper presents the path-tracking issue of terrestrial Autonomous Vehicles (AV) using a linear model predictive controller (LMPC) structure. In a cascade structure, the controller architecture takes into account both kinematic and dynamic control. In addition to ensuring tracking accuracy, the controller also takes vehicle dynamic stability into account during tracking. The goal of this research is for the AV to precisely track the route's specified waypoints, ensure vehicle stability, and satisfy the control system's reliable performance. The model of the autonomous vehicle was used AV as a model for the MPC. This study contains a comparative study between two scenarios where the first scenario was a route that requires the car to travel along a normal path without any barriers, while the second requires it to pass over a barrier that has been placed in the road without hitting it. Using MATLAB/Simulink R2022b, a study on the performance of the MPC was carried out. After improving the parameters for LMPC the results show that by changing the direction of the vehicle, the MPC delivers high-quality performance in both the precision of the path tracing and the smoothness of the steering angle. These results demonstrate that the suggested MPC structure is the one that best satisfies the target requirements.

Keywords: Autonomous vehicle (AV), Model predictive control, Path tracing process, Steering angle, Yaw angle.

INTRODUCTION

The emergence of the digital revolution and the industrial revolution resulted in the creation of many fresh technologies and technologies in the field of AVs. Many research articles have been published describing the technological advances and improvements that have been added to AVs[1]. Expectations indicate in 2045, autonomous vehicles(AV) will make up 50% of all land travel. [2]. While a vehicle has levels 3-5 automated systems, it is referred to as an AV as shown in Fig. 1.

0	1	2	3	4	5
NO AUTOMATION	**DRIVER ASSISTANCE**	**PARTIAL AUTOMATION**	**CONDITIONAL AUTOMATION**	**HIGH AUTOMATION**	**FULL AUTOMATION**
Manual control. The human performs all driving tasks (sreering, acceleration, braking, etc).	The vehicle features a single automated system (e.g. it monitors speed through cruise control).	ADAS, The vehicle can perform steering and acceleration. The human still monitor all tasks and can take control at any time.	Environoment al detection capabilities. The vehicle can perform most driving tasks, but human override is still required.	The vehicle performs all driving under specific circumstances. Geofencing is required. Human override is still an option	The vehicle performs all driving tasks under all condition. Zero human attention is requires
The Human Monitors The Driving Environment			**The Automated System Monitors The Driving Renvironment.**		

FIGURE1. Levels of Driving Automation.

2) Second paper

Improving the Dynamic Performance of Hybrid Storage System Provided by PV Solar Panels

Mohammed Albaker Najm Abed[a,*], Ali Abdul Razzaq Altahir[b], Ahmed Abdulhadi Al – Moadhen[c]

[a] University of Kerbala, Department of Electrical and Electronics Engineering, Kerbala, Iraq

[a] e09163265@s.uokerbala.edu.iq; https://orcid.org/0009-0001-6954-8205

[b] University of Kerbala, Department of Electrical and Electronics Engineering, Kerbala, Iraq

ali.altahir @uokerbala.edu.iq; https://orcid.org/0000-0002-8125-6600

[c] University of Kerbala, Department of Electrical and Electronics Engineering, Kerbala, Iraq

ahmedh1333@uokerbala.edu.iq; https://orcid.org/0000-0002-2035-3917

محمد الباقر نجم عبد[a]، علي عبد الرزاق عباس[b]، احمد عبد الهادي احمد[c]

[a] قسم الهندسة الكهربائية والالكترونية/ كلية هندسة / جامعة كربلاء /كربلاء-العراق

A B S T R A C T

Solar energy is one of the most reliable energy sources in the planet. Renewable energy sources have recently been used as charger sources for many applications, such as batteries and supercapacitors. They are utilizing rechargeable batteries, supercapacitors, and photovoltaic solar energy as an energy storage system. Batteries experience frequent charging and discharging cycles, which impact their lifespan. The dynamic performance of a hybrid storage system is improved, and a lower-capacity rechargeable battery can be installed by adding a supercapacitor to the energy storage system. Moreover, the supercapacitor smoothed out currents flowing to and from the battery, improving operating conditions and increasing energy efficiency. It is capable for utilizing a combination of storage technologies. That is Lithium-ion batteries will offer good capacity for long-term storage, while supercapacitors will handle rapid power fluctuations. That will create a system responding to short-term and long-term power demand changes. In the current paper, MPPT methods with charge controllers based on different DC-DC converters will be discussed and compared successfully. The supercapacitor is a helpful resource for choosing the suitable type of MPPT algorithm and DC-DC converter since it describes all scenarios' functionality, applications, benefits, and drawbacks. The energy management system between the solar panel, supercapacitor, and battery has been considered. Using a

3) Third paper

Kerbala Journal for Engineering Science
https://kjes.uokerbala.edu.iq/

A Review of Hybrid Electric Vehicle Configurations: Advances and Challenges

Mohammed Albaker Najm Abed[a]*, Prof. Dr. Ali Abdul Razzaq Altahir[b] ,
Assist. Prof. Dr. Ahmed Abdulhadi Ahmed[c]

[a,b,c] University of Kerbala, Department of Electrical and Electronics Engineering, Kerbala, Iraq
* Corresponding author, Email: e09163265@s.uokerbala.edu.iq; ali.altahir@uokerbala.edu.iq

https://orcid.org/0009-0001-6954-8205

Received; Revised:; Accepted:

Abstract

Hybrid electric vehicles (HEVs) are essential to achieving sustainable mobility objectives. The configurations used in HEVs are reviewed in this paper, along with their advancements and remaining challenges. The paper explores the fundamental parts of HEVs, such as motor controllers, energy storage systems, and powertrains. Different motor types and control techniques are analyzed, along with advancements in battery technology for improved energy density and lifespan. The role of maximum power point trackers in optimizing solar panel output for plug-in hybrids is explored. The paper emphasizes the critical function of DC-DC converters in regulating voltage levels and the importance of efficient energy management systems in optimizing HEV performance. A comparative analysis of parallel, series, and power-split hybrid powertrains highlights their unique advantages and limitations. Finally, the discussion section explores overall trends, advancements in HEV configurations, and challenges such as cost reduction, range limitations, and battery recycling. The conclusion emphasizes the potential of HEVs for sustainable transportation and briefly mentions future research directions for HEV configurations. Most of controllers have the same reaction with less distortion for the backstepping control. The main reason is that Backstepping control's efficacy depends on accurate controller tuning. Torque distortion can be considerably reduced with carefully selected parameters. This article summarizes multiple comprehensive reviews that studied different literature on hybrid electric vehicle configurations, advances and challenges. This work aims to provide a guide for researchers and practitioners to relate their work to existing research and gain insights into what their work can contribute to the field.

Keywords: Hybrid energy storage system, Backstepping control, Slide mode control, Enhanced field-oriented control, Speed control techniques, Maximum Power Point Tracking, Perturb and Observe, Incremental Conductance, Particle Swarm Optimization, Artificial Neural Network.

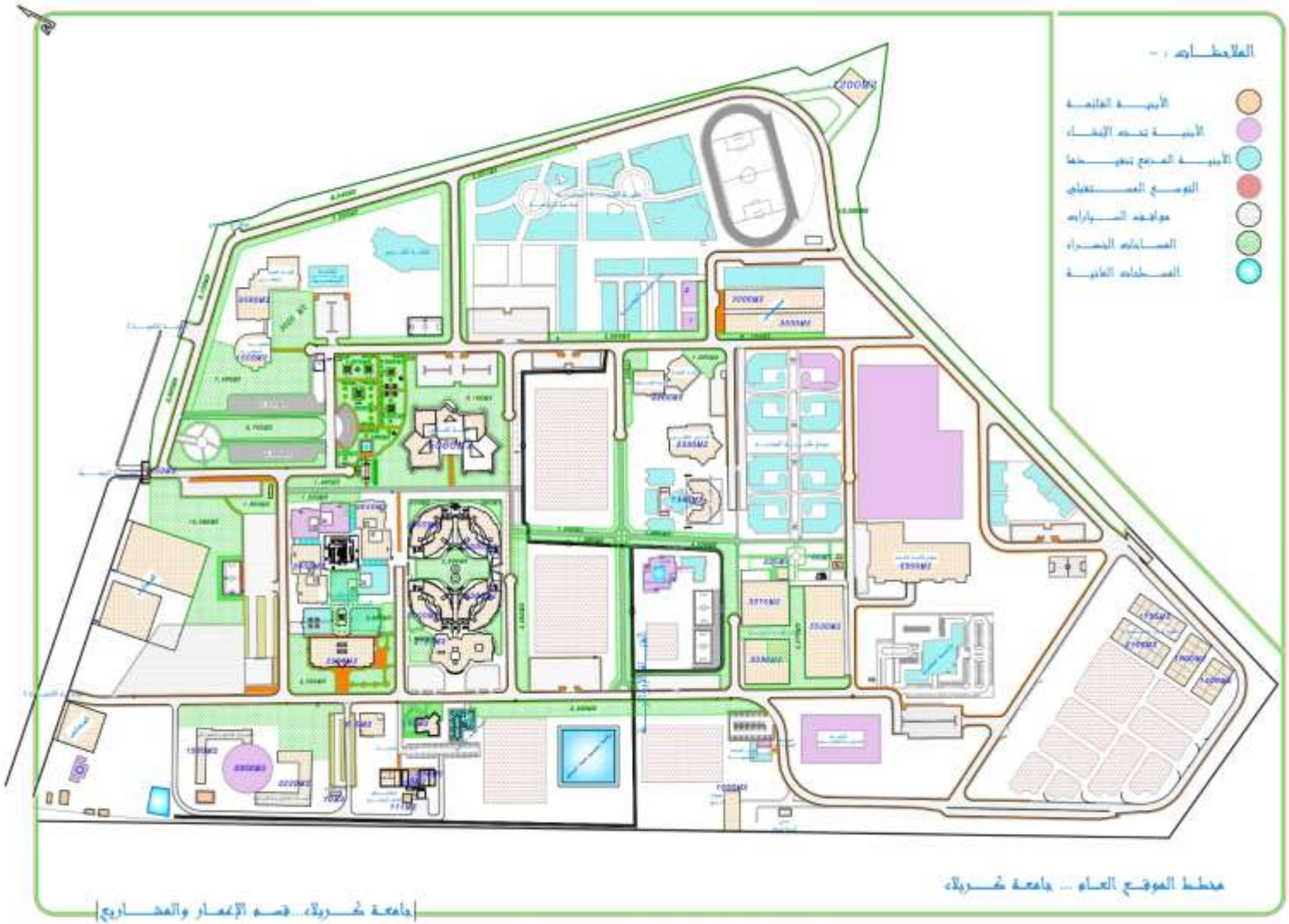
الملاحظات :-
الأبنية القائمة
الأبنية تحت الإنشاء
الأبنية المزمع تنفيذها
التوسع المستقبلي
مواقف السيارات
المساحات الخضراء
المسطحات المائية
مخطط الموقع العام ... جامعة شقراء
جامعة شقراء ... قسم الإعمار والمشاريع

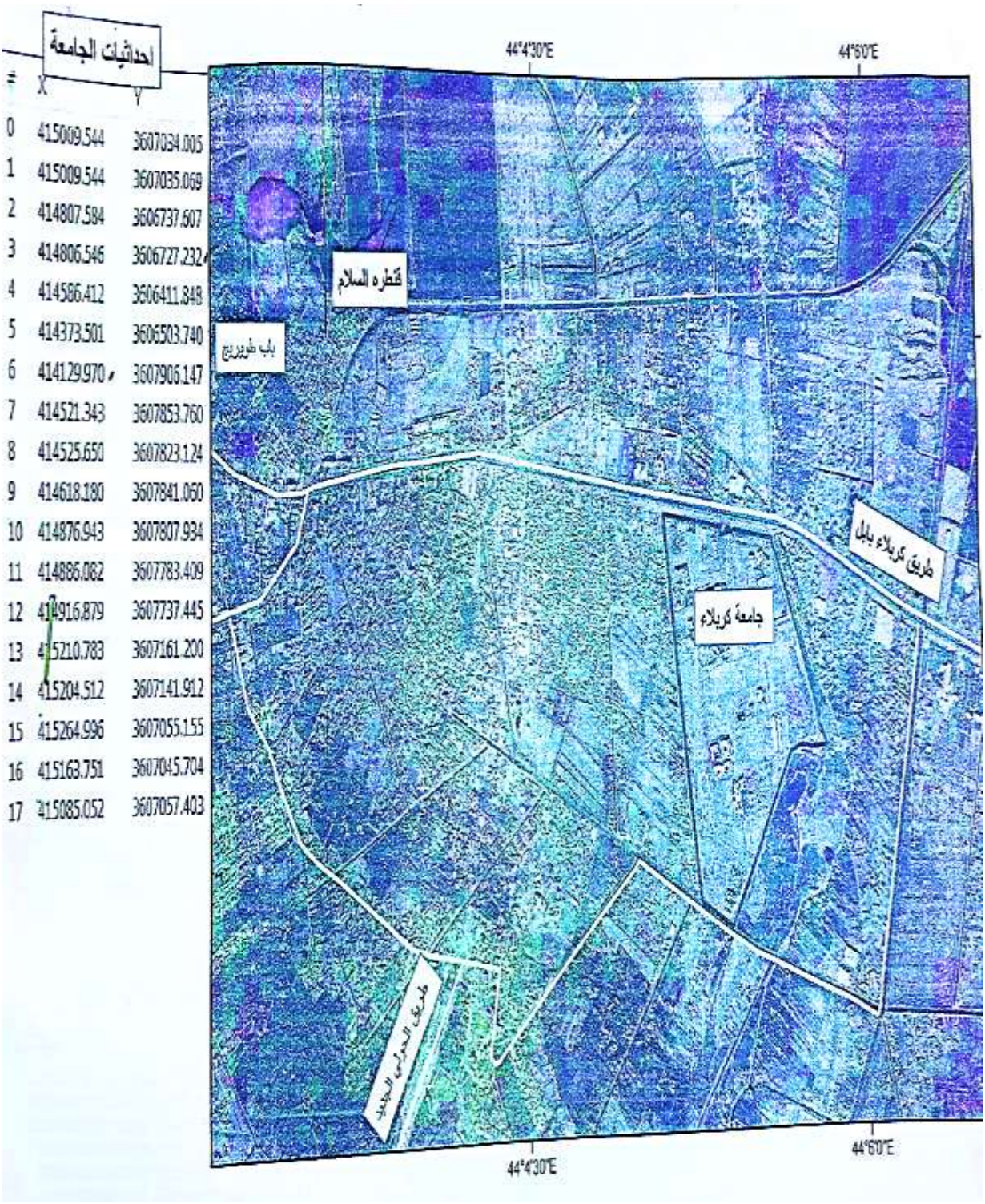

مرتسم يوضح موقع جامعة كربلاء مع الطرق الرئيسية المؤدية لها

الخلاصة

يظل قطاع النقل أحد المساهمين الرئيسيين في ظاهرة الاحتباس الحراري ، وذلك بشكل أساسي بسبب انبعاثات الغازات الدفيئة من المركبات التي تعمل بالبنزين .تقدم المركبات الكهربائية الهجينة حلاً قويًا ، حيث تقلل بشكل كبير من البصمة الكربونية .ومع ذلك ، فإن تحسين أداء أنظمة التحكم بها يمثل تحديات مستمرة .تناول هذا البحث هذه التحديات من خلال دراسة طرق تحسين أداء المركبات الكهربائية الهجينة واستكشاف إمكانية تحويلها إلى أنظمة مستقلة .توفر نتائج البحث رؤى قيمة للتطوير المستقبلي للمركبات الكهربائية الهجينة ودمجها مع تقنية القيادة الذاتية. حدد البحث مجالين رئيسيين لتحسين أداء المركبات الكهربائية الهجينة :تحكم المحرك وتحسين نظام تخزين الطاقة. قارنت الدراسة بين أنواع مختلفة من المحركات وطرق التحكم من خلال عمليات محاكاة مكثفة .برز المحرك ذو المغناطيس الدائم كخيار أمثل ، خاصة عند إقرانه بالتحكم المتتابع .أظهر المحرك ذو المغناطيس الدائم أداءً متفوقًا في جميع سيناريوهات الاختبار ، بما في ذلك السرعة المتغيرة وعزم الدوران ، مقارنة بالمحركات التيارالمستمر بدون فرشاة . وجد أن أفضل مزيج هو نظام المحرك ذو المغناطيس الدائم مع التحكم الخلفي. قدم المحرك ذو المغناطيس الدائم العديد من المزايا الهامة على المحركات التيارالمستمر بدون فرشاة وتقنيات التحكم الأخرى مثل التحكم في الوضع المنزلق و التحكم الموجه نحو المجال، بما في ذلك السماح بالتحكم المتتابع بتوصيل طاقة دقيق ، مما يقلل من فقدان الطاقة, قلل هذا المزيج بشكل فعال من تموج عزم الدوران ، وهي ظاهرة تسبب خرج عزم دوران غير متساوي واهتزازات. و قلل التحكم المتتابع من تقلبات السرعة وعزم الدوران ، مما أدى إلى تشغيل السيارة بسلاسة أكبر. خاضت الاطروحة في تحسين نظام تخزين الطاقة ، الذي يضم البطاريات والمكثفات الفائقة ونظام الطاقة الشمسية .كان التركيز على زيادة خرج الطاقة مع ضمان استقرار النظام .تم تقييم عدة تقنيات عبر فئات مختلفة. أثبتت طريقة المضايقة والملاحظة أنها الأكثر فعالية في استخراج أقصى قدر من الطاقة من الألواح الشمسية .يُترجم هذا إلى شحن أسرع للبطارية والمكثف الفائق ، مما يعزز الكفاءة العامة للطاقة في المركبات الكهربائية الهجينة .أظهر المحول سوبر ليو أداءً متفوقًا مقارنة بالمحول التعزيزي .لقد قدم تنظيمًا أفضل للجهود ، وقلل من التجاوز والتذبذبات في جهد الخرج ، وحسن كفاءة تتبع نقطة التشغيل الأقصى.أظهرت نتائج محاكاة الدراسة أن كفاءة مستويات العاكس المختلفة .برز العاكس متعدد المستويات ذو السبعة مستويات كالفائز الواضح ، حيث قلل من التقلبات والتموجات في السرعة وعزم الدوران .بالإضافة إلى ذلك ، فقد أثر بشكل

إيجابي على نظام تخزين الطاقة من خلال تقليل تقلبات التيار أثناء الشحن والتفريغ وتحسين خصائص تيار التشغيل. إلى جانب تحسين الأداء ، تم دراسة الجدوى الفنية لتحويل المركبات الكهربائية الهجينة إلى مركبات ذاتية القيادة .تم استخدام نموذج تحكم تنبؤي تكيفي من خلال عمليات محاكاة لتقييم فعاليته في التحكم في مسار مركبة كهربائية هجينة ذاتية القيادة .كانت النتائج مشجعة. أظهر استخدام نموذج تحكم تنبؤي تكيفي دقة عالية في تتبع المسارات المحددة مسبقًا. أظهرت النتائج أن دقة متحكم السرعة وعزم الدوران وصلت إلى 99.4%، وانخفض تموج عزم الدوران إلى 0.083% مع التحكم بالخطوة الخلفية. يتم زيادة الطاقة المستخرجة من اللوحة الشمسية إلى 15% عند استخدام P&O مع محول Super-lift Luo. يعتبر الوصول إلى كفاءة تتبع المسار بنسبة 99.2% بمثابة تتبع مسار دقيق للغاية.

جمهورية العراق
وزارة التعليم العالي و البحث العلمي
جامعة كربلاء
كلية الهندسة
قسم الهندسة الكهربائية والإلكترونية

أسناد المحرك الكهربائي في مركبة هجينة بمتحكم سرعة ذكي

رسالة مقدمة الى مجلس كلية الهندسة / جامعة كربلاء وهي جزء من متطلبات نيل درجة الماجستير في علوم الهندسة الكهربائية

من قبل:
محمد الباقر نجم عبد ضيول

باشراف :
أ.د. علي عبد الرزاق عباس الطاهر

أ.م.د. أحمد عبد الهادي أحمد

ذو الحجة - 1445

حزيران- 2024